Veröffentlichungen der DGK

Ausschuss Geodäsie der Bayerischen Akademie der Wissenschaften

Reihe C | Dissertationen | Heft Nr. 844

Cheng-Chieh Wu

The Measurement- and Model-based Structural Analysis for Damage Detection

München 2020

Verlag der Bayerischen Akademie der Wissenschaften

ISSN 0065-5325 | ISBN 978-3-7696-5256-7

Diese Arbeit ist gleichzeitig veröffentlicht in:
Universitätsbibliothek der Technischen Universität Berlin
http://dx.doi.org/10.14279/depositonce-8845, Berlin 2019

Veröffentlichungen der DGK

Ausschuss Geodäsie der Bayerischen Akademie der Wissenschaften

Reihe C | Dissertationen | Heft Nr. 844

The Measurement- and Model-based Structural Analysis for Damage Detection

Von der Fakultät – Planen Bauen Umwelt

der Technischen Universität Berlin

zur Erlangung des akademischen Grades

Doktor der Ingenieurwissenschaften (Dr.-Ing.)

genehmigte Dissertation

Vorgelegt von

Dipl.-Ing. Cheng-Chieh Wu

Geboren am 08.10.1983 in Taipeh

München 2020

Verlag der Bayerischen Akademie der Wissenschaften

ISSN 0065-5325 ISBN 978-3-7696-5256-7

Diese Arbeit ist gleichzeitig veröffentlicht in:
Universitätsbibliothek der Technischen Universität Berlin
http://dx.doi.org/10.14279/depositonce-8845, Berlin 2019

Adresse der DGK:



Ausschuss Geodäsie der Bayerischen Akademie der Wissenschaften (DGK)

Alfons-Goppel-Straße 11 ● D – 80 539 München

Telefon +49 – 331 – 288 1685 ● Telefax +49 – 331 – 288 1759

E-Mail post@dgk.badw.de ● http://www.dgk.badw.de

Promotionsausschuss:

Vorsitzender: Prof. Dr. phil. nat. Jürgen Oberst

Gutachter: Prof. Dr.-Ing. Frank Neitzel
Prof. Dr.-Ing. Andreas Eichhorn
Univ.-Prof. Dipl.-Ing. Dr.techn. Werner Lienhart
Prof. Dr.-Ing. Werner Daum

Tag der wissenschaftlichen Aussprache: 20.03.2019

© 2020 Bayerische Akademie der Wissenschaften, München

Alle Rechte vorbehalten. Ohne Genehmigung der Herausgeber ist es auch nicht gestattet,
die Veröffentlichung oder Teile daraus auf photomechanischem Wege (Photokopie, Mikrokopie) zu vervielfältigen

ISSN 0065-5325 ISBN 978-3-7696-5256-7

Summary

The present work is intended to make a contribution to the monitoring of civil engineering structures. The detection of damage to structures is based on the evaluation of spatially and temporally distributed hybrid measurements. The acquired data can be evaluated purely geometrically or physically. It is preferable to do the latter, since the cause of damage can be determined by means of geometrical-physical laws in order to be able to intervene in time and ensure the further use of the structures. For this reason, the continuum mechanical field equations in conjunction with the finite element method and hybrid measurements are combined into a single evaluation method by the adjustment calculation. This results in two challenges.

The first task deals with the relationship between the finite element method and the method of least squares. The finite element method solves certain problem classes, which are described by a system of elliptical partial differential equations. Whereas the method of least squares solves another class of problems, which is formulated as an overdetermined system of equations. The striking similarity between both methods is known since many decades. However, it remains unresolved why this resemblance exists. The contribution is to clarify this by examining the variational calculus, especially with regard to its methodological procedure. Although the well-known Gauss-Markov model within the method of least squares and the finite element method solve inherently different problem classes, it is shown that both methods can be derived by following the same methodological steps of the variational calculus. From a methodical viewpoint, this implies that both methods are not only similar, but actually the same. In addition, it is pointed out where a possible cross-connection to other methods exists.

The second task introduces a Measurement- and Model-based Structural Analysis (MeMoS) by integrating the finite element method into the adjustment calculation. It is shown in numerical examinations how this integrated analysis can be used for parameter identification of simple as well as arbitrarily shaped structural components. Based on this, it is examined with which observation types, with which precision and at which location of the structure these measurements must be carried out in order to determine the material parameters as precisely as possible. This serves to determine an optimal and economic measurement set-up. With this integrated analysis, a substitute model of a geometrically complex structure can also be determined. The issue of the detection and localisation of damage within a structure is studied by means of this structural analysis. The Measurement and Model-based Structural Analysis is validated using two different test setups, an aluminum model bridge and a bending beam.

Zusammenfassung

Die vorliegende Arbeit soll einen Beitrag zur Überwachung von Ingenieurbauwerken leisten. Die Detektion von Schäden an Bauwerken basiert auf der Auswertung von räumlich und zeitlich verteilten Hybridmessungen. Die erfassten Daten können rein geometrisch oder physikalisch ausgewertet werden. Letzteres ist vorzuziehen, da die Schadensursache mittels geometrisch-physikalischer Gesetze ermittelt werden kann, um rechtzeitig eingreifen und die weitere Nutzung der Bauwerke sicherstellen zu können. Aus diesem Grund werden die kontinuumsmechanischen Feldgleichungen in Verbindung mit der Finite-Elemente-Methode und Hybridmessungen durch die Ausgleichungsrechnung zu einer einzigen Auswertemethode kombiniert. Dabei ergeben sich zwei Aufgabenstellungen.

Die erste Aufgabe beschäftigt sich mit der Beziehung zwischen der Finite-Elemente-Methode und der Ausgleichungsrechnung. Die Finite-Elemente-Methode löst bestimmte Problemklassen, die durch ein System elliptischer partieller Differentialgleichungen beschrieben werden. Während die Methode der kleinsten Quadrate eine weitere Klasse von Problemen löst, die als ein überdeterminiertes Gleichungssystem formuliert ist. Die auffallende Ähnlichkeit zwischen den beiden Methoden ist seit vielen Jahrzehnten bekannt. Es bleibt jedoch ungeklärt, warum diese Ähnlichkeit besteht. Der Beitrag soll dies klären, indem die Variationsrechnung im Hinblick auf ihr methodisches Vorgehen untersucht wird. Obwohl das bekannte Gauss-Markov-Modell innerhalb der Methode der kleinsten Quadrate und die Finite-Elemente-Methode inhärent unterschiedliche Problemklassen lösen, wird gezeigt, dass beide Methoden durch die gleichen methodischen Schritte der Variationsrechnung abgeleitet werden können. Aus methodischer Sicht bedeutet dies, dass beide Methoden nicht nur ähnlich, sondern sogar gleich sind. Außerdem wird darauf hingewiesen, wo eine mögliche Querverbindung zu anderen Methoden besteht.

Die zweite Aufgabenstellung stellt eine Messungs- und Modellbasierte Strukturanalyse (MeMoS) durch die Integration der Finite-Elemente-Methode in die Ausgleichungsrechnung vor. In numerischen Untersuchungen wird gezeigt, wie diese integrierte Analyse zur Parameteridentifikation sowohl einfacher als auch beliebig geformter Strukturbauteile eingesetzt werden kann. Darauf aufbauend wird untersucht, mit welchen Beobachtungstypen, mit welcher Genauigkeit und an welcher Stelle der Struktur diese Messungen durchgeführt werden müssen, um die Materialparameter möglichst genau zu bestimmen. Dies dient der Ermittlung eines optimalen und wirtschaftlichen Messaufbaus. Mit dieser integrierten Analyse kann auch ein Ersatzmodell einer geometrisch komplexen Struktur ermittelt werden. Die Frage der Erkennung und Lokalisierung von Schäden innerhalb einer Struktur wird mit Hilfe dieser Strukturanalyse behandelt. Die Messungs- und Modellbasierte Strukturanalyse wird mit zwei verschiedenen Testaufbauten, einer Aluminium-Modellbrücke und einem Biegebalken, validiert.

Preface

The research presented in this dissertation was supported by the PhD funding programme “Menschen, Ideen, Strukturen” (“People, Ideas, Structures”) of the *Bundesanstalt für Materialforschung und -prüfung* (BAM). In addition, the *Technische Universität Berlin* (TUB) has enriched this doctoral programme through its infrastructure. I am grateful to the members of the appraisal committee Professor Dr. W. Daum, Professor Dr. F. Neitzel and Dr. K. Brandes for giving me the opportunity to write this dissertation.

I want to thank Professor Dr. W. Daum for his supervision and generous support. As the director of his department and deputy director of several departments, he nevertheless took time for me every week to discuss the progress of my dissertation. He was understanding and open to my concerns and gave me valuable advice and suggestions.

Furthermore, I want to thank Professor Dr. F. Neitzel for his kind support and guidance throughout this time. In Professor Dr. F. Neitzel I had a liberal supervisor who gave me the freedom to conduct my research according to my own ideas, while giving me encouragement and counsel. I appreciate his openness to accept even a non-geodesist like me to join his institute. Especially, he created an environment that promotes cooperation between different disciplines, in my case geodesy and continuum mechanics, in which this dissertation could develop. I appreciate his sense of humour, which has reduced my nervousness and anxiety. Nevertheless, he has always critically and rigorously questioned my chains of reasoning and derivations and provided valuable feedback.

I am grateful to Dr. K. Brandes for his visits and the insight into his wisdom and knowledge about bridges.

Furthermore, I would like to express my gratitude to Professor Dr. A. Eichhorn, Professor Dr. W. Lienhart and Professor Dr. W. Daum for the kind acceptance of the appraisal of this dissertation and also to Professor Dr. J. Oberst for accepting the chairmanship of the dissertation procedure.

I would like to thank my numerous colleagues at BAM and TUB: I want to express my appreciation to H. Kohlhoff, M. Fischer, J. Erdmann and S. Schendler who supported me in the planning and construction of the model bridge. In the group of Terrestrial Laser Scanning I would like to thank Dr. D. Wujanz and J. Feng. I wish to thank D. Kadoke and M. Burger in the Photogrammetry group. I am also grateful that my colleagues have kept my body in a healthy state, Dr. M. Bartholmai, U. and T. Braun, S. Fritzsche, G. Von-Drygalski and D. Hüllmann. I am especially indebted to the latter for additionally keeping my mind in a sane state. Many thanks to Dr. F. Richter for proofreading. Great thanks to A. Barthelmeß for helping me to order the books from various libraries all over Germany. Special thanks to B. Eule who took care of bureaucratic matters for me. My gratitude goes to my office colleague K.-P. Gründer who took care of me. My sincere thanks go to G. Malissiovas for the endless discussion about adjustment calculation. And I thank P. Neumann as a former office colleague.

My cordial thanks go to my colleagues who made it possible for me to obtain follow-up financing, Dr. E. Köppe, Dr. R. Helmerich, Dr. M. Bartholmai and Professor Dr. W. Daum.

I am particularly indebted to my mentor and office colleague at TUB S. Weisbrich. He took care of me when I was in a tough situation, both at work and privately. That’s how he kept me sane, so I could finish my dissertation. It is also valuable to me that we often have fierce and passionate disputes about mathematics in engineering sciences.

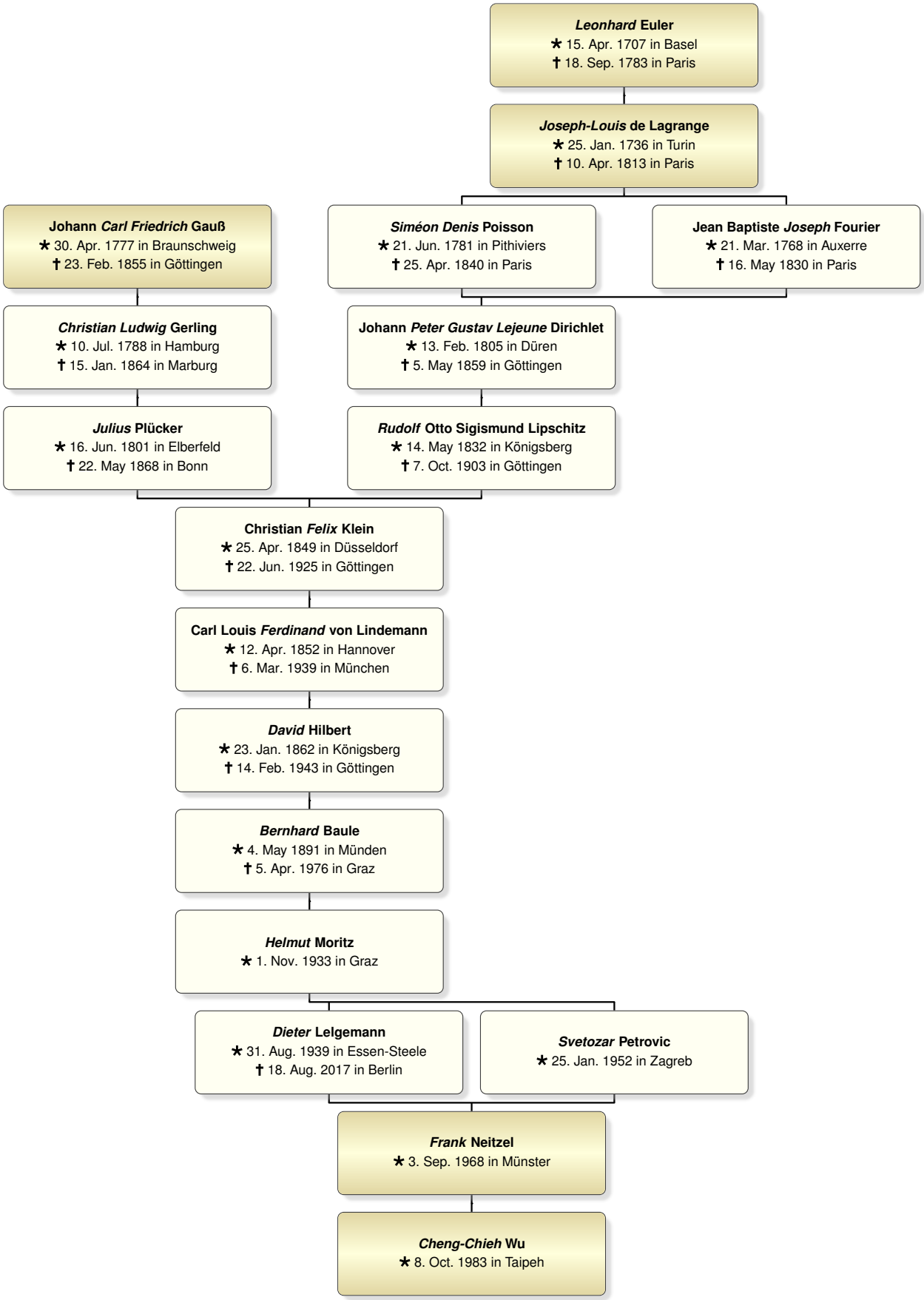
Finally, I would like to thank my parents, A.-T. Wu (吳安德) and M.-H. Wu Liu (吳 劉美華), for their support and encouragement as hard-working chefs in their own Taiwanese restaurant *Beef House* (牛稼莊) in Berlin throughout my education. I would also like to dedicate this dissertation to my grandmothers, C.-H. Liu Wu (劉 吳秋紅) and Y.-C. Yang (楊玉珍), and my late grandfathers, K.-L. Wu (吳桂林, a former chef) and P.-K. Liu (劉炳國, a former policeman). In particular, my late grandfather, P.-K. Liu, wanted me to do my doctorate.

Berlin, August 2019

Cheng-Chieh Wu (吳正覺)



Genealogy



Source: Mathematics Genealogy Project

Contents

1 Prologue 1

2 Basics of Continuum Mechanics 9

2.1 Notation 9

2.2 Kinematics 11

2.3 Regular Balance Equations 14

2.4 Material Equations 29

2.5 Field Equations 32

2.6 Numerical Treatment with Finite Element Method 39

3 Basics of Adjustment Calculation 55

3.1 Mathematical Model 55

3.2 Least Squares Adjustment Models 56

3.3 Statistical Hypothesis Inference Testing 59

4 Variational Calculus 67

4.1 A Brief History of Variational Calculus 68

4.2 Formulations of a Problem 68

4.3 Calculus of Variations and Least Squares Adjustment 71

4.4 Calculus of Variations and Finite Element Method 77

4.5 Calculus of Variations in Adjustment Theory 80

4.6 A first step towards a unified method 84

5 Measurement- and Model-based Structural Analysis 85

5.1 On Optimal Measurement Set-Ups for Material Parameter Determination 86

5.2 Damage Detection and Localisation within a slender beam 94

5.3 A Four-Point Bending Test Apparatus for Measurement- and Model-based Structural Analysis 97

5.4 Adjustment of Material Parameters from Displacement Field Measurement 114

5.5 Approximate Model for Geometrical Complex Structures 116

5.6 A Small Scale Test Bridge for Measurement- and Model-based Structural Analysis 130

6 Epilogue 147

A Source Codes C

List of Figures

1.1 A flowchart for classifying *Measurement- and Model-based Structural Analysis* as a dynamic deformation model or as an integrated deformation analysis according to Chrzanowski et al. (1990); the structure to be examined in the sense of system theory (top part); *Measurement- and Model-based Structural Analysis* (bottom part) 4

2.1 A four-point bending test apparatus. 33

2.2 The Method of Sections generates a *free-body diagram* for revealing the inner stresses within a beam. The forces F^p are applied on the rectangular traction areas with depth d and width w which are marked in red. 34

2.3 Explanation of the semi-inverse method. 35

2.4 Explanation of the semi-inverse method. 36

2.5 (Left) Assembly of the total stiffness matrix $\mathbf{K}$ from the element matrices ${}^{\zeta}\mathbf{K}$. (Right) Assembly of the total load vector $\mathbf{f}$ from the element load vectors ${}^{\zeta+1}\mathbf{f}$. 52

4.1 The representation of the trial function $\Phi = \sum_i c_i X_i$ as a neuron network. 84

5.1 Basic principle of the approaches for material parameter determination of complex samples as proposed by Eichhorn (2005) and Lienhart (2007) 86

5.2 The bending moment M 87

5.3 The exact solution of the beam differential equation, from top to bottom: strain ε, tangent of the inclination $\tan(\alpha)$, displacement u 89

5.4 Precision of the estimated elastic modulus $\sigma_{\hat{E}}$ depending on sensor position and three different precisions of a displacement sensor 92

5.5 Precision of the estimated elastic modulus $\sigma_{\hat{E}}$ depending on sensor position and three different precisions of a tilt sensor 92

5.6 Precision of the estimated elastic modulus $\sigma_{\hat{E}}$ depending on sensor position and three different precisions of a strain sensor 93

5.7 Precision of the estimated elastic modulus $\sigma_{\hat{E}}$ depending on number of sensors with fixed precision 93

5.8 Beam defects due to geometric changes or material changes (left) are simulated by material degradation (right) 94

5.9 Examination of predefined damage scenarios 96

5.10 Damage detection depending on material degradation (change of elastic modulus) and number of damaged elements 96

5.11 Damage localisation depending on material degradation (change of elastic modulus) and number of damaged elements 97

5.12 A six-point bending test apparatus for an aluminium beam specimen. This test device was partly enhanced by scrap such as lead battery, dumbbell, plastic box. 98

5.13 Deflection lines of the undamaged beam subjected to various external forces and the measured displacement from photogrammetry (top left), the corresponding residuals (top right), the complete residuals in one representation (middle) and the corresponding standardised residuals (bottom) 101

5.14 The position where damage is induced. 104

5.15 Undamaged beam subjected to external weight of $5.491\,\mathrm{kg}$, adjusted deflection line and measured displacement $\mathbf{u}_4$ (top left), the corresponding residuals as line representation (top right), the corresponding residuals as bar representation (middle), and the standardised residuals of the displacement observations (bottom); no damage detected 105

5.16 Undamaged beam subjected to external weight of $17.825\,\mathrm{kg}$, adjusted deflection line and measured displacement $\mathbf{u}_3$ (top left), the corresponding residuals as line representation (top right), the corresponding residuals as bar representation (middle), and the standardised residuals of the displacement observations (bottom); damage detected, false alarm 106

5.17 Damaged beam subjected to external weight of $3.546\,\mathrm{kg}$, adjusted deflection line and measured displacement $\mathbf{u}_{21}$ (top left), the corresponding residuals as line representation (top right), the corresponding residuals as bar representation (middle), and the standardised residuals of the displacement observations (bottom); no damage detected 107

5.18 Damaged beam subjected to external weight of $7.114\,\mathrm{kg}$, adjusted deflection line and measured displacement $\mathbf{u}_{25}$ (top left), the corresponding residuals as line representation (top right), the corresponding residuals as bar representation (middle), and the standardised residuals of the displacement observations (bottom); damage detected 108

5.19 Damaged beam subjected to external weight of $7.114\,\mathrm{kg}$, displacement measurements $\mathbf{u}_{25}$; elastic moduli of the beam (top), the residuals of the observed unknowns (middle), the standardised residuals of the observed unknowns (bottom); damage localisation at element node $\zeta = 15$ 109

5.20 Damaged beam subjected to external weight of $3.561\,\mathrm{kg}$, adjusted deflection line and measured displacement $\mathbf{u}_{27}$ (top left), the corresponding residuals as line representation (top right), the corresponding residuals as bar representation (middle), and the standardised residuals of the displacement observations (bottom); damage detected 110

5.21 Damaged beam subjected to external weight of $3.561\,\mathrm{kg}$, displacement measurements $\mathbf{u}_{27}$; elastic moduli of the beam (top), the residuals of the observed unknowns (middle), the standardised residuals of the observed unknowns (bottom); damage localisation at element node $\zeta = 22$ 111

5.22 Damaged beam subjected to external weight of $17.808\,\mathrm{kg}$, adjusted deflection line and measured displacement $\mathbf{u}_{31}$ (top left), the corresponding residuals as line representation (top right), the corresponding residuals as bar representation (middle), and the standardised residuals of the displacement observations (bottom); damage detected 112

5.23 Damaged beam subjected to external weight of $17.808\,\mathrm{kg}$, displacement measurements $\mathbf{u}_{31}$; elastic moduli of the beam (top), the residuals of the observed unknowns (middle), the standardised residuals of the observed unknowns (bottom); damage localisation at element node $\zeta = 22$ 113

5.24 Aluminium profile with a geometrical complex inner structure can be substituted by an approximate model 116

5.25 (a) Undeformed substitute model; (b) Undeformed original model; (c) Deformed original model; (d) Overlay comparison between the undeformed (grey) and deformed (red transparent) body of the original model; (e) Displacement field; (f) Overlay comparison between the undeformed (grey) and deformed (red transparent) body of the substitute model 117

5.26 An "inverted" compression test in x_1-axis direction on the surface normal in x_1-axis direction; *top left* A normal stress σ_{11} is applied to the original sample; *top right* A normal stress σ_{11} is applied to the substitute sample; *bottom left* An overlay comparison between the original and substitute samples in a deformed state; *bottom right* Parameter ① and also due to symmetry considerations parameter ❶ can be determined in this test 120

5.27 An "inverted" compression test in x_2-axis direction on the surface normal in x_2-axis direction; *top left* A normal stress σ_{22} is applied to the original sample; *top right* A normal stress σ_{22} is applied to the substitute sample; *bottom left* An overlay comparison between the original and substitute samples in a deformed state; *bottom right* Parameter ① and also due to symmetry considerations parameter ❶ can be determined in this test 121

5.28 An "inverted" compression test in x_3-axis direction on the surface normal in x_3-axis direction; *top left* A normal stress σ_{33} is applied to the original sample; *top right* A normal stress σ_{33} is applied to the substitute sample; *bottom left* An overlay comparison between the original and substitute samples in a deformed state; *bottom right* Parameter ② can be determined in this test 122

5.29 A simple shear test in x_2-axis direction on the surface normal in x_3-axis direction; *top left* A shear stress σ_{23} is applied to the original sample; *top right* A shear stress σ_{23} is applied to the substitute sample; *bottom left* An overlay comparison between the original and substitute samples in a deformed state; *bottom right* Parameter ③ and also due to symmetry considerations parameter ❸ can be determined in this test 123

5.30 A simple shear test in x_1-axis direction on the surface normal in x_3-axis direction; *top left* A shear stress σ_{13} is applied to the original sample; *top right* A shear stress σ_{13} is applied to the substitute sample; *bottom left* An overlay comparison between the original and substitute samples in a deformed state; *bottom right* Parameter ③ and also due to symmetry considerations parameter ❸ can be determined in this test 124

5.31 A simple shear test in x_1-axis direction on the surface normal in x_2-axis direction; *top left* A shear stress σ_{12} is applied to the original sample; *top right* A shear stress σ_{12} is applied to the substitute sample; *bottom left* An overlay comparison between the original and substitute samples in a deformed state; *bottom right* Parameter ④ can be determined in this test 125

5.32 An uniaxial tensile test in x_1-axis direction on the surface normal in x_1-axis direction; *top left* A normal stress σ_{11} is applied to the original sample; *top right* A normal stress σ_{11} is applied to the substitute sample; *bottom left* An overlay comparison between the original and substitute samples in a deformed state; *bottom right* Parameters ①, ②, ⑤ and ⑥ can be determined in this test 126

5.33 For the verification of the adjusted elastic parameters, a comparison between a original aluminium beam with a substitute beam is being made 127

5.34 Overlay comparison between original aluminium (grey) beam and substitute beam (red, transparent); length of the beams: 1520 mm; Three test set-ups: *top* Three-point bending test, *middle* one sided cantilever test and *bottom* double sided cantilever test; Three different forces: 50 N (blue), 500 N (yellow) and 5000 N (red) 127

5.35 Overlay comparison between original aluminium (grey) beam and substitute beam (red, transparent); length of the beams: 700 mm; Three test set-ups: *top* Three-point bending test, *middle* one sided cantilever test and *bottom* double sided cantilever test; Three different forces: 50 N (blue), 500 N (yellow) and 5000 N (red) 128

5.36 The bridge specimen on the pedestal, approximately 2147.6 N was applied 131

5.37 Terrestrial laser scanning of the bridge model, the coloured spheres indicate where screws are loosened to cause damage, damage level 1: red spheres, damage level 2: red and yellow spheres, damage level 3: red, yellow and blue spheres 133

5.38 Screws are released to induce artificial damages to the bridge model 134

5.39 The stiffness tensor has to be rotated in accordance to the different spatial orientations of the profiles 135

5.40 The standardised residuals of the observed unknowns NV_ζ for 598 chunks of the bridge specimen's finite element model by evaluation of the displacement measurements $\mathbf{L}_2$, two different perspectives of the bridge specimen (top and bottom) 142

5.41 The standardised residuals of the observed unknowns NV_ζ by evaluation of the displacement measurements $\mathbf{L}_2$ including the observed displacement vectors magnified 500 times, a profile is highlighted in green that indicates an additional displacement field induced by residual stress 143

5.42 The standardised residuals of the observed unknowns NV_ζ by evaluation of the displacement measurements $\mathbf{L}_3$ including the observed displacement vectors magnified 500 times 145

5.43 The standardised residuals of the observed unknowns NV_ζ by evaluation of the displacement measurements $\mathbf{L}_4$ including the observed displacement vectors magnified 500 times 146

List of Tables

4.1 An overview of the discussed methods. GAUSS-MARKOV model (GMM), continuous GAUSS-MARKOV model (cGMM), finite element method (FEM), least squares finite element method (LSFEM) 83

5.1 Specification of the four-point bending set-up and beam specimen for the finite element modelling. 90

5.2 Synthetic measurements on beam specimen 95

5.3 For each state s, weights (m_1, m_2, m_3) were attached to the undamaged beam specimen and n_{photo} images were taken. 99

5.4 For each state s, weights (m_1, m_2, m_3) were attached to the damaged beam specimen and n_{photo} images were taken. 102

5.5 The measurement data designation indicates whether the beam is actually damaged or undamaged, the displacement measurements set $\mathbf{u}_i$ from state s^0 to s, the theoretical reference standard deviation σ_0, the empirical reference standard deviation s_0, the test statistic χ^2_r, the threshold value for all cases $\chi^2_{r,1-\alpha} = 44.985$ for redundancy $r = 31$ and error probability $\alpha = 5\,\%$, if it holds $p : \chi^2_r > \chi^2_{r,1-\alpha}$ then reject H_0 in favour of H_A, the allegedly damaged finite element ζ respectively ${}^{\zeta}\hat{E}$, the ratio $r_{\text{el}} = \frac{{}^{22}\hat{E}}{\hat{E}}$ between the damaged and undamaged finite element, ${}^{22}\hat{E}$ and $\hat{E}$, the total attached weights m 103

5.6 Results of original and substitute beams that are subjected to three-point bending tests (TP), double sided cantilever tests (DC) and single sided cantilever tests (SC) and the total computational time (TCT) 129

5.7 Different spatial orientations of the aluminium profile 136

5.8 Calibration process of the reference state 139

5.9 Global test for different displacement measurements sets $\mathbf{L}_i$, the theoretical reference standard deviation σ_0, the empirical reference standard deviation s_0, the total redundancy r, test statistic χ^2_r, threshold value $\chi^2_{r,1-\alpha}$, if it holds $\chi^2_r > \chi^2_{r,1-\alpha}$ then reject H_0 in favour of H_A 141

1 Prologue

Nothing shocks me. I'm a scientist.

– Dr. Henry Walton "Indiana" Jones, Jr.,
Indiana Jones and the Temple of Doom (1984)

Technical Diagnostics (Czichos 2013) is concerned with diagnostic procedures and methods for the determination of *faults* or *failures* in technical objects. The examination may reveal *symptoms* or even *syndromes* (groups of symptoms) that indicate of abnormal condition. On a continuous or scheduled basis, the diagnosis can be carried out. The technical diagnostics may be principally broken down into two applications: *Condition Monitoring* (*ISO 13372:2012* 2012) and *Structural Health Monitoring* (SHM) (Farrar and Worden 2013). Both diagnostics are dedicated to the acquisition of data and to the process of information that indicate the state of a technical object. The scope of condition monitoring is mainly on machines, while the focus of structural health monitoring is set on civil engineering structures such as buildings, bridges, dams, main road, railways, processing plants, etc.

The objective of structural health monitoring is to guarantee the functionality, quality, reliability and safety of civil engineering structures. The important outcome from structural monitoring is to avoid catastrophic failures and unintended downtime, to identify suspicious behaviour before it becomes a problem, to support maintenance and overhaul management and to provide assistance to research and development for innovative structural designs and to standardised guidelines and practices. The monitoring procedure begins with data acquisition of structural behaviour to evaluate structural performance under designated environmental and operational conditions. Unexpected results may indicate the damage or deterioration of the structure and can be a valuable indicator of the state or condition of the structure.

Daum (2013, p. 413 ff) specifies a *generic design procedure* common to all structural health monitoring systems designs. This generic design process ultimately defines the basic concept of *monitoring* which can be summarised as:

1. characterisation of the structure and identification of the required measurands as well as of the significant parameters for damage evaluation,
2. selection of suitable sensors and data acquisition system,
3. application of an appropriate diagnostic method.

In this thesis, the *Measurement- and Model-based Structural Analysis* for early damage detection and localisation is presented following the term monitoring as defined above.

Firstly, the structural behaviour is described by means of a physical model. This in turn leads to field equations that connect the *primitive variables* to the *material parameters* as well as to a set of *boundary conditions*. Mass density, velocity, temperature, electric field, magnetic flux density and their spatial and temporal derivatives are considered as primitive variables. The boundary conditions describe the environmental and operational effects on engineering structure. The material parameters characterise the substances which the structure is made of. The required measurands for structural health monitoring are identified by determining the quantities that can be measured in the field equations and in the boundary conditions. Material parameters are regarded as unmeasurable as they can only be drawn from observations of measurable quantities. Furthermore, they serve as a key feature for the damage evaluation.

Secondly, once the measurands have been identified, decisions regarding the selection of suitable sensors and data acquisition system have to be made based on the following three criteria: performance and quantity of sensors,

environmental sensor operating conditions and economical aspects. A model-based *sensitivity analysis* is carried out to evaluate the impact of stochastic characteristics of sensors on the material parameters computation. The results of this analysis provide the information about the minimum requirement for the performance and quantity of sensors. Consequently, these results are used to assess the economic feasibility of a structural monitoring plan.

Thirdly and lastly, as stated in Worden et al. (2007), sensors are incapable to measure damage. However, from the measurements they collect, tangible features such as material parameters can be extracted. Then, structural damages are identified by comparing features from different states of the structure. In this comparison, hypothesis testings from statistical analysis are applied to detect and localise damages. The success rate of damage detection and localisation depends on the sensor precision, on the correctness of the physical modelling and on the structural damage severity. In a *Monte Carlo simulation* this dependence can be clarified beforehand.

Therefore, the *Measurement- and Model-based Structural Analysis* can be placed as part of the group of technical diagnostics. However, from a civil engineering perspective, the four main aims in structural health monitoring are

1. the detection,
2. the localisation,
3. the causes and
4. the prognoses of damages

in a structure. This perspective does not necessary contradict the generic design procedure of the technical diagnostics, rather the *physical* characterisation / description of the structure becomes utmost important. While structural damages can be detected and localised by non-physical approaches, the causes of damages and the following prognoses rely heavily on a physical model. Even though, the *Measurement- and Model-based Structural Analysis* does not claim to be the ultimate method that can determine all the causal links between measurements and the sources of damages, the presented analysis lays down the fundamental framework that will allow progressing toward the goal in further researches. Hence, the *Measurement- and Model-based Structural Analysis* requires a coherent evaluation between physical model and measurements by means of an adjustment method with the capability to assess statistically the results in regard of precision and reliability.

Related Works

According to Welsch and Heunecke (2001), engineering surveys are involved in all phases of the life cycle phase of a structure: Planning phase, construction, commissioning, operation and maintenance, renovation or demolition. *Deformation measurements* between commissioning, operation and maintenance are of particular importance. The main task of the deformation measurements and its corresponding analysis in these phases are to obtain a detailed and relevant description of the structure in order to examine its condition. The aim and purpose of the monitoring measures is the early detection of damages, failures and hazards for operational safety in order to be able to take measures in good time. Monitoring measures are only one aspect that improves operational safety. Therefore engineering surveying is unable to cover all aspects, however it is an important component. As a result, the monitoring of structures today is a multidisciplinary task.

In accordance with Welsch and Heunecke (2001), there are four *deformation models*: congruence, kinematic, static and dynamic model. Each individual model is discussed as follows.

Conventional deformation analysis aims to clarify the geometry of the structure and its motion geometry by capturing the structural body with discrete points at a given point in time. The causes of the movement are not examined. The captured motion of each point is then used to reconstruct the displacement and deformation of the structure.

The *congruence models* in conventional deformation analysis is a classical approach for monitoring a structure. The geometry of the structure is compared at two or more points in time. A statistical test is then carried out to determine whether a deformation has occurred or not. For example, Heunecke et al. (2013, p. 488 ff) examine a control point network that spans the surface of the structure. By means of stochastic evaluations, significant position changes of the points of the network are determined from different states of the structure.

In the conventional deformation analysis the congruence models can be understood as a special case of the so-called *kinematic models*. In these models, the motion functions of the discrete points are explicitly estimated from quasi-continuous measurements. The determined time-dependent motion functions can then be further analysed. For example, Welsch (1986) shows the determination of the velocity and strain rate field from continuous position measurements of a geodetic network. The results were developed with regard to the assessment of structure movements or distortions.

While conventional methods examine the spatial and temporal deformation changes of a structure purely geometrically, the *advanced deformation analysis* also considers the cause of deformation. Both the physical properties and the external influences of the structure are taken into account as the reason for the deformation. In terms of system theory, the causal forces are input parameters which are transformed by the structure as a transfer function into the resulting deformation as output quantities. This creates a causal chain that is referred to as a *dynamic system*. The modelling of this dynamic system is a complex issue that can only be successfully addressed through interdisciplinary collaboration. The advanced deformation analysis is formally divided into static and dynamic models, whereby the static variants can be understood as a special case of the dynamic cases.

First, the *static models* evaluate between different structural states in which the structure is in equilibrium with forces. The forces acting on the structure can differ between the equilibrium states. The advantage over the congruence model is that this makes it possible to compare deformation states of the structure under different external conditions in order to detect possible damage to the structure. For example, Brandes et al. (2012) evaluate two static states of a wooden bridge, one loaded with external forces and one unloaded. With the help of discrete displacement measurements on a wooden bridge and a mechanical model, combined with an evaluation method of the adjustment calculation with *Lagrange multipliers*, drilling damage could be detected.

Second, The *dynamic models* evaluate a structure in the non-equilibrium state. The structural motion under time-dependent influences is examined. For example, the vibration behaviour of the structure can be examined in order to determine possible damage. The *Ambient Vibration Monitoring* from Wenzel and Pichler (2005) analyses distinct dynamic structural behaviour. When a structure, such as a bridge, is monitored, it can be observed that the structure is constantly in motion due to the excitation by the environment. And for a brief moment, the structure might be relieved of the environmental influences. At that moment, a decaying vibration is observed. This behaviour suggests that a structure can be adequately described by a (physical) spring-damping system, i. e., structural deformation can be decomposed into two parts: reversible and irreversible. Deformation that recovers completely after removal of the external influences is considered as reversible and as such this part can be represented as spring components within a structural system. A remaining deformation is referred to as irreversible part that is imagined in a system as damping components. The *Forced Vibration Analysis* also analyses the dynamic structural behaviour as described above, see for example Brincker and Ventura (2015). The difference is that controlled vibration is induced.

If both the cause and the reactions of a structure are measurable, the transfer function can be determined from them. The formulation of a suitable mathematical representation of the transfer function of a dynamic system (dynamic and static models) is called *system identification*. The identification of the transfer function may be based on physical reasoning. This is called *parametric identification* in the terms of system theory. Alternatively, the system can be identified without rational justification by an empirical mathematical description which is referred to as *non-parametric identification*. In both cases, however, suitable input and output data must be available for a successful system identification.

A flowchart in Fig. 1.1, based on the idealized flowchart in Chrzanowski et al. (1990), is used to classify *Measurement- and Model-based Structural Analysis* with regard to deformation analysis. In Fig. 1.1, the upper part represents the structure to be examined. A deformable body, such as a structure, is deformed by external loads. Without loss of generality, two observers are shown who measure the deformation of the structure in different states. The first observer measures the deformation of the structure under defined loads in an essentially arbitrary reference state at initial times for which a damage-free state can be assumed. The second observer measures the deformation of the same structure at a later time under possible changed loads and under possible changed conditions of the structure. The lower part represents *Measurement- and Model-based Structural Analysis*. By means of continuum mechanics, a deterministic relationship is established between the two quantities, material parameters and structural deformation, in the form of a system of partial differential equations. Using the finite element method, the partial differential equations are converted into a system of equations, so that it is then possible to integrate

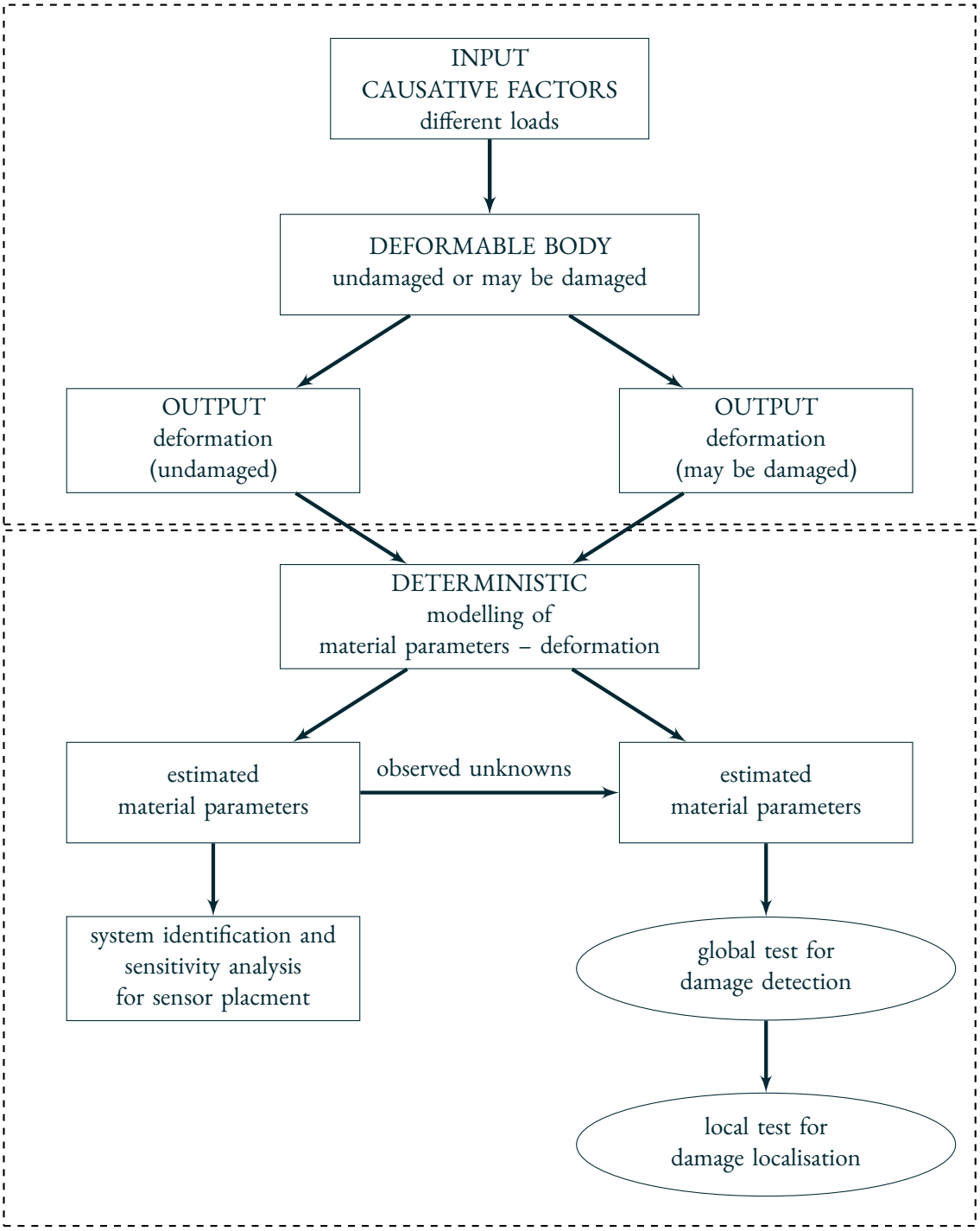


Figure 1.1: A flowchart for classifying *Measurement- and Model-based Structural Analysis* as a dynamic deformation model or as an integrated deformation analysis according to Chrzanowski et al. (1990); the structure to be examined in the sense of system theory (top part); *Measurement- and Model-based Structural Analysis* (bottom part)

them into the adjustment calculation. This makes it possible to estimate the material parameters from the deformation measurements (system identification). In addition, it is possible to perform sensitivity analyses using synthetic deformation measurements to identify the optimal sensor placement. The estimated material parameters from the undamaged state of the structure can be used as *observed unknowns* together with deformation measurements from later epochs to detect and localize possible damage to the structure.

In the sense of Welsch and Heunecke (2001) and Chrzanowski et al. (1990) it can be stated that *Measurement- and Model-based Structural Analysis* can be regarded as a dynamic deformation model or as an integrated deformation analysis. Due to computer limitations, there is a trade-off between dealing with dynamic topics or geometric complexity. Although the theoretical foundations for the treatment of time-dependent problems are discussed, this work deals only with the static issue. This decision has no influence on the fact that *Measurement- and Model-based Structural Analysis* is still a dynamic model.

The *Measurement- and Model-based Structural Analysis* is to be applied to bridge monitoring. In terms of Structural Health Monitoring, this dissertation implements a complete process of strategies and techniques for damage detection and localisation of engineering structures as proof-of-concept:

- construction of a small test bridge,
- acquisition of the bridge behaviour with suitable sensors,
- determination of damage-relevant quantities from the measurements,
- statistical analysis of the extracted parameters for the determination of the current structural condition.

Scope of the Work

Structural Health Monitoring requires interdisciplinary knowledge from various parts of engineering. The scope of this dissertation is to identify damage with a rigorous analysis by fusing the fundamentals belonging to continuum mechanics and geodesy. On one hand, continuum mechanics provides the framework to describe the behaviour of the structure in terms of the relationship between the primitive field quantities to the boundary conditions and to the material parameters. On the other hand, adjustment theory in geodesy provides methods to determine unknown parameters from observations and fixed values as well as to evaluate the results in regard to precision and reliability. The presented *Measurement- and Model-based Structural Analysis* is based on the expertise of these two engineering fields. Material parameters characterise and quantify physical properties of matters. Changes that occur to the substances are noticed in alteration in these parameters. In this thesis, material constants are used as main features for the assessment of early damage detection on structures. The challenge is to extract and to assess material parameters from the measurements of different epochs. The stochastic evaluation of material parameters leads to the detection of damage. If defects is detected in the structure, individual local material parameters are further analysed to locate the damage. In summary, the objectives of *Measurement- and Model-based Structural Analysis* can be addressed in the context of structural health monitoring as follows: Damage is to be detected and localised as well as explained by a decrease in the material parameter value. Since the focus here is on early detection of damage, the damage prognosis is omitted in this dissertation.

Aforesaid, structural health monitoring combines know-how from different fields of engineering. It should be generally understood that to include everything about engineering science would go beyond the scope in this dissertation. Even if there is a limitation to materials, say steel, concrete, wood, that are the usual building materials, it is still impossible to complete this dissertation in a reasonable time. As a matter of fact, there are different types of material, and they behave differently under the same conditions. Therefore, there are individual departments, each is dealing with specialised material such as department for metallic materials, department for construction chemistry, department for biological materials, etc. The common feature of all building materials is that they behave in a linearly elastic manner. This idealisation is a necessary simplification that has to be made. Anything that significantly deviates from this assumption can be interpreted as damage. Certainly, damping elements that are installed on bridges to shift the resonance frequency would disturb this premise immensely. However, in further research as well as the ambient vibration monitoring already suggests, one can use linear viscoelasticity, combination of linear elasticity and linear viscosity, to characterise the building materials to overcome this limitation. In this

dissertation, the foundation for a general method for structural health monitoring is laid: Continuum mechanics is known for its generality to analyse physical systems in an axiomatic deductive way. While adjustment theory, in a broader sense, is a general method to convert mathematical and physical relationships into useful results. Both have the generalisation in common. The commitment in this work is to keep approaches to any given task as general as possible.

The finite element method and the least squares adjustment are essential for the *Measurement- and Model-based Structural Analysis*. A more academic perspective in this dissertation deals with the relationship between those two methods. As stated in Lienhart (2007), he referred in his dissertation that many geodesists already knew about the striking similarity between the mentioned methods. Analogies between finite element method and least squares adjustment were presented, but the mentioned geodesists failed to show that both methods can be derived from the so-called *variational calculus* even though each method is apparently trying to solve different types of problems. While the development of the finite element method is often considered coming from mechanics, it is shown here that finite element method should be seen as a part of the adjustment theory.

Scientific and Technological Significance

Approximation, optimisation, filtering, projection, biological evolution, genetic algorithm, machine learning, data encryption and decryption, data compression, building information modelling, industry 4.0, internet of things and many more are in no doubt inherently different. But, what if all these notions can be consolidated, to be precise, the methodological approaches that are attached to those notions, in a single unified method, a unified adjustment theory? The advantages lie ahead: One would be able to comprehend all these different ideas and concepts in an instant, because they are perceived as similar. The benefit would be that they could be combined and be applied for different engineering tasks. This could lead to new and innovative approaches. In a long run, it is a lucrative objective to show the connections between, at first sight, different methods. In a short-term, in this dissertation, the connections between the finite element method and least squares adjustment are tied by means of the calculus of variations. Both methods share inherently different notions, while the finite element method solves certain classes of problems described by a system of elliptic partial differential equations, the method of least squares solves another class of problems formulated as overdetermined system of equations. At the end of the day, both methods follow the very same methodological steps that were developed by Lagrange and Euler back in 1755. The adjustment theory is more than a main tool used only in geodesy. In this dissertation, adjustment theory is being extended by assimilation of variation calculus in the hope of unifying all known methods. The aim is to reach the ultimate method that can solve any mathematically describable problem. In the end, when liberated from the burden of the many confusing origins and being unified, it will be simply called: *The Method*.

The aims that are demanded by structural health monitoring can only be reached by interdisciplinary collaborative effort of different engineering and scientific fields. Material science deals with research of designing and characterising materials. The civil engineers plan and construct structures. In computational science simulations of structures are performed. In order to combine their forces to achieve the aims of structural health monitoring, in a first step, a common framework has to be established. On the one hand, continuum mechanics appear in every branch of physical engineering. On the other hand, the adjustment theory comes into play when dealing with experimental data or parameter adjustments in simulation. This has made both, continuum mechanics and adjustment theory, a great unifying framework for structural health monitoring. Moreover, a more deductive path is followed to build up this framework. This rational way of working requires that well-established knowledge are integrated in the framework in the first place. Then, more experimental or more intuition-based approaches can be built on top of it. In doing so, the framework is more clearly arranged and enable problems to be solved in a problem-oriented way.

Research Topics

For the sake of clarity, the important points are summarised in the form of hypotheses and questions.

The finite element method and the least squares method can be derived from the variation calculus. Both methods solve fundamentally different problems. Nevertheless, both methods establish a system of linear equations that leads to the solution of their respective problem. From a geodetic perspective, the linear system of equations of the

finite element method is fascinating, since analogies can be drawn with respect to geodesy and mechanics. However, it has been ignored that the procedure of both methods is identical. Thus, the objective is to show that the *variational calculus* as an overarching method leads to both methods when the corresponding problem formulation is specified:

- What is *variational calculus*?
- What formulations are there to describe the same problem?
- How to show with simple examples that the two methods are related by means of *variational calculus*?
- What consequences result from the fact that both methods can be derived using the *variational calculus*?

Detect and locate damage with rigorous analysis by merging the basics of geodesy and continuum theory. After the finite element method and the least squares method have been discussed in detail, the two methods can be combined with each other to develop a test method suitable for monitoring civil engineering structures. The combination of the two methods is nothing new in itself, but so far the combination of the two methods has meant that they still work as a separate and independent module and only exchange information with each other. In this case, a combination is preferred in which the derived variables of both methods are used in each other so that the wanted quantities can be calculated directly from the given values. This requires a certain degree of rigour. From continuum mechanics, physical models can be derived, from whose components suitable measurands and parameters can be identified in order to find appropriate sensor types and damage parameters. Furthermore, the physical model establishes the causal relationship between the measurand and the desired parameters. Based on this, the adjustment calculation can calculate the desired parameters and their stochastic properties from redundant measurements. The questions of interest for monitoring can be examined:

- What quantity has to be measured where, with which sensor type and with which precision in order to detect and locate the damage?
- How can the concept of observed unknowns and deformation analysis from geodesy assist in deducing the location of the damage from the elastic parameters?

For any shaped body, the following problem must be solved beforehand:

- How to determine the elastic parameters from the measurements for any shape of body under any load?

Overly complicated shaped bodies can cause numerical complications, so it is inevitable to find a substitute model with the same deformational behaviour.

- How can the finite element method and the least squares method use their combined effort to find a substitute model?

Finally, appropriate experiments must be developed to validate the effectiveness of this integrated analysis to answer the question whether the *Measurement- and Model-based Structural Analysis* is capable of detecting and locating damage?

Since the focus of this thesis is on the structural evaluation of arbitrary geometric complexity, dynamic processes are not explicitly dealt with here due to limitations of the available computing speed and memory. However, it is wrong to conclude that this is a fundamental limitation of *Measurement- and Model-based Structural Analysis*. For example, by using the aforementioned substitute model in conjunction with specially developed finite elements, dynamic problems can be solved in a reasonable time by means of *Measurement- and Model-based Structural Analysis*. However, this goes beyond the scope of this dissertation.

Methods and Organisation of the Dissertation

In this dissertation, the finite element method and adjustment calculation are the main components. The relationship between these two methods as well as their combined utilisation for structural health monitoring are examined. In Chap. 2 the basics of continuum mechanics are recapitulated. Furthermore, an excursion to finite element method is enriched at the end of this chapter. The basic notions of continuum mechanics are presented as follows. Often used notations are briefly summarised in Sec. 2.1. This is followed by the three main ingredients to formulate a field equations system, namely: the kinematics also known as the geometrical description of motion in Sec. 2.2, the physical axioms in form of balance equations in Sec. 2.3 and material laws formulated as so-called constitutive equations in Sec. 2.4. Finally, this leads to field equations expressed as partial differential equations in Sec. 2.5. Then, a practical approach of finite element method with Python source codes in Sec. 2.6 completes the chapter. The basics of adjustment calculation are summarised in Chap. 3. Basic notions are briefly reviewed in Sec. 3.1. This is followed by the two models of the least squares adjustment in Sec. 3.2, namely: the Gauss-Helmert model and Gauss-Markov model. A practical approach to statistical assessments are recapitulated in Sec. 3.3. In Chap. 4 the *Variational Calculus* is introduced in order to discuss the relationship between finite element method and least squares adjustment. Finally, in Chap. 5, the finite element method and adjustment calculation are brought together. Detection and localisation of structural damage are being analysed in a shared effort in form of the *Measurement- and Model-based Structural Analysis*. As an initial examination in Sec. 5.1, the Euler-Bernoulli beam equation, expressed mathematically as an one-dimensional Poisson differential equation, is being treated numerically with finite element method. Afterwards, a sensitivity analysis is numerically conducted in regard to elastic parameter and to hybrid measurements for a slender beam. In a further numerical examination, a geodetic approach the *deformation analysis* is being recast and reused to detect and localise material degradation damage within a slender beam. Finally, the *Measurement- and Model-based Structural Analysis* is put into practical application. An experiment is carried out in Sec. 5.3. A slender aluminium beam is tested on a bending apparatus. However, in general, bridges are anything but slender beams. Therefore, in Sec. 5.4 the plunge was taken in this development and an geometrical arbitrary formed elastostatic body is being analysed in regard to its anisotropic elastic parameters and displacement field measurements. In Sec. 5.5, a workaround has to be elaborated. Due to computer memory limitation, a simple geometric substitute body has to be found to replace an original complex body. And to reaffirm this presented analysis, in Sec. 5.6 a small-sized aluminium bridge model is build as an experimental set-up. To complete this work, a concluding review is given in Chap. 6.

2 Basics of Continuum Mechanics

> Ray, pretend for a moment that I don't know anything about metallurgy, engineering, or physics, and just tell me what the Hell is going on.
>
> – Peter Venkman, Ph.D., Ghostbusters (1984)

When a deformable and thermal conductible body is subjected to external forces and heating, the body reacts with changes in its mass density, its velocity and its temperature. One of the main engineering objectives of examining such a body is to compute these continuously distributed responses that are depending on space and time. Continuum mechanics can assist for this purpose to derive the functional relationships between responses and material-specific parameters known as the *field equations*.

In continuum mechanics, as the name already suggest, a physical entity is modelled as a continuum body. It is a volume which is filled with continuously distributed matter. However, by this, the continuum mechanics is incapable to describe microscopic or mesoscopic properties in detail, such as molecular structure or materials with complex inner structure, e. g., concrete. Nevertheless, the continuum mechanics can comprehend these effects by means of equivalent descriptions. For instance, smeared or homogenized representation can be used. Likewise, results from statistical mechanics which set up relationships between microscopic and macroscopic properties can be incorporated. Apart from modelling of internal characteristics of a body, external influences have to taken into consideration. For that matter, a continuum body is divided into infinitesimal volume elements. These continuum particles obey the same law as in classical mechanics as well as thermodynamics. Thus, their methods may also be applied to continuum mechanics as well. In this view, continuum mechanics can be seen as a generalisation of (classical) particle mechanics augmented with thermodynamics.

Concerning the continuum mechanical approach, an (almost) well-defined procedure is followed. In Sec. 2.1, indicial notation that is used in this thesis is briefly introduced. Kinematic consideration is accounted for in Sec. 2.2. In Sec. 2.3, a number of balance laws are formulated. In accordance to the responses and environmental influences, one has to choose and use the suitable set of balance equations. Then, for materials in which the examined body is made of, adequate material laws have to be used. Selected material equations relevant for solid are presented in Sec. 2.4. Finally, the field equations result from the combination of balance and material laws. Three field equations of significant importance are presented in Sec. 2.5: elastodynamic equations, Euler-Bernoulli beam theory and heat equation. Field equations appear as coupled partial differential equations. This leads to the next issue: a field equation shows no direct link between responses and material-specific parameters. In order to solve differential equations, appropriate initial and boundary as well as transition conditions have to be provided. Further, a working method to solve the specific type of differential equation has to exist.

It is to be noted that regular balances in Cartesian coordinate system are covered in this thesis.

2.1 Notation

Since only the descriptions and representations in Cartesian coordinate system is used, aspects of arbitrary coordinates are not discussed. In this section, the basics of indicial notation, which are necessary to gain elementary insight into continuum mechanics, are briefly covered.

Einstein Summation Convention

The purpose to use the EINSTEIN summation convention is to simplify and clarify mathematical expressions by suppressing summation signs, see for example BRONSHTEIN et al. (2007, p. 262). This summation rule states that a term is implicitly summed over from 1 to 3 whenever an index occurs twice. Indices that appear twice are called *free indices*. To preserve this agreement, the number of appearance of each free index can not be exceeded than twice. Indices that occur once in a term are referred to as *bounded indices*. For adding up terms, each term is obliged to contain the same bounded indices.

For example:

$$z_i = \sum_{j=1}^{3} a_{ij} b_j + \sum_{j=1}^{3} \sum_{k=1}^{3} c_{ij} d_{jk} g_k \equiv a_{ij} b_j + c_{ij} d_{jk} g_k \,.$$

Kronecker Symbol

The KRONECKER delta (cf. BRONSHTEIN et al. 2007, p. 253) with indices i and j running over the set $\{1, 2, 3\}$ takes value

$$\delta_{ij} = \begin{cases} 1 & \text{for } \delta_{11}, \delta_{22}, \delta_{33} \,, \\ 0 & \text{else} \,. \end{cases} \tag{2.1}$$

Levi-Civita Symbol

The *completely antisymmetric tensor of third order* ε_{ijk}, also known as the *alternating tensor* in BRONSHTEIN et al. (2007, p. 265), with the indices i, j, k running over the set $\{1, 2, 3\}$ takes value

$$\varepsilon_{ijk} = \begin{cases} 1 & \text{for } \varepsilon_{123}, \varepsilon_{231}, \varepsilon_{312} \,, \\ -1 & \text{for } \varepsilon_{213}, \varepsilon_{132}, \varepsilon_{321} \,, \\ 0 & \text{else} \,. \end{cases} \tag{2.2}$$

The product of two alternating symbols can be described by KRONECKER deltas as follows

$$\begin{aligned} \varepsilon_{ijk}\varepsilon_{lmn} &= \begin{vmatrix} \delta_{il} & \delta_{im} & \delta_{in} \\ \delta_{jl} & \delta_{jm} & \delta_{jn} \\ \delta_{kl} & \delta_{km} & \delta_{kn} \end{vmatrix} \\ &= + \delta_{il}\delta_{jm}\delta_{kn} - \delta_{il}\delta_{jn}\delta_{km} \\ &\quad + \delta_{im}\delta_{jn}\delta_{kl} - \delta_{im}\delta_{jl}\delta_{kn} \\ &\quad + \delta_{in}\delta_{jl}\delta_{km} - \delta_{in}\delta_{jm}\delta_{kl} \,. \end{aligned} \tag{2.3}$$

From the above equation, the following useful identities can be derived

$$\varepsilon_{ijk}\varepsilon_{imn} = \delta_{jm}\delta_{kn} - \delta_{jn}\delta_{km} \,, \tag{2.4}$$

$$\varepsilon_{ijk}\varepsilon_{ijn} = 2\delta_{kn} \,, \tag{2.5}$$

$$\varepsilon_{ijk}\varepsilon_{ijk} = 6 \,. \tag{2.6}$$

The *LEVI-CIVITA symbol* can be used to represent the cross product of two vectors x_j^1 and x_k^2

$$\vec{x}^3 = \vec{x}^1 \times \vec{x}^2 \;\equiv\; x_i^3 = \varepsilon_{ijk} x_j^1 x_k^2 \,. \tag{2.7}$$

Furthermore, the *permutation symbol* can be applied to compute the determinant of a second order tensor X_{ij}

$$\det(\boldsymbol{X}) = \begin{vmatrix} X_{11} & X_{12} & X_{13} \\ X_{21} & X_{22} & X_{23} \\ X_{31} & X_{32} & X_{33} \end{vmatrix} = \varepsilon_{ijk} X_{1i} X_{2j} X_{3k} \,. \tag{2.8}$$

It can be explicitly shown by switching any pair of the indices 1, 2 and 3, the following identity holds

$$\varepsilon_{lmn} \det(\boldsymbol{X}) = \varepsilon_{ijk} X_{li} X_{mj} X_{nk} \,. \tag{2.9}$$

Multiply both sides with ε_{lmn} an useful expressions can be obtained

$$\det(\boldsymbol{X}) = \frac{1}{6} \varepsilon_{lmn} \varepsilon_{ijk} X_{li} X_{mj} X_{nk} \,. \tag{2.10}$$

2.2 Kinematics

The kinematics describes the geometrical aspect of motion (Gross, Hauger, Schröder, Wall, and Rajapakse 2009, p. 2). First, two equivalent descriptions of motion are introduced. Afterwards, a deformation mapping that connects between deformed and undeformed configuration is shown. Finally, this in turn serves as basis for the development of strain measures and geometric changes. The cause of movements is not covered by kinematics, but rather, the kinetics predicts the resulting motion due to the impact of mechanical and thermal loads. This will be discussed in the section of balance equations.

2.2.1 Description of Motion

In the *Eulerian spatial description* of motion (cf. Irgens 2008, p. 37 ff), a definitive property ψ_i within a fixed net of coordinates is expressed as a functional of time t and position vector x_j

$$\psi_i = \bar{\psi}_i(t, x_j) \,. \tag{2.11}$$

Whereas in the *Lagrangian material description* (cf. Irgens 2008, p. 37 ff), the movement of each body particle is governed by the continuous *motion*

$$x_j = \tilde{x}_j(t, X_k) \,. \tag{2.12}$$

In consideration of identifying uniquely the particles, a fixed reference time t_0 has to be chosen and each individual material point is distinguished by a functional in spatial perception

$$X_k = \bar{X}_k(t_0, x_j) \,. \tag{2.13}$$

Using the total differential on Eq. (2.12), the *velocity* can be calculated

$$\begin{aligned} \frac{\mathrm{d}x_j}{\mathrm{d}t} &= \frac{\mathrm{d}}{\mathrm{d}t}\Big(\tilde{x}_j(t, X_k)\Big) = \frac{\partial}{\partial t}\Big(\tilde{x}_j(t, X_k)\Big)\frac{\mathrm{d}t}{\mathrm{d}t} + \frac{\partial}{\partial X_k}\Big(\tilde{x}_j(t, X_k)\Big)\frac{\mathrm{d}X_k}{\mathrm{d}t} = \\ &= \frac{\partial}{\partial t}\Big(\tilde{x}_j(t, X_k)\Big) = \frac{\partial x_j}{\partial t} \equiv v_j \,, \end{aligned} \tag{2.14}$$

where

$$\frac{\mathrm{d}X_k}{\mathrm{d}t} = 0 \tag{2.15}$$

because the reference frame is time-independent by definition. The swap between both points of view is carried out as follows

$$\psi_i = \bar{\psi}_i(t, x_j) = \bar{\psi}_i\Big(t, \tilde{x}_j(t, X_k)\Big) = \tilde{\psi}_i(t, X_k) = \tilde{\psi}_i\Big(t, \bar{X}_k(t_0, x_j)\Big) = \bar{\psi}_i(t, x_j) \,, \tag{2.16}$$

where the functionals of the property ψ_i are marked with bar or tilde for notation in Eulerian or Lagrangian perception. Both descriptions have consequences in regard of time derivative. In the spatial description the focus lies on the observation of temporal change of a certain quantity ψ_i at a specific spatial position. The total differential is used to determine the change over time in the property ψ_i which is known as *material time derivative*

$$\frac{\mathrm{d}\psi_i}{\mathrm{d}t} = \frac{\mathrm{d}}{\mathrm{d}t}\Big(\bar{\psi}_i(t, x_j)\Big) = \frac{\partial}{\partial t}\Big(\bar{\psi}_i(t, x_j)\Big)\frac{\mathrm{d}t}{\mathrm{d}t} + \frac{\partial}{\partial x_j}\Big(\bar{\psi}_i(t, x_j)\Big)\frac{\mathrm{d}x_j}{\mathrm{d}t} =$$

$$= \frac{\partial}{\partial t}\Big(\bar{\psi}_i(t,x_j)\Big) + \frac{\partial}{\partial x_j}\Big(\bar{\psi}_i(t,x_j)\Big)v_j = \left[\frac{\partial \psi_i}{\partial t} + \frac{\partial \psi_i}{\partial x_j}v_j\right]_{\text{spatial}} . \tag{2.17}$$

Alternatively, in the material description, particles are specified in a reference configuration and their trajectories are examined by following the travel paths of material points. The material time derivative can be obtained by applying the total differential as follows

$$\begin{aligned}\frac{\mathrm{d}\psi_i}{\mathrm{d}t} &= \frac{\mathrm{d}}{\mathrm{d}t}\Big(\tilde{\psi}_i(t,X_k)\Big) = \frac{\partial}{\partial t}\Big(\tilde{\psi}_i(t,X_k)\Big)\frac{\mathrm{d}t}{\mathrm{d}t} + \frac{\partial}{\partial X_k}\Big(\tilde{\psi}_i(t,X_k)\Big)\frac{\mathrm{d}X_k}{\mathrm{d}t} = \\ &= \frac{\partial}{\partial t}\Big(\tilde{\psi}_i(t,X_k)\Big) = \left[\frac{\partial \psi_i}{\partial t}\right]_{\text{material}} .\end{aligned} \tag{2.18}$$

In both perceptions, the total temporal change of a quantity ψ_i is affected by a local change over time. Additionally, in spatial point of view, the quantity ψ_i is influenced by a convective part. This part describes the space of a spatial point in which particles may enter or leave. In contrast, there is no convective part in the material point of view, since a specific unique material particle is followed.

2.2.2 Deformation Gradient

The relationship between the infinitesimal distance of two neighbouring particles in a current configuration $\mathrm{d}x_j$ and in the corresponding reference frame $\mathrm{d}X_l$ can be calculated using the total derivative

$$\begin{aligned}\frac{\mathrm{d}x_j}{\mathrm{d}X_l} &= \frac{\mathrm{d}}{\mathrm{d}X_l}\Big(\tilde{x}_j(t,X_k)\Big) = \frac{\partial}{\partial t}\Big(\tilde{x}_j(t,X_k)\Big)\frac{\mathrm{d}t}{\mathrm{d}X_l} + \frac{\partial}{\partial X_k}\Big(\tilde{x}_j(t,X_k)\Big)\frac{\mathrm{d}X_k}{\mathrm{d}X_l} = \\ &= \frac{\partial x_j}{\partial X_k}\delta_{kl} = \frac{\partial x_j}{\partial X_l} \quad \Longrightarrow \quad \mathrm{d}x_j = \frac{\partial x_j}{\partial X_l}\mathrm{d}X_l ,\end{aligned} \tag{2.19}$$

where

$$F_{jl} = \frac{\partial x_j}{\partial X_l} \tag{2.20}$$

is known as *deformation gradient* (cf. Haupt 2010, p. 23 ff). Analogously, one can write

$$\begin{aligned}\frac{\mathrm{d}X_k}{\mathrm{d}x_i} &= \frac{\mathrm{d}}{\mathrm{d}x_i}\Big(\bar{X}_k(t_0,x_j)\Big) = \frac{\partial}{\partial x_j}\Big(\bar{X}_k(t_0,x_j)\Big)\frac{\mathrm{d}x_j}{\mathrm{d}x_i} = \frac{\partial X_k}{\partial x_j}\frac{\mathrm{d}x_j}{\mathrm{d}x_i} = \\ &= \frac{\partial X_k}{\partial x_j}\delta_{ji} = \frac{\partial X_k}{\partial x_i} \quad \Longrightarrow \quad \mathrm{d}X_k = \frac{\partial X_k}{\partial x_i}\mathrm{d}x_i = \big(F^{-1}\big)_{ki}\mathrm{d}x_i ,\end{aligned} \tag{2.21}$$

The deformation gradient F_{jl} rotates and stretches the infinitesimal neighbourhood in the reference state $\mathrm{d}X_l$ to the current frame $\mathrm{d}x_j$. In contrary, the deformation gradient $\big(F^{-1}\big)_{ki}$ reverses the transformation. The invertibility is only possible following the *inverse function theorem*, which the *Jacobian* J of the deformation gradient must have a non-zero positive value

$$J = \det\big(F_{jl}\big) > 0 . \tag{2.22}$$

The time-derivative of the deformation gradient is calculated as follows

$$\begin{aligned}\frac{\mathrm{d}F_{jl}}{\mathrm{d}t} &= \frac{\mathrm{d}}{\mathrm{d}t}\left(\frac{\partial x_j}{\partial X_l}\right) = \frac{\mathrm{d}}{\mathrm{d}t}\left(\frac{\partial}{\partial X_l}\Big(\tilde{x}_j(t,X_k)\Big)\right) = \\ &= \frac{\partial}{\partial t}\left(\frac{\partial x_j}{\partial X_l}\right)\frac{\mathrm{d}t}{\mathrm{d}t} + \frac{\partial}{\partial X_k}\left(\frac{\partial x_j}{\partial X_l}\right)\frac{\mathrm{d}X_k}{\mathrm{d}t} = \frac{\partial}{\partial t}\left(\frac{\partial x_j}{\partial X_l}\right) = \frac{\partial}{\partial X_l}\left(\frac{\partial x_j}{\partial t}\right) = \\ &= \frac{\partial}{\partial X_l}\left(\frac{\mathrm{d}x_j}{\mathrm{d}t}\right) = \frac{\partial v_j}{\partial X_l} = \frac{\mathrm{d}v_j}{\mathrm{d}X_l} = \frac{\mathrm{d}}{\mathrm{d}X_l}\Big(\bar{v}_j(t,x_m)\Big) = \\ &= \frac{\partial}{\partial t}\Big(\bar{v}_j(t,x_m)\Big)\frac{\mathrm{d}t}{\mathrm{d}X_l} + \frac{\partial}{\partial x_m}\Big(\bar{v}_j(t,x_m)\Big)\frac{\mathrm{d}x_m}{\mathrm{d}X_l} = \frac{\partial v_j}{\partial x_m}\frac{\partial x_m}{\partial X_l} = \\ &= \frac{\partial v_j}{\partial x_m}F_{ml} .\end{aligned} \tag{2.23}$$

2.2.3 Strain Tensor

A body undergoes a transformation, when it changes from a reference to a current configuration. However, the body deforms only due to a certain part of this transformation, the so-called non-rigid body transformation. The *strain* ε is a measure to capture the deformation (cf. Liu 2002, p. 8 ff). For example, the *Euler-Almansi strain* is defined as follows

$$\varepsilon = \frac{1}{2}\left(\frac{l^2 - L^2}{L^2}\right), \tag{2.24}$$

where L and l are the length of infinitesimal distance between two neighbouring particles within a body in the reference $\mathrm{d}X_j$ and the current configuration $\mathrm{d}x_i$. Accordantly, the Euler-Almansi strain tensor can be extracted as follows

$$\begin{aligned}
\varepsilon &= \frac{1}{2}\left(\frac{|\mathrm{d}x_i|^2 - |\mathrm{d}X_j|^2}{|\mathrm{d}x_k|^2}\right) = \frac{1}{2}\left(\frac{\mathrm{d}x_i \mathrm{d}x_i - \mathrm{d}X_j \mathrm{d}X_j}{\mathrm{d}x_k \mathrm{d}x_k}\right) \\
&= \frac{1}{2}\left(\frac{\delta_{il}\mathrm{d}x_l \delta_{im}\mathrm{d}x_m - \left(F^{-1}\right)_{jl}\mathrm{d}x_l \left(F^{-1}\right)_{jm}\mathrm{d}x_m}{\delta_{kl}\mathrm{d}x_l \delta_{km}\mathrm{d}x_m}\right) \\
&= \frac{1}{2}\left(\frac{\mathrm{d}x_l \delta_{lm}\mathrm{d}x_m - \mathrm{d}x_l \left(F^{-1}\right)_{jl}\left(F^{-1}\right)_{jm}\mathrm{d}x_m}{\mathrm{d}x_l \delta_{lm}\mathrm{d}x_m}\right) \\
&= \frac{1}{2}\left(\frac{\mathrm{d}x_l \left(\delta_{lm} - \left(F_{lj}\, F_{mj}\right)^{-1}\right)\mathrm{d}x_m}{\mathrm{d}x_l \delta_{lm}\mathrm{d}x_m}\right) \\
&= \frac{\mathrm{d}x_l e_{lm}\mathrm{d}x_m}{\mathrm{d}x_l \delta_{lm}\mathrm{d}x_m},
\end{aligned}$$

where

$$e_{lm} = \frac{1}{2}\left(\delta_{lm} - \left(F_{lj}\, F_{mj}\right)^{-1}\right) = \frac{1}{2}\left(\delta_{lm} - \left(B_{lm}\right)^{-1}\right) \tag{2.25}$$

is known as Euler-Almansi strain tensor with so-called *left Cauchy-Green deformation tensor*

$$B_{lm} = F_{lj}\, F_{mj} = F_{lj}\left(F^{\mathsf{T}}\right)_{jm}. \tag{2.26}$$

When a displacement vector u_i is introduced as follows

$$x_i = u_i + X_i, \tag{2.27}$$

the Euler-Almansi strain tensor can be recast as

$$\begin{aligned}
e_{lm} &= \frac{1}{2}\left(\delta_{lm} - \left(\frac{\partial x_l}{\partial X_j}\frac{\partial x_m}{\partial X_j}\right)^{-1}\right) = \frac{1}{2}\left(\delta_{lm} - \frac{\partial X_j}{\partial x_l}\frac{\partial X_j}{\partial x_m}\right) \\
&= \frac{1}{2}\left(\delta_{lm} - \frac{\partial}{\partial x_l}(x_j - u_j)\frac{\partial}{\partial x_m}(x_j - u_j)\right) \\
&= \frac{1}{2}\left(\delta_{lm} - \left(\frac{\partial x_j}{\partial x_l} - \frac{\partial u_j}{\partial x_l}\right)\left(\frac{\partial x_j}{\partial x_m} - \frac{\partial u_j}{\partial x_m}\right)\right) \\
&= \frac{1}{2}\left(\delta_{lm} - \left(\delta_{jl} - \frac{\partial u_j}{\partial x_l}\right)\left(\delta_{jm} - \frac{\partial u_j}{\partial x_m}\right)\right) \\
&= \frac{1}{2}\left(\delta_{lm} - \delta_{lj}\delta_{jm} + \delta_{lj}\frac{\partial u_j}{\partial x_m} + \delta_{mj}\frac{\partial u_j}{\partial x_l} - \frac{\partial u_j}{\partial x_l}\frac{\partial u_j}{\partial x_m}\right) \\
&= \frac{1}{2}\left(\frac{\partial u_l}{\partial x_m} + \frac{\partial u_m}{\partial x_l} - \frac{\partial u_j}{\partial x_l}\frac{\partial u_j}{\partial x_m}\right).
\end{aligned}$$

For small deformations, the second order term of the above strain tensor can be neglected, the *infinitesimal strain tensor*

$$\varepsilon_{ij} = \frac{1}{2}\left(\frac{\partial u_i}{\partial x_j} + \frac{\partial u_j}{\partial x_i}\right) \tag{2.28}$$

is obtained.

2.2.4 Volumetric Changes

The current infinitesimal volume $\mathrm{d}V$ and the volume element $\mathrm{d}V^0$ in the reference configuration can be computed by taking the triple product of three given infinitesimal distance vectors $\mathrm{d}x_i^1$, $\mathrm{d}x_j^2$, $\mathrm{d}x_k^3$ in the current and $\mathrm{d}X_i^1$, $\mathrm{d}X_j^2$, $\mathrm{d}X_k^3$ in the reference state

$$\begin{aligned} \mathrm{d}V &= \mathrm{d}\vec{x}^1 \cdot \left(\mathrm{d}\vec{x}^2 \times \mathrm{d}\vec{x}^3\right) = \mathrm{d}x_i^1\, \varepsilon_{ijk}\, \mathrm{d}x_j^2\, \mathrm{d}x_k^3 \quad \text{and} \\ \mathrm{d}V^0 &= \mathrm{d}\vec{X}^1 \cdot \left(\mathrm{d}\vec{X}^2 \times \mathrm{d}\vec{X}^3\right) = \mathrm{d}X_i^1\, \varepsilon_{ijk}\, \mathrm{d}X_j^2\, \mathrm{d}X_k^3\,. \end{aligned} \tag{2.29}$$

The volumetric changes of a particle between both states can be described by a ratio J as follows

$$\begin{aligned} \mathrm{d}V &= \mathrm{d}x_i^1\, \varepsilon_{ijk}\, \mathrm{d}x_j^2\, \mathrm{d}x_k^3 = \varepsilon_{ijk} \frac{\partial x_i^1}{\partial X_l^1}\, \mathrm{d}X_l^1 \frac{\partial x_j^2}{\partial X_m^2}\, \mathrm{d}X_m^2 \frac{\partial x_k^3}{\partial X_n^3}\, \mathrm{d}X_n^3 \\ &= \varepsilon_{ijk} \frac{\partial x_i^1}{\partial X_l^1} \frac{\partial x_j^2}{\partial X_m^2} \frac{\partial x_k^3}{\partial X_n^3}\, \mathrm{d}X_l^1\, \mathrm{d}X_m^2\, \mathrm{d}X_n^3 = \varepsilon_{ijk} F_{il}\, F_{jm}\, F_{kn}\, \mathrm{d}X_l^1\, \mathrm{d}X_m^2\, \mathrm{d}X_n^3 \\ &= \varepsilon_{lmn} \det\left(\boldsymbol{F}\right) \mathrm{d}X_l^1\, \mathrm{d}X_m^2\, \mathrm{d}X_n^3 = \det\left(\boldsymbol{F}\right) \varepsilon_{lmn}\, \mathrm{d}X_l^1\, \mathrm{d}X_m^2\, \mathrm{d}X_n^3 = J\, \mathrm{d}V^0\,. \end{aligned} \tag{2.30}$$

The ratio J (cf. Irgens 2008, p. 166) describes a local volume change

$$J = \det\left(\boldsymbol{F}\right) = \frac{1}{6} \varepsilon_{lmn} \varepsilon_{ijk} F_{li}\, F_{mj}\, F_{nk}\,. \tag{2.31}$$

The time-derivative of the volumetric change ratio (cf. Irgens 2008, p. 166) is computed as follows

$$\begin{aligned} \frac{\mathrm{d}J}{\mathrm{d}t} &= \frac{\mathrm{d}}{\mathrm{d}t}\Big(\det\left(\boldsymbol{F}\right)\Big) = \frac{1}{6} \varepsilon_{lmn} \varepsilon_{ijk} \frac{\mathrm{d}}{\mathrm{d}t}\left(F_{li}\, F_{mj}\, F_{nk}\right) = \\ &= \frac{1}{6} \varepsilon_{lmn} \varepsilon_{ijk} \frac{\mathrm{d}F_{li}}{\mathrm{d}t} F_{mj}\, F_{nk} + \frac{1}{6} \varepsilon_{lmn} \varepsilon_{ijk} F_{li} \frac{\mathrm{d}F_{mj}}{\mathrm{d}t} F_{nk} + \\ &\quad + \frac{1}{6} \varepsilon_{lmn} \varepsilon_{ijk} F_{li}\, F_{mj} \frac{\mathrm{d}F_{nk}}{\mathrm{d}t} \\ &= \frac{1}{6} \varepsilon_{lmn} \varepsilon_{ijk} \frac{\partial v_l}{\partial x_o} F_{oi}\, F_{mj}\, F_{nk} + \frac{1}{6} \varepsilon_{lmn} \varepsilon_{ijk} F_{li} \frac{\partial v_m}{\partial x_o} F_{oj}\, F_{nk} + \\ &\quad + \frac{1}{6} \varepsilon_{lmn} \varepsilon_{ijk} F_{li}\, F_{mj} \frac{\partial v_n}{\partial x_o} F_{ok} \\ &= \frac{1}{6} \varepsilon_{lmn} \varepsilon_{ijk} \frac{\partial v_l}{\partial x_o} F_{oi}\, F_{mj}\, F_{nk} + \frac{1}{6} \varepsilon_{lmn} \varepsilon_{ijk} \frac{\partial v_m}{\partial x_o} F_{oj}\, F_{li}\, F_{nk} + \\ &\quad + \frac{1}{6} \varepsilon_{lmn} \varepsilon_{ijk} \frac{\partial v_n}{\partial x_o} F_{ok}\, F_{li}\, F_{mj} \\ &= \frac{1}{6} \varepsilon_{lmn} \varepsilon_{ijk} \frac{\partial v_l}{\partial x_o} F_{oi}\, F_{mj}\, F_{nk} + \frac{1}{6} \left(-\varepsilon_{mln}\right)\left(-\varepsilon_{jik}\right) \frac{\partial v_m}{\partial x_o} F_{oj}\, F_{li}\, F_{nk} + \\ &\quad + \frac{1}{6} \varepsilon_{nlm} \varepsilon_{kij} \frac{\partial v_n}{\partial x_o} F_{ok}\, F_{li}\, F_{mj} \\ &= \frac{1}{2} \varepsilon_{lmn} \varepsilon_{ijk} \frac{\partial v_l}{\partial x_o} F_{oi}\, F_{mj}\, F_{nk} = \frac{1}{2} \varepsilon_{lmn} \varepsilon_{omn} \frac{\partial v_l}{\partial x_o} \det\left(\boldsymbol{F}\right) = \delta_{lo} \frac{\partial v_l}{\partial x_o} J = \frac{\partial v_l}{\partial x_l} J\,. \end{aligned} \tag{2.32}$$

2.3 Regular Balance Equations

A vector-valued extensive quantity Ψ_i of a physical body that can change in time t due to external as well as internal influences is described by a balance equation. Effects on and in the body are divided into three categories: flux $\mathcal{F}_i$, supply $\mathcal{S}_i$ and production $\mathcal{P}_i$. The flux manipulates the body across the surface, whereas the other occur within the body. The difference between supply and production is that the former can be regulated and the latter can not be controlled at all. The balance equation (cf. W. H. Müller 2014, p. 54) reads as follows

$$\frac{\mathrm{d}\Psi_i}{\mathrm{d}t} = \mathcal{F}_i + \mathcal{S}_i + \mathcal{P}_i\,. \tag{2.33}$$

Applying the balance equation to extended bodies, the above equation can be rewritten by means of densities in the following *global form*

$$\frac{\mathrm{d}}{\mathrm{d}t}\int \psi_i \,\mathrm{d}V = \int f_i \,\mathrm{d}A + \int s_i \,\mathrm{d}V + \int p_i \,\mathrm{d}V\,, \tag{2.34}$$

where ψ_i, f_i, s_i, p_i are the field density of the vector valued extensive quantity Ψ_i, the field densities of the flux, of the supply and of the production. In the Eulerian point of view, the fields depend on position x_i within a body and time t, and the flux density can be varied additionally by the surface normal unit n_i

$$\psi_i = \bar{\psi}_i(t, x_j)\,,\; f_i = \bar{f}_i(t, x_j, n_j)\,,\; s_i = \bar{s}_i(t, x_j)\,,\; p_i = \bar{p}_i(t, x_j)\,. \tag{2.35}$$

On the one hand, global balances are suitable for physical interpretation, but on the other hand they are inappropriate for computation of field quantities. For this purpose, integral balances are transformed into local form. The local balances have the advantage that the integrals are suppressed and the relationship between field densities are described in form of partial differential equations. Then, various methods are available for dealing with partial differential equations. To proceed from global form to local form, the left-hand side of Eq. (2.34) has to be reformulated into the Lagrangian description, so that it is possible to differentiate with respect to time t under the integral sign. The *Reynold's Transport Theorem* (cf. W. H. Müller 2014, p. 59) is utilized as follows

$$\begin{aligned}
\frac{\mathrm{d}}{\mathrm{d}t}\int_{V=V(t)} \psi_i \,\mathrm{d}V &= \frac{\mathrm{d}}{\mathrm{d}t}\int_{V^0=V(t_0)} \tilde{\psi}_i(t, X_k)\, J \,\mathrm{d}V^0 \\
&= \int \left(\frac{\mathrm{d}}{\mathrm{d}t}\left(\tilde{\psi}_i(t, X_k)\right) J + \tilde{\psi}_i(t, X_k)\frac{\mathrm{d}J}{\mathrm{d}t}\right)\mathrm{d}V^0 \\
&= \int \left(\frac{\mathrm{d}}{\mathrm{d}t}\left(\bar{\psi}_i(t, x_j)\right) J + \bar{\psi}_i(t, x_j)\frac{\partial v_j}{\partial x_j} J\right)\frac{1}{J}\,\mathrm{d}V \\
&= \int \left(\frac{\partial}{\partial t}\left(\bar{\psi}_i(t, x_j)\right) + \frac{\partial}{\partial x_j}\left(\bar{\psi}_i(t, x_j)\right) v_j + \bar{\psi}_i(t, x_j)\frac{\partial v_j}{\partial x_j}\right)\mathrm{d}V \\
&= \int \left(\frac{\partial \psi_i}{\partial t} + \frac{\partial \psi_i}{\partial x_j} v_j + \psi_i \frac{\partial v_j}{\partial x_j}\right)\mathrm{d}V = \int \left(\frac{\partial \psi_i}{\partial t} + \frac{\partial}{\partial x_j}(\psi_i v_j)\right)\mathrm{d}V \\
&= \int \frac{\partial \psi_i}{\partial t}\,\mathrm{d}V + \int \frac{\partial}{\partial x_j}(\psi_i v_j)\,\mathrm{d}V = \int \frac{\partial \psi_i}{\partial t}\,\mathrm{d}V + \int \psi_i v_j n_j \,\mathrm{d}A\,.
\end{aligned} \tag{2.36}$$

This theorem states that the quantity Ψ_i can be changed over time t either by the temporal change of the density ψ_i or by quantity transport across the surface or both. The volumetric change ratio J in Eq. (2.30) and its time-derivative in Eq. (2.32) as well as the time-independence of the reference volume V^0 are used to obtain the transport theorem. Furthermore, in the last step of the derivation *Gauss' Theorem* (cf. Tadmor et al. 2012, pp. 64–66) for $g = \psi_i v_j$ is applied so that

$$\begin{aligned}
\int g n_j \,\mathrm{d}A &= \sum_{\forall k} \int_{\partial V_k} g n_j \,\mathrm{d}A \\
&= \sum_{\forall k} \lim_{\Delta x_j \to 0}\left(\int_{\partial A_k} \bar{g}(x_j)(-n_j)\,\mathrm{d}A + \int_{\partial A_k} \bar{g}(x_j + \Delta x_j) n_j \,\mathrm{d}A\right) \\
&= \sum_{\forall k} \lim_{\Delta x_j \to 0}\left(-\bar{g}(x_j)\Delta A_k + \bar{g}(x_j + \Delta x_j)\Delta A_k\right) \\
&= \sum_{\forall k} \lim_{\Delta x_j \to 0}\left(\bar{g}(x_j + \Delta x_j)\frac{\Delta A_k}{\Delta V_k} - \bar{g}(x_j)\frac{\Delta A_k}{\Delta V_k}\right)\Delta V_k \\
&= \sum_{\forall k} \lim_{\Delta x_j \to 0}\left(\frac{\bar{g}(x_j + \Delta x_j) - \bar{g}(x_j)}{\Delta x_j}\right)\Delta V_k = \sum_{\forall k} \frac{\partial g}{\partial x_j}\Delta V_k \\
&= \int \frac{\partial g}{\partial x_j}\,\mathrm{d}V\,.
\end{aligned} \tag{2.37}$$

The divergence theorem states that net flux of g in and out of the body is equal to the source and sink of g within the body. For the proof of this theorem, the body is virtually divided into k number of cubes. Then, for each cube two opposing sides in normal direction n_j are evaluated with the *mean value theorem*. The partial derivative is obtained by examining the limit $\Delta x_j \to 0$. Reconstructing all cubes into the body yields the theorem in Eq. (2.37). The Reynold's transport theorem and Gauss' divergence theorem are used in context with the global balance equation to obtain

$$\int \left(\frac{\partial \psi_i}{\partial t} + \frac{\partial}{\partial x_j}(\psi_i v_j) - s_i - p_i \right) \mathrm{d}V = \int f_i \ \mathrm{d}A \,. \tag{2.38}$$

For the sake of clarity, the left-hand side integrand can be written with ϕ_i as

$$\int \phi_i \, \mathrm{d}V = \int f_i \ \mathrm{d}A \,. \tag{2.39}$$

To proceed, the flux on the right-hand side with the *Cauchy's Theorem* (cf. Tadmor et al. 2012, pp. 113–117) is examined. The purpose of this theorem is to show that the flux density f_i , besides being a function of position x_j and time t, depends *linearly* on normal vector to a surface n_j. Here, the focus is mainly on vector valued flux density f_i , for example, force- and couple-traction, t_i and μ_i. Forces and couples are acting across the body surface. Consequently, flux vectors depend on time, position and the direction of the surface normal. The Cauchy's tetrahedron is studied to show the linear dependence between flux vector and normal of the surface. Four fluxes are acting on the surface of the tetrahedron

$$\begin{aligned}
\int_{V_{\text{tetrahedron}}} \phi_i \, \mathrm{d}V &= \int_{\partial V_1} \bar{f}_i \left(-\boldsymbol{e}_1\right) \mathrm{d}A + \int_{\partial V_2} \bar{f}_i \left(-\boldsymbol{e}_2\right) \mathrm{d}A + \int_{\partial V_3} \bar{f}_i \left(-\boldsymbol{e}_3\right) \mathrm{d}A + \int_{\partial V_4} \bar{f}_i \left(\boldsymbol{n}\right) \mathrm{d}A \\
\phi_i^* \int_{V_{\text{tetrahedron}}} \mathrm{d}V &= \bar{f}_i^*\left(-\boldsymbol{e}_1\right) \int_{\partial V_1} \mathrm{d}A + \bar{f}_i^*\left(-\boldsymbol{e}_2\right) \int_{\partial V_2} \mathrm{d}A + \bar{f}_i^*\left(-\boldsymbol{e}_3\right) \int_{\partial V_3} \mathrm{d}A + \bar{f}_i^*\left(\boldsymbol{n}\right) \int_{\partial V_4} \mathrm{d}A \\
\phi_i^* \frac{1}{3} A_4 h &= \bar{f}_i^*\left(-\boldsymbol{e}_1\right) A_1 + \bar{f}_i^*\left(-\boldsymbol{e}_2\right) A_2 + \bar{f}_i^*\left(-\boldsymbol{e}_3\right) A_3 + \bar{f}_i^*\left(\boldsymbol{n}\right) A_4 \\
\phi_i^* \frac{1}{3} A_4 h &= \bar{f}_i^*\left(-\boldsymbol{e}_1\right) A_4 n_1 + \bar{f}_i^*\left(-\boldsymbol{e}_2\right) A_4 n_2 + \bar{f}_i^*\left(-\boldsymbol{e}_3\right) A_4 n_3 + \bar{f}_i^*\left(\boldsymbol{n}\right) A_4 \\
\phi_i^* \frac{1}{3} h &= \bar{f}_i^*\left(-\boldsymbol{e}_1\right) n_1 + \bar{f}_i^*\left(-\boldsymbol{e}_2\right) n_2 + \bar{f}_i^*\left(-\boldsymbol{e}_3\right) n_3 + \bar{f}_i^*\left(\boldsymbol{n}\right) \\
\phi_i^* \frac{1}{3} h &= -\bar{f}_i^*\left(\boldsymbol{e}_1\right) n_1 - \bar{f}_i^*\left(\boldsymbol{e}_2\right) n_2 - \bar{f}_i^*\left(\boldsymbol{e}_3\right) n_3 + \bar{f}_i^*\left(\boldsymbol{n}\right) .
\end{aligned}$$

For the derivation, the mean value theorem as well as the area projection $A_j = A_4 n_j$ are used. Additionally, for the last step the reaction-principle is applied as follows. For this purpose, imagine a small cylinder that is virtually cut out of the body in order to compute the Eq. (2.39)

$$\begin{aligned}
\int_{V_{\text{cylinder}}} \phi_i \, \mathrm{d}V &= \int_{\partial V_{\text{top}}} \bar{f}_i \left(n_j\right) \mathrm{d}A + \int_{\partial V_{\text{bottom}}} \bar{f}_i \left(-n_j\right) \mathrm{d}A + \int_{\partial V_{\text{barrel}}} \bar{f}_i \left(n_j^\star\right) \mathrm{d}A \\
\phi_i^* \int_{V_{\text{cylinder}}} \mathrm{d}V &= \bar{f}_i^*\left(n_j\right) \int_{\partial V_{\text{top}}} \mathrm{d}A + \bar{f}_i^*\left(-n_j\right) \int_{\partial V_{\text{bottom}}} \mathrm{d}A + \bar{f}_i^*\left(n_j^\star\right) \int_{\partial V_{\text{barrel}}} \mathrm{d}A \\
\phi_i^* \pi r^2 h &= \bar{f}_i^*\left(n_j\right) \pi r^2 + \bar{f}_i^*\left(-n_j\right) \pi r^2 + \bar{f}_i^*\left(n_j^\star\right) 2\pi r h
\end{aligned}$$

For $h \to 0$ and divided by πr^2,

$$\bar{f}_i \left(-n_j\right) = -\bar{f}_i \left(n_j\right) \tag{2.40}$$

is obtained. In the same way for the tetrahedron, for $h \to 0$, this gives

$$\bar{f}_i \left(\boldsymbol{n}\right) = \bar{f}_i \left(\boldsymbol{e}_1\right) n_1 + \bar{f}_i \left(\boldsymbol{e}_2\right) n_2 + \bar{f}_i \left(\boldsymbol{e}_3\right) n_3 = \bar{f}_i \left(\boldsymbol{e}_j\right) n_j \,. \tag{2.41}$$

One can write

$$f_i = f_{ij} \, n_j \,, \tag{2.42}$$

if the second order tensor

$$f_{ij} = \bar{f}_i\left(\boldsymbol{e}_j\right) \tag{2.43}$$

is identified as stress tensor $f_{ij} \equiv \sigma_{ij}$ for force traction $f_i \equiv t_i$ or surface couple-stress tensor $f_{ij} \equiv m_{ij}$ for couple traction $f_i \equiv \mu_i$. Using CAUCHY's formula as well as the divergence theorem in Eq. (2.38) yields

$$\int \left(\frac{\partial \psi_i}{\partial t} + \frac{\partial}{\partial x_j}(\psi_i v_j) - \frac{\partial f_{ij}}{\partial x_j} - s_i - p_i \right) \mathrm{d}V = 0\,. \tag{2.44}$$

By means of *fundamental lemma of calculus of variations*, it becomes possible to obtain the local balance (cf. W. H. MÜLLER 2014, pp. 70–71) in Eulerian framework

$$\frac{\mathrm{d}\psi_i}{\mathrm{d}t} + \psi_i \frac{\partial v_j}{\partial x_j} = \frac{\partial f_{ij}}{\partial x_j} + s_i + p_i\,. \tag{2.45}$$

In the next sections, this local balance equation is applied to different mechanical and thermodynamical quantities: *mass*, *linear momentum*, *angular momentum* and *total energy*. And based on these local balances, the following balance laws can be established: *moment of linear momentum*, *intrinsic moment of linear momentum*, *kinetic* and *internal energies* as well as *entropy*.

2.3.1 Mass

A body is a well-defined virtual *region of interest*. In this confined system, mass can not be created or destroyed, i. e., mass abides by the conservation law. Furthermore, mass is not allowed to move into or out of this region. This means that the total mass m of the body does not change over time t and can be expressed by

$$\frac{\mathrm{d}m}{\mathrm{d}t} = 0\,. \tag{2.46}$$

The total mass m can be rewritten for an extended body by means of mass density ϱ as

$$m = \int \varrho \,\mathrm{d}V \text{ with } \varrho = \bar{\varrho}\left(t, x_j\right)\,. \tag{2.47}$$

Consequently, the global balance of mass becomes

$$\frac{\mathrm{d}}{\mathrm{d}t} \int \varrho \,\mathrm{d}V = 0\,. \tag{2.48}$$

Following the global balance in Eq. (2.34) for scalar valued case, one recognizes

$$\psi = \varrho\,,\ f = 0\,,\ s = 0\,,\ p = 0\,. \tag{2.49}$$

According to Eq. (2.45), this in turn yields the local balance law of mass (cf. W. H. MÜLLER 2014, p. 72)

$$\frac{\mathrm{d}\varrho}{\mathrm{d}t} + \varrho \frac{\partial v_i}{\partial x_i} = 0\,. \tag{2.50}$$

This equation will be used to facilitate other balance laws.

2.3.2 Linear Momentum

The state of translational motion of a body is characterised by the linear momentum P_i, while the change of the linear movement is influenced by addictive forces. These forces can be categorised into two types: short-range and long-range forces, T_i and F_i. Surface forces are mostly identified as short-range, as this force type is only able to interact with the body when it is acting in close range, i. e., on the body surface. In contrast, the long-range type of forces can influence not only a body from long distance, but it has also the capability to interact directly with

every particle of the inside of the body, for example gravity forces. The balance law of linear momentum (cf. W. H. Müller 2014, p. 52) can be written as follows

$$\frac{\mathrm{d}P_i}{\mathrm{d}t} = T_i + F_i \,. \tag{2.51}$$

For an extended body, the global balance law of linear momentum is written as

$$\frac{\mathrm{d}}{\mathrm{d}t}\int \varrho v_i \,\mathrm{d}V = \int t_i \,\mathrm{d}A + \int \varrho f_i \,\mathrm{d}V \tag{2.52}$$

with the densities

$$v_i = \bar{v}_i(t, x_j) \,,\; t_i = \bar{t}_i(t, x_j) \,,\; f_i = \bar{f}_i(t, x_j) \,, \tag{2.53}$$

where v_i, t_i, f_i are the velocity, the force-traction and the specific volume force field. Following the global balance in Eq. (2.34), one recognises

$$\psi_i = \varrho v_i \,,\; f_i = t_i \,,\; s_i = \varrho f_i \,,\; p_i = 0 \,. \tag{2.54}$$

The force traction t_i can be imagined as hooks that are continuously distributed over and attached to the surface of a body. Each hook can pull or push with different intensity. As shown with the Cauchy's tetrahedron argument, the force traction t_i linearly depends on the normal vector n_j where the coefficients σ_{ij} are called stress tensor

$$t_i = \sigma_{ij} n_j \,. \tag{2.55}$$

The specific volume force f_i is mainly associated with the gravitational acceleration to compute the dead load. The zero-valued production density p_i indicates that the balance equation of linear momentum obeys the conservation law. Following Eq. (2.45), it yields

$$\frac{\mathrm{d}}{\mathrm{d}t}(\varrho v_i) + \varrho v_i \frac{\partial v_j}{\partial x_j} = \frac{\partial \sigma_{ij}}{\partial x_j} + \varrho f_i \tag{2.56}$$

The expression on the left-hand side can be rewritten as

$$\frac{\mathrm{d}}{\mathrm{d}t}(\varrho v_i) + \varrho v_i \frac{\partial v_j}{\partial x_j} = \frac{\mathrm{d}\varrho}{\mathrm{d}t} v_i + \varrho \frac{\mathrm{d}v_i}{\mathrm{d}t} + \varrho v_i \frac{\partial v_j}{\partial x_j} = \left(\frac{\mathrm{d}\varrho}{\mathrm{d}t} + \varrho \frac{\partial v_j}{\partial x_j}\right) v_i + \varrho \frac{\mathrm{d}v_i}{\mathrm{d}t} \,. \tag{2.57}$$

Hereby, the local balance law of linear momentum results

$$\left(\frac{\mathrm{d}\varrho}{\mathrm{d}t} + \varrho \frac{\partial v_j}{\partial x_j}\right) v_i + \varrho \frac{\mathrm{d}v_i}{\mathrm{d}t} = \frac{\partial \sigma_{ij}}{\partial x_j} + \varrho f_i \,. \tag{2.58}$$

This local balance equation is the origin of *translational kinetic energy* and *moment of linear momentum*. Inserting the local balance of mass from Eq. (2.50), the local balance of linear momentum that satisfies the local balance of mass results

$$\varrho \frac{\mathrm{d}v_i}{\mathrm{d}t} = \frac{\partial \sigma_{ij}}{\partial x_j} + \varrho f_i \,. \tag{2.59}$$

Combined with appropriate material laws for stress tensor σ_{ij} and volume force f_i, the primary usage of the above local balance is to formulate field equations for the velocity or displacement.

2.3.3 Translational Kinetic Energy

The translational kinetic energy (cf. W. H. Müller 2014, p. 75) can be derived by multiplying the local balance of linear momentum in Eq. (2.58) with velocity v_i. This yields

$$\left(\frac{\mathrm{d}\varrho}{\mathrm{d}t} + \varrho \frac{\partial v_j}{\partial x_j}\right) v_i v_i + \varrho v_i \frac{\mathrm{d}v_i}{\mathrm{d}t} = v_i \frac{\partial \sigma_{ij}}{\partial x_j} + \varrho v_i f_i \,. \tag{2.60}$$

The second term on the left-hand side can be rewritten as

$$\varrho v_i \frac{\mathrm{d}v_i}{\mathrm{d}t} = \frac{1}{2}\varrho \frac{\mathrm{d}}{\mathrm{d}t}(v_i v_i) \tag{2.61}$$

and the first expression on the right-hand side as

$$v_i \frac{\partial \sigma_{ij}}{\partial x_j} = \frac{\partial}{\partial x_j}(v_i \sigma_{ij}) - \frac{\partial v_i}{\partial x_j}\sigma_{ij} \tag{2.62}$$

to obtain the local balance of translational kinetic energy

$$\left(\frac{\mathrm{d}\varrho}{\mathrm{d}t} + \varrho \frac{\partial v_j}{\partial x_j}\right) v_i v_i + \frac{1}{2}\varrho \frac{\mathrm{d}}{\mathrm{d}t}(v_i v_i) = \frac{\partial}{\partial x_j}(v_i \sigma_{ij}) + \varrho v_i f_i - \frac{\partial v_i}{\partial x_j}\sigma_{ij}\,. \tag{2.63}$$

In order to derive the global balance law, the following identity to reformulate the left-hand side of the local balance is used

$$\begin{aligned}
&\frac{1}{2}\frac{\partial}{\partial t}(\varrho v_i v_i) + \frac{1}{2}\frac{\partial}{\partial x_j}(\varrho v_i v_i v_j) = \\
&\quad = \frac{1}{2}\frac{\partial \varrho}{\partial t} v_i v_i + \varrho \frac{\partial v_i}{\partial t} v_i + \frac{1}{2}\frac{\partial \varrho}{\partial x_j} v_i v_i v_j + \varrho \frac{\partial v_i}{\partial x_j} v_i v_j + \frac{1}{2}\varrho v_i v_i \frac{\partial v_j}{\partial x_j} \\
&\quad = \frac{1}{2}\left(\frac{\partial \varrho}{\partial t} + \frac{\partial \varrho}{\partial x_j} v_j + \varrho \frac{\partial v_j}{\partial x_j}\right) v_i v_i + \varrho \frac{\partial v_i}{\partial t} v_i + \varrho \frac{\partial v_i}{\partial x_j} v_i v_j \\
&\quad = \frac{1}{2}\left(\frac{\mathrm{d}\varrho}{\mathrm{d}t} + \varrho \frac{\partial v_j}{\partial x_j}\right) v_i v_i + \frac{1}{2}\varrho \frac{\mathrm{d}}{\mathrm{d}t}(v_i v_i)\,.
\end{aligned} \tag{2.64}$$

Applying the integration and using the Reynold's Transport followed by the Gauss' theorem gives the global balance of the translational kinetic energy

$$\begin{aligned}
&\int \frac{1}{2}\left(\frac{\mathrm{d}\varrho}{\mathrm{d}t} + \varrho \frac{\partial v_j}{\partial x_j}\right) v_i v_i \,\mathrm{d}V + \frac{\mathrm{d}}{\mathrm{d}t}\int \frac{1}{2}\varrho v_i v_i \,\mathrm{d}V = \\
&\qquad = \int v_i \sigma_{ij} n_j \,\mathrm{d}A + \int \varrho v_i f_i \,\mathrm{d}V - \int \frac{\partial v_i}{\partial x_j}\sigma_{ij} \,\mathrm{d}V\,.
\end{aligned} \tag{2.65}$$

With the exception of the first term, we can identify by means of scalar valued version of Eq. (2.34)

$$\psi = \frac{1}{2}\varrho v_i v_i\,,\; f = v_i \sigma_{ij} n_j\,,\; s = \varrho v_i f_i\,,\; p = -\frac{\partial v_i}{\partial x_j}\sigma_{ij}\,. \tag{2.66}$$

Due to the existence of a production term p, translational kinetic energy does not obey the conservation law. The first expression of the global and local balance of translational kinetic energy in Eq. (2.65) and in Eq. (2.63) vanish by satisfying the local balance of mass from Eq. (2.50). We have the translational kinetic energy balance as global form

$$\frac{\mathrm{d}}{\mathrm{d}t}\int \frac{1}{2}\varrho v_i v_i \,\mathrm{d}V = \int v_i \sigma_{ij} n_j \,\mathrm{d}A + \int \varrho v_i f_i \,\mathrm{d}V - \int \frac{\partial v_i}{\partial x_j}\sigma_{ij} \,\mathrm{d}V \tag{2.67}$$

and local form

$$\frac{1}{2}\varrho \frac{\mathrm{d}}{\mathrm{d}t}(v_i v_i) = \frac{\partial}{\partial x_j}(v_i \sigma_{ij}) + \varrho v_i f_i - \frac{\partial v_i}{\partial x_j}\sigma_{ij}\,. \tag{2.68}$$

The most common use of (translational) kinetic energy is to find the production term of the internal energy from the total energy.

2.3.4 Moment of Linear Momentum

The rotational counterpart to translational momentum is, in part, the moment of linear momentum (cf. W. H. Müller 2014, p. 79). By applying the cross product to the local balance of linear momentum in Eq. (2.58) with x_l, we find

$$\left(\frac{\mathrm{d}\varrho}{\mathrm{d}t} + \varrho\frac{\partial v_j}{\partial x_j}\right)\varepsilon_{kli}x_l v_i + \varrho\varepsilon_{kli}x_l\frac{\mathrm{d}v_i}{\mathrm{d}t} = \varepsilon_{kli}x_l\frac{\partial \sigma_{ij}}{\partial x_j} + \varrho\varepsilon_{kli}x_l f_i \,. \tag{2.69}$$

We rewrite the second expression on the left-hand side as

$$\varrho\varepsilon_{kli}x_l\frac{\mathrm{d}v_i}{\mathrm{d}t} = \varrho\frac{\mathrm{d}}{\mathrm{d}t}\left(\varepsilon_{kli}x_l v_i\right) - \varrho\varepsilon_{kli}\frac{\mathrm{d}x_l}{\mathrm{d}t}v_i = \varrho\frac{\mathrm{d}}{\mathrm{d}t}\left(\varepsilon_{kli}x_l v_i\right) . \tag{2.70}$$

To proceed, it is opportune to use the angular velocity

$$v_i = \varepsilon_{irs}\omega_r x_s \,, \tag{2.71}$$

so that the expression becomes

$$\begin{aligned}\varepsilon_{kli}x_l v_i &= \varepsilon_{kli}x_l\varepsilon_{irs}\omega_r x_s = \varepsilon_{ikl}\varepsilon_{irs}x_l x_s\omega_r = \left(\delta_{kr}\delta_{ls} - \delta_{ks}\delta_{lr}\right)x_l x_s\omega_r = \\ &= \left(\delta_{kr}x_l\delta_{ls}x_s - \delta_{ks}x_s x_l\delta_{lr}\right)\omega_r = \left(\delta_{kr}x_l x_l - x_k x_r\right)\omega_r = \theta_{kr}\omega_r \,,\end{aligned} \tag{2.72}$$

where the specific inertia tensor is introduced as

$$\theta_{kr} = \delta_{kr}x_l x_l - x_k x_r \,. \tag{2.73}$$

We reformulate the first term on the right-hand side as

$$\begin{aligned}\varepsilon_{kli}x_l\frac{\partial \sigma_{ij}}{\partial x_j} &= \frac{\partial}{\partial x_j}\left(\varepsilon_{kli}x_l\sigma_{ij}\right) - \varepsilon_{kli}\frac{\partial x_l}{\partial x_j}\sigma_{ij} = \frac{\partial}{\partial x_j}\left(\varepsilon_{kli}x_l\sigma_{ij}\right) - \varepsilon_{kli}\delta_{lj}\sigma_{ij} = \\ &= \frac{\partial}{\partial x_j}\left(\varepsilon_{kli}x_l\sigma_{ij}\right) - \varepsilon_{kji}\sigma_{ij} = \frac{\partial}{\partial x_j}\left(\varepsilon_{kli}x_l\sigma_{ij}\right) + \varepsilon_{kij}\sigma_{ij} \,.\end{aligned} \tag{2.74}$$

The local balance of moment of linear momentum is

$$\left(\frac{\mathrm{d}\varrho}{\mathrm{d}t} + \varrho\frac{\partial v_j}{\partial x_j}\right)\theta_{kr}\omega_r + \varrho\frac{\mathrm{d}}{\mathrm{d}t}\left(\theta_{kr}\omega_r\right) = \frac{\partial}{\partial x_j}\left(\varepsilon_{kli}x_l\sigma_{ij}\right) + \varrho\varepsilon_{kli}x_l f_i + \varepsilon_{kij}\sigma_{ij} \,. \tag{2.75}$$

For the global variant of moment of linear momentum, we substitute the following identity into the local form of moment of linear momentum

$$\begin{aligned}&\frac{\partial}{\partial t}\left(\varrho\theta_{kr}\omega_r\right) + \frac{\partial}{\partial x_j}\left(\varrho\theta_{kr}\omega_r v_j\right) = \\ &= \frac{\partial\varrho}{\partial t}\theta_{kr}\omega_r + \varrho\frac{\partial}{\partial t}\left(\theta_{kr}\omega_r\right) + \frac{\partial\varrho}{\partial x_j}\theta_{kr}\omega_r v_j + \varrho\frac{\partial}{\partial x_j}\left(\theta_{kr}\omega_r\right)v_j + \varrho\theta_{kr}\omega_r\frac{\partial v_j}{\partial x_j} \\ &= \frac{\partial\varrho}{\partial t}\theta_{kr}\omega_r + \frac{\partial\varrho}{\partial x_j}\theta_{kr}\omega_r v_j + \varrho\theta_{kr}\omega_r\frac{\partial v_j}{\partial x_j} + \varrho\frac{\partial}{\partial t}\left(\theta_{kr}\omega_r\right) + \varrho\frac{\partial}{\partial x_j}\left(\theta_{kr}\omega_r\right)v_j \\ &= \left(\frac{\partial\varrho}{\partial t} + \frac{\partial\varrho}{\partial x_j}v_j + \varrho\frac{\partial v_j}{\partial x_j}\right)\theta_{kr}\omega_r + \varrho\frac{\mathrm{d}}{\mathrm{d}t}\left(\theta_{kr}\omega_r\right) \\ &= \left(\frac{\mathrm{d}\varrho}{\mathrm{d}t} + \varrho\frac{\partial v_j}{\partial x_j}\right)\theta_{kr}\omega_r + \varrho\frac{\mathrm{d}}{\mathrm{d}t}\left(\theta_{kr}\omega_r\right) .\end{aligned} \tag{2.76}$$

Applying the integration and using the Reynold's Transport followed by the Gauss' theorem gives the global balance of moment of linear momentum

$$\frac{\mathrm{d}}{\mathrm{d}t}\int \varrho\theta_{kr}\omega_r \,\mathrm{d}V = \int \varepsilon_{kli}x_l\sigma_{ij}n_j \,\mathrm{d}A + \int \varrho\varepsilon_{kli}x_l f_i \,\mathrm{d}V + \int \varepsilon_{kij}\sigma_{ij} \,\mathrm{d}V \,. \tag{2.77}$$

By means of Eq. (2.34), we can identify

$$\psi_k = \varrho\theta_{kr}\omega_r \,,\; f_k = \varepsilon_{kli}x_l\sigma_{ij}n_j \,,\; s_k = \varrho\varepsilon_{kli}x_l f_i \,,\; p_k = \varepsilon_{kij}\sigma_{ij} \,. \tag{2.78}$$

As a result of a non-zero production term p_k, the moment of linear momentum is not conserved. Note that due to the cross product the moment of linear momentum is independent of linear momentum. By satisfying the balance of mass in Eq. (2.50), the local balance of moment of linear momentum in Eq. (2.75) can be written as

$$\varrho\frac{\mathrm{d}}{\mathrm{d}t}(\theta_{kr}\omega_r) = \frac{\partial}{\partial x_j}(\varepsilon_{kli}x_l\sigma_{ij}) + \varrho\varepsilon_{kli}x_l f_i + \varepsilon_{kij}\sigma_{ij} \,. \tag{2.79}$$

This balance equation can be used to derive the Euler-Bernoulli beam equation.

2.3.5 Rotational Kinetic Energy

To get the balance of rotational kinetic energy (cf. Serway and Jewett 2008, pp. 287–289), we multiply the local balance of moment of linear momentum in Eq. (2.75) with angular velocity ω_k

$$\begin{aligned}\Big(\frac{\mathrm{d}\varrho}{\mathrm{d}t} + \varrho\frac{\partial v_j}{\partial x_j}\Big)\omega_k\theta_{kr}\omega_r + \varrho\omega_k\frac{\mathrm{d}}{\mathrm{d}t}(\theta_{kr}\omega_r) = \\ = \omega_k\frac{\partial}{\partial x_j}(\varepsilon_{kli}x_l\sigma_{ij}) + \varrho\omega_k\varepsilon_{kli}x_l f_i + \omega_k\varepsilon_{kij}\sigma_{ij} \,.\end{aligned} \tag{2.80}$$

Exploiting the symmetry of the specific inertia tensor θ_{kr}, the second expression on the left-hand side of the above equation can be rewritten as

$$\begin{aligned}\varrho\omega_k\frac{\mathrm{d}}{\mathrm{d}t}(\theta_{kr}\omega_r) &= \varrho\omega_k\frac{\mathrm{d}\theta_{kr}}{\mathrm{d}t}\omega_r + \varrho\omega_k\theta_{kr}\frac{\mathrm{d}\omega_r}{\mathrm{d}t} \\ &= \Big(\frac{1}{2}\varrho\omega_k\frac{\mathrm{d}\theta_{kr}}{\mathrm{d}t}\omega_r + \frac{1}{2}\varrho\omega_k\frac{\mathrm{d}\theta_{kr}}{\mathrm{d}t}\omega_r\Big) + \Big(\frac{1}{2}\varrho\omega_k\theta_{kr}\frac{\mathrm{d}\omega_r}{\mathrm{d}t} + \frac{1}{2}\varrho\omega_r\theta_{rk}\frac{\mathrm{d}\omega_k}{\mathrm{d}t}\Big) \\ &= \frac{1}{2}\varrho\omega_k\frac{\mathrm{d}\theta_{kr}}{\mathrm{d}t}\omega_r + \Big(\frac{1}{2}\varrho\omega_k\theta_{kr}\frac{\mathrm{d}\omega_r}{\mathrm{d}t} + \frac{1}{2}\varrho\omega_k\frac{\mathrm{d}\theta_{kr}}{\mathrm{d}t}\omega_r + \frac{1}{2}\varrho\frac{\mathrm{d}\omega_k}{\mathrm{d}t}\theta_{kr}\omega_r\Big) \\ &= \frac{1}{2}\varrho\frac{\mathrm{d}}{\mathrm{d}t}(\omega_k\theta_{kr}\omega_r) \,,\end{aligned} \tag{2.81}$$

where this identity is used in the last step

$$\begin{aligned}\omega_k\frac{\mathrm{d}\theta_{kr}}{\mathrm{d}t}\omega_r &= \omega_k\frac{\mathrm{d}}{\mathrm{d}t}(\delta_{kr}x_l x_l - x_k x_r)\omega_r = \\ &= \omega_k\Big(2\delta_{kr}\frac{\mathrm{d}x_l}{\mathrm{d}t}x_l - \frac{\mathrm{d}x_k}{\mathrm{d}t}x_r - x_k\frac{\mathrm{d}x_r}{\mathrm{d}t}\Big)\omega_r \\ &= \omega_k\big(2\delta_{kr}v_l x_l - v_k x_r - x_k v_r\big)\omega_r \\ &= \omega_k\big(2\delta_{kr}\varepsilon_{lmn}\omega_m x_n x_l - \varepsilon_{kmn}\omega_m x_n x_r - x_k\varepsilon_{rmn}\omega_m x_n\big)\omega_r \\ &= 2\omega_r\omega_r\big(x_l\varepsilon_{lmn}x_n\big)\omega_m - \big(\omega_k\varepsilon_{kmn}\omega_m\big)x_n x_r\omega_r - \omega_k x_k\big(\omega_r\varepsilon_{rmn}\omega_m\big)x_n \\ &= 0 \,.\end{aligned} \tag{2.82}$$

The first term on the right-hand side can be rewritten as

$$\begin{aligned}\omega_k\frac{\partial}{\partial x_j}(\varepsilon_{kli}x_l\sigma_{ij}) &= \frac{\partial}{\partial x_j}(\omega_k\varepsilon_{kli}x_l\sigma_{ij}) - \frac{\partial\omega_k}{\partial x_j}\varepsilon_{kli}x_l\sigma_{ij} \\ &= \frac{\partial}{\partial x_j}(\omega_k\varepsilon_{kli}x_l\sigma_{ij}) - \frac{\partial}{\partial x_j}(\omega_k\varepsilon_{kli}x_l)\sigma_{ij} + \omega_k\varepsilon_{kli}\frac{\partial x_l}{\partial x_j}\sigma_{ij} \\ &= \frac{\partial}{\partial x_j}(\varepsilon_{ikl}\omega_k x_l\sigma_{ij}) - \frac{\partial}{\partial x_j}(\varepsilon_{ikl}\omega_k x_l)\sigma_{ij} + \omega_k\varepsilon_{kli}\delta_{lj}\sigma_{ij}\end{aligned}$$

$$= \frac{\partial}{\partial x_j}\left(\varepsilon_{ikl}\omega_k x_l \sigma_{ij}\right) - \frac{\partial}{\partial x_j}\left(\varepsilon_{ikl}\omega_k x_l\right)\sigma_{ij} + \omega_k \varepsilon_{kji}\sigma_{ij}$$
$$= \frac{\partial}{\partial x_j}\left(\varepsilon_{ikl}\omega_k x_l \sigma_{ij}\right) - \frac{\partial}{\partial x_j}\left(\varepsilon_{ikl}\omega_k x_l\right)\sigma_{ij} - \omega_k \varepsilon_{kij}\sigma_{ij} \,. \tag{2.83}$$

This yields the local balance of rotational kinetic energy

$$\left(\frac{\mathrm{d}\varrho}{\mathrm{d}t} + \varrho\frac{\partial v_j}{\partial x_j}\right)\omega_k\theta_{kr}\omega_r + \frac{1}{2}\varrho\frac{\mathrm{d}}{\mathrm{d}t}\left(\omega_k\theta_{kr}\omega_r\right) =$$
$$= \frac{\partial}{\partial x_j}\left(\varepsilon_{ikl}\omega_k x_l \sigma_{ij}\right) + \varrho\omega_k\varepsilon_{kli}x_l f_i - \frac{\partial}{\partial x_j}\left(\varepsilon_{ikl}\omega_k x_l\right)\sigma_{ij} \,. \tag{2.84}$$

To compute the global balance equation of the rotational kinetic energy, we substitute the following expression into the local balance

$$\frac{\partial}{\partial t}\left(\varrho\omega_k\theta_{kr}\omega_r\right) + \frac{\partial}{\partial x_j}\left(\varrho\omega_k\theta_{kr}\omega_r v_j\right) =$$
$$= \frac{\partial\varrho}{\partial t}\omega_k\theta_{kr}\omega_r + \varrho\frac{\partial}{\partial t}\left(\omega_k\theta_{kr}\omega_r\right) +$$
$$+ \frac{\partial\varrho}{\partial x_j}\omega_k\theta_{kr}\omega_r v_j + \varrho\frac{\partial}{\partial x_j}\left(\omega_k\theta_{kr}\omega_r\right)v_j + \varrho\omega_k\theta_{kr}\omega_r\frac{\partial v_j}{\partial x_j}$$
$$= \frac{\partial\varrho}{\partial t}\omega_k\theta_{kr}\omega_r + \frac{\partial\varrho}{\partial x_j}\omega_k\theta_{kr}\omega_r v_j + \varrho\omega_k\theta_{kr}\omega_r\frac{\partial v_j}{\partial x_j} +$$
$$+ \varrho\frac{\partial}{\partial t}\left(\omega_k\theta_{kr}\omega_r\right) + \varrho\frac{\partial}{\partial x_j}\left(\omega_k\theta_{kr}\omega_r\right)v_j$$
$$= \left(\frac{\partial\varrho}{\partial t} + \frac{\partial\varrho}{\partial x_j}v_j + \varrho\frac{\partial v_j}{\partial x_j}\right)\omega_k\theta_{kr}\omega_r + \varrho\frac{\mathrm{d}}{\mathrm{d}t}\left(\omega_k\theta_{kr}\omega_r\right)$$
$$= \left(\frac{\mathrm{d}\varrho}{\mathrm{d}t} + \varrho\frac{\partial v_j}{\partial x_j}\right)\omega_k\theta_{kr}\omega_r + \varrho\frac{\mathrm{d}}{\mathrm{d}t}\left(\omega_k\theta_{kr}\omega_r\right) \,. \tag{2.85}$$

We integrate and use the Reynold's Transport as well as the Gauss' theorem to get the global balance of rotational kinetic energy

$$\int \frac{1}{2}\left(\frac{\mathrm{d}\varrho}{\mathrm{d}t} + \varrho\frac{\partial v_j}{\partial x_j}\right)\omega_k\theta_{kr}\omega_r \,\mathrm{d}V + \frac{\mathrm{d}}{\mathrm{d}t}\int \frac{1}{2}\varrho\omega_k\theta_{kr}\omega_r \,\mathrm{d}V =$$
$$= \int \varepsilon_{ikl}\omega_k x_l \sigma_{ij} n_j \,\mathrm{d}A + \int \varrho\varepsilon_{ikl}\omega_k x_l f_i \,\mathrm{d}V - \int \frac{\partial}{\partial x_j}\left(\varepsilon_{ikl}\omega_k x_l\right)\sigma_{ij} \,\mathrm{d}V \,. \tag{2.86}$$

With the exception of the first term, we can identify each terms by means of Eq. (2.34) as follows

$$\psi = \frac{1}{2}\varrho\omega_k\theta_{kr}\omega_r \,,\; f = \varepsilon_{ikl}\omega_k x_l \sigma_{ij} n_j \,,\; s = \varrho\varepsilon_{ikl}\omega_k x_l f_i \,,\; p = -\frac{\partial}{\partial x_j}\left(\varepsilon_{ikl}\omega_k x_l\right)\sigma_{ij} \,. \tag{2.87}$$

Also here the production term p is non-zero, thus the rotational kinetic energy does not abide by the conservation law. By means of Eq. (2.71) and Eq. (2.72), it can be shown that the balance of rotational kinetic energy can be rewritten as translational kinetic energy and vice versa. As the case arise, the representation of kinetic energy can be expressed in one way or the other, or a combination of both. But care must be taken to avoid double counting of the kinetic energy balance.

2.3.6 Angular Momentum

The state of rotational motion of a body is described by the angular momentum L_k (cf. Serway and Jewett 2008, p. 315). The rate of change of the angular momentum is governed by the sum of short-range and long-range torques:

torque flux M_k^{flux} and torque supply M_k^{supply}. Analogously to short-range and long-range forces, the torque flux is interacting on the body surface, whereas the torque supply has an impact on the body volume. The balance equation of angular momentum reads as follows

$$\frac{\mathrm{d}L_k}{\mathrm{d}t} = M_k^{\text{flux}} + M_k^{\text{supply}} . \tag{2.88}$$

The total angular momentum of a body L_k constitutes of the sum of moment of linear momentum L_k^{moment} and spin L_k^{spin}

$$L_k = L_k^{\text{moment}} + L_k^{\text{spin}} . \tag{2.89}$$

The moment of linear momentum is identified on the left-hand side in Eq. (2.77)

$$L_k^{\text{moment}} = \int \varrho \theta_{kr} \omega_r \, \mathrm{d}V \tag{2.90}$$

and the spin for extended body is written as

$$L_k^{\text{spin}} = \int \varrho s_k \, \mathrm{d}V , \tag{2.91}$$

where s_k is the specific spin. The torque flux

$$M_k^{\text{flux}} = \int \varepsilon_{kli} x_l \sigma_{ij} n_j \, \mathrm{d}A + \int \mu_k \, \mathrm{d}A \tag{2.92}$$

compromises of two additive parts. The first one is induced by surface force that is the first expression on the right-hand side in Eq. (2.77) and the second one is caused by force couple. Similarly, the torque supply

$$M_k^{\text{supply}} = \int \varrho \varepsilon_{kli} x_l f_i \, \mathrm{d}V + \int \varrho l_k \, \mathrm{d}V . \tag{2.93}$$

consists additively of the volume force term that can be found in the second expression on the right-hand side in Eq. (2.77) and volume couple term. In the forthcoming section the spin, the surface and volume couples will be discussed. The global balance law of angular momentum can be rewritten as follows

$$\frac{\mathrm{d}}{\mathrm{d}t} \int \varrho \big(\theta_{kr} \omega_r + s_k\big) \, \mathrm{d}V = \int \big(\varepsilon_{kli} x_l \sigma_{ij} n_j + \mu_k\big) \, \mathrm{d}A + \int \varrho \big(\varepsilon_{kli} x_l f_i + l_k\big) \, \mathrm{d}V . \tag{2.94}$$

According to Eq. (2.34), we recognise

$$\psi_k = \varrho \big(\theta_{kr} \omega_r + s_k\big) , \; f_k = \varepsilon_{kli} x_l \sigma_{ij} n_j + \mu_k , \; s_k = \varrho \big(\varepsilon_{kli} x_l f_i + l_k\big) , \; p_k = 0 . \tag{2.95}$$

We recall that the production term p_k vanished due to the conservation of angular momentum. The sum of Eq. (2.75) and Eq. (2.103) yields the local balance of angular momentum

$$\begin{aligned} &\left(\frac{\mathrm{d}\varrho}{\mathrm{d}t} + \varrho \frac{\partial v_j}{\partial x_j}\right)\big(\theta_{kr} \omega_r + s_k\big) + \varrho \frac{\mathrm{d}}{\mathrm{d}t}\big(\theta_{kr} \omega_r + s_k\big) = \\ &\quad = \frac{\partial}{\partial x_j}\big(\varepsilon_{kli} x_l \sigma_{ij} + m_{kj}\big) + \varrho \big(\varepsilon_{kli} x_l f_i + l_k\big) . \end{aligned} \tag{2.96}$$

In order to write the balance of spin, its the production term needs to be determined. This is possible by using conservation property of the balance of angular momentum in conjunction with the balance of moment of linear momentum.

2.3.7 Spin

Another rotational counterpart to translational momentum is the *intrinsic moment of momentum* (cf. W. H. Müller 2014, p. 78), or in short: *spin*. This approach is applied for Cosserat continuum (E. Cosserat and F. Cosserat 1909) or *micropolar bodies* (Eringen 2012). These are materials with complex inner microstructure such as foams, porous media, liquid crystals (Warner and Terentjev 2003), concrete (Chesnais et al. 2011), rock masses (Stojanović 1972). Besides their apparent translational or rotational motion, these materials have an additional internal degrees of freedom in form of an intrinsic rotation. An overview about this topic can be found in (Altenbach et al. 2011).

By subtracting the global balance of angular momentum in Eq. (2.94) from the balance law of moment of linear momentum in Eq. (2.77), we obtain the global balance equation of spin

$$\frac{\mathrm{d}}{\mathrm{d}t}\int \varrho s_k \,\mathrm{d}V = \int \mu_k \,\mathrm{d}A + \int \varrho l_k \,\mathrm{d}V - \int \varepsilon_{kij}\sigma_{ij} \,\mathrm{d}V \tag{2.97}$$

with the densities

$$s_k = \bar{s}_k(t, x_j)\ ,\ \mu_k = \bar{\mu}_k(t, x_j)\ ,\ l_k = \bar{l}_k(t, x_j) \tag{2.98}$$

where s_k, μ_k, l_k are the specific spin, the surface couple and the specific volume couple density. Following the global balance in Eq. (2.34), we can identify

$$\psi_k = \varrho s_k\ ,\ f_k\ = \mu_k\ ,\ s_k\ = \varrho l_k\ ,\ p_k = -\varepsilon_{kij}\sigma_{ij}\ . \tag{2.99}$$

The surface couple μ_k can be imagined as screwdrivers that are continuously distributed over and attached to the surface of a body. Each screwdriver turns and twists with different intensity. Following the Cauchy's tetrahedron argument, the surface couple μ_k linearly depends on the normal vector n_j where the coefficients m_{kj} are called surface couple stress tensor

$$\mu_k = m_{kj} n_j\ . \tag{2.100}$$

The specific volume couple field l_k can be associated with electromagnetic induction that affects the lattice. Therefore, this field effects the spin balance within the interior of a body. Following Eq. (2.45), we write

$$\frac{\mathrm{d}}{\mathrm{d}t}(\varrho s_k) + \varrho s_k \frac{\partial v_j}{\partial x_j} = \frac{\partial m_{kj}}{\partial x_j} + \varrho l_k - \varepsilon_{kij}\sigma_{ij}\ . \tag{2.101}$$

The expression on the left hand side can be reformulated as

$$\frac{\mathrm{d}}{\mathrm{d}t}(\varrho s_k) + \varrho s_k \frac{\partial v_j}{\partial x_j} = \frac{\mathrm{d}\varrho}{\mathrm{d}t} s_k + \varrho \frac{\mathrm{d}s_k}{\mathrm{d}t} + \varrho s_k \frac{\partial v_j}{\partial x_j} = \left(\frac{\mathrm{d}\varrho}{\mathrm{d}t} + \varrho \frac{\partial v_j}{\partial x_j}\right) s_k + \varrho \frac{\mathrm{d}s_k}{\mathrm{d}t}\ . \tag{2.102}$$

The local balance law of spin reads

$$\left(\frac{\mathrm{d}\varrho}{\mathrm{d}t} + \varrho \frac{\partial v_j}{\partial x_j}\right) s_k + \varrho \frac{\mathrm{d}s_k}{\mathrm{d}t} = \frac{\partial m_{kj}}{\partial x_j} + \varrho l_k - \varepsilon_{kij}\sigma_{ij}\ . \tag{2.103}$$

The aspect of spin can be ignored for materials with simple inner structure such as steel and negligible spin-affecting torques. If this holds true, the specific spin s_k, the surface couple μ_k and the specific volume couple density l_k vanished. Thus, we have

$$0 = \varepsilon_{kij}\sigma_{ij}\ . \tag{2.104}$$

As a consequence we have a symmetric stress tensor by expanding the above equation, see I. Müller (1973, p. 32)

$$\sigma_{ij} = \sigma_{ji}\ . \tag{2.105}$$

2.3.8 Kinetic Energy of Spin

To obtain the kinetic energy balance of spin as briefly mentioned in Yamaguchi (2008, p. 56), the local balance of spin is multiplied with the angular velocity ω_k

$$\left(\frac{\mathrm{d}\varrho}{\mathrm{d}t}+\varrho\frac{\partial v_j}{\partial x_j}\right)\omega_k s_k+\varrho\omega_k\frac{\mathrm{d}s_k}{\mathrm{d}t}=\omega_k\frac{\partial m_{kj}}{\partial x_j}+\varrho\omega_k l_k-\omega_k\varepsilon_{kij}\sigma_{ij}\,. \tag{2.106}$$

If it is admissible to assume that the spin features a symmetric *intrinsic specific inertia tensor* j_{kr}, so that we can write

$$s_k=j_{kr}\omega_r\,, \tag{2.107}$$

then the second expression on the left-hand side can be rearranged in a similar way to moment of linear momentum as

$$\varrho\omega_k\frac{\mathrm{d}s_k}{\mathrm{d}t}=\frac{1}{2}\varrho\frac{\mathrm{d}}{\mathrm{d}t}(\omega_k s_k)\,. \tag{2.108}$$

To proceed, we transform the first term of the right-hand side

$$\omega_k\frac{\partial m_{kj}}{\partial x_j}=\frac{\partial}{\partial x_j}(\omega_k m_{kj})-\frac{\partial\omega_k}{\partial x_j}m_{kj}\,. \tag{2.109}$$

The local balance of spin energy reads

$$\begin{aligned}&\left(\frac{\mathrm{d}\varrho}{\mathrm{d}t}+\varrho\frac{\partial v_j}{\partial x_j}\right)\omega_k s_k+\frac{1}{2}\varrho\frac{\mathrm{d}}{\mathrm{d}t}(\omega_k s_k)=\\&\quad=\frac{\partial}{\partial x_j}(\omega_k m_{kj})+\varrho\omega_k l_k-\left(\frac{\partial\omega_k}{\partial x_j}m_{kj}+\omega_k\varepsilon_{kij}\sigma_{ij}\right).\end{aligned}$$

To get the global variant of spin energy, the following identity is used

$$\begin{aligned}&\frac{\partial}{\partial t}(\varrho\omega_k s_k)+\frac{\partial}{\partial x_j}(\varrho\omega_k s_k v_j)=\\&\quad=\frac{\partial\varrho}{\partial t}\omega_k s_k+\varrho\frac{\partial}{\partial t}(\omega_k s_k)+\frac{\partial\varrho}{\partial x_j}\omega_k s_k v_j+\varrho\frac{\partial}{\partial x_j}(\omega_k s_k)v_j+\varrho\omega_k s_k\frac{\partial v_j}{\partial x_j}\\&\quad=\frac{\partial\varrho}{\partial t}\omega_k s_k+\frac{\partial\varrho}{\partial x_j}\omega_k s_k v_j+\varrho\omega_k s_k\frac{\partial v_j}{\partial x_j}+\varrho\frac{\partial}{\partial t}(\omega_k s_k)+\varrho\frac{\partial}{\partial x_j}(\omega_k s_k)v_j\\&\quad=\left(\frac{\partial\varrho}{\partial t}+\frac{\partial\varrho}{\partial x_j}v_j+\varrho\frac{\partial v_j}{\partial x_j}\right)\omega_k s_k+\varrho\frac{\mathrm{d}}{\mathrm{d}t}(\omega_k s_k)\\&\quad=\left(\frac{\mathrm{d}\varrho}{\mathrm{d}t}+\varrho\frac{\partial v_j}{\partial x_j}\right)\omega_k s_k+\varrho\frac{\mathrm{d}}{\mathrm{d}t}(\omega_k s_k)\,.\end{aligned} \tag{2.110}$$

This in turn yields the global balance of spin energy after the integration, followed by Reynold's transport and applying the Gauss' theorem

$$\begin{aligned}&\int\frac{1}{2}\left(\frac{\mathrm{d}\varrho}{\mathrm{d}t}+\varrho\frac{\partial v_j}{\partial x_j}\right)\omega_k s_k\,\mathrm{d}V+\int\frac{1}{2}\varrho\omega_k s_k\,\mathrm{d}V=\\&\quad=\int\omega_k m_{kj}n_j\,\mathrm{d}A+\int\varrho\omega_k l_k\,\mathrm{d}V-\int\left(\frac{\partial\omega_k}{\partial x_j}m_{kj}+\omega_k\varepsilon_{kij}\sigma_{ij}\right)\mathrm{d}V\,.\end{aligned} \tag{2.111}$$

With the exception of the first term, we analyse each terms by means of Eq. (2.34) as follows

$$\psi=\frac{1}{2}\varrho\omega_k s_k\,,\ f=\omega_k m_{kj}n_j\,,\ s=\varrho\omega_k l_k\,,\ p=-\left(\frac{\partial\omega_k}{\partial x_j}m_{kj}+\omega_k\varepsilon_{kij}\sigma_{ij}\right). \tag{2.112}$$

The spin energy does not obey the conservation law due to the non-zero production term p.

2.3.9 Total Energy

The conservation of the total sum of energies is known as the *first law of thermodynamics*. We can write the sum of the global equation of translational, rotational and spin energies in Eq. (2.65), Eq. (2.86) and Eq. (2.111) as the total sum of kinetic energies. However, we observe that the production term of the total kinetic energy still remains. Thus, an other kind of energy has to be identified in order to complete the total energy: It is the *internal energy*. The global balance of total energy (cf. W. H. Müller 2014, p. 77) reads as follows

$$\int \frac{1}{2}\left(\frac{\mathrm{d}\varrho}{\mathrm{d}t} + \varrho\frac{\partial v_j}{\partial x_j}\right)\left(v_i v_i + \omega_k \theta_{kr}\omega_r + \omega_k s_k\right)\mathrm{d}V + \frac{\mathrm{d}}{\mathrm{d}t}\left(E+U\right) = \dot{\mathcal{W}} + \dot{\mathcal{Q}}\,, \tag{2.113}$$

where $E, U, \dot{\mathcal{W}}, \dot{\mathcal{Q}}$ are the total kinetic energy, the internal energy, work and heat transfer rate. By writing the sum of the global balance of kinetic energies, we recognize that the total kinetic energy is

$$E = \int \frac{1}{2}\varrho v_i v_i \,\mathrm{d}V + \int \frac{1}{2}\varrho\omega_k\theta_{kr}\omega_r \,\mathrm{d}V + \int \frac{1}{2}\varrho\omega_k s_k \,\mathrm{d}V \tag{2.114}$$

and the work transfer rate is

$$\begin{aligned}\dot{\mathcal{W}} = &\int \left(v_i\sigma_{ij}n_j + \varepsilon_{ikl}\omega_k x_l \sigma_{ij}n_j + \omega_k m_{kj}n_j\right)\mathrm{d}A + \\ &+ \int \left(\varrho v_i f_i + \varrho\varepsilon_{ikl}\omega_k x_l f_i + \varrho\omega_k l_k\right)\mathrm{d}V\,.\end{aligned} \tag{2.115}$$

The internal energy U can be rewritten for extended body by means of specific internal energy u

$$U = \int \varrho u \,\mathrm{d}V \tag{2.116}$$

and the heat transfer rate $\dot{\mathcal{Q}}$ consists of additive heat conduction and radiation components

$$\dot{\mathcal{Q}} = -\int q_i n_i \,\mathrm{d}A + \int \varrho r \,\mathrm{d}V\,, \tag{2.117}$$

where q_i, r are the heat flux and the specific radiation. The internal energy as well as the heat transfer is discussed in the next section. The global balance of total energy is

$$\begin{aligned}&\int \frac{1}{2}\left(\frac{\mathrm{d}\varrho}{\mathrm{d}t} + \varrho\frac{\partial v_j}{\partial x_j}\right)\left(v_i v_i + \omega_k\theta_{kr}\omega_r + \omega_k s_k\right)\mathrm{d}V + \\ &\quad + \frac{\mathrm{d}}{\mathrm{d}t}\int\left(\frac{1}{2}\varrho v_i v_i + \frac{1}{2}\varrho\omega_k\theta_{kr}\omega_r + \frac{1}{2}\varrho\omega_k s_k + \varrho u\right)\mathrm{d}V = \\ &= \int \left(v_i\sigma_{ij}n_j + \varepsilon_{ikl}\omega_k x_l\sigma_{ij}n_j + \omega_k m_{kj}n_j - q_j n_j\right)\mathrm{d}A + \\ &\quad + \int\left(\varrho v_i f_i + \varrho\varepsilon_{ikl}\omega_k x_l f_i + \varrho\omega_k l_k + \varrho r\right)\mathrm{d}V\,,\end{aligned} \tag{2.118}$$

According to the scalar valued version of Eq. (2.34), we can identify with exception of the first term on the left-hand side that

$$\begin{aligned}\psi &= \frac{1}{2}\varrho v_i v_i + \frac{1}{2}\varrho\omega_k\theta_{kr}\omega_r + \frac{1}{2}\varrho\omega_k s_k + \varrho u\,,\\ f &= v_i\sigma_{ij}n_j + \varepsilon_{ikl}\omega_k x_l\sigma_{ij}n_j + \omega_k m_{kj}n_j - q_j n_j\,,\\ s &= \varrho v_i f_i + \varrho\varepsilon_{ikl}\omega_k x_l f_i + \varrho\omega_k l_k + \varrho r\,,\\ p &= 0\,.\end{aligned}$$

The absence of the production p shows that the balance of total energy is conserved.

2.3.10 Internal Energy

Velocity is a measure for the kinetic energy of continuum particles and describes the apparent motion of them. In addition, *temperature* is introduced to incorporate the imperceptible and random movement of molecules or atoms within the continuum particles. The temperature is a measure for the intrinsic mean kinetic energy of molecules or atoms, or in short: *internal energy* (cf. I. Müller 2007, pp. 59–64). By subtracting the global balance of total energy in Eq. (2.118) from the global equations of total sum of kinetic energies in Eq. (2.65), Eq. (2.86) and Eq. (2.111), the global balance law of internal energy reads

$$\begin{aligned}\frac{\mathrm{d}}{\mathrm{d}t}\int \varrho u \,\mathrm{d}V = -\int q_i n_i \,\mathrm{d}A + \int \varrho r \,\mathrm{d}V + \\ + \int \left(\frac{\partial v_i}{\partial x_j}\sigma_{ij} + \frac{\partial \omega_k}{\partial x_j}\varepsilon_{kli} x_l \sigma_{ij} + \frac{\partial \omega_k}{\partial x_j} m_{kj} \right) \mathrm{d}V\end{aligned} \tag{2.119}$$

with densities

$$u = \bar{u}\big(t, x_j\big)\,,\; q_i = \bar{q}_i\big(t, x_j\big)\,,\; r = \bar{r}\big(t, x_j\big)\,, \tag{2.120}$$

where u, q_i, r are the specific internal energy, the heat flux and the specific radiation. According to Eq. (2.34) in scalar valued variant, we can identify

$$\psi = \varrho u\,,\; f = -q_i n_i\,,\; s = \varrho r\,,\; p = \frac{\partial v_i}{\partial x_j}\sigma_{ij} + \frac{\partial \omega_k}{\partial x_j}\varepsilon_{kli} x_l \sigma_{ij} + \frac{\partial \omega_k}{\partial x_j} m_{kj}\,. \tag{2.121}$$

Following Eq. (2.45), we write

$$\frac{\mathrm{d}}{\mathrm{d}t}\big(\varrho u\big) + \varrho u \frac{\partial v_j}{\partial x_j} = -\frac{\partial q_i}{\partial x_i} + \varrho r + \frac{\partial v_i}{\partial x_j}\sigma_{ij} + \frac{\partial \omega_k}{\partial x_j}\varepsilon_{kli} x_l \sigma_{ij} + \frac{\partial \omega_k}{\partial x_j} m_{kj}\,. \tag{2.122}$$

The expression on the left hand side can be rewritten as

$$\frac{\mathrm{d}}{\mathrm{d}t}\big(\varrho u\big) + \varrho u \frac{\partial v_j}{\partial x_j} = \frac{\mathrm{d}\varrho}{\mathrm{d}t} u + \varrho \frac{\mathrm{d}u}{\mathrm{d}t} + \varrho u \frac{\partial v_j}{\partial x_j} = \left(\frac{\mathrm{d}\varrho}{\mathrm{d}t} + \varrho \frac{\partial v_j}{\partial x_j} \right) u + \varrho \frac{\mathrm{d}u}{\mathrm{d}t}\,. \tag{2.123}$$

The local balance law of internal energy reads

$$\left(\frac{\mathrm{d}\varrho}{\mathrm{d}t} + \varrho \frac{\partial v_i}{\partial x_i} \right) u + \varrho \frac{\mathrm{d}u}{\mathrm{d}t} = -\frac{\partial q_i}{\partial x_i} + \varrho r + \frac{\partial v_i}{\partial x_j}\sigma_{ij} + \frac{\partial \omega_k}{\partial x_j}\varepsilon_{kli} x_l \sigma_{ij} + \frac{\partial \omega_k}{\partial x_j} m_{kj}\,. \tag{2.124}$$

We obtain the local balance law of internal energy that satisfies the local balance of mass by inserting the Eq. (2.50) into the above equation. Further, ignoring any rotational motion, we have

$$\varrho \frac{\mathrm{d}u}{\mathrm{d}t} = -\frac{\partial q_i}{\partial x_i} + \varrho r + \frac{\partial v_i}{\partial x_j}\sigma_{ij}\,. \tag{2.125}$$

Combined with suitable material equations for specific internal energy u, heat flux q_i, specific radiation r and stress tensor σ_{ij}, we can formulate a field equation for the temperature T.

2.3.11 Entropy

The entropy principle is applied to prevent construction of cyclic devices that are impossible to operate. This also known as the second law of thermodynamics. This principle serves us to reduce the degrees of freedom of material equations by restricting their properties, i. e., form and dependency, see for example (Abali 2014, p. 21 ff). Furthermore, the entropy production can be used to evaluate process models and define them as possible, ideal or impossible. Further insight to this topic can be found in, e. g., (W. H. Müller 2014, p. 307 ff), (I. Müller 1973) as well as (Eckart 1940).

We follow Tadmor et al. (2012, p. 148 ff) and assume that the internal energy is completely determined by the independent state variables specific entropy s and extensive kinematic variables Γ_i

$$u = \breve{u}(s, \Gamma_i) \,. \tag{2.126}$$

The total differential of internal energy is known as *entropy form of the first law* and it reads

$$\mathrm{d}u = \frac{\partial u}{\partial s}\,\mathrm{d}s + \sum_{i=1}^{n} \frac{\partial u}{\partial \Gamma_i}\,\mathrm{d}\Gamma_i = T\,\mathrm{d}s + \sum_{i=1}^{n} \varpi_i\,\mathrm{d}\Gamma_i \,, \tag{2.127}$$

where T is the *absolute temperature* and ϖ_i is the *thermodynamic tensions*. Inserting the above equation into the local balance of internal energy and divided by absolute temperature T, it yields

$$\begin{aligned}\left(\frac{\mathrm{d}\varrho}{\mathrm{d}t} + \varrho\frac{\partial v_i}{\partial x_i}\right)\frac{1}{T}u + \varrho\frac{\mathrm{d}s}{\mathrm{d}t} = &-\frac{1}{T}\frac{\partial q_i}{\partial x_i} + \\ &+ \frac{1}{T}\varrho r + \frac{1}{T}\frac{\partial v_i}{\partial x_j}\sigma_{ij} + \frac{1}{T}\frac{\partial \omega_k}{\partial x_j}\varepsilon_{kli}x_l\sigma_{ij} + \frac{1}{T}\frac{\partial \omega_k}{\partial x_j}m_{kj} - \sum_{i=1}^{n}\frac{1}{T}\varrho\varpi_i\frac{\mathrm{d}\Gamma_i}{\mathrm{d}t} \,.\end{aligned} \tag{2.128}$$

The first expression on the right-hand side can be rewritten as

$$\begin{aligned}-\frac{1}{T}\frac{\partial q_i}{\partial x_i} &= -\frac{\partial}{\partial x_i}\left(\frac{1}{T}q_i\right) + \frac{\partial\left(\frac{1}{T}\right)}{\partial x_i}q_i = -\frac{\partial}{\partial x_i}\left(\frac{1}{T}q_i\right) + \frac{\partial\left(\frac{1}{T}\right)}{\partial T}\frac{\partial T}{\partial x_i}q_i = \\ &= -\frac{\partial}{\partial x_i}\left(\frac{1}{T}q_i\right) - \frac{1}{T^2}\frac{\partial T}{\partial x_i}q_i \,.\end{aligned} \tag{2.129}$$

The local balance of entropy follows as

$$\begin{aligned}\left(\frac{\mathrm{d}\varrho}{\mathrm{d}t} + \varrho\frac{\partial v_i}{\partial x_i}\right)\frac{u}{T} + \varrho\frac{\mathrm{d}s}{\mathrm{d}t} = &-\frac{\partial}{\partial x_i}\left(\frac{1}{T}q_i\right) + \frac{1}{T}\varrho r - \\ &- \frac{1}{T^2}\frac{\partial T}{\partial x_i}q_i + \frac{1}{T}\frac{\partial v_i}{\partial x_j}\sigma_{ij} + \frac{1}{T}\frac{\partial \omega_k}{\partial x_j}\varepsilon_{kli}x_l\sigma_{ij} + \frac{1}{T}\frac{\partial \omega_k}{\partial x_j}m_{kj} - \sum_{i=1}^{n}\frac{1}{T}\varrho\varpi_i\frac{\mathrm{d}\Gamma_i}{\mathrm{d}t} \,.\end{aligned} \tag{2.130}$$

To determine the global balance of entropy, the following identity is used

$$\begin{aligned}\frac{\partial}{\partial t}(\varrho s) + \frac{\partial}{\partial x_i}(\varrho s v_i) &= \frac{\partial \varrho}{\partial t}s + \varrho\frac{\partial s}{\partial t} + \frac{\partial \varrho}{\partial x_i}s v_i + \varrho\frac{\partial s}{\partial x_i}v_i + \varrho s\frac{\partial v_i}{\partial x_i} \\ &= \frac{\partial \varrho}{\partial t}s + \frac{\partial \varrho}{\partial x_i}s v_i + \varrho s\frac{\partial v_i}{\partial x_i} + \varrho\frac{\partial s}{\partial t} + \varrho\frac{\partial s}{\partial x_i}v_i \\ &= \left(\frac{\partial \varrho}{\partial t} + \frac{\partial \varrho}{\partial x_i}v_i + \varrho\frac{\partial v_i}{\partial x_i}\right)s + \varrho\frac{\mathrm{d}s}{\mathrm{d}t} \\ &= \left(\frac{\mathrm{d}\varrho}{\mathrm{d}t} + \varrho\frac{\partial v_i}{\partial x_i}\right)s + \varrho\frac{\mathrm{d}s}{\mathrm{d}t} \,.\end{aligned} \tag{2.131}$$

Applying the integration and using the Reynold's Transport followed by the Gauss' theorem gives the global balance of entropy

$$\begin{aligned}\int\left(\frac{\mathrm{d}\varrho}{\mathrm{d}t} + \varrho\frac{\partial v_i}{\partial x_i}\right)\left(\frac{u}{T} - s\right)\mathrm{d}V + \frac{\mathrm{d}}{\mathrm{d}t}\int \varrho s\,\mathrm{d}V = &-\int\frac{1}{T}q_i n_i\,\mathrm{d}A + \int\frac{1}{T}\varrho r\,\mathrm{d}V + \\ &+ \int\left(-\frac{1}{T^2}\frac{\partial T}{\partial x_i}q_i + \frac{1}{T}\frac{\partial v_i}{\partial x_j}\sigma_{ij} + \frac{1}{T}\frac{\partial \omega_k}{\partial x_j}\varepsilon_{kli}x_l\sigma_{ij} + \frac{1}{T}\frac{\partial \omega_k}{\partial x_j}m_{kj} - \right. \\ &\left. - \sum_{i=1}^{n}\frac{1}{T}\varrho\varpi_i\frac{\mathrm{d}\Gamma_i}{\mathrm{d}t}\right)\mathrm{d}V \,.\end{aligned} \tag{2.132}$$

Ignoring the first term, we can identify by means of scalar valued version of Eq. (2.34)

$$\psi = \varrho s\,,\; f = -\frac{1}{T} q_i n_i\,,\; s = \frac{1}{T}\varrho r\,,$$
$$p = -\frac{1}{T^2}\frac{\partial T}{\partial x_i} q_i + \frac{1}{T}\frac{\partial v_i}{\partial x_j}\sigma_{ij} + \frac{1}{T}\frac{\partial \omega_k}{\partial x_j}\varepsilon_{kli} x_l \sigma_{ij} + \frac{1}{T}\frac{\partial \omega_k}{\partial x_j} m_{kj} - \sum_{i=1}^{n} \frac{1}{T}\varrho\varpi_i \frac{\mathrm{d}\Gamma_i}{\mathrm{d}t}\,. \tag{2.133}$$

The thermodynamic compatibility of material equations can be examined in conjunction with the entropy production term p. The second law of thermodynamics states that if

$$p > 0\,, \tag{2.134}$$

it is possible that the material equations exist. For idealised material behaviour or processes, it is $p = 0$.

2.4 Material Equations

The balance laws alone are insufficient to formulate the field equations that describe the functional relationship between the responses (mass density, velocity and temperature) and material-specific parameters. Additional equations are required to cover the material-specific response behaviour (cf. W. H. Müller 2014, pp. 129–130), specifically for the stress tensor σ_{ij}, the internal energy u, the heat flux q_i, the specific volume force f_i and specific radiation r. For linear elastic solids, we will present the material laws for the first three quantities. For the latter two, we will use the gravitational acceleration for the specific volume force and the specific radiation will be assumed to be known.

2.4.1 Linear Elastic Deformation and Thermal Expansion

The total linear strain for small deformation ε_{kl} can be additive decompose into different summands (cf. Hetnarski and Eslami 2009, p. 21). Each strain part is associated to an phenomenon such as elastic deformation and thermal expansion

$$\varepsilon_{kl} = \varepsilon_{kl}^{\text{elastic}} + \varepsilon_{kl}^{\text{thermal}}\,. \tag{2.135}$$

Other types of strain can be added to cover more phenomena, e. g., plasticity or viscosity, but they are beyond the scope of this work. For small elastic deformation and ignoring the aspect of spin, the symmetric stress σ_{ij} in Eq. (2.105) and elastic strain tensor $\varepsilon_{kl}^{\text{elastic}}$ relation has a linear proportional. The elastic response is described by Hooke's law

$$\sigma_{ij} = C_{ijkl}\varepsilon_{kl}^{\text{elastic}}\,, \tag{2.136}$$

where C_{ijkl} is the elasticity tensor with 81 entries. By using the symmetrical properties of the stress, see Eq. (2.105), as well as the strain tensor, the number of the parameters is reduced to 36. Within the range of linear elastic deformation, the stored energy is equal to its complementary part. Therefore, the number of parameters is further decreased to 21 independent constants for anisotropic elastic materials. Thus, the Hooke's law can be rewritten as Voigt's matrix notation as follows

$$\begin{bmatrix} \sigma_{11} \\ \sigma_{22} \\ \sigma_{33} \\ \sigma_{23} \\ \sigma_{13} \\ \sigma_{12} \end{bmatrix} = \begin{bmatrix} C_{1111} & C_{1122} & C_{1133} & C_{1123} & C_{1113} & C_{1112} \\ & C_{2222} & C_{2233} & C_{2223} & C_{2213} & C_{2212} \\ & & C_{3333} & C_{3323} & C_{3313} & C_{3312} \\ & & & C_{2323} & C_{2313} & C_{2312} \\ & & & & C_{1313} & C_{1312} \\ \text{symmetrical} & & & & & C_{1212} \end{bmatrix} \begin{bmatrix} \varepsilon_{11}^{\text{elastic}} \\ \varepsilon_{22}^{\text{elastic}} \\ \varepsilon_{33}^{\text{elastic}} \\ 2\varepsilon_{23}^{\text{elastic}} \\ 2\varepsilon_{13}^{\text{elastic}} \\ 2\varepsilon_{12}^{\text{elastic}} \end{bmatrix} \tag{2.137}$$

respectively in matrix notation

$$\boldsymbol{\sigma} = \mathbf{C}\boldsymbol{\varepsilon}^{\text{elastic}}\,. \tag{2.138}$$

An overview of the eight different symmetry classes (triclinic, monoclinic, orthotropic, tetragonal, trigonal, hexagonal, cubic, isotropic) of the elasticity tensor can be found in Chadwick et al. (2001). The linear thermal expansion

is described as a relation between thermal strain $\varepsilon_{kl}^{\text{thermal}}$ and the change of the temperature ΔT from a reference to a current state

$$\varepsilon_{kl}^{\text{thermal}} = \alpha_{kl}\left(T - T^{\text{Reference}}\right) = \alpha_{kl}\Delta T\,, \tag{2.139}$$

where α_{kl} is the coefficient of thermal expansion. The stress to strain and temperature change relationship for anisotropic materials can be obtained by inserting elastic strain from Eq. (2.135) into Hooke's law in Eq. (2.136) and followed by the linear thermal expansion law in Eq. (2.139)

$$\sigma_{ij} = C_{ijkl}\left(\varepsilon_{kl} - \varepsilon_{kl}^{\text{thermal}}\right) = C_{ijkl}\left(\varepsilon_{kl} - \alpha_{kl}\Delta T\right). \tag{2.140}$$

For isotropic elastic materials, the following elasticity tensor applies

$$C_{ijkl} = \lambda\delta_{ij}\delta_{kl} + \mu\left(\delta_{ik}\delta_{jl} + \delta_{il}\delta_{jk}\right) \tag{2.141}$$

or respectively in Voigt's notation

$$\mathbf{C} = \begin{bmatrix} \lambda+2\mu & \lambda & \lambda & & & \\ & \lambda+2\mu & \lambda & & & \\ & & \lambda+2\mu & & & \\ & & & \mu & & \\ & & & & \mu & \\ \text{symmetrical} & & & & & \mu \end{bmatrix}, \tag{2.142}$$

where the parameters λ and μ are called Lamé constants. The conversion to Young's modulus E and Poisson's ratio ν can be found for example in Szabó (1966, p. 93)

$$\lambda = \frac{E\nu}{\left(1+\nu\right)\left(1-2\nu\right)}\,,\ \mu = \frac{E}{2\left(1+\nu\right)}\,. \tag{2.143}$$

The Hooke's law reads

$$\sigma_{ij} = \lambda\delta_{ij}\varepsilon_{kk}^{\text{elastic}} + 2\mu\varepsilon_{ij}^{\text{elastic}}\,. \tag{2.144}$$

The following thermal expansion coefficient is applied for isotropic materials

$$\alpha_{kl} = \alpha\delta_{kl}\,. \tag{2.145}$$

Refer to, for example, Grote and Antonsson (2009, p. 124), to find thermal expansion coefficients for selected materials. The relationship of stress to strain and to temperature change for isotropic materials can be computed by inserting the elasticity tensor in Eq. (2.141) and thermal expansion coefficient in Eq. (2.145) into Eq. (2.139). Taking the linear strain from Eq. (2.135) into account, we have

$$\sigma_{ij} = \lambda\delta_{ij}\varepsilon_{kk} + 2\mu\varepsilon_{ij} - \left(3\lambda+2\mu\right)\alpha\delta_{ij}\Delta T\,. \tag{2.146}$$

2.4.2 Caloric State Equation for Solids

Recall an obsolete unit for energy: the *Calorie*, see e. g. (I. Müller and W. H. Müller 2008, p. 54). The definition was the amount of heat energy that is needed to increase one gram of water by one Kelvin. Furthermore, the specific heat capacity of water that was used to define the Calorie was fixed at atmospheric pressure and at initial water temperature of $T_0 = 15\,^{\circ}\text{C}$. Observe the local balance of internal energy in Eq. (2.125) where the local balance of mass is satisfied and spin and rotational influences are neglected

$$\varrho\frac{\mathrm{d}u}{\mathrm{d}t} = -\frac{\partial q_i}{\partial x_i} + \varrho r + \frac{\partial v_i}{\partial x_j}\sigma_{ij}\,. \tag{2.125}$$

For a fluid almost at rest, we can use a simplified Navier-Stokes Equation where the frictional parts are ignored

$$\sigma_{ij} = -p\delta_{ij}\,, \tag{2.147}$$

where p is the pressure. This in turn yields

$$\frac{\mathrm{d}u}{\mathrm{d}t} = -\frac{1}{\varrho}\frac{\partial q_i}{\partial x_i} + r - \frac{1}{\varrho}\frac{\partial v_i}{\partial x_i}p = \dot{q} - \frac{\mathrm{d}v}{\mathrm{d}t}p\,, \tag{2.148}$$

where the heat flux and radiation parts are combined as heat transfer rate

$$\dot{q} = -\frac{1}{\varrho}\frac{\partial q_i}{\partial x_i} + r\,. \tag{2.149}$$

The specific volume is $v = 1/\varrho$ so that the local balance of mass in Eq. (2.50) can be rewritten as

$$\frac{\mathrm{d}v_i}{\mathrm{d}x_i} = -\frac{1}{\varrho}\frac{\mathrm{d}\varrho}{\mathrm{d}t} = -v\frac{\mathrm{d}(1/v)}{\mathrm{d}t} = -v\frac{\mathrm{d}(1/v)}{\mathrm{d}v}\frac{\mathrm{d}v}{\mathrm{d}t} = \frac{1}{v}\frac{\mathrm{d}v}{\mathrm{d}t}\,. \tag{2.150}$$

For the right-hand side of Eq. (2.148), we assume that the specific internal energy is completely determined by the temperature T and specific volume v

$$u = \breve{u}(T, v)\,. \tag{2.151}$$

This leads to

$$\frac{\partial u}{\partial T}\frac{\mathrm{d}T}{\mathrm{d}t} + \frac{\partial u}{\partial v}\frac{\mathrm{d}v}{\mathrm{d}t} + p\frac{\mathrm{d}v}{\mathrm{d}t} = \frac{\partial u}{\partial T}\frac{\mathrm{d}T}{\mathrm{d}t} + \left(\frac{\partial u}{\partial v} + p\right)\frac{\mathrm{d}v}{\mathrm{d}t} = c_v\frac{\mathrm{d}T}{\mathrm{d}t} + \left(\frac{\partial u}{\partial v} + p\right)\frac{\mathrm{d}v}{\mathrm{d}t} = \dot{q}\,. \tag{2.152}$$

For isochoric process $\mathrm{d}v = 0$, we can obtain the heat capacity at constant specific volume $c_v = \breve{c}_v(T = T_0)$ for an initial temperature T_0 by measuring the transferred heat energy $Q = \int \dot{q}\,\mathrm{d}t$ as well as the rise of temperature ΔT

$$c_v\frac{\mathrm{d}T}{\mathrm{d}t} = \dot{q} \;\Rightarrow\; \int c_v\,\mathrm{d}T = \int \dot{q}\,\mathrm{d}t \;\Rightarrow\; \breve{c}_v(T = T_0) = \frac{Q}{\Delta T}\,. \tag{2.153}$$

Since the above equation is inappropriate to compute the heat capacity at constant pressure $c_p = \breve{c}_p(T = T_0)$ for an reference temperature T_0, we reformulate the equation by means of specific volume that is completely determined by the temperature T and pressure p

$$v = \breve{v}(T, p) \tag{2.154}$$

and this yields

$$\begin{aligned} c_v\frac{\mathrm{d}T}{\mathrm{d}t} + \left(\frac{\partial u}{\partial v} + p\right)\left(\frac{\partial v}{\partial T}\frac{\mathrm{d}T}{\mathrm{d}t} + \frac{\partial v}{\partial p}\frac{\mathrm{d}p}{\mathrm{d}t}\right) = \\ = \left(c_v + \left(\frac{\partial u}{\partial v} + p\right)\frac{\partial v}{\partial T}\right)\frac{\mathrm{d}T}{\mathrm{d}t} + \left(\left(\frac{\partial u}{\partial v} + p\right)\frac{\partial v}{\partial p}\right)\frac{\mathrm{d}p}{\mathrm{d}t} = \\ = c_p\frac{\mathrm{d}T}{\mathrm{d}t} + \left(\left(\frac{\partial u}{\partial v} + p\right)\frac{\partial v}{\partial p}\right)\frac{\mathrm{d}p}{\mathrm{d}t} = \dot{q}\,. \end{aligned}$$

For isobaric process $\mathrm{d}p = 0$, we can compute the heat capacity at constant pressure $c_p = \breve{c}_p(T = T_0)$ for a starting temperature T_0 by measuring the transferred heat energy $Q = \int \dot{q}\,\mathrm{d}t$ as well as the increase of temperature ΔT

$$c_p\frac{\mathrm{d}T}{\mathrm{d}t} = \dot{q} \;\Rightarrow\; \int c_p\,\mathrm{d}T = \int \dot{q}\,\mathrm{d}t \;\Rightarrow\; \breve{c}_p(T = T_0) = \frac{Q}{\Delta T}\,. \tag{2.155}$$

For ideal solid, a different approach is followed. First, the internal energy is completely determined by temperature T and linear strain ε_{kl}

$$u = \breve{u}(T, \varepsilon_{kl})\,. \tag{2.156}$$

Second, for isostrain process $\mathrm{d}\varepsilon_{kl} = 0$, the heat capacity at constant strain $c_{\varepsilon_{kl}}$ is described by the Dulong-Petit law

$$c_{\varepsilon_{kl}} = 3\frac{R}{M}\,, \tag{2.157}$$

where R is the *universal gas constant* and M is the *atomic* or *molecular weight*. This law is derived by means of statistical mechanics, see for example (Grifalco 2000, p. 104), and is valid for room temperature and above.

2.4.3 Law of Heat Conduction

The heat conduction law by FOURIER described the heat transfer rate per area element q_i. The heat transfer occurs in the normal direction of an infinitesimal cubic element with a thickness in the same direction ∂x_i when the two opposing sides have different temperatures, i. e., temperature difference ∂T. The FOURIER's law reads

$$q_i = -\kappa \frac{\partial T}{\partial x_i}\,, \tag{2.158}$$

where κ is the thermal conductivity. For example in GROTE and ANTONSSON (2009, p. 281), the thermal conductivities of some materials can be found. An historical overview about the development and influences of FOURIER's heat conduction equation can be found in NARASIMHAN (1999).

2.5 Field Equations

The field equations connect the responses and material-specific parameters in form of partial differential equations (cf. W. H. MÜLLER 2014, pp. 153–154). They can be obtained by combining the balance equations and material laws. Each response type is associated with a balance law. The mass density field ϱ is linked to the balance of mass. The velocity field v_i is connected with the balance of linear momentum. The angular velocity ω_r field is intertwined with the balance of angular momentum. The temperature field T is tied to the balance of internal energy. The material-specific parameters originate from the material equations.

2.5.1 Elastodynamic Equations

Inserting the HOOKE's law with linear thermal expansion in Eq. (2.140) into the local balance of linear moment which satisfies the balance of mass in Eq. (2.59) and using the linear strain for small deformation in Eq. (2.28) (cf. ABALI 2017, pp. 2–9), this results

$$\begin{aligned}
\varrho \frac{\mathrm{d}v_i}{\mathrm{d}t} &= \frac{\partial}{\partial x_j}\Big(C_{ijkl}\big(\varepsilon_{kl} - \alpha_{kl}\Delta T\big)\Big) + \varrho f_i = \frac{\partial}{\partial x_j}\big(C_{ijkl}\varepsilon_{kl} - C_{ijkl}\alpha_{kl}\Delta T\big) + \varrho f_i = \\
&= C_{ijkl}\frac{\partial \varepsilon_{kl}}{\partial x_j} - C_{ijkl}\alpha_{kl}\frac{\partial T}{\partial x_j} + \varrho f_i = \\
&= C_{ijkl}\frac{\partial}{\partial x_j}\Big(\frac{1}{2}\Big(\frac{\partial u_k}{\partial x_l} + \frac{\partial u_l}{\partial x_k}\Big)\Big) - C_{ijkl}\alpha_{kl}\frac{\partial T}{\partial x_j} + \varrho f_i = \\
&= \frac{1}{2}C_{ijkl}\frac{\partial^2 u_k}{\partial x_j \partial x_l} + \frac{1}{2}\underbrace{C_{ijkl}}_{=C_{ijlk}}\frac{\partial^2 u_l}{\partial x_j \partial x_k} - C_{ijkl}\alpha_{kl}\frac{\partial T}{\partial x_j} + \varrho f_i = \\
&= C_{ijkl}\frac{\partial^2 u_k}{\partial x_j \partial x_l} - C_{ijkl}\alpha_{kl}\frac{\partial T}{\partial x_j} + \varrho f_i\,.
\end{aligned} \tag{2.159}$$

For the right-hand side, the velocity v_i can be rewritten as

$$v_i = \frac{\mathrm{d}x_i}{\mathrm{d}t} = \frac{\mathrm{d}}{\mathrm{d}t}\big(u_i + X_i\big) = \frac{\mathrm{d}u_i}{\mathrm{d}t}. \tag{2.160}$$

This yields the elastodynamic equations

$$\varrho \frac{\mathrm{d}^2 u_i}{\mathrm{d}t^2} = C_{ijkl}\frac{\partial^2 u_k}{\partial x_j \partial x_l} - C_{ijkl}\alpha_{kl}\frac{\partial T}{\partial x_j} + \varrho f_i\,. \tag{2.161}$$

One special case of dynamic is the static equilibrium. In this steady state, the displacement is time-independent and therefore the left-hand side of the elastodynamic equations can be omitted. The specific volume force f_i is mostly associated with the gravitational acceleration and is used to incorporate the aspect of the dead load. It can

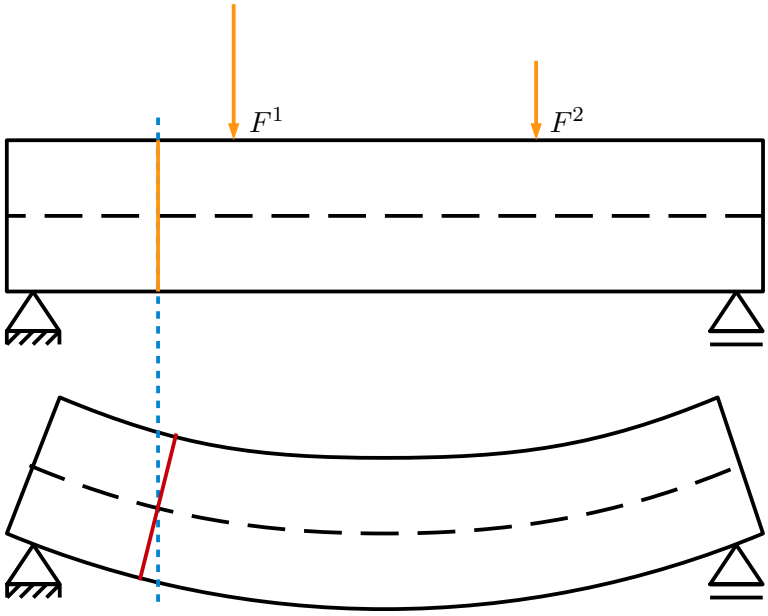


Figure 2.1: A four-point bending test apparatus.

be ignored if the applied forces are much greater than the force of gravitation. When the body has an overall constant temperature, the temperature gradient drops out from the analysis. Thus, the thermal expansion part can be neglected. For a body consists of isotropic material, the so-called Lamé-Navier equations (cf. W. H. Müller 2014, p. 161)

$$\begin{aligned} 0 = C_{ijkl}\frac{\partial^2 u_k}{\partial x_j \partial x_l} &= \lambda \frac{\partial^2 u_k}{\partial x_i \partial x_k} + \mu\left(\frac{\partial^2 u_i}{\partial x_j \partial x_j} + \frac{\partial^2 u_j}{\partial x_j \partial x_i}\right) = \\ &= (\lambda+\mu)\frac{\partial^2 u_j}{\partial x_i \partial x_j} + \mu \frac{\partial^2 u_i}{\partial x_j \partial x_j} \implies 0 = \frac{\partial^2 u_i}{\partial x_j \partial x_j} + \left(\frac{\lambda}{\mu}+1\right)\frac{\partial^2 u_j}{\partial x_i \partial x_j} \end{aligned} \tag{2.162}$$

is obtained.

2.5.2 Euler-Bernoulli Beam Theory

A bending test is an experimental set-up to determine structural deformation behaviour by applying predefined forces to a specimen, see Fig. 2.1. For a bending test, a specimen is shaped as a slender beam with specific geometry. Then the beam specimen is clamped with bearings. At specific positions on top of the beam, forces of predefined strength are applied. For a given bending test configuration, the deflection of the beam in the deformed state can be computed by the Euler-Bernoulli beam equation (cf. Gross, Hauger, Schröder, Wall, and Bonet 2011, pp. 125–129). To this, observe the local balance of angular momentum in Eq. (2.96) which satisfies the balance of mass in Eq. (2.50)

$$\varrho \frac{\mathrm{d}}{\mathrm{d}t}\left(\theta_{kr}\omega_r + s_k\right) = \frac{\partial}{\partial x_j}\left(\varepsilon_{kli}x_l\sigma_{ij} + m_{kj}\right) + \varrho\left(\varepsilon_{kli}x_l f_i + l_k\right). \tag{2.163}$$

For materials with non-complex inner structure, the spin s_k as well as the influences of the surface and volume couple, m_{kj} and l_k, are neglected, thus we have a symmetric stress tensor in Eq. (2.105). For statically bended beams, the dynamic part in the left-hand side of the balance equation vanishes. Furthermore, the gravitational specific volume force f_i can be ignored due to the much greater applied bending forces. Consequently, we obtain the momentum equilibrium

$$0 = \frac{\partial}{\partial x_j}\left(\varepsilon_{kli}x_l\sigma_{ij}\right). \tag{2.164}$$

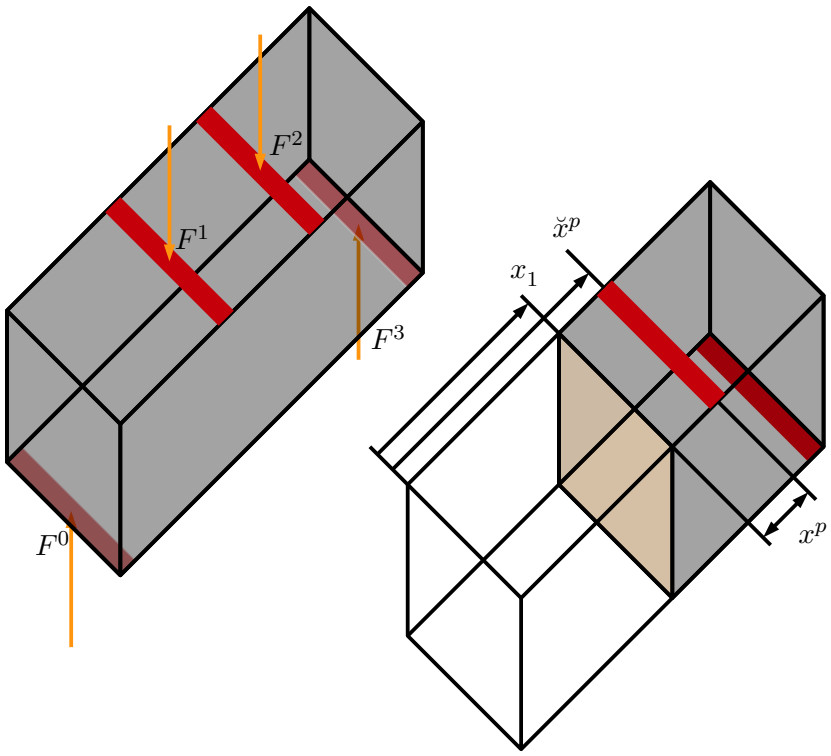


Figure 2.2: The Method of Sections generates a *free-body diagram* for revealing the inner stresses within a beam. The forces F^p are applied on the rectangular traction areas with depth d and width w which are marked in red.

Integrating over the volume of the beam body, followed by the application of the GAUSS' theorem, we find

$$0 = \int \frac{\partial}{\partial x_j}(\varepsilon_{kli} x_l \sigma_{ij}) \, \mathrm{d}V = \int \varepsilon_{kli} x_l \sigma_{ij} n_j \, \mathrm{d}A = \\ = \int_{\partial \mathcal{B}_{\text{internal}}} \varepsilon_{kli} x_l \sigma_{ij} n_j \, \mathrm{d}A + \int_{\partial \mathcal{B}_{\text{external}}} \varepsilon_{kli} x_l t_i \, \mathrm{d}A = M_k^{\text{internal}} + M_k^{\text{external}} . \tag{2.165}$$

In the last step, we decompose the total momentum into internal and external parts in order to reveal the interior stress of the beam. This is possible by means of the *method of sections*, see for example in GROSS, HAUGER, SCHRÖDER, WALL, and RAJAPAKSE (2009, p. 10) or in GERE and GOODNO (2013, p. 8). As shown in Fig. 2.2, we section a imaginary cut to the beam perpendicular to direction 1 at position x_1 and examine the right-hand side part. The internal momentum M_k^{internal} is computed from the cutting area at the cutting point x_1. In a bending testing apparatus, the beam specimen is subjected to two types of external forces F^p: active and reactive. Predefined line forces, applied on top of the beam at specific positions x^p, are considered active, while the reactive forces occurs as a response to the constraints induced by the supports at positions x^p. The superscript p identifies uniquely the active and reactive forces and are numbered from 0 to N. A line force comprises the acting force F^p that are distributed on rectangular area of depth d and width w at position x^p. The rectangular areas are marked in red in Fig. 2.2. The external momentum M_k^{external} is determined by the external forces F^p on the right-hand side part at the cutting point x_1.

To proceed, we apply the so-called *semi-inverse method* for

$$M_k^{\text{internal}} = \int_{\partial \mathcal{B}_{\text{internal}}} \varepsilon_{kli} x_l \sigma_{ij} n_j \, \mathrm{d}A \, . \tag{2.166}$$

In this method, the displacement functions are supposed to have certain form by geometrical considerations and simplified assumptions. For the EULER-BERNOULLI beam theory, we have to ensure that the tested beam specimen fulfils the BERNOULLI's hypothesis that the cross sections of the beam remain plane and perpendicular in the bent

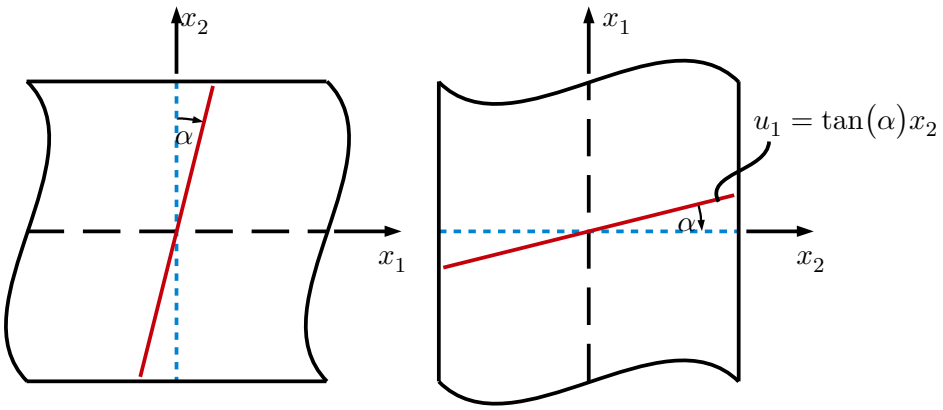


Figure 2.3: Explanation of the semi-inverse method.

configuration to the set of lines that don't extend or contract. This can be ascertained for small deformation. The black dashed line in Fig. 2.1 indicates this set of lines that is known as the *neutral surface*. Furthermore, in Fig. 2.1, the red line shows that the cross section remains perpendicular in the deformed beam. This in turn leads to the following displacement functions

$$u_1 = \tan(\alpha)x_2 = \frac{\partial u}{\partial x_1}x_2\,,\; u_2 = u = \breve{u}(x_1)\,,\; u_3 = 0\,. \tag{2.167}$$

The displacement u_3 vanishes due to the set-up of the bending apparatus that excludes deformation in direction 3. For small deformation, the displacement u_2 depends only on x_1. The displacement u_1 is determined by the cross section in the bent configuration of the beam, see Fig. 2.3. While u_1 is a function of x_1 and x_2, its slope $\tan(\alpha)$ depends only on x_1 due to the BERNOULLI's hypothesis. The slope $\tan(\alpha)$ is determined as depicted in Fig. 2.4. It shows that the slope $\tan(\alpha)$ is also determined by an infinitesimal change of displacement u_2, ∂u_2, divided by an infinitesimal change of position x_1, ∂x_1.

For small deformation, we use the linear strain in Eq. (2.28) with the displacement functions to determine non-zero strains as follows

$$\varepsilon_{11} = \frac{\partial u_1}{\partial x_1} = \frac{\partial^2 u}{\partial {x_1}^2}x_2 \text{ and } \varepsilon_{12} = \frac{1}{2}\left(\frac{\partial u_1}{\partial x_2} + \frac{\partial u_2}{\partial x_1}\right) = \frac{\partial u}{\partial x_1}\,. \tag{2.168}$$

Since the total length of a slender beam is much greater than the deflection for small deformation, it is feasible to assume that the inclination of the deformed beam is negligibly small

$$\frac{\partial u}{\partial x_1} \approx 0\,. \tag{2.169}$$

Furthermore, the beam consists of isotropic material which obeys HOOKE's law. This results in the following non-zero entries of the stress tensor

$$\sigma_{11} = (\lambda + 2\mu)\varepsilon_{11}\,,\; \sigma_{22} = \sigma_{33} = \lambda\varepsilon_{11}\,. \tag{2.170}$$

The POISSON's ratio ν vanishes as a consequence of the chosen displacement functions

$$\nu = -\frac{\varepsilon_{22}}{\varepsilon_{11}} = -\frac{\varepsilon_{33}}{\varepsilon_{11}} = 0\,, \tag{2.171}$$

therefore the LAMÉ constants become

$$\lambda = 0\,,\; \mu = \frac{E}{2}\,. \tag{2.172}$$

The only non-vanishing stress entry left is

$$\sigma_{11} = E\varepsilon_{11}\,. \tag{2.173}$$

Therefore, the remaining internal momentums are

$$M_2^{\text{internal}} = \int \varepsilon_{231}x_3\sigma_{11}n_1\,\mathrm{d}A = \int x_3\sigma_{11}\,\mathrm{d}x_2\,\mathrm{d}x_3 = \int x_3 E\varepsilon_{11}\,\mathrm{d}x_2\,\mathrm{d}x_3 =$$

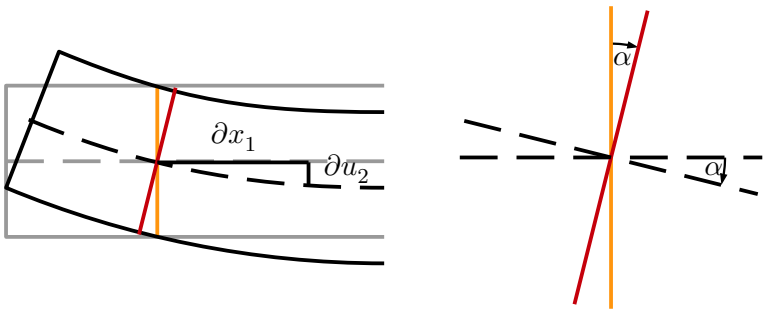


Figure 2.4: Explanation of the semi-inverse method.

$$= \int x_3 E x_2 \frac{\partial^2 u}{\partial {x_1}^2} \,\mathrm{d}x_2 \,\mathrm{d}x_3 = E \frac{\partial^2 u}{\partial {x_1}^2} \int_{-\frac{h}{2}}^{\frac{h}{2}} x_2 \,\mathrm{d}x_2 \int_{-\frac{w}{2}}^{\frac{w}{2}} x_3 \,\mathrm{d}x_3 =$$

$$= E \frac{\partial^2 u}{\partial {x_1}^2} \frac{1}{2} \underbrace{\left[{x_2}^2\right]_{-\frac{h}{2}}^{\frac{h}{2}}}_{=0} \frac{1}{2} \underbrace{\left[{x_3}^2\right]_{-\frac{w}{2}}^{\frac{w}{2}}}_{=0} = 0 \tag{2.174}$$

and

$$M_3^{\text{internal}} = \int \varepsilon_{321} x_2 \sigma_{11} n_1 \,\mathrm{d}A = \int -x_2 \sigma_{11} (-1) \,\mathrm{d}x_2 \,\mathrm{d}x_3 = \int x_2 E \varepsilon_{11} \,\mathrm{d}x_2 \,\mathrm{d}x_3 =$$

$$= \int x_2 E x_2 \frac{\partial^2 u}{\partial {x_1}^2} \,\mathrm{d}x_2 \,\mathrm{d}x_3 = E \frac{\partial^2 u}{\partial {x_1}^2} \underbrace{\int_{-\frac{w}{2}}^{\frac{w}{2}} \int_{-\frac{h}{2}}^{\frac{h}{2}} {x_2}^2 \,\mathrm{d}x_2 \,\mathrm{d}x_3}_{=I_{22}} = E I_{22} \frac{\partial^2 u}{\partial {x_1}^2} \,,$$

where I_{22} is known as *moment of inertia of plane area*.

For the external momentum

$$M_k^{\text{external}} = \int_{\partial \mathcal{B}_{\text{external}}} \varepsilon_{kli} x_l t_i \,\mathrm{d}A \,, \tag{2.175}$$

the tractions t_i that are acting on the beam are considered. Due to the apparatus set-up, the active and reactive forces point along the direction x_2-axis. Therefore, the only remaining traction vector component is

$$t_2 = \breve{t}(x_1, x_2) = \begin{cases} t^p & \text{for } x_1 \in \left[x^p - \frac{d}{2} \,,\, x^p + \frac{d}{2}\right] \,,\; x_2 = \;\; \frac{h}{2} \,, \\ t^p & \text{for } x_1 \in \left[x^p - \frac{d}{2} \,,\, x^p + \frac{d}{2}\right] \,,\; x_2 = -\frac{h}{2} \,, \\ 0 & \text{otherwise} \,, \end{cases} \tag{2.176}$$

where t^p is a constant for each acting force point p. The remaining external momentums are

$$M_1^{\text{external}} = \int \varepsilon_{132} x_3 t_2 \,\mathrm{d}A = \int -x_3 t_2 \,\mathrm{d}A = \int \varepsilon_{132} x_3 t_2 \,\mathrm{d}A = \int -x_3 t_2 \,\mathrm{d}x_1 \,\mathrm{d}x_3 =$$

$$= \sum_{p=1}^{N} \int_{-\frac{w}{2}}^{\frac{w}{2}} \int_{x^p - \frac{d}{2}}^{x^p + \frac{d}{2}} -x_3 t^p \,\mathrm{d}x_1 \,\mathrm{d}x_3 = \sum_{p=1}^{N} -\frac{1}{2} \underbrace{\left[{x_3}^2\right]_{-\frac{w}{2}}^{\frac{w}{2}}}_{=0} t^p d = 0 \,. \tag{2.177}$$

and

$$M_3^{\text{external}} = \int \varepsilon_{312} x_1 t_2 \,\mathrm{d}A = \int x_1 t_2 \,\mathrm{d}A = \int x_1 t_2 \,\mathrm{d}x_1 \,\mathrm{d}x_3 =$$

$$= \sum_{p=1}^{N} \int_{-\frac{w}{2}}^{\frac{w}{2}} \int_{x^p-\frac{d}{2}}^{x^p+\frac{d}{2}} x_1 t^p \, \mathrm{d}x_1 \, \mathrm{d}x_3 = \sum_{p=1}^{N} x^p \underbrace{t^p dw}_{=F^p} = \sum_{p=1}^{N} x^p F^p \,. \tag{2.178}$$

We obtain the momentum equilibrium for the Euler-Bernoulli beam as follows

$$0 = M_3^{\text{internal}} + M_3^{\text{external}} = EI_{22} \frac{\partial^2 u}{\partial {x_1}^2} + \sum_{p=1}^{N} x^p F^p \,. \tag{2.179}$$

For $k = 1$ and $k = 2$ momentum equilibrium are fulfilled without contradiction. The bending moment M in dependence of position x_1 is determined as resistive moment of the external momentum M_3^{external} at sectioning point x_1. Each moment lever arm x^p is computed by the distance between the imaginary cut position x_1 and the force acting point $\breve{x}_p$

$$x^p = x_1 - \breve{x}^p \,. \tag{2.180}$$

The bending moment is computed as follows

$$M_3^{\text{external}} = \sum_{p=1}^{N} x^p F^p = \sum_{p=1}^{N} \big(x_1 - \breve{x}^p\big) F^p = \breve{M}\big(x_1\big) = M \,. \tag{2.181}$$

We rewrite the momentum equilibrium in the form known as the Euler-Bernoulli beam equation

$$EI_{22} \frac{\partial^2 u}{\partial {x_1}^2} = -M \,. \tag{2.182}$$

2.5.3 Heat Equation

To examine a solid which is heated solely by thermal conduction and radiation, the temperature distribution within its body is computed (cf. W. H. Müller 2014, pp. 176–178). Observe the local balance of internal energy in Eq. (2.125) where we exclude rotational influences

$$\varrho \frac{\mathrm{d}u}{\mathrm{d}t} = -\frac{\partial q_i}{\partial x_i} + \varrho r + \frac{\partial v_i}{\partial x_j} \sigma_{ij} \,. \tag{2.125}$$

We assume that the internal energy is completely determined by the state variables specific entropy s and linear strain ε_{kl}

$$u = \breve{u}\big(s, \varepsilon_{kl}\big) \,. \tag{2.183}$$

The total differential of internal energy leads to

$$\mathrm{d}u = \frac{\partial u}{\partial s} \, \mathrm{d}s + \frac{\partial u}{\partial \varepsilon_{kl}} \, \mathrm{d}\varepsilon_{kl} = T \, \mathrm{d}s + \frac{1}{\varrho} \sigma_{kl} \, \mathrm{d}\varepsilon_{kl} \,, \tag{2.184}$$

where by means of Gibbs' equation the partial derivatives are identified as $\frac{\partial u}{\partial s} = T$ and $\frac{\partial u}{\partial \varepsilon_{kl}} = \frac{1}{\varrho} \sigma_{kl}$. Since the specific entropy is irrelevant, the dependency of the internal energy has to be converted

$$u = \breve{u}\big(s, \varepsilon_{kl}\big) \;\longrightarrow\; u = \breve{u}\big(T, \varepsilon_{kl}\big) \,. \tag{2.185}$$

This is obtained by assuming that for solids the specific entropy is completely determined by the state variables temperature and linear strain

$$s = \breve{s}\big(T, \varepsilon_{kl}\big) \,. \tag{2.186}$$

The total differential of specific entropy is

$$\mathrm{d}s = \frac{\partial s}{\partial T} \, \mathrm{d}T + \frac{\partial s}{\partial \varepsilon_{kl}} \, \mathrm{d}\varepsilon_{kl} \,. \tag{2.187}$$

Inserting the above equation into the GIBBS' equation in Eq. (2.184), we find the internal energy with the dependency of temperature and linear strain on right-hand side as follows

$$\mathrm{d}u = T\frac{\partial s}{\partial T}\,\mathrm{d}T + T\frac{\partial s}{\partial \varepsilon_{kl}}\,\mathrm{d}\varepsilon_{kl} + \frac{1}{\varrho}\sigma_{kl}\,\mathrm{d}\varepsilon_{kl} = T\frac{\partial s}{\partial T}\,\mathrm{d}T + \left(T\frac{\partial s}{\partial \varepsilon_{kl}} + \frac{1}{\varrho}\sigma_{kl}\right)\mathrm{d}\varepsilon_{kl}\,. \tag{2.188}$$

The left-hand side of the equation above can now be rewritten as

$$\mathrm{d}u = \frac{\partial u}{\partial T}\,\mathrm{d}T + \frac{\partial u}{\partial \varepsilon_{kl}}\,\mathrm{d}\varepsilon_{kl} \tag{2.189}$$

and we find

$$\frac{\partial u}{\partial T}\,\mathrm{d}T + \frac{\partial u}{\partial \varepsilon_{kl}}\,\mathrm{d}\varepsilon_{kl} = T\frac{\partial s}{\partial T}\,\mathrm{d}T + \left(T\frac{\partial s}{\partial \varepsilon_{kl}} + \frac{1}{\varrho}\sigma_{kl}\right)\mathrm{d}\varepsilon_{kl}\,. \tag{2.190}$$

The first partial derivative on the left-hand side is identified as the heat capacity at constant linear strain which obeys the law of DULONG-PETIT law in Eq. (2.157)

$$\frac{\partial u}{\partial T} = c_{\varepsilon_{kl}}\,. \tag{2.191}$$

To identify the second derivative $\frac{\partial u}{\partial \varepsilon_{kl}}$, we equate the coefficients to obtain

$$\frac{\partial u}{\partial T} = T\frac{\partial s}{\partial T} \qquad \text{and} \tag{2.192}$$

$$\frac{\partial u}{\partial \varepsilon_{kl}} = T\frac{\partial s}{\partial \varepsilon_{kl}} + \frac{1}{\varrho}\sigma_{kl}\,. \tag{2.193}$$

A mutual differentiation is applied on the above equations by differentiating the first one with respect to linear strain and the second one with respect to temperature

$$\frac{\partial^2 u}{\partial \varepsilon_{kl}\partial T} = T\frac{\partial^2 s}{\partial \varepsilon_{kl}\partial T} \qquad \text{and} \tag{2.194}$$

$$\frac{\partial^2 u}{\partial T\partial \varepsilon_{kl}} = \frac{\partial s}{\partial \varepsilon_{kl}} + T\frac{\partial^2 s}{\partial T\partial \varepsilon_{kl}} + \frac{1}{\varrho}\frac{\partial \sigma_{kl}}{\partial T}\,. \tag{2.195}$$

Subtracting the second equation with the first one, we have

$$\frac{\partial s}{\partial \varepsilon_{kl}} = -\frac{1}{\varrho}\frac{\partial \sigma_{kl}}{\partial T}\,. \tag{2.196}$$

By inserting the above relation into Eq. (2.193), the second derivative is found

$$\frac{\partial u}{\partial \varepsilon_{kl}} = -\frac{T}{\varrho}\frac{\partial \sigma_{kl}}{\partial T} + \frac{1}{\varrho}\sigma_{kl}\,. \tag{2.197}$$

Substitute both derivatives, Eq. (2.191) and Eq. (2.197), into Eq. (2.189) for left-hand side of the local balance of total energy in Eq. (2.125) gives

$$\varrho c_{\varepsilon_{kl}}\frac{\mathrm{d}T}{\mathrm{d}t} - T\frac{\partial \sigma_{kl}}{\partial T}\frac{\mathrm{d}\varepsilon_{kl}}{\mathrm{d}t} + \sigma_{kl}\frac{\mathrm{d}\varepsilon_{kl}}{\mathrm{d}t} = -\frac{\partial q_j}{\partial x_j} + \varrho r + \frac{\partial v_i}{\partial x_j}\sigma_{ij}\,. \tag{2.198}$$

The third expression on the left-hand side can be rewritten as

$$\sigma_{kl}\frac{\mathrm{d}\varepsilon_{kl}}{\mathrm{d}t} = \sigma_{kl}\frac{\mathrm{d}}{\mathrm{d}t}\left(\frac{1}{2}\left(\frac{\partial u_k}{\partial x_l} + \frac{\partial u_l}{\partial x_k}\right)\right) = \frac{1}{2}\sigma_{kl}\frac{\mathrm{d}}{\mathrm{d}t}\left(\frac{\partial u_k}{\partial x_l}\right) + \frac{1}{2}\underbrace{\sigma_{kl}}_{=\sigma_{lk}}\frac{\mathrm{d}}{\mathrm{d}t}\left(\frac{\partial u_k}{\partial x_l}\right) =$$

$$= \sigma_{kl}\frac{\mathrm{d}}{\mathrm{d}t}\left(\frac{\partial u_k}{\partial x_l}\right) = \sigma_{kl}\frac{\partial}{\partial t}\left(\frac{\partial u_k}{\partial x_l}\right) + \sigma_{kl}\frac{\partial}{\partial x_m}\left(\frac{\partial u_k}{\partial x_l}\right)v_m =$$

$$= \sigma_{kl}\left(\frac{\partial^2 u_k}{\partial t \partial x_l} + \frac{\partial^2 u_k}{\partial x_m \partial x_l} v_m\right) = \sigma_{kl}\frac{\partial}{\partial x_l}\left(\frac{\partial u_k}{\partial t} + \frac{\partial u_k}{\partial x_m} v_m\right) =$$
$$= \sigma_{kl}\frac{\partial}{\partial x_l}\left(\frac{\mathrm{d}u_k}{\mathrm{d}t}\right) = \sigma_{kl}\frac{\partial}{\partial x_l}\left(\frac{\mathrm{d}}{\mathrm{d}t}(x_k - X_k)\right) = \sigma_{kl}\frac{\partial}{\partial x_l}\left(\frac{\mathrm{d}x_k}{\mathrm{d}t}\right) = \sigma_{kl}\frac{\partial v_k}{\partial x_l} \tag{2.199}$$

and is recognized as the production term of internal energy. It cancels the third expression on the right-hand side out. Then, the heat equation reads

$$\varrho c_{\varepsilon_{kl}} \frac{\mathrm{d}T}{\mathrm{d}t} = -\frac{\partial q_j}{\partial x_j} + \varrho r + T\frac{\partial \sigma_{kl}}{\partial T}\frac{\mathrm{d}\varepsilon_{kl}}{\mathrm{d}t} \,. \tag{2.200}$$

Applying the Fourier's law for heat conduction q_j in Eq. (2.158) with constant thermal conductivity κ as well as the Hooke's law for the stress tensor σ_{kl} in Eq. (2.140), we find

$$\varrho c_{\varepsilon_{kl}} \frac{\mathrm{d}T}{\mathrm{d}t} = \kappa \frac{\partial^2 T}{\partial x_j \partial x_j} + \varrho r - T C_{klij}\alpha_{ij}\frac{\mathrm{d}\varepsilon_{kl}}{\mathrm{d}t} \,. \tag{2.201}$$

A special case is where the solid is at rest $v_j = 0$. For this, the material time derivative is applied for the temporal change of temperature on the left-hand side

$$\frac{\mathrm{d}T}{\mathrm{d}t} = \frac{\partial T}{\partial t} + \frac{\partial T}{\partial x_j} v_j \tag{2.202}$$

and the thermal expansion on right-hand side

$$\frac{\mathrm{d}\varepsilon_{kl}}{\mathrm{d}t} = \frac{\partial \varepsilon_{kl}}{\partial t} + \frac{\partial \varepsilon_{kl}}{\partial x_j} v_j \,. \tag{2.203}$$

This in turn yields

$$\varrho c_{\varepsilon_{kl}} \frac{\partial T}{\partial t} = \kappa \frac{\partial^2 T}{\partial x_j \partial x_j} + \varrho r - T C_{klij}\alpha_{ij}\frac{\partial \varepsilon_{kl}}{\partial t} \,. \tag{2.204}$$

For isotropic materials in Eq. (2.146), we obtain

$$\varrho c_{\varepsilon_{kl}} \frac{\partial T}{\partial t} = \kappa \frac{\partial^2 T}{\partial x_j \partial x_j} + \varrho r - T(3\lambda + 2\mu)\alpha\frac{\partial \varepsilon_{kk}}{\partial t} \,. \tag{2.205}$$

Further simplification is obtained by assuming that the process of thermal expansion is slow, thus the effect of the strain rate can be neglected. This gives

$$\varrho c_{\varepsilon_{kl}} \frac{\partial T}{\partial t} = \kappa \frac{\partial^2 T}{\partial x_j \partial x_j} + \varrho r \,. \tag{2.206}$$

2.6 Numerical Treatment with Finite Element Method

Continuum mechanics serves as the basic to cover the thermomechanical modelling of an engineering problem. The model has to describe the task as close to reality as possible, but on condition that the task can be accomplished in a feasible manner. Therefore, whenever it is possible one has to simplify the model by using admissible assumptions. We end up with the field equations that describe the problem in form of partial differential equations. In this formulation, we find the relationship between the derivatives of the responses and material constants. However, we are more interested in the direct dependency between the responses and the material-specific parameters. And that is the solutions of the differential equations. For certain classes of differential equations, their unique solution is known to exist and can be obtained by taking into account the problem-specific geometry, initial and boundary conditions. Still, it is not always possible to determine a close-form solution for it. This is often the case for complex-shaped structures made of non-linear materials. Consequently, it is more convenient to approximate the solution by applying a numerical method like, for instance, finite element method.

The finite element method is mainly applied to second order partial differential equations of elliptic, parabolic or hyperbolic type. This method transforms partial differential equations into a system of linear equations by subdividing the whole structure into parts with simpler shape, which are called elements. The response behaviour of each element is then approximated by a function such as polynomial function. Thus, the summation over all elements yields the numerical solution. A profound introduction to finite element method is provided by the standard text books by, for example, (Zienkiewicz et al. 2013) and (Strang and Fix 2008).

For a numerical treatment of the field equations with finite element method, we follow the procedure that is known as the Ritz-Galerkin method in mechanics. Although, according to Gander and Wanner (2012), Galerkin (1915) himself refer this method as Ritz method that is published in (Ritz 1908) and (Ritz 1909). Firstly, we convert the differential equations into their *variational form* as follows. Each differential equation is multiplied by a so-called *test function* that is associated with the primary response variable in the field equation. The at least once differentiable test functions are arbitrary but compatible. To fulfil the compatibility, the test functions have to vanish at Dirichlet boundaries. In this area, the primary response variables take given values as conditions. Furthermore, in regard of compatibility, the capability to assemble a square matrix at the end has to be guaranteed by the choice of suitable function to approximate the test functions. Then, we integrate over the whole body. Using integration by parts, the order of spatial differentiation in the integral is reduced. At this end, we find the variational formulation of the field equations. Secondly, the complete structure is discretised into a finite number of elements. Finally, for each element, we approximate its response by a polynomial function. Thus, the sum of all polynomial functions represents the approximated response of the whole structure. Since the test function is associated with the response, we chose the same polynomial function as for the response to approximate the test function. Additionally to Ritz-Galerkin method, considerations are required for dealing with transient part in the variational formulation and numerical integration.

From Secs. 2.6.1 to 2.6.8, we apply the finite element method to the elastodynamic field equations to show a step-by-step work flow to transform hyperbolic partial differential equations to a system of linear equations. For this purpose, linear tetrahedron elements are used. In Sec. 2.6.9, it is shown how non-linear finite elements can be utilised. To this end, we apply the finite element method for non-linear elements to Euler-Bernoulli beam equation.

2.6.1 Variational Formulation

The first step of applying of the Ritz-Galerkin method is to reformulate the field equations into their variational form. Consider the elastodynamic equations in Eq. (2.161), uncoupled from the temperature field,

$$\varrho \frac{\mathrm{d}^2 u_i}{\mathrm{d}t^2} = C_{ijkl} \frac{\partial^2 u_k}{\partial x_j \partial x_l} + \varrho f_i \,, \tag{2.207}$$

where the mass density ϱ and the specific volume force f_i are given as constants. The primary response variable is the displacement u_i. Therefore, we multiply each equation by its associated test function δu_i and obtain after integration over the whole body

$$\int \varrho \delta u_i \frac{\mathrm{d}^2 u_i}{\mathrm{d}t^2} \,\mathrm{d}V = \int \delta u_i C_{ijkl} \frac{\partial^2 u_k}{\partial x_j \partial x_l} \,\mathrm{d}V + \int \varrho \delta u_i f_i \,\mathrm{d}V \,. \tag{2.208}$$

The transient part is on the left-hand side of above equation. The temporal differentiation can be approximated with the *finite difference method*

$$\frac{\mathrm{d}^2 u_i}{\mathrm{d}t^2} \approx \frac{u_i - 2u_i^{t-1} + u_i^{t-2}}{\Delta t^2} \,, \tag{2.209}$$

where $t-1$ and $t-2$ denote the previous and pre-previous time step. The first expression on the right-hand side is the elliptic part. By applying integration by parts, the order of spatial differentiation of the displacement u_k can be reduced by increasing the order of spatial differentiation of the test function δu_i as follows

$$\int C_{ijkl} \frac{\partial}{\partial x_j} \left(\delta u_i \frac{\partial u_k}{\partial x_l} \right) \mathrm{d}V = \int \delta u_i C_{ijkl} \frac{\partial^2 u_k}{\partial x_j \partial x_l} \,\mathrm{d}V + \int C_{ijkl} \frac{\partial \delta u_i}{\partial x_j} \frac{\partial u_k}{\partial x_l} \,\mathrm{d}V \,. \tag{2.210}$$

Furthermore, the term on the left-hand side of above equation can be rewritten as

$$\int C_{ijkl} \frac{\partial}{\partial x_j} \left(\delta u_i \frac{\partial u_k}{\partial x_l} \right) \mathrm{d}V = \int \delta u_i C_{ijkl} \frac{\partial u_k}{\partial x_l} n_j \, \mathrm{d}A = \int \delta u_i t_i \, \mathrm{d}A \,, \tag{2.211}$$

where the GAUSS theorem of Eq. (2.37) is used followed by Eq. (2.159), the HOOKE's law in Eq. (2.136) and the traction in Eq. (2.55). The variational form of the elastodynamic equations in Eq. (2.207) is

$$\begin{aligned} &\int \varrho \delta u_i \frac{u_i - 2u_i^{t-1} + u_i^{t-2}}{\Delta t^2} \mathrm{d}V = \\ &= -\int C_{ijkl} \frac{\partial \delta u_i}{\partial x_j} \frac{\partial u_k}{\partial x_l} \mathrm{d}V + \int \delta u_i t_i \, \mathrm{d}A + \int \varrho \delta u_i f_i \, \mathrm{d}V \,. \end{aligned} \tag{2.212}$$

The variational form can be further rearranged as

$$\begin{aligned} &\int \frac{\varrho}{\Delta t^2} \delta u_i u_i \, \mathrm{d}V + \int C_{ijkl} \frac{\partial \delta u_i}{\partial x_j} \frac{\partial u_k}{\partial x_l} \mathrm{d}V = \\ &= \int \frac{\varrho}{\Delta t^2} \delta u_i \left(2u_i^{t-1} - u_i^{t-2} \right) \mathrm{d}V + \int \delta u_i t_i \, \mathrm{d}A + \int \varrho \delta u_i f_i \, \mathrm{d}V \,. \end{aligned} \tag{2.213}$$

In this arrangement, we have a first glance on the final form of the finite element approach. The method transforms the partial differential equations into linear algebraic systems that then can be solved with known algorithm such as Gaussian elimination. The expressions of the left-side hand side becomes the so-called *stiffness matrix* and *displacement vector*. The terms on the right-hand side lead to the so-called *load vector* and contain the natural (first and last terms) and NEUMANN boundary conditions (second terms).

2.6.2 Discretisation in Linear Tetrahedron Elements

The complete body is discretised into a finite number of elements N. Here, we explicitly use tetrahedron elements for 3-D problems. The presented approach is also applicable for triangular elements for 2-D problems and straight elements for 1-D problems. Every element and every node have to be uniquely identified. Therefore, each node ν and each element ζ are numbered with natural numbers, where n is the number of nodes and N is the number of elements. The unique identifier and the coordinate of each node, as well as the identification number and the corner nodes for each element can be stored in tables, e. g.,

ν	x_1	x_2	x_3
1			
$\vdots$			
n			

and

ζ	ν_1	ν_2	ν_3	ν_4
1				
$\vdots$				
N				

.

2.6.3 Approximation with Linear Functions

The displacement field ${}^{\zeta}u_k$ within each element ζ can be approximated with a linear function such as

$${}^{\zeta}u_k \approx {}^{\zeta}a_0 + {}^{\zeta}a_1 x_1 + {}^{\zeta}a_2 x_2 + {}^{\zeta}a_3 x_3 \tag{2.214}$$

in such a way that the sum of all linear functions yields the approximated displacement field

$$u_k \approx \sum_{\zeta=1}^{N} {}^{\zeta}u_k \,, \tag{2.215}$$

where the scalar valued constants ${}^{\zeta}a_0$, ${}^{\zeta}a_1$, ${}^{\zeta}a_2$, ${}^{\zeta}a_3$ are the coefficients of the linear function. But, it is a frequent practice in finite element method that the linear function in Eq. (2.214) is rewritten, so that

$${}^{\zeta}a_0 + {}^{\zeta}a_1 x_1 + {}^{\zeta}a_2 x_2 + {}^{\zeta}a_3 x_3 = {}_{\nu_1}{}^{\zeta}u_k \, {}^{\zeta}\xi_{\nu_1} + {}_{\nu_2}{}^{\zeta}u_k \, {}^{\zeta}\xi_{\nu_2} + {}_{\nu_3}{}^{\zeta}u_k \, {}^{\zeta}\xi_{\nu_3} + {}_{\nu_4}{}^{\zeta}u_k \, {}^{\zeta}\xi_{\nu_4} \,, \tag{2.216}$$

where the coefficients ${}^{\zeta}_{\nu_1}u_k$, ${}^{\zeta}_{\nu_2}u_k$, ${}^{\zeta}_{\nu_3}u_k$, ${}^{\zeta}_{\nu_4}u_k$ correspond to displacement values at the corner points of each element ζ with ${}^{\zeta}\xi_{\nu_1}$, ${}^{\zeta}\xi_{\nu_2}$, ${}^{\zeta}\xi_{\nu_3}$ and ${}^{\zeta}\xi_{\nu_4}$ as their basis functions. The advantage of rewriting the polynomial functions is that the converted set of coefficients $\left({}^{\zeta}_{\nu_1}u_k, {}^{\zeta}_{\nu_2}u_k, {}^{\zeta}_{\nu_3}u_k, {}^{\zeta}_{\nu_4}u_k\right)$ are the sought values at that positions. Meanwhile, using the original set of coefficients $\left({}^{\zeta}a_0, {}^{\zeta}a_1, {}^{\zeta}a_2, {}^{\zeta}a_3\right)$ in Eq. (2.214), the displacement value for a specific position has to be computed once the original set of coefficients is determined. To rewrite the expression as shown in the above equation, we write

$$
\begin{aligned}
{}^{\zeta}_{\nu_1}u_k &= {}^{\zeta}a_0 + {}^{\zeta}a_1 {}^{\zeta}_{\nu_1}x_1 + {}^{\zeta}a_2 {}^{\zeta}_{\nu_1}x_2 + {}^{\zeta}a_3 {}^{\zeta}_{\nu_1}x_3 \\
{}^{\zeta}_{\nu_2}u_k &= {}^{\zeta}a_0 + {}^{\zeta}a_1 {}^{\zeta}_{\nu_2}x_1 + {}^{\zeta}a_2 {}^{\zeta}_{\nu_2}x_2 + {}^{\zeta}a_3 {}^{\zeta}_{\nu_2}x_3 \\
{}^{\zeta}_{\nu_3}u_k &= {}^{\zeta}a_0 + {}^{\zeta}a_1 {}^{\zeta}_{\nu_3}x_1 + {}^{\zeta}a_2 {}^{\zeta}_{\nu_3}x_2 + {}^{\zeta}a_3 {}^{\zeta}_{\nu_3}x_3 \\
{}^{\zeta}_{\nu_4}u_k &= {}^{\zeta}a_0 + {}^{\zeta}a_1 {}^{\zeta}_{\nu_4}x_1 + {}^{\zeta}a_2 {}^{\zeta}_{\nu_4}x_2 + {}^{\zeta}a_3 {}^{\zeta}_{\nu_4}x_3 \,,
\end{aligned}
\tag{2.217}
$$

where the coordinates ${}^{\zeta}_{\nu_z}x_1$, ${}^{\zeta}_{\nu_z}x_2$, ${}^{\zeta}_{\nu_z}x_3$ of the four corner nodes ($z = 1, 2, 3, 4$) forming a tetrahedron element ζ are inserted in the left-hand side of Eq. (2.216). At each of the corners z, the linear function takes the displacement value ${}^{\zeta}_{\nu_z}u_k$. It is helpful to use matrix notation for Eq. (2.217)

$$
\begin{bmatrix} {}^{\zeta}_{\nu_1}u_k \\ {}^{\zeta}_{\nu_2}u_k \\ {}^{\zeta}_{\nu_3}u_k \\ {}^{\zeta}_{\nu_4}u_k \end{bmatrix} = \begin{bmatrix} 1 & {}^{\zeta}_{\nu_1}x_1 & {}^{\zeta}_{\nu_1}x_2 & {}^{\zeta}_{\nu_1}x_3 \\ 1 & {}^{\zeta}_{\nu_2}x_1 & {}^{\zeta}_{\nu_2}x_2 & {}^{\zeta}_{\nu_2}x_3 \\ 1 & {}^{\zeta}_{\nu_3}x_1 & {}^{\zeta}_{\nu_3}x_2 & {}^{\zeta}_{\nu_3}x_3 \\ 1 & {}^{\zeta}_{\nu_4}x_1 & {}^{\zeta}_{\nu_4}x_2 & {}^{\zeta}_{\nu_4}x_3 \end{bmatrix} \begin{bmatrix} {}^{\zeta}a_0 \\ {}^{\zeta}a_1 \\ {}^{\zeta}a_2 \\ {}^{\zeta}a_3 \end{bmatrix}
\tag{2.218}
$$

and for Eq. (2.216)

$$
\begin{bmatrix} 1 & x_1 & x_2 & x_3 \end{bmatrix} \begin{bmatrix} {}^{\zeta}a_0 \\ {}^{\zeta}a_1 \\ {}^{\zeta}a_2 \\ {}^{\zeta}a_3 \end{bmatrix} = \begin{bmatrix} {}^{\zeta}\xi_{\nu_1} & {}^{\zeta}\xi_{\nu_2} & {}^{\zeta}\xi_{\nu_3} & {}^{\zeta}\xi_{\nu_4} \end{bmatrix} \begin{bmatrix} {}^{\zeta}_{\nu_1}u_k \\ {}^{\zeta}_{\nu_2}u_k \\ {}^{\zeta}_{\nu_3}u_k \\ {}^{\zeta}_{\nu_4}u_k \end{bmatrix} .
\tag{2.219}
$$

Substituting Eq. (2.218) into Eq. (2.219), we have after equating coefficients

$$
\begin{bmatrix} 1 \\ x_1 \\ x_2 \\ x_3 \end{bmatrix} = \begin{bmatrix} 1 & 1 & 1 & 1 \\ {}^{\zeta}_{\nu_1}x_1 & {}^{\zeta}_{\nu_2}x_1 & {}^{\zeta}_{\nu_3}x_1 & {}^{\zeta}_{\nu_4}x_1 \\ {}^{\zeta}_{\nu_1}x_2 & {}^{\zeta}_{\nu_2}x_2 & {}^{\zeta}_{\nu_3}x_2 & {}^{\zeta}_{\nu_4}x_2 \\ {}^{\zeta}_{\nu_1}x_3 & {}^{\zeta}_{\nu_2}x_3 & {}^{\zeta}_{\nu_3}x_3 & {}^{\zeta}_{\nu_4}x_3 \end{bmatrix} \begin{bmatrix} {}^{\zeta}\xi_{\nu_1} \\ {}^{\zeta}\xi_{\nu_2} \\ {}^{\zeta}\xi_{\nu_3} \\ {}^{\zeta}\xi_{\nu_4} \end{bmatrix} .
\tag{2.220}
$$

The above matrix equation shows the conversion between normalized Barycentric (or Areal) and Cartesian coordinates

$$
\begin{bmatrix} x_1 \\ x_2 \\ x_3 \end{bmatrix} = {}^{\zeta}\xi_{\nu_1} \begin{bmatrix} {}^{\zeta}_{\nu_1}x_1 \\ {}^{\zeta}_{\nu_1}x_2 \\ {}^{\zeta}_{\nu_1}x_3 \end{bmatrix} + {}^{\zeta}\xi_{\nu_2} \begin{bmatrix} {}^{\zeta}_{\nu_2}x_1 \\ {}^{\zeta}_{\nu_2}x_2 \\ {}^{\zeta}_{\nu_2}x_3 \end{bmatrix} + {}^{\zeta}\xi_{\nu_3} \begin{bmatrix} {}^{\zeta}_{\nu_3}x_1 \\ {}^{\zeta}_{\nu_3}x_2 \\ {}^{\zeta}_{\nu_3}x_3 \end{bmatrix} + {}^{\zeta}\xi_{\nu_4} \begin{bmatrix} {}^{\zeta}_{\nu_4}x_1 \\ {}^{\zeta}_{\nu_4}x_2 \\ {}^{\zeta}_{\nu_4}x_3 \end{bmatrix}
\tag{2.221}
$$

with normalization relation

$$
1 = {}^{\zeta}\xi_{\nu_1} + {}^{\zeta}\xi_{\nu_2} + {}^{\zeta}\xi_{\nu_3} + {}^{\zeta}\xi_{\nu_4} \,.
\tag{2.222}
$$

The basis functions ${}^{\zeta}\xi_{\nu_1}$, ${}^{\zeta}\xi_{\nu_2}$, ${}^{\zeta}\xi_{\nu_3}$, ${}^{\zeta}\xi_{\nu_4}$ occur on the right-hand side in Eq. (2.216) are barycentric basis functions that can be determined as follows

$$
\begin{bmatrix} {}^{\zeta}\xi_{\nu_1} \\ {}^{\zeta}\xi_{\nu_2} \\ {}^{\zeta}\xi_{\nu_3} \\ {}^{\zeta}\xi_{\nu_4} \end{bmatrix} = \begin{bmatrix} 1 & 1 & 1 & 1 \\ {}^{\zeta}_{\nu_1}x_1 & {}^{\zeta}_{\nu_2}x_1 & {}^{\zeta}_{\nu_3}x_1 & {}^{\zeta}_{\nu_4}x_1 \\ {}^{\zeta}_{\nu_1}x_2 & {}^{\zeta}_{\nu_2}x_2 & {}^{\zeta}_{\nu_3}x_2 & {}^{\zeta}_{\nu_4}x_2 \\ {}^{\zeta}_{\nu_1}x_3 & {}^{\zeta}_{\nu_2}x_3 & {}^{\zeta}_{\nu_3}x_3 & {}^{\zeta}_{\nu_4}x_3 \end{bmatrix}^{-1} \begin{bmatrix} 1 \\ x_1 \\ x_2 \\ x_3 \end{bmatrix}
$$

$$= \begin{bmatrix} M_{11} & M_{12} & M_{13} & M_{14} \\ M_{21} & M_{22} & M_{23} & M_{24} \\ M_{31} & M_{32} & M_{33} & M_{34} \\ M_{41} & M_{42} & M_{43} & M_{44} \end{bmatrix} \begin{bmatrix} 1 \\ x_1 \\ x_2 \\ x_3 \end{bmatrix} . \tag{2.223}$$

Now the rewritten linear function with barycentric basis functions is applied to approximate the displacement field vector

$$u_k \approx \sum_{\zeta=1}^{N} {}^{\zeta}u_k = \sum_{\zeta=1}^{N} {}^{\zeta}_{\nu_1}u_k \, {}^{\zeta}\xi_{\nu_1} + {}^{\zeta}_{\nu_2}u_k \, {}^{\zeta}\xi_{\nu_2} + {}^{\zeta}_{\nu_3}u_k \, {}^{\zeta}\xi_{\nu_3} + {}^{\zeta}_{\nu_4}u_k \, {}^{\zeta}\xi_{\nu_4} . \tag{2.224}$$

Since the test function δu_i is associated with the displacement field u_k, we also approximate the test function with linear function with barycentric basis functions

$$\delta u_i \approx \sum_{\zeta=1}^{N} {}^{\zeta}\delta u_i = \sum_{\zeta=1}^{N} {}^{\zeta}_{\nu_1}\delta u_i \, {}^{\zeta}\xi_{\nu_1} + {}^{\zeta}_{\nu_2}\delta u_i \, {}^{\zeta}\xi_{\nu_2} + {}^{\zeta}_{\nu_3}\delta u_i \, {}^{\zeta}\xi_{\nu_3} + {}^{\zeta}_{\nu_4}\delta u_i \, {}^{\zeta}\xi_{\nu_4} . \tag{2.225}$$

As stated previously, the test function is arbitrary but compatible and at least once differentiable. Due to the use of linear functions with barycentric basis functions for the test function, the stated requirements are satisfied. Any linear function can be differentiated once. The test functions are arbitrary due to their coefficients that can take any values. In part for compatibility, the coefficients are able to vanish at DIRICHLET boundaries. The other part regarding the compatibility is that the outcome has to result in square matrices. We shall later see that it is true due to the approach to use the same form of the linear function as in the displacement field for the test function. Note that the coefficients for the displacement field approximation are treated as unknowns, while the coefficients of the test function are considered to be known.

2.6.4 Stiffness Matrix

Observe the second expression on the left-hand side of Eq. (2.213)

$$\begin{aligned} \int C_{ijkl} \frac{\partial \delta u_i}{\partial x_j} \frac{\partial u_k}{\partial x_l} \, \mathrm{d}V &\approx \sum_{\zeta=1}^{N} \int C_{ijkl} \frac{\partial^{\zeta} \delta u_i}{\partial x_j} \frac{\partial^{\zeta} u_k}{\partial x_l} \, \mathrm{d}^{\zeta}V = \\ &= \sum_{\zeta=1}^{N} C_{ijkl} \frac{\partial^{\zeta} \delta u_i}{\partial x_j} \frac{\partial^{\zeta} u_k}{\partial x_l} \int \mathrm{d}^{\zeta}V = \\ &= \sum_{\zeta=1}^{N} C_{ijkl} \frac{\partial^{\zeta} \delta u_i}{\partial x_j} \frac{\partial^{\zeta} u_k}{\partial x_l} {}^{\zeta}V , \end{aligned} \tag{2.226}$$

where we know that the elasticity tensor C_{ijkl} as well as the partial derivatives are constants. We substitute the displacement vector and its test functions with the approximation in Eq. (2.224) and in Eq. (2.225) and obtain for each tetrahedron element ζ

$$C_{ijkl} \frac{\partial^{\zeta} \delta u_i}{\partial x_j} \frac{\partial^{\zeta} u_k}{\partial x_l} {}^{\zeta}V = \sum_{m=1}^{4} \sum_{n=1}^{4} C_{ijkl} \, {}^{\zeta}_{\nu_m}\delta u_i \, {}^{\zeta}_{\nu_n}u_k \frac{\partial^{\zeta} \xi_{\nu_m}}{\partial x_j} \frac{\partial^{\zeta} \xi_{\nu_n}}{\partial x_l} {}^{\zeta}V = {}^{\zeta}\mathbf{u}^{\mathsf{T}} \, {}^{\zeta}\mathbf{K} \, {}^{\zeta}\boldsymbol{\delta}\mathbf{u} \, {}^{\zeta}V . \tag{2.227}$$

After the last equal sign, the matrix notation is introduced where

$${}^{\zeta}\mathbf{u}^{\mathsf{T}} = \begin{bmatrix} {}^{\zeta}_{\nu_1}u_k & {}^{\zeta}_{\nu_2}u_k & {}^{\zeta}_{\nu_3}u_k & {}^{\zeta}_{\nu_4}u_k \end{bmatrix} ,$$

$${}^{\zeta}\mathbf{K} = \begin{bmatrix} C_{ijkl} \frac{\partial^{\zeta} \xi_{\nu_1}}{\partial x_j} \frac{\partial^{\zeta} \xi_{\nu_1}}{\partial x_l} & C_{ijkl} \frac{\partial^{\zeta} \xi_{\nu_1}}{\partial x_j} \frac{\partial^{\zeta} \xi_{\nu_2}}{\partial x_l} & C_{ijkl} \frac{\partial^{\zeta} \xi_{\nu_1}}{\partial x_j} \frac{\partial^{\zeta} \xi_{\nu_3}}{\partial x_l} & C_{ijkl} \frac{\partial^{\zeta} \xi_{\nu_1}}{\partial x_j} \frac{\partial^{\zeta} \xi_{\nu_4}}{\partial x_l} \\ C_{ijkl} \frac{\partial^{\zeta} \xi_{\nu_2}}{\partial x_j} \frac{\partial^{\zeta} \xi_{\nu_1}}{\partial x_l} & C_{ijkl} \frac{\partial^{\zeta} \xi_{\nu_2}}{\partial x_j} \frac{\partial^{\zeta} \xi_{\nu_2}}{\partial x_l} & C_{ijkl} \frac{\partial^{\zeta} \xi_{\nu_2}}{\partial x_j} \frac{\partial^{\zeta} \xi_{\nu_3}}{\partial x_l} & C_{ijkl} \frac{\partial^{\zeta} \xi_{\nu_2}}{\partial x_j} \frac{\partial^{\zeta} \xi_{\nu_4}}{\partial x_l} \\ C_{ijkl} \frac{\partial^{\zeta} \xi_{\nu_3}}{\partial x_j} \frac{\partial^{\zeta} \xi_{\nu_1}}{\partial x_l} & C_{ijkl} \frac{\partial^{\zeta} \xi_{\nu_3}}{\partial x_j} \frac{\partial^{\zeta} \xi_{\nu_2}}{\partial x_l} & C_{ijkl} \frac{\partial^{\zeta} \xi_{\nu_3}}{\partial x_j} \frac{\partial^{\zeta} \xi_{\nu_3}}{\partial x_l} & C_{ijkl} \frac{\partial^{\zeta} \xi_{\nu_3}}{\partial x_j} \frac{\partial^{\zeta} \xi_{\nu_4}}{\partial x_l} \\ C_{ijkl} \frac{\partial^{\zeta} \xi_{\nu_4}}{\partial x_j} \frac{\partial^{\zeta} \xi_{\nu_1}}{\partial x_l} & C_{ijkl} \frac{\partial^{\zeta} \xi_{\nu_4}}{\partial x_j} \frac{\partial^{\zeta} \xi_{\nu_2}}{\partial x_l} & C_{ijkl} \frac{\partial^{\zeta} \xi_{\nu_4}}{\partial x_j} \frac{\partial^{\zeta} \xi_{\nu_3}}{\partial x_l} & C_{ijkl} \frac{\partial^{\zeta} \xi_{\nu_4}}{\partial x_j} \frac{\partial^{\zeta} \xi_{\nu_4}}{\partial x_l} \end{bmatrix} ,$$

$$
{}^{\zeta}\boldsymbol{\delta}\mathbf{u} = \begin{bmatrix} {}^{\zeta}_{\nu_1}\delta u_i \\ {}^{\zeta}_{\nu_2}\delta u_i \\ {}^{\zeta}_{\nu_3}\delta u_i \\ {}^{\zeta}_{\nu_4}\delta u_i \end{bmatrix} , \tag{2.228}
$$

where ${}^{\zeta}\mathbf{K}$, ${}^{\zeta}\mathbf{u}$, ${}^{\zeta}\boldsymbol{\delta}\mathbf{u}$ are the stiffness matrix, the displacement vector and the vector containing the coefficients of the test function of a single tetrahedron element ζ. Moreover, each entry in the above stiffness matrix ${}^{\zeta}\mathbf{K}$ contains a 3×3 sub-matrix. Therefore, the total size of the stiffness matrix ${}^{\zeta}\mathbf{K}$ is 12×12. Likewise, the size of the vectors ${}^{\zeta}\mathbf{u}$ and ${}^{\zeta}\boldsymbol{\delta}\mathbf{u}$ is 12. An implementation in Python to generate the stiffness matrix ${}^{\zeta}\mathbf{K}$ of a single tetrahedron element ζ is given in Listing A.1.

2.6.5 Mass Matrix

Observe the first expression on the left-hand side of Eq. (2.213) that is approximated by a finite number of tetrahedron elements

$$
\int \frac{\varrho}{\Delta t^2}\delta u_i u_i \,\mathrm{d}V \approx \sum_{\zeta=1}^{N} \int \frac{\varrho}{\Delta t^2}\,{}^{\zeta}\delta u_i\,{}^{\zeta}u_i \,\mathrm{d}^{\zeta}V \,. \tag{2.229}
$$

For each tetrahedron element, we substitute the displacement vector and its test function with Eq. (2.224) and Eq. (2.225) and arrive at

$$
\begin{aligned}
\int \frac{\varrho}{\Delta t^2}\,{}^{\zeta}\delta u_i\,{}^{\zeta}u_i \,\mathrm{d}^{\zeta}V &= \int \frac{\varrho}{\Delta t^2}\left({}^{\zeta}_{\nu_1}\delta u_i\,{}^{\zeta}\xi_{\nu_1} + {}^{\zeta}_{\nu_2}\delta u_i\,{}^{\zeta}\xi_{\nu_2} + {}^{\zeta}_{\nu_3}\delta u_i\,{}^{\zeta}\xi_{\nu_3} + {}^{\zeta}_{\nu_4}\delta u_i\,{}^{\zeta}\xi_{\nu_4}\right) \\
&\qquad \left({}^{\zeta}_{\nu_1}u_i\,{}^{\zeta}\xi_{\nu_1} + {}^{\zeta}_{\nu_2}u_i\,{}^{\zeta}\xi_{\nu_2} + {}^{\zeta}_{\nu_3}u_i\,{}^{\zeta}\xi_{\nu_3} + {}^{\zeta}_{\nu_4}u_i\,{}^{\zeta}\xi_{\nu_4}\right) \mathrm{d}^{\zeta}V \\
&= {}^{\zeta}\mathbf{u}^{\mathsf{T}}\,{}^{\zeta}\mathbf{M}\,{}^{\zeta}\boldsymbol{\delta}\mathbf{u} \,.
\end{aligned} \tag{2.230}
$$

The matrix notation is used after the last equal sign and where the components of this equation are

$$
{}^{\zeta}\mathbf{u}^{\mathsf{T}} = \begin{bmatrix} {}^{\zeta}_{\nu_1}u_k & {}^{\zeta}_{\nu_2}u_k & {}^{\zeta}_{\nu_3}u_k & {}^{\zeta}_{\nu_4}u_k \end{bmatrix} ,
$$

$$
{}^{\zeta}\mathbf{M} = \begin{bmatrix}
m_{11} & & & m_{12} & & & m_{13} & & & m_{14} & & \\
 & m_{11} & & & m_{12} & & & m_{13} & & & m_{14} & \\
 & & m_{11} & & & m_{12} & & & m_{13} & & & m_{14} \\
m_{21} & & & m_{22} & & & m_{23} & & & m_{24} & & \\
 & m_{21} & & & m_{22} & & & m_{23} & & & m_{24} & \\
 & & m_{21} & & & m_{22} & & & m_{23} & & & m_{24} \\
m_{31} & & & m_{32} & & & m_{33} & & & m_{34} & & \\
 & m_{31} & & & m_{32} & & & m_{33} & & & m_{34} & \\
 & & m_{31} & & & m_{32} & & & m_{33} & & & m_{34} \\
m_{41} & & & m_{42} & & & m_{43} & & & m_{44} & & \\
 & m_{41} & & & m_{42} & & & m_{43} & & & m_{44} & \\
 & & m_{41} & & & m_{42} & & & m_{43} & & & m_{44}
\end{bmatrix}
$$

$$
\text{with } m_{mn} = \int \frac{\varrho}{\Delta t^2}\,{}^{\zeta}\xi_{\nu_m}\,{}^{\zeta}\xi_{\nu_n}\,\mathrm{d}^{\zeta}V \,,
$$

$$
{}^{\zeta}\boldsymbol{\delta}\mathbf{u} = \begin{bmatrix} {}^{\zeta}_{\nu_1}\delta u_i \\ {}^{\zeta}_{\nu_2}\delta u_i \\ {}^{\zeta}_{\nu_3}\delta u_i \\ {}^{\zeta}_{\nu_4}\delta u_i \end{bmatrix} . \tag{2.231}
$$

Here, for each tetrahedron element ζ, we define ${}^{\zeta}\mathbf{M}$ as mass matrix, and ${}^{\zeta}\mathbf{u}$ and ${}^{\zeta}\boldsymbol{\delta}\mathbf{u}$ are the displacement vector and the vector containing the coefficients of the test function. The 12×12 entries m_{mn} in the mass matrix ${}^{\zeta}\mathbf{M}$

can be computed by means of barycentric coordinates (cf. Deb 2006, pp. 346–348) as follows

$$m_{mn} = \int \frac{\varrho}{\Delta t^2} {}^{\zeta}\xi_{\nu_m} {}^{\zeta}\xi_{\nu_n} \,\mathrm{d}^{\zeta}V = \int_0^{a_3}\int_0^{a_2}\int_0^{a_1} \frac{\varrho}{\Delta t^2} {}^{\zeta}\xi_{\nu_m} {}^{\zeta}\xi_{\nu_n}\, 6\, {}^{\zeta}V \,\mathrm{d}{}^{\zeta}\xi_{\nu_1} \,\mathrm{d}{}^{\zeta}\xi_{\nu_2} \,\mathrm{d}{}^{\zeta}\xi_{\nu_3} \,, \tag{2.232}$$

where for $m, n = 1, 2, 3, 4$ the limits are $a_3 = 1$, $a_2 = 1 - {}^{\zeta}\xi_{\nu_3}$ and $a_1 = 1 - {}^{\zeta}\xi_{\nu_3} - {}^{\zeta}\xi_{\nu_2}$. Afterwards, the above expression can be computed by means of Gauss-Legendre quadrature as follows

$$\begin{aligned}
&\int_0^{a_3}\int_0^{a_2}\int_0^{a_1} \frac{\varrho}{\Delta t^2} {}^{\zeta}\xi_{\nu_m} {}^{\zeta}\xi_{\nu_n}\, 6\, {}^{\zeta}V \,\mathrm{d}{}^{\zeta}\xi_{\nu_1} \,\mathrm{d}{}^{\zeta}\xi_{\nu_2} \,\mathrm{d}{}^{\zeta}\xi_{\nu_3} = \\
&= \int_0^{a_3}\int_0^{a_2} \sum_r \frac{a_1}{2}\omega_r \frac{\varrho}{\Delta t^2} {}^{\zeta}\xi_{\nu_m} {}^{\zeta}\xi_{\nu_n}\, 6\, {}^{\zeta}V \Big|_{{}^{\zeta}\xi_{\nu_1} = \frac{a_1}{2} n_r + \frac{a_1}{2}} \,\mathrm{d}{}^{\zeta}\xi_{\nu_2} \,\mathrm{d}{}^{\zeta}\xi_{\nu_3} \\
&= \int_0^{a_3} \sum_q \sum_r \frac{a_2}{2}\omega_q \frac{a_1}{2}\omega_r \frac{\varrho}{\Delta t^2} {}^{\zeta}\xi_{\nu_m} {}^{\zeta}\xi_{\nu_n}\, 6\, {}^{\zeta}V \Big|_{{}^{\zeta}\xi_{\nu_2} = \frac{a_2}{2} n_q + \frac{a_2}{2}} \,\mathrm{d}{}^{\zeta}\xi_{\nu_3} \\
&= \sum_p \sum_q \sum_r \frac{a_3}{2}\omega_p \frac{a_2}{2}\omega_q \frac{a_1}{2}\omega_r \frac{\varrho}{\Delta t^2} {}^{\zeta}\xi_{\nu_m} {}^{\zeta}\xi_{\nu_n}\, 6\, {}^{\zeta}V \Big|_{{}^{\zeta}\xi_{\nu_3} = \frac{a_3}{2} n_p + \frac{a_3}{2}} \\
&= \sum_p \sum_q \sum_r a_3\omega_p a_2\omega_q a_1\omega_r \frac{\varrho}{\Delta t^2} {}^{\zeta}\xi_{\nu_m} {}^{\zeta}\xi_{\nu_n}\, \frac{3}{4}\, {}^{\zeta}V \,.
\end{aligned} \tag{2.233}$$

An implementation to generate the mass matrix ${}^{\zeta}\mathbf{M}$ of a single tetrahedron element ζ is provided in Listing A.2.

2.6.6 Load Vector

The evaluation of the three terms

$$\int \frac{\varrho}{\Delta t^2} \delta u_i \left(2u_i^{t-1} - u_i^{t-2}\right) \mathrm{d}V \,, \quad \int \delta u_i t_i \,\mathrm{d}A \text{ and } \int \varrho \delta u_i f_i \,\mathrm{d}V \tag{2.234}$$

on the right-hand side of Eq. (2.213) leads to the load vector. We observe that the first and third expressions are volume integrals. Hence, they can be evaluated with the same computational method that is described in the following section about load vector of volume forces. The second term is a surface integral and its calculation is presented in the following section about load vector of surface forces.

In order to evaluate the integrals, two aspects must be respected. Firstly, for convenient computation, the integrals have to be reformulated in barycentric coordinate system. For the reformulation, useful relations and proofs can be found in Eisenberg and Malvern (1973). Secondly, we obtain definite integrals that can be approximate numerically by means of Gaussian quadrature. More detailed information on quadrature can be obtained for example in Dasgupta (2006, pp. 238–244).

Load Vector of Volume Forces

To evaluate the third expression on the right-hand side of Eq. (2.213)

$$\int \varrho \delta u_i f_i \,\mathrm{d}V \approx \sum_{\zeta=1}^{N} \int \varrho^{\zeta} \delta u_i f_i \,\mathrm{d}^{\zeta}V \,, \tag{2.235}$$

we substitute the test functions δu_i with the approximation in Eq. (2.225). For each tetrahedron element ζ, we have

$$\int \varrho^{\zeta} \delta u_i f_i \,\mathrm{d}^{\zeta}V = \int \varrho \left({}^{\zeta}_{\nu_1}\delta u_i \, {}^{\zeta}\xi_{\nu_1} + {}^{\zeta}_{\nu_2}\delta u_i \, {}^{\zeta}\xi_{\nu_2} + {}^{\zeta}_{\nu_3}\delta u_i \, {}^{\zeta}\xi_{\nu_3} + {}^{\zeta}_{\nu_4}\delta u_i \, {}^{\zeta}\xi_{\nu_4} \right) f_i \,\mathrm{d}^{\zeta}V$$

$$= {}^{\zeta}\mathbf{f}_{f_i}^{\mathsf{T}}\,{}^{\zeta}\boldsymbol{\delta}\mathbf{u}\,, \tag{2.236}$$

where matrix notation is used after the last equal sign and where

$$\begin{aligned}
{}^{\zeta}\mathbf{f}_{f_i}^{\mathsf{T}} &= \begin{bmatrix} \int {}^{\zeta}\xi_{\nu_1}\,\varrho f_i\,\mathrm{d}^{\zeta}V & \int {}^{\zeta}\xi_{\nu_2}\,\varrho f_i\,\mathrm{d}^{\zeta}V & \int {}^{\zeta}\xi_{\nu_3}\,\varrho f_i\,\mathrm{d}^{\zeta}V & \int {}^{\zeta}\xi_{\nu_4}\,\varrho f_i\,\mathrm{d}^{\zeta}V \end{bmatrix}\,, \\
{}^{\zeta}\boldsymbol{\delta}\mathbf{u} &= \begin{bmatrix} {}^{\zeta}_{\nu_1}\delta u_i \\ {}^{\zeta}_{\nu_2}\delta u_i \\ {}^{\zeta}_{\nu_3}\delta u_i \\ {}^{\zeta}_{\nu_4}\delta u_i \end{bmatrix}\,.
\end{aligned} \tag{2.237}$$

The entries in the load vector for the long range forces ${}^{\zeta}\mathbf{f}_{f_i}^{\mathsf{T}}$ can be computed by means of barycentric coordinates (cf. Deb 2006, pp. 346–348) as follows

$$\int {}^{\zeta}\xi_{\nu_m}\,\varrho f_i\,\mathrm{d}^{\zeta}V = \int_0^{a_3}\int_0^{a_2}\int_0^{a_1} {}^{\zeta}\xi_{\nu_m}\,\varrho f_i\,6\,{}^{\zeta}V\,\mathrm{d}^{\zeta}\xi_{\nu_1}\,\mathrm{d}^{\zeta}\xi_{\nu_2}\,\mathrm{d}^{\zeta}\xi_{\nu_3}\,, \tag{2.238}$$

where for $m = 1, 2, 3, 4$ the limits are $a_3 = 1$, $a_2 = 1 - {}^{\zeta}\xi_{\nu_3}$ and $a_1 = 1 - {}^{\zeta}\xi_{\nu_3} - {}^{\zeta}\xi_{\nu_2}$. Then, the above expression can be approximated with Gauss-Legendre quadrature as follows

$$\begin{aligned}
&\int_0^{a_3}\int_0^{a_2}\int_0^{a_1} {}^{\zeta}\xi_{\nu_m}\,\varrho f_i\,6\,{}^{\zeta}V\,\mathrm{d}^{\zeta}\xi_{\nu_1}\,\mathrm{d}^{\zeta}\xi_{\nu_2}\,\mathrm{d}^{\zeta}\xi_{\nu_3} = \\
&\quad= \int_0^{a_3}\int_0^{a_2}\sum_r \frac{a_1}{2}\omega_r\,{}^{\zeta}\xi_{\nu_m}\,\varrho f_i\,6\,{}^{\zeta}V\Big|_{{}^{\zeta}\xi_{\nu_1}=\frac{a_1}{2}n_r+\frac{a_1}{2}}\,\mathrm{d}^{\zeta}\xi_{\nu_2}\,\mathrm{d}^{\zeta}\xi_{\nu_3} \\
&\quad= \int_0^{a_3}\sum_q\sum_r \frac{a_2}{2}\omega_q\frac{a_1}{2}\omega_r\,{}^{\zeta}\xi_{\nu_m}\,\varrho f_i\,6\,{}^{\zeta}V\Big|_{{}^{\zeta}\xi_{\nu_2}=\frac{a_2}{2}n_q+\frac{a_2}{2}}\,\mathrm{d}^{\zeta}\xi_{\nu_3} \\
&\quad= \sum_p\sum_q\sum_r \frac{a_3}{2}\omega_p\frac{a_2}{2}\omega_q\frac{a_1}{2}\omega_r\,{}^{\zeta}\xi_{\nu_m}\,\varrho f_i\,6\,{}^{\zeta}V\Big|_{{}^{\zeta}\xi_{\nu_3}=\frac{a_3}{2}n_p+\frac{a_3}{2}} \\
&\quad= \sum_p\sum_q\sum_r a_3\omega_p a_2\omega_q a_1\omega_r\,{}^{\zeta}\xi_{\nu_m}\,\varrho f_i\,\frac{3}{4}{}^{\zeta}V\,.
\end{aligned} \tag{2.239}$$

The implementation to compute the load vector for volume integral of a single tetrahedron is given in Listing A.3.

Mass Vector

The first term on the right-hand side of Eq. (2.213) can be evaluated in exactly the same fashion as for the volume forces. Instead of computing the integrand part ϱf_i, we can replace it by $\frac{\varrho}{\Delta t^2}\left(2u_i^{t-1} - u_i^{t-2}\right)$. We obtain

$$\int \frac{\varrho}{\Delta t^2}\delta u_i\left(2u_i^{t-1} - u_i^{t-2}\right)\mathrm{d}V \approx \sum_{\zeta=1}^{N}\int \frac{\varrho}{\Delta t^2}\,{}^{\zeta}\delta u_i\left(2u_i^{t-1} - u_i^{t-2}\right)\mathrm{d}^{\zeta}V\,, \tag{2.240}$$

where for each tetrahedron element we have

$$\int \frac{\varrho}{\Delta t^2}\,{}^{\zeta}\delta u_i\left(2u_i^{t-1} - u_i^{t-2}\right)\mathrm{d}^{\zeta}V = {}^{\zeta}\mathbf{f}_t^{\mathsf{T}}\,{}^{\zeta}\boldsymbol{\delta}\mathbf{u}\,. \tag{2.241}$$

Here we define ${}^{\zeta}\mathbf{f}_t^{\mathsf{T}}$ as mass vector and it can be implemented as shown in Listing A.3.

Load Vector of Surface Forces

To compute the second expression on the right-hand side of Eq. (2.213)

$$\int \delta u_i t_i \, \mathrm{d}A \approx \sum_{\zeta=1}^{N} \int {}^{\zeta}\delta u_i t_i \, \mathrm{d}^{\zeta}A \,, \tag{2.242}$$

we substitute the test functions δu_i with the approximation in Eq. (2.225). For each tetrahedron ζ, we write

$$\begin{aligned} \int {}^{\zeta}\delta u_i t_i \, \mathrm{d}^{\zeta}A &= \int \Big({}^{\zeta}_{\nu_1}\delta u_i \, {}^{\zeta}\xi_{\nu_1} + {}^{\zeta}_{\nu_2}\delta u_i \, {}^{\zeta}\xi_{\nu_2} + {}^{\zeta}_{\nu_3}\delta u_i \, {}^{\zeta}\xi_{\nu_3} + {}^{\zeta}_{\nu_4}\delta u_i \, {}^{\zeta}\xi_{\nu_4} \Big) t_i \, \mathrm{d}^{\zeta}A \\ &= {}^{\zeta}\mathbf{f}_{t_i}^{\mathsf{T}} \, {}^{\zeta}\boldsymbol{\delta}\mathbf{u} \,, \end{aligned} \tag{2.243}$$

where we use the matrix notation for

$$\begin{aligned} {}^{\zeta}\mathbf{f}_{t_i}^{\mathsf{T}} &= \begin{bmatrix} \int {}^{\zeta}\xi_{\nu_1} t_i \, \mathrm{d}^{\zeta}A & \int {}^{\zeta}\xi_{\nu_2} t_i \, \mathrm{d}^{\zeta}A & \int {}^{\zeta}\xi_{\nu_3} t_i \, \mathrm{d}^{\zeta}A & \int {}^{\zeta}\xi_{\nu_4} t_i \, \mathrm{d}^{\zeta}A \end{bmatrix} , \\ {}^{\zeta}\boldsymbol{\delta}\mathbf{u} &= \begin{bmatrix} {}^{\zeta}_{\nu_1}\delta u_i \\ {}^{\zeta}_{\nu_2}\delta u_i \\ {}^{\zeta}_{\nu_3}\delta u_i \\ {}^{\zeta}_{\nu_4}\delta u_i \end{bmatrix} . \end{aligned} \tag{2.244}$$

For each entry in the load vector for short-range forces ${}^{\zeta}\mathbf{f}_{t_i}^{\mathsf{T}}$, we can calculate it as follows

$$\int {}^{\zeta}\xi_{\nu_m} t_i \, \mathrm{d}^{\zeta}A = \int_0^{a_2} \int_0^{a_1} {}^{\zeta}\xi_{\nu_m} t_i 2 \, {}^{\zeta}A \, \mathrm{d}^{\zeta}\xi_{\nu_1} \, \mathrm{d}^{\zeta}\xi_{\nu_2} \,, \tag{2.245}$$

where for $m = 1, 2, 3, 4$ the limits are $a_2 = 1$ and $a_1 = 1 - {}^{\zeta}\xi_{\nu_2}$. Using Gauss-Legendre quadrature, we find the approximation for the definite integral

$$\begin{aligned} &\int_0^{a_2} \int_0^{a_1} {}^{\zeta}\xi_{\nu_m} t_i 2 \, {}^{\zeta}A \, \mathrm{d}^{\zeta}\xi_{\nu_1} \, \mathrm{d}^{\zeta}\xi_{\nu_2} = \\ &= \int_0^{a_2} \sum_q \frac{a_1}{2} \omega_q \, {}^{\zeta}\xi_{\nu_m} t_i 2 \, {}^{\zeta}A \Big|_{{}^{\zeta}\xi_{\nu_1} = \frac{a_1}{2} n_q + \frac{a_1}{2}} \mathrm{d}^{\zeta}\xi_{\nu_2} \\ &= \sum_p \sum_q \frac{a_2}{2} \omega_p \frac{a_1}{2} \omega_q \, {}^{\zeta}\xi_{\nu_m} t_i 2 \, {}^{\zeta}A \Big|_{{}^{\zeta}\xi_{\nu_2} = \frac{a_2}{2} n_p + \frac{a_2}{2}} \\ &= \sum_p \sum_q a_2 \omega_p a_1 \omega_q \, {}^{\zeta}\xi_{\nu_m} t_i \frac{1}{2} \, {}^{\zeta}A \,. \end{aligned} \tag{2.246}$$

The implementation to compute the load vector for surface integral is provided in Listing A.4.

2.6.7 Assembly

The assembly describes the process on how to build the stiffness matrix and load vector for the complete body from all its finite element parts. In our case, we claim that the condition of continuity has to be fulfilled. As a result, the nodes of each element serve as the connecting points of its neighbouring elements. Apart from this, some vertices are shared by many elements. Nevertheless, this information is stored in tables as shown in Sec. 2.6.2 and is used to assemble the stiffness matrix and load vector. The continuity condition can be seen as constraints and can be implemented by means of the Lagrangian multiplier method. But, it will considerably enlarge the stiffness matrix and hence the computational time is increased. Therefore, in practise, another approach is used. First, the

global stiffness matrix is initialised by defining a $m \times n$ matrix in which each entry contains a 3×3 zero sub-matrix. Afterwards, for each computed local stiffness matrix, its sub-matrices are assigned to the global stiffness matrix in accordance to the table. The table contains the global numbering of local nodes for all elements. In case of multiple assignment to an entry of the global stiffness matrix due to sharing of a single node with multiple elements, the sub-matrices are summed up. Similarly, the load vector is assembled following the same rules.

By inserting the Eq. (2.230) into Eq. (2.229), Eq. (2.227) into Eq. (2.226), Eq. (2.241) into Eq. (2.240), Eq. (2.236) into Eq. (2.235) and Eq. (2.243) into Eq. (2.242), we obtain

$$\begin{aligned}
\int \frac{\varrho}{\Delta t^2} \delta u_i u_i \, \mathrm{d}V &\approx \sum_{\zeta=1}^{N} {}^{\zeta}\mathbf{u}^{\mathsf{T}} {}^{\zeta}\mathbf{M} {}^{\zeta}\delta\mathbf{u} = \mathbf{u}^{\mathsf{T}}\mathbf{M}\delta\mathbf{u} \,, \\
\int C_{ijkl} \frac{\partial \delta u_i}{\partial x_j} \frac{\partial u_k}{\partial x_l} \, \mathrm{d}V &\approx \sum_{\zeta=1}^{N} {}^{\zeta}\mathbf{u}^{\mathsf{T}} {}^{\zeta}\mathbf{K} {}^{\zeta}\delta\mathbf{u} {}^{\zeta}V = \mathbf{u}^{\mathsf{T}}\mathbf{K}\delta\mathbf{u} \,, \\
\int \frac{\varrho}{\Delta t^2} \delta u_i \left(2u_i^{t-1} - u_i^{t-2}\right) \mathrm{d}V &\approx \sum_{\zeta=1}^{N} {}^{\zeta}\mathbf{f}_t^{\mathsf{T}} {}^{\zeta}\delta\mathbf{u} = \mathbf{f}_t^{\mathsf{T}}\delta\mathbf{u} \,, \\
\int \varrho \delta u_i f_i \, \mathrm{d}V &\approx \sum_{\zeta=1}^{N} {}^{\zeta}\mathbf{f}_{f_i}^{\mathsf{T}} {}^{\zeta}\delta\mathbf{u} = \mathbf{f}_{f_i}^{\mathsf{T}}\delta\mathbf{u} \,, \\
\int \delta u_i t_i \, \mathrm{d}A &\approx \sum_{\zeta=1}^{N} {}^{\zeta}\mathbf{f}_{t_i}^{\mathsf{T}} {}^{\zeta}\delta\mathbf{u} = \mathbf{f}_{t_i}^{\mathsf{T}}\delta\mathbf{u} \,,
\end{aligned} \tag{2.247}$$

where $\mathbf{M}, \mathbf{K}, \mathbf{u}, \mathbf{f}_t, \mathbf{f}_{f_i}, \mathbf{f}_{t_i}, \delta\mathbf{u}$ are the global variant of the mass matrix, the stiffness matrix, the displacement vector, the mass vector, the load vector for volume and surface forces and the vector containing the coefficients of the test function. The above equations are used to evaluate the expression in Eq. (2.213). Equating the coefficients by $\delta\mathbf{u}$ and transposing gives

$$\begin{aligned}
\mathbf{u}^{\mathsf{T}}\mathbf{M}\delta\mathbf{u} + \mathbf{u}^{\mathsf{T}}\mathbf{K}\delta\mathbf{u} &= \mathbf{f}_t^{\mathsf{T}}\delta\mathbf{u} + \mathbf{f}_{f_i}^{\mathsf{T}}\delta\mathbf{u} + \mathbf{f}_{t_i}^{\mathsf{T}}\delta\mathbf{u} \\
\mathbf{u}^{\mathsf{T}}\mathbf{M} + \mathbf{u}^{\mathsf{T}}\mathbf{K} &= \mathbf{f}_t^{\mathsf{T}} + \mathbf{f}_{f_i}^{\mathsf{T}} + \mathbf{f}_{t_i}^{\mathsf{T}} \\
\mathbf{u}^{\mathsf{T}}\left(\mathbf{M} + \mathbf{K}\right) &= \mathbf{f}^{\mathsf{T}} \\
\mathbf{u}^{\mathsf{T}}\mathbf{K}_t &= \mathbf{f}^{\mathsf{T}} \\
\mathbf{K}_t\mathbf{u} &= \mathbf{f} \,.
\end{aligned} \tag{2.248}$$

2.6.8 Incorporating the Dirichlet Boundary Conditions

The Dirichlet boundary conditions prescribe certain values that the solution has to take at the pre-specified boundaries. To incorporate the Dirichlet boundary conditions, we can also apply the Lagrangian multiplier method as the Dirichlet boundary conditions can be interpreted as constraints. But, using this method, the computational effort is increased due to the enlargement of the stiffness matrix. Therefore, we choose an alternative way to incorporate the boundary conditions. First, the row in the stiffness matrix and load vector in Eq. (2.248) to which the conditions apply are determined by means of the table in Sec. 2.6.2. Second, for each condition, the entries of the associated row and column in the stiffness matrix are overwritten with zeros. At the intersection of the row and column line, the entry takes the value one. At the same time, the row entry of the load vector takes the given value of the prescribed condition.

2.6.9 Non-linear Finite Elements

To improve the approximation of the solution, two possible options are available. The number of finite elements can be increased or a higher order polynomial for the elements can be used. The latter one is attractive and we show how a fifth-order polynomial can be used to approximate field quantity in finite element method. Observe

the EULER-BERNOULLI beam equation in Eq. (2.182)

$$\frac{\partial^2 u}{\partial {x_1}^2} = -\frac{M}{EI_{22}}\,, \tag{2.249}$$

where u, x_1, M, E and I_{22} are the deflection, the position, the bending moment, the YOUNG's modulus and the moment of inertia. Due to the set-up of the bending apparatus, the course of the bending moment M is given. Apart from this, the geometry of the beam specimen is also known, therefore the moment of inertia I_{22} is determined from the specimen cross section. The field variable is the displacement u, hence we multiply the differential equation by its associated test function δu. We obtain the variational form of the beam equation after integration over the whole beam body respectively the total beam length

$$\begin{aligned}
\int_0^l \frac{\partial^2 u}{\partial {x_1}^2}\delta u \,\mathrm{d}x_1 &= -\int_0^l \frac{M}{EI_{22}}\delta u \,\mathrm{d}x_1 \\
\int_0^l \frac{\partial}{\partial x_1}\left(\frac{\partial u}{\partial x_1}\delta u\right)\mathrm{d}x_1 - \int_0^l \frac{\partial u}{\partial x_1}\frac{\partial \delta u}{\partial x_1}\,\mathrm{d}x_1 &= -\int_0^l \frac{M}{EI_{22}}\delta u \,\mathrm{d}x_1 \\
\frac{\partial u}{\partial x_1}\bigg|_{x=l}\delta u\bigg|_{x=l} - \frac{\partial u}{\partial x_1}\bigg|_{x=0}\delta u\bigg|_{x=0} - \int_0^l \frac{\partial u}{\partial x_1}\frac{\partial \delta u}{\partial x_1}\,\mathrm{d}x_1 &= -\int_0^l \frac{M}{EI_{22}}\delta u \,\mathrm{d}x_1 \\
\int_0^l \frac{\partial u}{\partial x_1}\frac{\partial \delta u}{\partial x_1}\,\mathrm{d}x_1 &= \int_0^l \frac{M}{EI_{22}}\delta u \,\mathrm{d}x_1\,,
\end{aligned} \tag{2.250}$$

where integration by parts is applied and we benefit from the property that the test function vanishes on the DIRICHLET boundary conditions $\delta u\big|_{x=l} = \delta u\big|_{x=0} = 0$. Then, we discretise the beam into a finite number of straight elements N with the length of $\left|{}^{\zeta}\nu_2 - {}^{\zeta}\nu_1\right|$ for each element ζ. Within each element ζ, the displacement ${}^{\zeta}u$ is approximated by a LAGRANGE basis polynomial up to fifth order

$${}^{\zeta}u \approx {}^{\zeta}a_0 + {}^{\zeta}a_1\,{}^{\zeta}\tilde{x} + {}^{\zeta}a_2\,{}^{\zeta}\tilde{x}^2 + {}^{\zeta}a_3\,{}^{\zeta}\tilde{x}^3 + {}^{\zeta}a_4\,{}^{\zeta}\tilde{x}^4 + {}^{\zeta}a_5\,{}^{\zeta}\tilde{x}^5\,, \tag{2.251}$$

where the scalar-valued constants ${}^{\zeta}a_0$, ${}^{\zeta}a_1$, ${}^{\zeta}a_2$, ${}^{\zeta}a_3$, ${}^{\zeta}a_4$, ${}^{\zeta}a_5$ are the coefficients of the basis function

$${}^{\zeta}\tilde{x} = \frac{x_1 - {}^{\zeta}\nu_1}{{}^{\zeta}\nu_2 - {}^{\zeta}\nu_1}\,. \tag{2.252}$$

And thus, the sum of all polynomial functions results in the approximated displacement field

$$u \approx \sum_{\zeta=1}^{N} {}^{\zeta}u\,, \tag{2.253}$$

Now, we rewrite the non-linear function in Eq. (2.251), so that we can compute the values of the deflection $\left({}^{\zeta}_{\nu_1}u, {}^{\zeta}_{\nu_2}u\right)$, the first $\left({}^{\zeta}_{\nu_1}u', {}^{\zeta}_{\nu_2}u'\right)$ and the second derivatives $\left({}^{\zeta}_{\nu_1}u'', {}^{\zeta}_{\nu_2}u''\right)$ at both ends ${}^{\zeta}\nu_1$ and ${}^{\zeta}\nu_2$ of an element

$$\begin{aligned}
&{}^{\zeta}a_0 + {}^{\zeta}a_1\,{}^{\zeta}\tilde{x} + {}^{\zeta}a_2\,{}^{\zeta}\tilde{x}^2 + {}^{\zeta}a_3\,{}^{\zeta}\tilde{x}^3 + {}^{\zeta}a_4\,{}^{\zeta}\tilde{x}^4 + {}^{\zeta}a_5\,{}^{\zeta}\tilde{x}^5 = \\
&\quad = {}^{\zeta}_{\nu_1}u\,{}^{\zeta}h_{00} + {}^{\zeta}_{\nu_2}u\,{}^{\zeta}h_{01} + {}^{\zeta}_{\nu_1}u'\,{}^{\zeta}h_{10} + {}^{\zeta}_{\nu_2}u'\,{}^{\zeta}h_{11} + {}^{\zeta}_{\nu_1}u''\,{}^{\zeta}h_{20} + {}^{\zeta}_{\nu_2}u''\,{}^{\zeta}h_{21}\,,
\end{aligned} \tag{2.254}$$

where ${}^{\zeta}h_{00}$, ${}^{\zeta}h_{01}$, ${}^{\zeta}h_{10}$, ${}^{\zeta}h_{11}$, ${}^{\zeta}h_{20}$, ${}^{\zeta}h_{21}$ are another set of basis functions. To convert the expression as shown in the above equation, we evaluate Eq. (2.254) and its first and second derivatives on both ends of a straight element at ${}^{\zeta}\tilde{x} = 0$ and ${}^{\zeta}\tilde{x} = 1$

$${}^{\zeta}_{\nu_1}u = {}^{\zeta}a_0$$

$$
\begin{aligned}
{}^{\zeta}_{\nu_2}u &= {}^{\zeta}a_0 + {}^{\zeta}a_1 + {}^{\zeta}a_2 + {}^{\zeta}a_3 + {}^{\zeta}a_4 + {}^{\zeta}a_5 \\
{}^{\zeta}_{\nu_1}u' &= \frac{1}{{}^{\zeta}l}\,{}^{\zeta}a_1 \\
{}^{\zeta}_{\nu_2}u' &= \frac{1}{{}^{\zeta}l}\left({}^{\zeta}a_1 + 2\,{}^{\zeta}a_2 + 3\,{}^{\zeta}a_3 + 4\,{}^{\zeta}a_4 + 5\,{}^{\zeta}a_5\right) \\
{}^{\zeta}_{\nu_1}u'' &= \frac{2}{{}^{\zeta}l^2}\,{}^{\zeta}a_2 \\
{}^{\zeta}_{\nu_2}u'' &= \frac{1}{{}^{\zeta}l^2}\left(2\,{}^{\zeta}a_2 + 6\,{}^{\zeta}a_3 + 12\,{}^{\zeta}a_4 + 20\,{}^{\zeta}a_5\right),
\end{aligned}
\tag{2.255}
$$

where ${}^{\zeta}l = {}^{\zeta}\nu_2 - {}^{\zeta}\nu_1$ is the length of a straight element ζ. It is helpful to use matrix notation for the above equations

$$
\begin{bmatrix}
{}^{\zeta}_{\nu_1}u \\ {}^{\zeta}_{\nu_2}u \\ {}^{\zeta}_{\nu_1}u' \\ {}^{\zeta}_{\nu_2}u' \\ {}^{\zeta}_{\nu_1}u'' \\ {}^{\zeta}_{\nu_2}u''
\end{bmatrix}
=
\begin{bmatrix}
1 & 0 & 0 & 0 & 0 & 0 \\
1 & 1 & 1 & 1 & 1 & 1 \\
0 & \frac{1}{{}^{\zeta}l} & 0 & 0 & 0 & 0 \\
0 & \frac{1}{{}^{\zeta}l} & \frac{2}{{}^{\zeta}l} & \frac{3}{{}^{\zeta}l} & \frac{4}{{}^{\zeta}l} & \frac{5}{{}^{\zeta}l} \\
0 & 0 & \frac{2}{{}^{\zeta}l^2} & 0 & 0 & 0 \\
0 & 0 & \frac{2}{{}^{\zeta}l^2} & \frac{6}{{}^{\zeta}l^2} & \frac{12}{{}^{\zeta}l^2} & \frac{20}{{}^{\zeta}l^2}
\end{bmatrix}
\begin{bmatrix}
{}^{\zeta}a_0 \\ {}^{\zeta}a_1 \\ {}^{\zeta}a_2 \\ {}^{\zeta}a_3 \\ {}^{\zeta}a_4 \\ {}^{\zeta}a_5
\end{bmatrix}
\tag{2.256}
$$

and for Eq. (2.254)

$$
\begin{bmatrix} 1 & {}^{\zeta}\tilde{x} & {}^{\zeta}\tilde{x}^2 & {}^{\zeta}\tilde{x}^3 & {}^{\zeta}\tilde{x}^4 & {}^{\zeta}\tilde{x}^5 \end{bmatrix}
\begin{bmatrix}
{}^{\zeta}a_0 \\ {}^{\zeta}a_1 \\ {}^{\zeta}a_2 \\ {}^{\zeta}a_3 \\ {}^{\zeta}a_4 \\ {}^{\zeta}a_5
\end{bmatrix} =
$$

$$
= \begin{bmatrix} {}^{\zeta}h_{00} & {}^{\zeta}h_{01} & {}^{\zeta}h_{10} & {}^{\zeta}h_{11} & {}^{\zeta}h_{20} & {}^{\zeta}h_{21} \end{bmatrix}
\begin{bmatrix}
{}^{\zeta}_{\nu_1}u \\ {}^{\zeta}_{\nu_2}u \\ {}^{\zeta}_{\nu_1}u' \\ {}^{\zeta}_{\nu_2}u' \\ {}^{\zeta}_{\nu_1}u'' \\ {}^{\zeta}_{\nu_2}u''
\end{bmatrix}.
\tag{2.257}
$$

Substituting Eq. (2.256) into Eq. (2.257), we have after equating coefficients

$$
\begin{bmatrix}
1 \\ {}^{\zeta}\tilde{x} \\ {}^{\zeta}\tilde{x}^2 \\ {}^{\zeta}\tilde{x}^3 \\ {}^{\zeta}\tilde{x}^4 \\ {}^{\zeta}\tilde{x}^5
\end{bmatrix}
=
\begin{bmatrix}
1 & 1 & 0 & 0 & 0 & 0 \\
0 & 1 & \frac{1}{{}^{\zeta}l} & \frac{1}{{}^{\zeta}l} & 0 & 0 \\
0 & 1 & 0 & \frac{2}{{}^{\zeta}l} & \frac{2}{{}^{\zeta}l^2} & \frac{2}{{}^{\zeta}l^2} \\
0 & 1 & 0 & \frac{3}{{}^{\zeta}l} & 0 & \frac{6}{{}^{\zeta}l^2} \\
0 & 1 & 0 & \frac{4}{{}^{\zeta}l} & 0 & \frac{12}{{}^{\zeta}l^2} \\
0 & 1 & 0 & \frac{5}{{}^{\zeta}l} & 0 & \frac{20}{{}^{\zeta}l^2}
\end{bmatrix}
\begin{bmatrix}
{}^{\zeta}h_{00} \\ {}^{\zeta}h_{01} \\ {}^{\zeta}h_{10} \\ {}^{\zeta}h_{11} \\ {}^{\zeta}h_{20} \\ {}^{\zeta}h_{21}
\end{bmatrix}.
\tag{2.258}
$$

Solving the above system of linear equations, we obtain

$$
\begin{bmatrix}
{}^{\zeta}h_{00} \\ {}^{\zeta}h_{01} \\ {}^{\zeta}h_{10} \\ {}^{\zeta}h_{11} \\ {}^{\zeta}h_{20} \\ {}^{\zeta}h_{21}
\end{bmatrix}
=
\begin{bmatrix}
1 & 0 & 0 & -10 & 15 & -6 \\
0 & 0 & 0 & 10 & -15 & 6 \\
0 & {}^{\zeta}l & 0 & -6\,{}^{\zeta}l & 8\,{}^{\zeta}l & -3\,{}^{\zeta}l \\
0 & 0 & 0 & -4\,{}^{\zeta}l & 7\,{}^{\zeta}l & -3\,{}^{\zeta}l \\
0 & 0 & \frac{1}{2}\,{}^{\zeta}l^2 & -\frac{3}{2}\,{}^{\zeta}l^2 & \frac{3}{2}\,{}^{\zeta}l^2 & -\frac{1}{2}\,{}^{\zeta}l^2 \\
0 & 0 & 0 & \frac{1}{2}\,{}^{\zeta}l^2 & -{}^{\zeta}l^2 & \frac{1}{2}\,{}^{\zeta}l^2
\end{bmatrix}
\begin{bmatrix}
1 \\ {}^{\zeta}\tilde{x} \\ {}^{\zeta}\tilde{x}^2 \\ {}^{\zeta}\tilde{x}^3 \\ {}^{\zeta}\tilde{x}^4 \\ {}^{\zeta}\tilde{x}^5
\end{bmatrix}
\tag{2.259}
$$

respectively

$$
\begin{aligned}
{}^{\zeta}h_{00} &= 1 - 10{}^{\zeta}\tilde{x}^3 + 15{}^{\zeta}\tilde{x}^4 - 6{}^{\zeta}\tilde{x}^5 \\
{}^{\zeta}h_{01} &= 10{}^{\zeta}\tilde{x}^3 - 15{}^{\zeta}\tilde{x}^4 + 6{}^{\zeta}\tilde{x}^5 \\
{}^{\zeta}h_{10} &= {}^{\zeta}l\left({}^{\zeta}\tilde{x} - 6{}^{\zeta}\tilde{x}^3 + 8{}^{\zeta}\tilde{x}^4 - 3{}^{\zeta}\tilde{x}^5\right) \\
{}^{\zeta}h_{11} &= {}^{\zeta}l\left(-4{}^{\zeta}\tilde{x}^3 + 7{}^{\zeta}\tilde{x}^4 - 3{}^{\zeta}\tilde{x}^5\right) \\
{}^{\zeta}h_{20} &= {}^{\zeta}l^2\left(\frac{1}{2}{}^{\zeta}\tilde{x}^2 - \frac{3}{2}{}^{\zeta}\tilde{x}^3 + \frac{3}{2}{}^{\zeta}\tilde{x}^4 - \frac{1}{2}{}^{\zeta}\tilde{x}^5\right) \\
{}^{\zeta}h_{21} &= {}^{\zeta}l^2\left(\frac{1}{2}{}^{\zeta}\tilde{x}^3 - {}^{\zeta}\tilde{x}^4 + \frac{1}{2}{}^{\zeta}\tilde{x}^5\right),
\end{aligned}
\tag{2.260}
$$

where ${}^{\zeta}h_{00}$, ${}^{\zeta}h_{01}$, ${}^{\zeta}h_{10}$, ${}^{\zeta}h_{11}$, ${}^{\zeta}h_{20}$, ${}^{\zeta}h_{21}$ are known as quintic HERMITE basis functions, see for example NEUSER (1992, p. 57). The rewritten non-linear basis functions are applied to approximate the displacement as follows

$$
u \approx \sum_{\zeta=1}^{N} {}^{\zeta}_{\nu_1}u\,{}^{\zeta}h_{00} + {}^{\zeta}_{\nu_2}u\,{}^{\zeta}h_{01} + {}^{\zeta}_{\nu_1}u'\,{}^{\zeta}h_{10} + {}^{\zeta}_{\nu_2}u'\,{}^{\zeta}h_{11} + {}^{\zeta}_{\nu_1}u''\,{}^{\zeta}h_{20} + {}^{\zeta}_{\nu_2}u''\,{}^{\zeta}h_{21}\,. \tag{2.261}
$$

Likewise, the HERMITE basis functions are used for the representation of the associated test function

$$
\delta u \approx \sum_{\zeta=1}^{N} {}^{\zeta}_{\nu_1}\delta u\,{}^{\zeta}h_{00} + {}^{\zeta}_{\nu_2}\delta u\,{}^{\zeta}h_{01} + {}^{\zeta}_{\nu_1}\delta u'\,{}^{\zeta}h_{10} + {}^{\zeta}_{\nu_2}\delta u'\,{}^{\zeta}h_{11} + {}^{\zeta}_{\nu_1}\delta u''\,{}^{\zeta}h_{20} + {}^{\zeta}_{\nu_2}\delta u''\,{}^{\zeta}h_{21}\,. \tag{2.262}
$$

The above two approximation functions are inserted in Eq. (2.250). In a similar fashion to the one spelled out in Sec. 2.6.4 and Sec. 2.6.6, we find a system of linear equations of each straight element as follows

$$
\underbrace{\begin{bmatrix}
{}^{\zeta}k_{00,00} & {}^{\zeta}k_{00,01} & {}^{\zeta}k_{00,10} & {}^{\zeta}k_{00,11} & {}^{\zeta}k_{00,20} & {}^{\zeta}k_{00,21} \\
{}^{\zeta}k_{01,00} & {}^{\zeta}k_{01,01} & {}^{\zeta}k_{01,10} & {}^{\zeta}k_{01,11} & {}^{\zeta}k_{01,20} & {}^{\zeta}k_{01,21} \\
{}^{\zeta}k_{10,00} & {}^{\zeta}k_{10,01} & {}^{\zeta}k_{10,10} & {}^{\zeta}k_{10,11} & {}^{\zeta}k_{10,20} & {}^{\zeta}k_{10,21} \\
{}^{\zeta}k_{11,00} & {}^{\zeta}k_{11,01} & {}^{\zeta}k_{11,10} & {}^{\zeta}k_{11,11} & {}^{\zeta}k_{11,20} & {}^{\zeta}k_{11,21} \\
{}^{\zeta}k_{20,00} & {}^{\zeta}k_{20,01} & {}^{\zeta}k_{20,10} & {}^{\zeta}k_{20,11} & {}^{\zeta}k_{20,20} & {}^{\zeta}k_{20,21} \\
{}^{\zeta}k_{21,00} & {}^{\zeta}k_{21,01} & {}^{\zeta}k_{21,10} & {}^{\zeta}k_{21,11} & {}^{\zeta}k_{21,20} & {}^{\zeta}k_{21,21}
\end{bmatrix}}_{={}^{\zeta}\mathbf{K}}
\underbrace{\begin{bmatrix}
{}^{\zeta}_{\nu_1}u \\ {}^{\zeta}_{\nu_2}u \\ {}^{\zeta}_{\nu_1}u' \\ {}^{\zeta}_{\nu_2}u' \\ {}^{\zeta}_{\nu_1}u'' \\ {}^{\zeta}_{\nu_2}u''
\end{bmatrix}}_{={}^{\zeta}\mathbf{u}}
= \underbrace{\begin{bmatrix}
{}^{\zeta}f_{00} \\ {}^{\zeta}f_{01} \\ {}^{\zeta}f_{10} \\ {}^{\zeta}f_{11} \\ {}^{\zeta}f_{20} \\ {}^{\zeta}f_{21}
\end{bmatrix}}_{={}^{\zeta}\mathbf{f}},
\tag{2.263}
$$

where

$$
{}^{\zeta}k_{ij,kl} = \int_{{}^{\zeta}_{\nu_1}}^{{}^{\zeta}_{\nu_2}} \frac{\partial\,{}^{\zeta}h_{ij}}{\partial x_1}\frac{\partial\,{}^{\zeta}h_{kl}}{\partial x_1}\,\mathrm{d}x_1 \tag{2.264}
$$

and

$$
{}^{\zeta}f_{ij} = \int_{{}^{\zeta}_{\nu_1}}^{{}^{\zeta}_{\nu_2}} \frac{M}{EI_{22}}\,{}^{\zeta}h_{ij}\,\mathrm{d}x_1 \tag{2.265}
$$

is used to compute the entry values in the element stiffness matrix ${}^{\zeta}\mathbf{K}$ and element load vector ${}^{\zeta}\mathbf{f}$. The entries in the element stiffness matrix ${}^{\zeta}\mathbf{K}$ can be explicitly calculated as

$$
{}^{\zeta}\mathbf{K} = \left[\begin{array}{cc|cc|cc}
\frac{10}{7{}^{\zeta}l} & -\frac{10}{7{}^{\zeta}l} & \frac{3}{14} & \frac{3}{14} & \frac{{}^{\zeta}l}{84} & -\frac{{}^{\zeta}l}{84} \\
-\frac{10}{7{}^{\zeta}l} & \frac{10}{7{}^{\zeta}l} & -\frac{3}{14} & -\frac{3}{14} & -\frac{{}^{\zeta}l}{84} & \frac{{}^{\zeta}l}{84} \\
\hline
\frac{3}{14} & -\frac{3}{14} & \frac{8{}^{\zeta}l}{35} & -\frac{{}^{\zeta}l}{70} & \frac{{}^{\zeta}l^2}{60} & \frac{{}^{\zeta}l^2}{210} \\
\frac{3}{14} & -\frac{3}{14} & -\frac{{}^{\zeta}l}{70} & \frac{8{}^{\zeta}l}{35} & -\frac{{}^{\zeta}l^2}{210} & -\frac{{}^{\zeta}l^2}{60} \\
\hline
\frac{{}^{\zeta}l}{84} & -\frac{{}^{\zeta}l}{84} & \frac{{}^{\zeta}l^2}{60} & -\frac{{}^{\zeta}l^2}{210} & \frac{{}^{\zeta}l^3}{630} & \frac{{}^{\zeta}l^3}{1260} \\
-\frac{{}^{\zeta}l}{84} & \frac{{}^{\zeta}l}{84} & \frac{{}^{\zeta}l^2}{210} & -\frac{{}^{\zeta}l^2}{60} & \frac{{}^{\zeta}l^3}{1260} & \frac{{}^{\zeta}l^3}{630}
\end{array}\right]
\tag{2.266}
$$

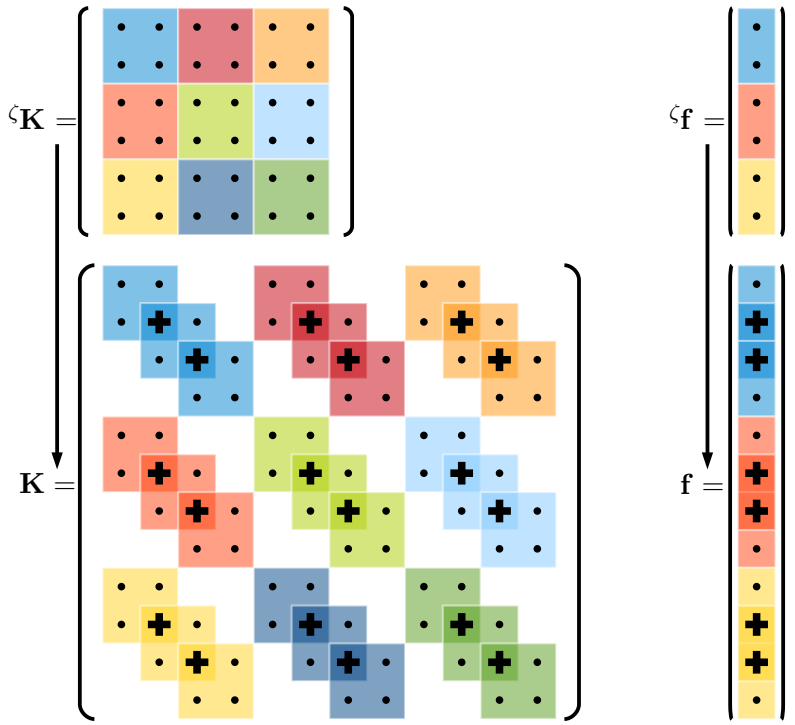


Figure 2.5: (Left) Assembly of the total stiffness matrix $\mathbf{K}$ from the element matrices ${}^{\zeta}\mathbf{K}$. (Right) Assembly of the total load vector $\mathbf{f}$ from the element load vectors ${}^{\zeta+1}\mathbf{f}$.

and the load vector entries can be computed by means of Gauss-Legendre quadrature.

In order to assemble the whole beam, every element needs to be connected to its respective neighbours. The assembly of the total stiffness matrix $\mathbf{K}$ and the total load vector $\mathbf{f}$ is shown in Fig. 2.5. Depending on the total number of elements N, the size of matrix $\mathbf{K}$ is $3(N+1) \times 3(N+1)$ and the size of vector $\mathbf{f}$ is $3(N+1)$. To connect two neighbouring straight elements ζ and $\zeta+1$, the assembly of the total stiffness matrix $\mathbf{K}$ results by adding the upper left corner of every sub-matrices in ${}^{\zeta+1}\mathbf{K}$ to the lower right corner of every sub-matrices in ${}^{\zeta}\mathbf{K}$, see Fig. 2.5 left. For the assembly of the total load vector $\mathbf{f}$, the upper entry in ${}^{\zeta+1}\mathbf{f}$ is being added to the lower entry in ${}^{\zeta}\mathbf{f}$, see Fig. 2.5 right. The vector $\mathbf{u}$ that contains the nodal values appears in this order: the deflection, its first and the second derivatives; in other words,

$$\mathbf{u}^{\star} = \begin{bmatrix} \mathbf{u} & \mathbf{u}' & \mathbf{u}'' \end{bmatrix}^{\mathsf{T}} \tag{2.267}$$

consists of the discrete beam deflection values

$$\mathbf{u} = \begin{bmatrix} u_1 & u_2 & \cdots & u_n \end{bmatrix}^{\mathsf{T}},$$

the discrete beam inclination values

$$\mathbf{u}' = \begin{bmatrix} u'_1 & u'_2 & \cdots & u'_n \end{bmatrix}^{\mathsf{T}},$$

the discrete beam longitudinal strain values

$$\mathbf{u}'' = \begin{bmatrix} u''_1 & u''_2 & \cdots & u''_n \end{bmatrix}^{\mathsf{T}},$$

where n denotes the total number of nodes and $n = N+1$. For the sake of clarity, the vector $\mathbf{u}$ can be rewritten as

$$\mathbf{u}^{\star} = \begin{bmatrix} u_1 & u_2 & \cdots & u_n \mid u'_1 & u'_2 & \cdots & u'_n \mid u''_1 & u''_2 & \cdots & u''_n \end{bmatrix}^{\mathsf{T}}. \tag{2.268}$$

It is opportune to introduce a set of running indices for the vector $\mathbf{u}$ as follows

$$\mathbf{u}^{\star} = \begin{bmatrix} u^{\star}_1 & u^{\star}_2 & \cdots & u^{\star}_n \mid u^{\star}_{n+1} & u^{\star}_{n+2} & \cdots & u^{\star}_{2n} \mid u^{\star}_{2n+1} & u^{\star}_{2n+2} & \cdots & u^{\star}_{3n} \end{bmatrix}^{\mathsf{T}}. \tag{2.269}$$

This enables one to rewrite Eq. (2.250) in compact form as

$$\mathbf{K}\mathbf{u}^{\star} = \mathbf{f} \tag{2.270}$$

respectively

$$\sum_{o=1}^{3n} k_{mo} u_o^\star = f_m \tag{2.271}$$

for $m = 1, \ldots, 3n$.

3 Basics of Adjustment Calculation

> If my calculations are correct, when this baby hits 88 miles per hour, you're gonna see some serious shit.
>
> – Emmett Lathrop "Doc" Brown, Ph.D.,
> Back to the Future (1985)

Adjustment calculation has to be carried out whenever unknown parameters and their precision have to be determined from conducted experimental and redundant measurements. Furthermore, adjustment calculation deals with statistical hypothesis testing for verifying the significance of the computed results. Profound standard text books on adjustment calculation are, e. g., (Mikhail and Ackermann 1976), (Mikhail and Gracie 1981) and (Teunissen 2000), (Niemeier 2008), (Ghilani 2010).

3.1 Mathematical Model

The mathematical model of the adjustment calculation consists of *functional model* and *stochastic model*. On the one hand, the functional model is based on a given set of algebraic equations. A functional model is defined by specifying all variables within the algebraic equations either as *observations*, *fixed values* or *unknowns*. All measured quantities are considered to be observations. Variables that can be regarded as error-free are fixed values. Parameters to be computed are called unknowns. Thus, a functional model describes the relationship between the measurements and the wanted parameters. In addition, different functional models can be defined by the same set of equations, depending on how the variables are defined in the algebraic equations as observations, fixed values or unknowns. A functional model $\boldsymbol{\Psi}$ can be formulated as an implicit representation as

$$\boldsymbol{\Psi}\left(\mathbf{L}, \mathbf{X}\right) = \mathbf{0}\,, \tag{3.1}$$

where the *vector of observations* $\mathbf{L}$ contains measurements and quantities to be computed are kept in the *vector of unknowns* $\mathbf{X}$. To the extent possible, an explicit functional model $\boldsymbol{\Phi}$ can be presented as a special case of the implicit functional model as

$$\boldsymbol{\Psi}\left(\mathbf{L}, \mathbf{X}\right) = \boldsymbol{\Phi}\left(\mathbf{X}\right) - \mathbf{L} = \mathbf{0} \text{ respectively } \boldsymbol{\Phi}\left(\mathbf{X}\right) = \mathbf{L}\,. \tag{3.2}$$

On the other hand, the stochastic model describes the probabilistic properties of measurements. Precision and correlations of measurements are taken into consideration as they have direct influence to the calculation results of unknowns. In case it can be ensured that the measurements are free of systematic deviations and blunders, the measurements are nevertheless subjected to random errors. Suppose that the tendency of observations have a normal or Gaussian distribution, then it is possible to apply least squares adjustment to compute the most probable solution for the unknowns. The stochastic model for normal distributed measurements can be expressed as *variance-covariance matrix of the observations*

$$\boldsymbol{\Sigma}_{\mathbf{LL}} = \begin{bmatrix} \sigma_{l_1}\sigma_{l_1} & \rho_{12}\sigma_{l_1}\sigma_{l_2} & \cdots & \rho_{1N}\sigma_{l_1}\sigma_{l_N} \\ \rho_{21}\sigma_{l_2}\sigma_{l_1} & \sigma_{l_2}\sigma_{l_2} & \cdots & \rho_{2N}\sigma_{l_2}\sigma_{l_N} \\ \vdots & \vdots & \ddots & \vdots \\ \rho_{N1}\sigma_{l_N}\sigma_{l_1} & \rho_{N2}\sigma_{l_N}\sigma_{l_2} & \cdots & \sigma_{l_N}\sigma_{l_N} \end{bmatrix}, \tag{3.3}$$

where the main diagonal contains variances and the secondary diagonals contain covariances of the observations. The standard deviations are denoted as σ_i and the correlation between two observations l_i and l_j is represented as ρ_{ij}.

3.2 Least Squares Adjustment Models

The functional model $\boldsymbol{\Psi}$ is usually inconsistent due to the random error in the measurements. Consequently, the functional model in Eq. (3.1) can never be satisfied. In order to find the most probable solution for the unknowns $\mathbf{X}$, the discrepancy in the functional model can be eased by introducing a *vector of residuals* $\mathbf{v}$ that provides as additive corrections to the vector of observations $\mathbf{L}$. With the introduction of the vector of residuals $\mathbf{v}$, the functional model reads

$$\boldsymbol{\Psi} = \boldsymbol{\Psi}\big(\mathbf{L} + \mathbf{v}, \hat{\mathbf{X}}\big) = \boldsymbol{\Psi}\big(\mathbf{v}, \hat{\mathbf{X}}\big) = \mathbf{0}\,. \tag{3.4}$$

But by doing this, instead of computing the unknowns $\mathbf{X}$ as in Eq. (3.1), the adjusted unknowns $\hat{\mathbf{X}}$ is now being calculated. Moreover, the possible values that the vector of residuals $\mathbf{v}$ and the adjusted unknowns $\hat{\mathbf{X}}$ can take are infinite, therefore an additional demand has to be stated for the vector of residuals $\mathbf{v}$. We seek values in $\mathbf{v}$ that yield the maximum of the normal density function

$$p = p\big(\mathbf{k}, \mathbf{v}, \hat{\mathbf{X}}\big) = \frac{1}{\sqrt{(2\pi)^N \det\big(\boldsymbol{\Sigma}_{\mathbf{LL}}\big)}} \exp\!\left(-\frac{1}{2}\mathbf{v}^{\mathsf{T}}\boldsymbol{\Sigma}_{\mathbf{LL}}^{-1}\mathbf{v}\right) - 2\mathbf{k}^{\mathsf{T}}\boldsymbol{\Psi} \;\rightarrow\; \text{maximum}\,, \tag{3.5}$$

where we impose the functional model $\boldsymbol{\Psi}$ as an *adjustment condition* respectively as a constraint by means of the *vector of* Lagrange *multipliers* $\mathbf{k}$. In case that this request is satisfied, the adjusted unknowns $\hat{\mathbf{X}}$ form the most probable the solution. By observing the argument of the exponential function, the above equation can be rewritten equivalently as a minimizing problem

$$\Omega = \Omega\big(\mathbf{k}, \mathbf{v}, \hat{\mathbf{X}}\big) = \mathbf{v}^{\mathsf{T}}\mathbf{P}\mathbf{v} - 2\mathbf{k}^{\mathsf{T}}\boldsymbol{\Psi} \;\rightarrow\; \text{minimum}\,, \tag{3.6}$$

where the *weight matrix of the observation*

$$\mathbf{P} = \mathbf{Q}_{\mathbf{LL}}^{-1} \tag{3.7}$$

is introduced. It is assumed that the *cofactor matrix of the observation*

$$\mathbf{Q}_{\mathbf{LL}} = \frac{1}{\sigma_0^2}\boldsymbol{\Sigma}_{\mathbf{LL}} \tag{3.8}$$

is regular. σ_0 is known as the *theoretical reference standard deviation*.

3.2.1 The rigorous solution from iteratively linearised Gauss-Helmert Model

In order to obtain the solution of the quadratic form in Eq. (3.6) that is known as the *rigorous solution from the iteratively linearized* Gauss-Helmert *Model*, the approach presented in L. Lenzmann and E. Lenzmann (2004) is followed. It is also known as the *most general case of least squares adjustment*. The corresponding standard is referenced in the fourth part in *DIN18709* (1995). The solution can be determined after linearisation of the adjustment condition $\boldsymbol{\Psi}$. We use the total differential to compute the infinitesimal change of the adjustment condition

$$\mathrm{d}\boldsymbol{\Psi} = \mathrm{d}\Big(\boldsymbol{\Psi}\big(\mathbf{v}, \hat{\mathbf{X}}\big)\Big) = \frac{\partial}{\partial \mathbf{v}}\Big(\boldsymbol{\Psi}\big(\mathbf{v}, \hat{\mathbf{X}}\big)\Big)\,\mathrm{d}\mathbf{v} + \frac{\partial}{\partial \hat{\mathbf{X}}}\Big(\boldsymbol{\Psi}\big(\mathbf{v}, \hat{\mathbf{X}}\big)\Big)\,\mathrm{d}\hat{\mathbf{X}} = \frac{\partial \boldsymbol{\Psi}}{\partial \mathbf{v}}\,\mathrm{d}\mathbf{v} + \frac{\partial \boldsymbol{\Psi}}{\partial \hat{\mathbf{X}}}\,\mathrm{d}\hat{\mathbf{X}}\,. \tag{3.9}$$

Fixing at starting values for $\mathbf{v} = \mathbf{v}^0$ and $\hat{\mathbf{X}} = \hat{\mathbf{X}}^0$, we obtain from the above equation

$$\begin{aligned}
\Delta\boldsymbol{\Psi} &= \left.\frac{\partial \boldsymbol{\Psi}}{\partial \mathbf{v}}\right|_{\substack{\mathbf{v}=\mathbf{v}^0 \\ \hat{\mathbf{X}}=\hat{\mathbf{X}}^0}} \Delta\mathbf{v} + \left.\frac{\partial \boldsymbol{\Psi}}{\partial \hat{\mathbf{X}}}\right|_{\substack{\mathbf{v}=\mathbf{v}^0 \\ \hat{\mathbf{X}}=\hat{\mathbf{X}}^0}} \Delta\hat{\mathbf{X}} \\
\boldsymbol{\Psi}\big(\mathbf{v}, \hat{\mathbf{X}}\big) - \boldsymbol{\Psi}\big(\mathbf{v}^0, \hat{\mathbf{X}}^0\big) &= \underbrace{\left.\frac{\partial \boldsymbol{\Psi}}{\partial \mathbf{v}}\right|_{\substack{\mathbf{v}=\mathbf{v}^0 \\ \hat{\mathbf{X}}=\hat{\mathbf{X}}^0}}}_{=\mathbf{B}} \big(\mathbf{v} - \mathbf{v}^0\big) + \underbrace{\left.\frac{\partial \boldsymbol{\Psi}}{\partial \hat{\mathbf{X}}}\right|_{\substack{\mathbf{v}=\mathbf{v}^0 \\ \hat{\mathbf{X}}=\hat{\mathbf{X}}^0}}}_{=\mathbf{A}} \big(\hat{\mathbf{X}} - \hat{\mathbf{X}}^0\big) \\
\boldsymbol{\Psi}\big(\mathbf{v}, \hat{\mathbf{X}}\big) &= \boldsymbol{\Psi}\big(\mathbf{v}^0, \hat{\mathbf{X}}^0\big) + \mathbf{B}\big(\mathbf{v} - \mathbf{v}^0\big) + \mathbf{A}\big(\hat{\mathbf{X}} - \hat{\mathbf{X}}^0\big)
\end{aligned}$$

$$\boldsymbol{\Psi}\left(\mathbf{v},\hat{\mathbf{X}}\right) = \mathbf{B}\mathbf{v} + \mathbf{A}\underbrace{\left(\hat{\mathbf{X}} - \hat{\mathbf{X}}^0\right)}_{=\Delta\hat{\mathbf{X}}} \underbrace{-\mathbf{B}\mathbf{v}^0 + \boldsymbol{\Psi}\left(\mathbf{v}^0,\hat{\mathbf{X}}^0\right)}_{=\mathbf{w}}$$

$$\boldsymbol{\Psi} = \mathbf{B}\mathbf{v} + \mathbf{A}\Delta\hat{\mathbf{X}} + \mathbf{w}\,, \tag{3.10}$$

where the *design matrices*

$$\mathbf{B} = \left.\frac{\partial\boldsymbol{\Psi}}{\partial\mathbf{v}}\right|_{\substack{\mathbf{v}=\mathbf{v}^0\\ \hat{\mathbf{X}}=\hat{\mathbf{X}}^0}} \text{ and } \mathbf{A} = \left.\frac{\partial\boldsymbol{\Psi}}{\partial\hat{\mathbf{X}}}\right|_{\substack{\mathbf{v}=\mathbf{v}^0\\ \hat{\mathbf{X}}=\hat{\mathbf{X}}^0}}\,, \tag{3.11}$$

the *vector of misclosures*

$$\mathbf{w} = -\mathbf{B}\mathbf{v}^0 + \boldsymbol{\Psi}\left(\mathbf{v}^0,\hat{\mathbf{X}}^0\right) \tag{3.12}$$

and the *vector of adjusted reduced unknowns*

$$\Delta\hat{\mathbf{X}} = \hat{\mathbf{X}} - \hat{\mathbf{X}}^0\,. \tag{3.13}$$

By inserting the above equation into Eq. (3.6), we obtain the linearised quadratic form

$$\Omega = \mathbf{v}^\mathsf{T}\mathbf{P}\mathbf{v} - 2\mathbf{k}^\mathsf{T}\left(\mathbf{B}\mathbf{v} + \mathbf{A}\Delta\hat{\mathbf{X}} + \mathbf{w}\right) \;\rightarrow\; \text{minimum}\,. \tag{3.14}$$

In order to determine the minimum of Ω, its partial derivatives with respect to $\Delta\hat{\mathbf{X}}$, $\mathbf{v}$ and $\mathbf{k}$ have to be set to zero

$$\frac{\partial\Omega}{\partial\Delta\hat{\mathbf{X}}} = -2\mathbf{k}^\mathsf{T}\mathbf{A} = \mathbf{0}^\mathsf{T}\,, \tag{3.15}$$

$$\frac{\partial\Omega}{\partial\mathbf{v}} = 2\mathbf{v}^\mathsf{T}\mathbf{P} - 2\mathbf{k}^\mathsf{T}\mathbf{B} = \mathbf{0}^\mathsf{T}\,, \tag{3.16}$$

$$\frac{\partial\Omega}{\partial\mathbf{k}^\mathsf{T}} = -2\left(\mathbf{B}\mathbf{v} + \mathbf{A}\Delta\hat{\mathbf{X}} + \mathbf{w}\right) = \mathbf{0}\,. \tag{3.17}$$

The above equations can be rewritten by dividing them by -2 and transposing the first and second equations, Eq. (3.15) and Eq. (3.16), as

$$\mathbf{A}^\mathsf{T}\mathbf{k} = \mathbf{0}\,, \tag{3.18}$$

$$\mathbf{P}\mathbf{v} - \mathbf{B}^\mathsf{T}\mathbf{k} = \mathbf{0}\,, \tag{3.19}$$

$$\mathbf{B}\mathbf{v} + \mathbf{A}\Delta\hat{\mathbf{X}} = -\mathbf{w}\,. \tag{3.20}$$

Likewise, we can obtain a compact representation of the above equations by means of matrix notation

$$\begin{bmatrix}\mathbf{0} & \mathbf{0} & \mathbf{A}^\mathsf{T}\\ \mathbf{0} & \mathbf{P} & -\mathbf{B}^\mathsf{T}\\ \mathbf{A} & \mathbf{B} & \mathbf{0}\end{bmatrix}\begin{bmatrix}\Delta\hat{\mathbf{X}}\\ \mathbf{v}\\ \mathbf{k}\end{bmatrix} = \begin{bmatrix}\mathbf{0}\\ \mathbf{0}\\ -\mathbf{w}\end{bmatrix}\,. \tag{3.21}$$

The solution for $\mathbf{k}$, $\mathbf{v}$ and $\Delta\hat{\mathbf{X}}$ of the Gauss-Helmert model is achieved by iterating the above equation. If we are interested only in $\mathbf{k}$ and $\Delta\hat{\mathbf{X}}$ or just in $\Delta\hat{\mathbf{X}}$, other possible equivalent representation of the solution can be found. We can rewrite Eq. (3.19) in term of vector of residuals $\mathbf{v}$ by multiplying the inverse weight matrix (or cofactor matrix) of the observation $\mathbf{P}^{-1} = \mathbf{Q}_{\mathbf{LL}}$ as

$$\begin{aligned}\mathbf{P}^{-1}\mathbf{P}\mathbf{v} - \mathbf{P}^{-1}\mathbf{B}^\mathsf{T}\mathbf{k} &= \mathbf{0}\\ \mathbf{v} &= \mathbf{Q}_{\mathbf{LL}}\mathbf{B}^\mathsf{T}\mathbf{k}\,.\end{aligned} \tag{3.22}$$

Inserting the above equation into Eq. (3.20), we obtain

$$\mathbf{B}\mathbf{Q}_{\mathbf{LL}}\mathbf{B}^\mathsf{T}\mathbf{k} + \mathbf{A}\Delta\hat{\mathbf{X}} = -\mathbf{w}\,. \tag{3.23}$$

The above equation and Eq. (3.18) yields, in matrix notation,

$$\begin{bmatrix}\mathbf{B}\mathbf{Q}_{\mathbf{LL}}\mathbf{B}^\mathsf{T} & \mathbf{A}\\ \mathbf{A}^\mathsf{T} & \mathbf{0}\end{bmatrix}\begin{bmatrix}\mathbf{k}\\ \Delta\hat{\mathbf{X}}\end{bmatrix} = \begin{bmatrix}-\mathbf{w}\\ \mathbf{0}\end{bmatrix}\,. \tag{3.24}$$

If we are looking for the vector of reduced unknowns $\Delta\hat{\mathbf{X}}$, we can reformulate Eq. (3.23) as

$$\mathbf{k} = -\left(\mathbf{B}\mathbf{Q}_{\mathbf{LL}}\mathbf{B}^{\mathsf{T}}\right)^{-1}\left(\mathbf{A}\Delta\hat{\mathbf{X}} + \mathbf{w}\right) \tag{3.25}$$

and inserting in Eq. (3.18) leads to

$$-\mathbf{A}^{\mathsf{T}}\left(\mathbf{B}\mathbf{Q}_{\mathbf{LL}}\mathbf{B}^{\mathsf{T}}\right)^{-1}\mathbf{A}\Delta\hat{\mathbf{X}} = \mathbf{A}^{\mathsf{T}}\left(\mathbf{B}\mathbf{Q}_{\mathbf{LL}}\mathbf{B}^{\mathsf{T}}\right)^{-1}\mathbf{w} \tag{3.26}$$

or, in matrix notation, to

$$\left[-\mathbf{A}^{\mathsf{T}}\left(\mathbf{B}\mathbf{Q}_{\mathbf{LL}}\mathbf{B}^{\mathsf{T}}\right)^{-1}\mathbf{A}\right]\left[\Delta\hat{\mathbf{X}}\right] = \left[\mathbf{A}^{\mathsf{T}}\left(\mathbf{B}\mathbf{Q}_{\mathbf{LL}}\mathbf{B}^{\mathsf{T}}\right)^{-1}\mathbf{w}\right] . \tag{3.27}$$

The above equation can be rewritten as

$$\mathbf{N}\Delta\hat{\mathbf{X}} = \mathbf{n} , \tag{3.28}$$

where

$$\mathbf{N} = -\mathbf{A}^{\mathsf{T}}\left(\mathbf{B}\mathbf{Q}_{\mathbf{LL}}\mathbf{B}^{\mathsf{T}}\right)^{-1}\mathbf{A} = -\mathbf{A}^{\mathsf{T}}\mathbf{M}^{-1}\mathbf{A} \tag{3.29}$$

is the *normal matrix* and

$$\mathbf{n} = \mathbf{A}^{\mathsf{T}}\left(\mathbf{B}\mathbf{Q}_{\mathbf{LL}}\mathbf{B}^{\mathsf{T}}\right)^{-1}\mathbf{w} = \mathbf{A}^{\mathsf{T}}\mathbf{M}^{-1}\mathbf{w} \tag{3.30}$$

is the *vector of absolute values* for the GAUSS-HELMERT model. The auxiliary matrix $\mathbf{M}$ is defined as

$$\mathbf{M} = \mathbf{B}\mathbf{Q}_{\mathbf{LL}}\mathbf{B}^{\mathsf{T}} . \tag{3.31}$$

3.2.2 The solution from iteratively linearised Gauss-Markov Model

The GAUSS-MARKOV model is a special case of the GAUSS-HELMERT model. A non-linear functional model is given as an overdetermined system of equations

$$\mathbf{L} = \mathbf{\Phi} , \tag{3.32}$$

where $\mathbf{\Phi} = \mathbf{\Phi}(\mathbf{X})$ are vector of non-linear functions of the unknowns $\mathbf{X}$. The overdetermined system of equations can not be solved without contradiction due to the measurements subjected to random errors in $\mathbf{L}$. For the sake of avoiding this discrepancy, we ease the restriction by introducing a vector of residuals $\mathbf{v}$

$$\mathbf{L} + \mathbf{v} = \mathbf{\Phi}(\hat{\mathbf{X}}) . \tag{3.33}$$

The above observation equations can be written as an adjustment condition by using Eq. (3.4) as

$$\mathbf{\Psi} = \mathbf{\Psi}(\mathbf{L} + \mathbf{v}, \hat{\mathbf{X}}) = \mathbf{\Phi}(\hat{\mathbf{X}}) - \mathbf{L} - \mathbf{v} = \mathbf{0} . \tag{3.34}$$

According to Eq. (3.26), the design matrices $\mathbf{B}$ and $\mathbf{A}$ can be determined from Eq. (3.11) as follows

$$\mathbf{B} = \left.\frac{\partial\mathbf{\Psi}}{\partial\mathbf{v}}\right|_{\substack{\mathbf{v}=\mathbf{v}^0\\ \hat{\mathbf{X}}=\hat{\mathbf{X}}^0}} = -\left.\frac{\partial\mathbf{v}}{\partial\mathbf{v}}\right|_{\substack{\mathbf{v}=\mathbf{v}^0\\ \hat{\mathbf{X}}=\hat{\mathbf{X}}^0}} = -\mathbf{I} \text{ and } \mathbf{A} = \left.\frac{\partial\mathbf{\Psi}}{\partial\hat{\mathbf{X}}}\right|_{\substack{\mathbf{v}=\mathbf{v}^0\\ \hat{\mathbf{X}}=\hat{\mathbf{X}}^0}} = \left.\frac{\partial\mathbf{\Phi}}{\partial\hat{\mathbf{X}}}\right|_{\hat{\mathbf{X}}=\hat{\mathbf{X}}^0} . \tag{3.35}$$

Within the GAUSS-MARKOV model, the design matrix $\mathbf{B}$ is identity matrix $\mathbf{I}$. Due to this fact, the vector of misclosures in Eq. (3.12) reads

$$\mathbf{w} = -\mathbf{B}\mathbf{v}^0 + \mathbf{\Psi}(\mathbf{v}^0, \hat{\mathbf{X}}^0) = \mathbf{v}^0 + \mathbf{\Phi}(\hat{\mathbf{X}}^0) - \mathbf{L} - \mathbf{v}^0 = \mathbf{\Phi}(\hat{\mathbf{X}}^0) - \mathbf{L} = -\mathbf{l} , \tag{3.36}$$

where $\mathbf{l} = \mathbf{L} - \mathbf{\Phi}(\hat{\mathbf{X}}^0)$ is also known as the *vector of reduced observations*. In addition, the expression $\left(\mathbf{B}\mathbf{Q}_{\mathbf{LL}}\mathbf{B}^{\mathsf{T}}\right)^{-1}$ on both sides in Eq. (3.26) becomes the weight matrix of the observation

$$\left(\mathbf{B}\mathbf{Q}_{\mathbf{LL}}\mathbf{B}^{\mathsf{T}}\right)^{-1} = \left(-\mathbf{I}\mathbf{Q}_{\mathbf{LL}}-\mathbf{I}^{\mathsf{T}}\right)^{-1} = \mathbf{Q}_{\mathbf{LL}}^{-1} = \mathbf{P} . \tag{3.37}$$

Inserting Eq. (3.36) and Eq. (3.37) into Eq. (3.26), the normal equations reads

$$-\mathbf{A}^{\mathsf{T}}\mathbf{P}\mathbf{A}\Delta\hat{\mathbf{X}} = -\mathbf{A}^{\mathsf{T}}\mathbf{P}\mathbf{l}$$

$$\mathbf{A}^{\mathsf{T}}\mathbf{P}\mathbf{A}\Delta\hat{\mathbf{X}} = \mathbf{A}^{\mathsf{T}}\mathbf{P}\mathbf{l} \tag{3.38}$$

or, in matrix notation,

$$\left[\mathbf{A}^{\mathsf{T}}\mathbf{P}\mathbf{A}\right]\left[\Delta\hat{\mathbf{X}}\right] = \left[\mathbf{A}^{\mathsf{T}}\mathbf{P}\mathbf{l}\right] \tag{3.39}$$

for the solution of the non-linear Gauss-Markov model. For linear function model, we have

$$\boldsymbol{\Phi} = \boldsymbol{\Phi}(\mathbf{X}) = \mathbf{A}\mathbf{X}\,. \tag{3.40}$$

The computation of the solution for linear Gauss-Markov model is obtained by inserting the above equation into Eq. (3.38). This leads to

$$\begin{aligned}
\mathbf{A}^{\mathsf{T}}\mathbf{P}\mathbf{A}(\hat{\mathbf{X}} - \hat{\mathbf{X}}^0) &= \mathbf{A}^{\mathsf{T}}\mathbf{P}\Big(\mathbf{L} - \boldsymbol{\Phi}(\hat{\mathbf{X}}^0)\Big) \\
\mathbf{A}^{\mathsf{T}}\mathbf{P}\mathbf{A}\hat{\mathbf{X}} &= \mathbf{A}^{\mathsf{T}}\mathbf{P}\mathbf{L} + \mathbf{A}^{\mathsf{T}}\mathbf{P}\mathbf{A}\hat{\mathbf{X}}^0 - \mathbf{A}^{\mathsf{T}}\mathbf{P}\underbrace{\boldsymbol{\Phi}(\hat{\mathbf{X}}^0)}_{=\mathbf{A}\hat{\mathbf{X}}^0} \\
\mathbf{A}^{\mathsf{T}}\mathbf{P}\mathbf{A}\hat{\mathbf{X}} &= \mathbf{A}^{\mathsf{T}}\mathbf{P}\mathbf{L}\,,
\end{aligned} \tag{3.41}$$

or, in matrix notation,

$$\left[\mathbf{A}^{\mathsf{T}}\mathbf{P}\mathbf{A}\right]\left[\hat{\mathbf{X}}\right] = \left[\mathbf{A}^{\mathsf{T}}\mathbf{P}\mathbf{L}\right]\,. \tag{3.42}$$

The above equation can be rewritten as

$$\mathbf{N}\hat{\mathbf{X}} = \mathbf{n}\,, \tag{3.43}$$

where $\mathbf{N} = \mathbf{A}^{\mathsf{T}}\mathbf{P}\mathbf{A}$ is the *normal matrix* and $\mathbf{n} = \mathbf{A}^{\mathsf{T}}\mathbf{P}\mathbf{L}$ is the *vector of absolute values* for the Gauss-Markov model. This normal equations is solved in one iteration.

3.3 Statistical Hypothesis Inference Testing

The statistical assessments of adjusted results are being discussed. The propagation of observation errors is studied by means of how triggering of infinitesimal random changes in the observations influences the unknowns and their expectation. This leads to the development of the quality assessment of adjusted results. Especially, the statistical hypothesis testing is used to analyse significant changes in an object. The following derivation can also be done differently, e.g., by means of *block matrix inversion* in Niemeier (2008, pp. 176–180). In this dissertation, a direct respectively straightforward approach is preferred.

3.3.1 The propagation of observation errors

After the adjustment, the vector of adjusted unknown $\hat{\mathbf{X}}$ as well as the vector of residuals $\mathbf{v}$ are determined. Now, the observation errors that propagates to the adjusted unknowns as well as to the residuals can be estimated. We approximate that the observation errors in the vector of misclosures $\mathbf{w}$ predominantly affect the adjusted unknowns. We know that Eq. (3.27) can be solved with respect to adjusted unknowns as follows

$$\begin{aligned}
\Delta\hat{\mathbf{X}} &= \left[-\mathbf{A}^{\mathsf{T}}\left(\mathbf{B}\mathbf{Q}_{\mathbf{LL}}\mathbf{B}^{\mathsf{T}}\right)^{-1}\mathbf{A}\right]^{-1}\mathbf{A}^{\mathsf{T}}\left(\mathbf{B}\mathbf{Q}_{\mathbf{LL}}\mathbf{B}^{\mathsf{T}}\right)^{-1}\mathbf{w} \\
\hat{\mathbf{X}} &= \left[-\mathbf{A}^{\mathsf{T}}\left(\mathbf{B}\mathbf{Q}_{\mathbf{LL}}\mathbf{B}^{\mathsf{T}}\right)^{-1}\mathbf{A}\right]^{-1}\mathbf{A}^{\mathsf{T}}\left(\mathbf{B}\mathbf{Q}_{\mathbf{LL}}\mathbf{B}^{\mathsf{T}}\right)^{-1}\mathbf{w} + \hat{\mathbf{X}}^0\,.
\end{aligned} \tag{3.44}$$

The total differential of the above equation with respect to the vector of misclosures $\mathbf{w}$ leads to

$$\mathrm{d}\hat{\mathbf{X}} = \frac{\partial\hat{\mathbf{X}}}{\partial\mathbf{w}}\,\mathrm{d}\mathbf{w}\,. \tag{3.45}$$

The division by $\mathrm{d}\mathbf{L}$ yields

$$\frac{\mathrm{d}\hat{\mathbf{X}}}{\mathrm{d}\mathbf{L}} = \frac{\partial\hat{\mathbf{X}}}{\partial\mathbf{w}}\frac{\mathrm{d}\mathbf{w}}{\mathrm{d}\mathbf{L}} = \left[-\mathbf{A}^{\mathsf{T}}\left(\mathbf{B}\mathbf{Q}_{\mathbf{LL}}\mathbf{B}^{\mathsf{T}}\right)^{-1}\mathbf{A}\right]^{-1}\mathbf{A}^{\mathsf{T}}\left(\mathbf{B}\mathbf{Q}_{\mathbf{LL}}\mathbf{B}^{\mathsf{T}}\right)^{-1}\frac{\mathrm{d}\mathbf{w}}{\mathrm{d}\mathbf{L}}\,. \tag{3.46}$$

The total differential of $\mathbf{w}$ with respect to $\mathbf{L}$ can be found by means of Eq. (3.12)

$$\mathrm{d}\mathbf{w} = \frac{\partial \mathbf{w}}{\partial \mathbf{L}}\,\mathrm{d}\mathbf{L} \;\Rightarrow\; \frac{\mathrm{d}\mathbf{w}}{\mathrm{d}\mathbf{L}} = \frac{\partial \mathbf{w}}{\partial \mathbf{L}} = \frac{\partial}{\partial \mathbf{L}}\Big(-\mathbf{B}\mathbf{v}^0 + \boldsymbol{\Psi}\big(\mathbf{L}+\mathbf{v}^0, \hat{\mathbf{X}}^0\big)\Big) = \frac{\partial \boldsymbol{\Psi}}{\partial \mathbf{L}} = \mathbf{B}\,. \tag{3.47}$$

Inserting the above equation into Eq. (3.46), we have

$$\mathrm{d}\hat{\mathbf{X}} = \Big[-\mathbf{A}^\mathsf{T}\big(\mathbf{B}\mathbf{Q}_{\mathbf{LL}}\mathbf{B}^\mathsf{T}\big)^{-1}\mathbf{A}\Big]^{-1}\mathbf{A}^\mathsf{T}\big(\mathbf{B}\mathbf{Q}_{\mathbf{LL}}\mathbf{B}^\mathsf{T}\big)^{-1}\mathbf{B}\,\mathrm{d}\mathbf{L} = \mathbf{N}^{-1}\mathbf{A}^\mathsf{T}\mathbf{M}^{-1}\mathbf{B}\,\mathrm{d}\mathbf{L}\,, \tag{3.48}$$

where the normal matrix $\mathbf{N}$ in Eq. (3.29) and the auxiliary matrix $\mathbf{M}$ in Eq. (3.31) are used. In Eq. (3.48), we observe how an infinitesimal change of the vector of observations $\mathrm{d}\mathbf{L}$ affects the adjusted unknowns express as an infinitesimal change of the vector of adjusted unknowns $\mathrm{d}\hat{\mathbf{X}}$. The vector $\mathrm{d}\mathbf{L}$ can either contain *vectors of random deviations* in case the expectation of each observation $\mu_{\mathbf{L}_i}$ is known or the vectors of residuals in case the expectation of each observation is unknown and instead the mean value of each observation $\bar{L}_i$ is used,

$$\mathrm{d}\mathbf{L} = \begin{bmatrix}\boldsymbol{\varepsilon}_1^\mathsf{T}\\ \boldsymbol{\varepsilon}_2^\mathsf{T}\\ \vdots\\ \boldsymbol{\varepsilon}_N^\mathsf{T}\end{bmatrix} \text{ or } \mathrm{d}\mathbf{L} = \begin{bmatrix}\mathbf{v}_1^\mathsf{T}\\ \mathbf{v}_2^\mathsf{T}\\ \vdots\\ \mathbf{v}_N^\mathsf{T}\end{bmatrix}\,. \tag{3.49}$$

The vector of random deviations and vector of residuals are determined as follows

$$\boldsymbol{\varepsilon}_i = \mathbf{L}_i - \mu_{\mathbf{L}_i}\mathbf{e} \text{ or } \mathbf{v}_i = \bar{L}_i\mathbf{e} - \mathbf{L}_i\,, \tag{3.50}$$

where $\mathbf{e}$ is the all-ones vector. The *variance* and *covariance* of the observations express as a matrix $\boldsymbol{\Sigma}_{\mathbf{LL}}$ can be approximated by the *empirical variance-covariance matrix* $\mathbf{S}_{\mathbf{LL}}$. Taking the outer product of $\mathrm{d}\mathbf{L}$ and $\mathrm{d}\mathbf{L}^\mathsf{T}$ followed by the division of the realisation number N from the observations yields

$$\begin{aligned}\boldsymbol{\Sigma}_{\mathbf{LL}} \approx \mathbf{S}_{\mathbf{LL}} = \frac{1}{N}\mathrm{d}\mathbf{L}\mathrm{d}\mathbf{L}^\mathsf{T} = \frac{1}{N}\begin{bmatrix}\boldsymbol{\varepsilon}_1^\mathsf{T}\\ \boldsymbol{\varepsilon}_2^\mathsf{T}\\ \vdots\\ \boldsymbol{\varepsilon}_N^\mathsf{T}\end{bmatrix}\begin{bmatrix}\boldsymbol{\varepsilon}_1 & \boldsymbol{\varepsilon}_2 & \cdots & \boldsymbol{\varepsilon}_N\end{bmatrix} =\\ = \frac{1}{N}\begin{bmatrix}\boldsymbol{\varepsilon}_1^\mathsf{T}\boldsymbol{\varepsilon}_1 & \boldsymbol{\varepsilon}_1^\mathsf{T}\boldsymbol{\varepsilon}_2 & \cdots & \boldsymbol{\varepsilon}_1^\mathsf{T}\boldsymbol{\varepsilon}_N\\ \boldsymbol{\varepsilon}_2^\mathsf{T}\boldsymbol{\varepsilon}_1 & \boldsymbol{\varepsilon}_2^\mathsf{T}\boldsymbol{\varepsilon}_2 & \cdots & \boldsymbol{\varepsilon}_2^\mathsf{T}\boldsymbol{\varepsilon}_N\\ \vdots & \vdots & \ddots & \vdots\\ \boldsymbol{\varepsilon}_N^\mathsf{T}\boldsymbol{\varepsilon}_1 & \boldsymbol{\varepsilon}_1^\mathsf{T}\boldsymbol{\varepsilon}_N & \cdots & \boldsymbol{\varepsilon}_N^\mathsf{T}\boldsymbol{\varepsilon}_N\end{bmatrix}\,.\end{aligned} \tag{3.51}$$

Apart from this, $\boldsymbol{\Sigma}_{\mathbf{LL}}$ can be also estimated by means of the residuals

$$\begin{aligned}\boldsymbol{\Sigma}_{\mathbf{LL}} \approx \mathbf{S}_{\mathbf{LL}} = \frac{1}{N-1}\mathrm{d}\mathbf{L}\mathrm{d}\mathbf{L}^\mathsf{T} = \frac{1}{N-1}\begin{bmatrix}\mathbf{v}_1^\mathsf{T}\\ \mathbf{v}_2^\mathsf{T}\\ \vdots\\ \mathbf{v}_N^\mathsf{T}\end{bmatrix}\begin{bmatrix}\mathbf{v}_1 & \mathbf{v}_2 & \cdots & \mathbf{v}_N\end{bmatrix} =\\ = \frac{1}{N-1}\begin{bmatrix}\mathbf{v}_1^\mathsf{T}\mathbf{v}_1 & \mathbf{v}_1^\mathsf{T}\mathbf{v}_2 & \cdots & \mathbf{v}_1^\mathsf{T}\mathbf{v}_N\\ \mathbf{v}_2^\mathsf{T}\mathbf{v}_1 & \mathbf{v}_2^\mathsf{T}\mathbf{v}_2 & \cdots & \mathbf{v}_2^\mathsf{T}\mathbf{v}_N\\ \vdots & \vdots & \ddots & \vdots\\ \mathbf{v}_N^\mathsf{T}\mathbf{v}_1 & \mathbf{v}_1^\mathsf{T}\mathbf{v}_N & \cdots & \mathbf{v}_N^\mathsf{T}\mathbf{v}_N\end{bmatrix}\,.\end{aligned} \tag{3.52}$$

For $N \to \infty$, the empirical variance-covariance matrix $\mathbf{S}_{\mathbf{LL}}$ converges to the theoretical variance-covariance matrix

$$\lim_{N\to\infty}\mathbf{S}_{\mathbf{LL}} = \begin{Bmatrix}\mathrm{E}\big(\boldsymbol{\varepsilon}_i^\mathsf{T}\boldsymbol{\varepsilon}_j\big)\\ \mathrm{E}\big(\mathbf{v}_i^\mathsf{T}\mathbf{v}_j\big)\end{Bmatrix} \quad \text{for } i,j = 1,\ldots,N \Bigg\} \equiv \boldsymbol{\Sigma}_{\mathbf{LL}}\,, \tag{3.53}$$

where E is the expectation operator. To examine the variance-covariance propagation of observation errors induced by $\mathrm{d}\mathbf{L}$, we write the outer product of $\mathrm{d}\hat{\mathbf{X}}$ and $\mathrm{d}\hat{\mathbf{X}}^\mathsf{T}$ as follows

$$\mathrm{d}\hat{\mathbf{X}}\mathrm{d}\hat{\mathbf{X}}^\mathsf{T} = \mathbf{N}^{-1}\mathbf{A}^\mathsf{T}\mathbf{M}^{-1}\mathbf{B}\,\mathrm{d}\mathbf{L}\,\mathrm{d}\mathbf{L}^\mathsf{T}\mathbf{B}^\mathsf{T}\big(\mathbf{M}^{-1}\big)^\mathsf{T}\mathbf{A}\big(\mathbf{N}^{-1}\big)^\mathsf{T}\,. \tag{3.54}$$

By applying the expectation operator on both sides yields

$$\begin{aligned}
\underbrace{\mathrm{E}\left(\mathrm{d}\hat{\mathbf{X}}\mathrm{d}\hat{\mathbf{X}}^{\mathsf{T}}\right)}_{=\boldsymbol{\Sigma}_{\hat{\mathbf{X}}\hat{\mathbf{X}}}} &= \mathbf{N}^{-1}\mathbf{A}^{\mathsf{T}}\mathbf{M}^{-1}\mathbf{B}\underbrace{\mathrm{E}\left(\mathrm{d}\mathbf{L}\,\mathrm{d}\mathbf{L}^{\mathsf{T}}\right)}_{=\boldsymbol{\Sigma}_{\mathbf{LL}}}\mathbf{B}^{\mathsf{T}}\left(\mathbf{M}^{-1}\right)^{\mathsf{T}}\mathbf{A}\left(\mathbf{N}^{-1}\right)^{\mathsf{T}} \\
\boldsymbol{\Sigma}_{\hat{\mathbf{X}}\hat{\mathbf{X}}} &= \mathbf{N}^{-1}\mathbf{A}^{\mathsf{T}}\mathbf{M}^{-1}\mathbf{B}\underbrace{\boldsymbol{\Sigma}_{\mathbf{LL}}}_{=\sigma_0^2\mathbf{Q}_{\mathbf{LL}}}\mathbf{B}^{\mathsf{T}}\left(\mathbf{M}^{-1}\right)^{\mathsf{T}}\mathbf{A}\left(\mathbf{N}^{-1}\right)^{\mathsf{T}} \\
&= \mathbf{N}^{-1}\mathbf{A}^{\mathsf{T}}\mathbf{M}^{-1}\mathbf{B}\sigma_0^2\mathbf{Q}_{\mathbf{LL}}\mathbf{B}^{\mathsf{T}}\left(\mathbf{M}^{-1}\right)^{\mathsf{T}}\mathbf{A}\left(\mathbf{N}^{-1}\right)^{\mathsf{T}} \\
&= \sigma_0^2\mathbf{N}^{-1}\mathbf{A}^{\mathsf{T}}\mathbf{M}^{-1}\underbrace{\mathbf{B}\mathbf{Q}_{\mathbf{LL}}\mathbf{B}^{\mathsf{T}}}_{=\mathbf{M}}\left(\mathbf{M}^{-1}\right)^{\mathsf{T}}\mathbf{A}\left(\mathbf{N}^{-1}\right)^{\mathsf{T}} \\
&= \sigma_0^2\mathbf{N}^{-1}\mathbf{A}^{\mathsf{T}}\underbrace{\mathbf{M}^{-1}\mathbf{M}}_{=\mathbf{I}}\left(\mathbf{M}^{-1}\right)^{\mathsf{T}}\mathbf{A}\left(\mathbf{N}^{-1}\right)^{\mathsf{T}} \\
&= \sigma_0^2\mathbf{N}^{-1}\underbrace{\mathbf{A}^{\mathsf{T}}\left(\mathbf{M}^{-1}\right)^{\mathsf{T}}\mathbf{A}}_{=\mathbf{A}^{\mathsf{T}}\mathbf{M}^{-1}\mathbf{A}=-\mathbf{N}}\left(\mathbf{N}^{-1}\right)^{\mathsf{T}} \\
&= -\sigma_0^2\underbrace{\mathbf{N}^{-1}\mathbf{N}}_{=\mathbf{I}}\left(\mathbf{N}^{-1}\right)^{\mathsf{T}} \\
&= -\sigma_0^2\mathbf{N}^{-1}\,,
\end{aligned} \tag{3.55}$$

where we used the fact that the inverse of a symmetric matrix is still symmetric, i. e. $\left(\mathbf{N}^{-1}\right)^{\mathsf{T}} = \mathbf{N}^{-1}$ and $\left(\mathbf{M}^{-1}\right)^{\mathsf{T}} = \mathbf{M}^{-1}$.

In order to examine the variance-covariance propagation of the observation $\boldsymbol{\Sigma}_{\mathbf{LL}}$ that affects the residuals, we write the total differential of Eq. (3.22) as

$$\mathrm{d}\mathbf{v} = \frac{\partial \mathbf{v}}{\partial \mathbf{k}}\,\mathrm{d}\mathbf{k} \tag{3.56}$$

and the division by $\mathrm{d}\mathbf{L}$ yields

$$\frac{\mathrm{d}\mathbf{v}}{\mathrm{d}\mathbf{L}} = \frac{\partial \mathbf{v}}{\partial \mathbf{k}}\frac{\mathrm{d}\mathbf{k}}{\mathrm{d}\mathbf{L}} = \mathbf{Q}_{\mathbf{LL}}\mathbf{B}^{\mathsf{T}}\frac{\mathrm{d}\mathbf{k}}{\mathrm{d}\mathbf{L}}\,. \tag{3.57}$$

The differential $\mathbf{k}$ with respect to the vector of observations $\mathbf{L}$ in the above equation can be obtained by means of Eq. (3.25), where we write its total differential as follows

$$\mathrm{d}\mathbf{k} = \frac{\partial \mathbf{k}}{\partial \Delta\hat{\mathbf{X}}}\,\mathrm{d}\Delta\hat{\mathbf{X}} + \frac{\partial \mathbf{k}}{\partial \mathbf{w}}\,\mathrm{d}\mathbf{w}\,. \tag{3.58}$$

By dividing with $\mathrm{d}\mathbf{L}$, we have

$$\begin{aligned}
\frac{\mathrm{d}\mathbf{k}}{\mathrm{d}\mathbf{L}} &= \frac{\partial \mathbf{k}}{\partial \Delta\hat{\mathbf{X}}}\frac{\mathrm{d}\Delta\hat{\mathbf{X}}}{\mathrm{d}\mathbf{L}} + \frac{\partial \mathbf{k}}{\partial \mathbf{w}}\frac{\mathrm{d}\mathbf{w}}{\mathrm{d}\mathbf{L}} = -\mathbf{M}^{-1}\mathbf{A}\frac{\mathrm{d}\hat{\mathbf{X}}}{\mathrm{d}\mathbf{L}} - \mathbf{M}^{-1}\mathbf{B} = \\
&= -\mathbf{M}^{-1}\mathbf{A}\mathbf{N}^{-1}\mathbf{A}^{\mathsf{T}}\mathbf{M}^{-1}\mathbf{B} - \mathbf{M}^{-1}\mathbf{B} = -\mathbf{M}^{-1}\left(\mathbf{A}\mathbf{N}^{-1}\mathbf{A}^{\mathsf{T}}\mathbf{M}^{-1} + \mathbf{I}\right)\mathbf{B}\,.
\end{aligned} \tag{3.59}$$

Inserting the above equation into Eq. (3.57), we find

$$\mathrm{d}\mathbf{v} = -\mathbf{Q}_{\mathbf{LL}}\mathbf{B}^{\mathsf{T}}\mathbf{M}^{-1}\left(\mathbf{A}\mathbf{N}^{-1}\mathbf{A}^{\mathsf{T}}\mathbf{M}^{-1} + \mathbf{I}\right)\mathbf{B}\,\mathrm{d}\mathbf{L} \tag{3.60}$$

The equation above shows how an infinitesimal change of the vector of observations $\mathrm{d}\mathbf{L}$ affects the vector of residuals in form of an infinitesimal change $\mathrm{d}\mathbf{v}$. In a similar fashion, we can obtain the variance-covariance matrix of the residuals $\boldsymbol{\Sigma}_{\mathbf{vv}}$ by writing the outer product of $\mathrm{d}\mathbf{v}$ and $\mathrm{d}\mathbf{v}^{\mathsf{T}}$ follow by applying the expectation operator on both sides

$$\underbrace{\mathrm{E}\left(\mathrm{d}\mathbf{v}\mathrm{d}\mathbf{v}^{\mathsf{T}}\right)}_{=\boldsymbol{\Sigma}_{\mathbf{vv}}} = \mathbf{Q}_{\mathbf{LL}}\mathbf{B}^{\mathsf{T}}\mathbf{M}^{-1}\left(\mathbf{A}\mathbf{N}^{-1}\mathbf{A}^{\mathsf{T}}\mathbf{M}^{-1} + \mathbf{I}\right)\mathbf{B}\underbrace{\mathrm{E}\left(\mathrm{d}\mathbf{L}\,\mathrm{d}\mathbf{L}^{\mathsf{T}}\right)}_{=\boldsymbol{\Sigma}_{\mathbf{LL}}}\mathbf{B}^{\mathsf{T}}\left(\mathbf{M}^{-1}\left(\mathbf{A}\mathbf{N}^{-1}\mathbf{A}^{\mathsf{T}}\mathbf{M}^{-1} + \mathbf{I}\right)\right)^{\mathsf{T}}\mathbf{B}\mathbf{Q}_{\mathbf{LL}}^{\mathsf{T}}$$

$$
\begin{aligned}
\boldsymbol{\Sigma}_{\mathbf{vv}} &= \mathbf{Q}_{\mathbf{LL}}\mathbf{B}^{\mathsf{T}}\mathbf{M}^{-1}(\mathbf{A}\mathbf{N}^{-1}\mathbf{A}^{\mathsf{T}}\mathbf{M}^{-1}+\mathbf{I})\mathbf{B}\underbrace{\boldsymbol{\Sigma}_{\mathbf{LL}}}_{=\sigma_0^2\mathbf{Q}_{\mathbf{LL}}}\mathbf{B}^{\mathsf{T}}\Big(\mathbf{M}^{-1}(\mathbf{A}\mathbf{N}^{-1}\mathbf{A}^{\mathsf{T}}\mathbf{M}^{-1}+\mathbf{I})\Big)^{\mathsf{T}}\mathbf{B}\mathbf{Q}_{\mathbf{LL}} \\
&= \mathbf{Q}_{\mathbf{LL}}\mathbf{B}^{\mathsf{T}}\mathbf{M}^{-1}(\mathbf{A}\mathbf{N}^{-1}\mathbf{A}^{\mathsf{T}}\mathbf{M}^{-1}+\mathbf{I})\mathbf{B}\sigma_0^2\mathbf{Q}_{\mathbf{LL}}\mathbf{B}^{\mathsf{T}}\Big(\mathbf{M}^{-1}(\mathbf{A}\mathbf{N}^{-1}\mathbf{A}^{\mathsf{T}}\mathbf{M}^{-1}+\mathbf{I})\Big)^{\mathsf{T}}\mathbf{B}\mathbf{Q}_{\mathbf{LL}} \\
&= \sigma_0^2\mathbf{Q}_{\mathbf{LL}}\mathbf{B}^{\mathsf{T}}\mathbf{M}^{-1}(\mathbf{A}\mathbf{N}^{-1}\mathbf{A}^{\mathsf{T}}\mathbf{M}^{-1}+\mathbf{I})\underbrace{\mathbf{B}\mathbf{Q}_{\mathbf{LL}}\mathbf{B}^{\mathsf{T}}}_{=\mathbf{M}}\Big(\mathbf{M}^{-1}(\mathbf{A}\mathbf{N}^{-1}\mathbf{A}^{\mathsf{T}}\mathbf{M}^{-1}+\mathbf{I})\Big)^{\mathsf{T}}\mathbf{B}\mathbf{Q}_{\mathbf{LL}} \\
&= \sigma_0^2\mathbf{Q}_{\mathbf{LL}}\mathbf{B}^{\mathsf{T}}\mathbf{M}^{-1}(\mathbf{A}\mathbf{N}^{-1}\mathbf{A}^{\mathsf{T}}\mathbf{M}^{-1}+\mathbf{I})\mathbf{M}(\mathbf{A}\mathbf{N}^{-1}\mathbf{A}^{\mathsf{T}}\mathbf{M}^{-1}+\mathbf{I})^{\mathsf{T}}(\mathbf{M}^{-1})^{\mathsf{T}}\mathbf{B}\mathbf{Q}_{\mathbf{LL}} \\
&= \sigma_0^2\mathbf{Q}_{\mathbf{LL}}\mathbf{B}^{\mathsf{T}}(\mathbf{M}^{-1}\mathbf{A}\mathbf{N}^{-1}\mathbf{A}^{\mathsf{T}}\underbrace{\mathbf{M}^{-1}\mathbf{M}}_{=\mathbf{I}}+\underbrace{\mathbf{M}^{-1}\mathbf{M}}_{=\mathbf{I}})(\mathbf{M}^{-1}\mathbf{A}\mathbf{N}^{-1}\mathbf{A}^{\mathsf{T}}+\mathbf{I})\mathbf{M}^{-1}\mathbf{B}\mathbf{Q}_{\mathbf{LL}} \\
&= \sigma_0^2\mathbf{Q}_{\mathbf{LL}}\mathbf{B}^{\mathsf{T}}(\mathbf{M}^{-1}\mathbf{A}\mathbf{N}^{-1}\mathbf{A}^{\mathsf{T}}+\mathbf{I})(\mathbf{M}^{-1}\mathbf{A}\mathbf{N}^{-1}\mathbf{A}^{\mathsf{T}}\mathbf{M}^{-1}+\mathbf{M}^{-1})\mathbf{B}\mathbf{Q}_{\mathbf{LL}} \\
&= \sigma_0^2\mathbf{Q}_{\mathbf{LL}}\mathbf{B}^{\mathsf{T}}(\mathbf{M}^{-1}\mathbf{A}\mathbf{N}^{-1}\underbrace{\mathbf{A}^{\mathsf{T}}\mathbf{M}^{-1}\mathbf{A}}_{=-\mathbf{N}}\mathbf{N}^{-1}\mathbf{A}^{\mathsf{T}}\mathbf{M}^{-1}+\mathbf{M}^{-1}\mathbf{A}\mathbf{N}^{-1}\mathbf{A}^{\mathsf{T}}\mathbf{M}^{-1}+ \\
&\qquad +\mathbf{M}^{-1}\mathbf{A}\mathbf{N}^{-1}\mathbf{A}^{\mathsf{T}}\mathbf{M}^{-1}+\mathbf{M}^{-1})\mathbf{B}\mathbf{Q}_{\mathbf{LL}} \\
&= \sigma_0^2\mathbf{Q}_{\mathbf{LL}}\mathbf{B}^{\mathsf{T}}\Big(-\mathbf{M}^{-1}\mathbf{A}\underbrace{\mathbf{N}^{-1}\mathbf{N}}_{=\mathbf{I}}\mathbf{N}^{-1}\mathbf{A}^{\mathsf{T}}\mathbf{M}^{-1}+\mathbf{M}^{-1}\mathbf{A}\mathbf{N}^{-1}\mathbf{A}^{\mathsf{T}}\mathbf{M}^{-1}+ \\
&\qquad +\mathbf{M}^{-1}(\mathbf{A}\mathbf{N}^{-1}\mathbf{A}^{\mathsf{T}}\mathbf{M}^{-1}+\mathbf{I})\Big)\mathbf{B}\mathbf{Q}_{\mathbf{LL}} \\
&= \sigma_0^2\mathbf{Q}_{\mathbf{LL}}\mathbf{B}^{\mathsf{T}}\Big(\underbrace{-\mathbf{M}^{-1}\mathbf{A}\mathbf{N}^{-1}\mathbf{A}^{\mathsf{T}}\mathbf{M}^{-1}+\mathbf{M}^{-1}\mathbf{A}\mathbf{N}^{-1}\mathbf{A}^{\mathsf{T}}\mathbf{M}^{-1}}_{=\mathbf{0}}+ \\
&\qquad +\mathbf{M}^{-1}(\mathbf{A}\mathbf{N}^{-1}\mathbf{A}^{\mathsf{T}}\mathbf{M}^{-1}+\mathbf{I})\Big)\mathbf{B}\mathbf{Q}_{\mathbf{LL}} \\
&= \sigma_0^2\mathbf{Q}_{\mathbf{LL}}\mathbf{B}^{\mathsf{T}}\mathbf{M}^{-1}(\mathbf{A}\mathbf{N}^{-1}\mathbf{A}^{\mathsf{T}}\mathbf{M}^{-1}+\mathbf{I})\mathbf{B}\mathbf{Q}_{\mathbf{LL}}\,.
\end{aligned}
\tag{3.61}
$$

The variance-covariance matrix of the unknowns and of the residuals, $\boldsymbol{\Sigma}_{\hat{\mathbf{X}}\hat{\mathbf{X}}}$ and $\boldsymbol{\Sigma}_{\mathbf{vv}}$, are utilized as measures for the quality assessment of the adjusted results.

3.3.2 Quality Assessment of Adjustment Results

The quality assessment of the adjustment calculation deals with the adjusted results, i. e., the measurements and the determined unknown parameters. We can categorize the quality into two distinct parts: *Precision* and *Reliability*. The precision expresses how precise the unknowns have been determined, provided that an appropriate functional and stochastic model are chosen as well as that blunders have little or no influences on the resulting unknowns. All common precision measures are calculated from the variance-covariance matrix of the unknowns $\boldsymbol{\Sigma}_{\hat{\mathbf{X}}\hat{\mathbf{X}}}$. The reliability refers the possibility of control of the observations to detect blunders. Apart from this, the reliability measures can be used to describe the influences of blunders to the unknown parameters. The variance-covariance matrix of the residuals $\boldsymbol{\Sigma}_{\mathbf{vv}}$ is the primary source to obtain reliability measures.

Redundancy Number

The reliability measures can be retrieved from the variance-covariance matrix of the residuals $\boldsymbol{\Sigma}_{\mathbf{vv}}$. We multiply the Eq. (3.61) with $\mathbf{Q}_{\mathbf{LL}}^{-1} = \mathbf{P}$ from the left and obtain by division with ${\sigma_0}^2$

$$
\begin{aligned}
\mathbf{Q}_{\mathbf{vv}}\mathbf{Q}_{\mathbf{LL}}^{-1} &= \mathbf{Q}_{\mathbf{LL}}\mathbf{B}^{\mathsf{T}}\mathbf{M}^{-1}(\mathbf{A}\mathbf{N}^{-1}\mathbf{A}^{\mathsf{T}}\mathbf{M}^{-1}+\mathbf{I})\mathbf{B}\underbrace{\mathbf{Q}_{\mathbf{LL}}\mathbf{Q}_{\mathbf{LL}}^{-1}}_{=\mathbf{I}} \\
\mathbf{Q}_{\mathbf{vv}}\mathbf{P} &= \mathbf{Q}_{\mathbf{LL}}\mathbf{B}^{\mathsf{T}}\mathbf{M}^{-1}(\mathbf{A}\mathbf{N}^{-1}\mathbf{A}^{\mathsf{T}}\mathbf{M}^{-1}+\mathbf{I})\mathbf{B}\,.
\end{aligned}
\tag{3.62}
$$

Inserting the above equation into Eq. (3.60) yields

$$
\mathrm{d}\mathbf{v} = -\mathbf{Q}_{\mathbf{vv}}\mathbf{P}\,\mathrm{d}\mathbf{L} = -\mathbf{R}\,\mathrm{d}\mathbf{L}\,, \tag{3.63}
$$

where the transfer matrix $\mathbf{R} = \mathbf{Q}_{\mathbf{vv}}\mathbf{P}$ is introduced. Observe if any one component $\mathrm{d}L_i$ in $\mathrm{d}\mathbf{L}$ contains an error, and, in that case how this error will influence all residuals by $\mathrm{d}\mathbf{v}$ due to the transfer matrix $\mathbf{R}$. The diagonal element R_{ii} in $\mathbf{R}$ is a transfer factor that shows the (partly) impact of the erroneous component $\mathrm{d}L_i$ on the corresponding residual v_i in $\mathbf{v}$. This transfer factor is knowns as *redundancy number* of the observation L_i

$$r_i = R_{ii}\,. \tag{3.64}$$

Each redundancy number r_i has a value between 0 and 1. In the extreme case of $r_i = 1$, an error in the observation l_i can be completely detected in the residuals v_i, while in the other extreme case of $r_i = 0$, an error in the observation l_i is undetectable. Therefore, it is required that the sum of all redundancy numbers, the total redundancy r, is large enough to detect blunders in the observations. The trace of the matrix $\mathbf{R}$ leads to the total redundancy r as follows

$$\mathrm{trace}(\mathbf{R}) = \sum_{i=1}^{N} r_i = r\,. \tag{3.65}$$

The redundancy number can be represented as a percentage EV that is known as *influence on the residuals* (German: *Einfluss auf die Verbesserung*)

$$EV = r_i\,100\,\%\,. \tag{3.66}$$

The following rating scale to evaluate the redundancy numbers has gained ground in the practise:

$0\,\%$	$\leq$	EV	$<$	$1\,\%$	observation is not controlled,
$1\,\%$	$\leq$	EV	$<$	$10\,\%$	observation is poorly controlled,
$10\,\%$	$\leq$	EV	$<$	$30\,\%$	observation is sufficiently controlled,
$30\,\%$	$\leq$	EV	$<$	$70\,\%$	observation well controlled,
$70\,\%$	$\leq$	EV	$<$	$100\,\%$	observation can be removed without loss of reliability.

Blunders Detection and Localisation

In order to prevent incorrect adjustment results due to outliers, blunders have to be detected and removed from the observations. A *global test* is performed as follows to find out if the observations contains blunders. According to Nuzzo (2014), the original purpose of a *hypothesis test* by Fischer is to study if the adjusted results are predominately occur due to randomness of the observations (null hypothesis). If it is not the case, the mathematical model might be incorrect or the observations might contain blunders (alternative hypothesis). Before we question the mathematical model, we have to be sure that the observations contain no blunders by examining if the *empirical reference standard deviation* after the adjustment

$$s_0 = \sqrt{\frac{\mathbf{v}^{\mathsf{T}}\mathbf{P}\mathbf{v}}{r}}\,. \tag{3.67}$$

coincides with the theoretical reference standard deviation σ_0 before the adjustment. We can state the null hypothesis H_0 as

$$H_0 : \mathrm{E}(s_0^2) = \sigma_0^2\,. \tag{3.68}$$

The alternative hypothesis H_A can take one of the following forms

$$H_\mathrm{A} : \mathrm{E}(s_0^2) \neq \sigma_0^2\,, \tag{3.69}$$
$$H_\mathrm{A} : \mathrm{E}(s_0^2) > \sigma_0^2\,, \tag{3.70}$$
$$H_\mathrm{A} : \mathrm{E}(s_0^2) < \sigma_0^2\,. \tag{3.71}$$

Now, we have to consider the statistical distribution of s_0^2. We rearrange Eq. (3.67) as follows

$$s_0^2 = \frac{\mathbf{v}^{\mathsf{T}}\mathbf{P}\mathbf{v}}{r} = \frac{\sigma_0^2}{\sigma_0^2}\frac{\mathbf{v}^{\mathsf{T}}\mathbf{Q}_{\mathbf{LL}}^{-1}\mathbf{v}}{r} = \sigma_0^2\frac{\mathbf{v}^{\mathsf{T}}\boldsymbol{\Sigma}_{\mathbf{LL}}^{-1}\mathbf{v}}{r} \;\Rightarrow\; r\frac{s_0^2}{\sigma_0^2} = \mathbf{v}^{\mathsf{T}}\boldsymbol{\Sigma}_{\mathbf{LL}}^{-1}\mathbf{v}\,. \tag{3.72}$$

The residuals $\mathbf{v}$ are assumed to be normal distributed random variables. Then, the squared residuals are weighted by the inverse of the variance-covariance matrix $\mathbf{\Sigma}_{\mathbf{LL}}^{-1}$. This in turn yields residuals that are divided by their corresponding variances. Consequently, they are variables that follow a standard normal distribution. According to PEARSON, the sum of their squares is conforming to χ^2-distribution with r degrees of freedom. In other words, the variable

$$\chi_r^2 = r\frac{s_0^2}{\sigma_0^2} \tag{3.73}$$

is χ^2-distributed. Therefore, we choose the above variable as *test statistic*. To determine the *threshold value* $\chi_{r,\alpha}^2$, an arbitrary chosen error probability α respectively confidence level $S = 1 - \alpha$ has to be considered. Then, we compare the test statistic with the threshold value for the following four statements

$$\chi_r^2 < \chi_{r,1-\frac{\alpha}{2}}^2 \text{ and } \chi_r^2 > \chi_{r,\frac{\alpha}{2}}^2 \;\Rightarrow\; \text{Reject } H_0 \text{ in favor of } H_\text{A} : \mathrm{E}\big(s_0^2\big) \neq \sigma_0^2\,, \tag{3.74}$$

$$\chi_r^2 > \chi_{r,1-\alpha}^2 \;\Rightarrow\; \text{Reject } H_0 \text{ in favor of } H_\text{A} : \mathrm{E}\big(s_0^2\big) > \sigma_0^2\,, \tag{3.75}$$

$$\chi_r^2 < \chi_{r,\alpha}^2 \;\Rightarrow\; \text{Reject } H_0 \text{ in favor of } H_\text{A} : \mathrm{E}\big(s_0^2\big) < \sigma_0^2\,, \tag{3.76}$$

otherwise we fail to reject the null hypothesis H_0. But, in case we reject the null hypothesis, we have to look for individual blunders in the observations. To introduce a measure for removing a single observation that likely contains gross error, we assume that the error in an observation mainly affects its corresponding residual. The measure *standardised residual* (German: *Normierte Verbesserung*) is defined as

$$NV_i = \frac{|v_i|}{\sigma_{v_i}}\,. \tag{3.77}$$

The computational purpose, we can find an alternative way for computing NV_i. We rewrite Eq. (3.61) by means of Eq. (3.62) and the transfer matrix as

$$\mathbf{\Sigma}_{\mathbf{vv}} = \sigma_0^2\mathbf{Q}_{\mathbf{vv}}\mathbf{P}\mathbf{Q}_{\mathbf{LL}} = \mathbf{R}\mathbf{\Sigma}_{\mathbf{LL}}\,. \tag{3.78}$$

It is often the case that the variance-covariance matrix $\mathbf{\Sigma}_{\mathbf{LL}}$ is a diagonal matrix. In this case, we can determine the standard deviation of the residual v_i as follows

$$\sigma_{v_i} = \sqrt{r_i}\sigma_{l_i}\,. \tag{3.79}$$

Inserting the above into Eq. (3.77) yields

$$NV_i = \frac{|v_i|}{\sqrt{r_i}\sigma_{l_i}}\,. \tag{3.80}$$

The standardised residual NV_i follows a standard normal distribution due to the division of the normal distributed residual v_i by its corresponding standard deviation σ_{v_i}. A standardised normal test or a *local test* has to be performed to evaluate if an observation contains gross error. But in practise, we can use the following rating scale to assess the standardised residual:

$$\begin{array}{rcccl} 2.5 & < & NV & \leq & 4 \quad \text{gross error possible,} \\ & & NV & > & 4 \quad \text{gross error most likely.} \end{array}$$

After we identified an observation as blunder, we can introduce a measure to quantify the magnitude of the gross error ε_i, *potential blunder* (German: *Grober Fehler*)

$$GF_i = \frac{\varepsilon_i}{r_i} = \frac{-v_i}{r_i}\,. \tag{3.81}$$

This ratio describes how the diagonal component r_i of the transfer matrix $\mathbf{R}$ affects its corresponding gross error ε_i respectively $-v_i$. Another question that arises is how large a blunder GF_i must be that we are able to detect it. A measure of detectability of blunder, the *boundary value* (German: *Grenzwert*) is introduced as follows

$$GRZW_i = \frac{\sigma_{l_i}\delta_0}{\sqrt{r_i}}\,, \tag{3.82}$$

where $\delta_0 = 4.13$ is the non-centrality parameter; for the derivation see Baarda (1968). Consequently, errors that are smaller than the *GRZW* has to be regarded as random and therefore they are undetectable.

The workflow of the blunders detection by means of a global test as well as the localisation and removal of blunders as known as *data snooping* can summarise as follows. First, after the adjustment, a global test respectively a χ^2-test is performed. If we fail to reject the null hypothesis H_0 in favour of the alternative hypothesis H_A, it means that the final result is obtained. Otherwise, we have to pinpoint the blunders in the observations by means of the standardised residuals. Second, the observation l_i with largest standardised residual NV_i has to be removed from the observation vector $\mathbf{L}$. Third, an adjustment calculation has to be performed and start this workflow from the beginning until we fail to reject the null hypothesis.

The influence of observation error on the parameters

Detectable and removable blunders and their influences are examined in the *internal reliability*. The affection of non-detectable blunders on the unknowns analysed in the *external reliability*. A measure that describes the impact of the boundary value on the coordinates of the corresponding point (German: *Einfluss des Grenzwertes auf die Koordinaten* der berührenden Punkte) is introduced as

$$EGK_i = \big(1 - r_i\big) GRZW_i \; . \tag{3.83}$$

The other measure that describes the impact of a potential blunder on a point corresponding to the measurement (German: *Einfluss eines eventuellen groben Fehlers auf den die Messung berührenden Punkt*) is introduced as follows

$$EP_i = \big(1 - r_i\big) GF_i \; . \tag{3.84}$$

For the derivation refer to Baarda (1968).

3.3.3 Deformation Analysis

The deformation analysis deals with assessment of the significant temporal changes of an object. The basis of significance evaluation are the observations from different time samples (*epochs*). Even though this analysis was mainly developed for determination of significant geometrical changes that occur over the time, we can apply the deformation analysis beyond geodetic problems. We follow Niemeier (1979) and focus on his method that is known as *congruence test* (German: *Kongruenztest*). According to Welsch and Heunecke (2001), this method is one of many ways to perform deformation analysis.

Consider an object where measurements from two epochs $\mathbf{L}_1$ and $\mathbf{L}_2$ were performed. We assume that the observations of the two time samples are not correlated, therefore we have the following stochastic model

$$\mathbf{\Sigma_{LL}} = \sigma_0^2 \begin{bmatrix} \mathbf{Q}_{\mathbf{L}_1\mathbf{L}_1} & \mathbf{0} \\ \mathbf{0} & \mathbf{Q}_{\mathbf{L}_2\mathbf{L}_2} \end{bmatrix} \; , \tag{3.85}$$

where the one and only variance factor σ_0^2 has to be computed by means of *variance-covariance components estimation*, see Grafarend (1984). At a first step, we want to figure out whether the unknowns, $\hat{\mathbf{X}}_1$ and $\hat{\mathbf{X}}_2$, that are adjusted from the observation from two time samples, $\mathbf{L}_1$ and $\mathbf{L}_2$, are significantly different. If it is true that the unknowns has altered from $\hat{\mathbf{X}}_1$ to $\hat{\mathbf{X}}_2$, then at a second step we have to apply a localisation strategy to seek out the cause. A global congruent test can be expressed as null and alternative hypothesis as follows

$$H_0 : \mathrm{E}\big(\hat{\mathbf{X}}_1\big) = \mathrm{E}\big(\hat{\mathbf{X}}_2\big) \text{ and } H_\mathrm{A} : \mathrm{E}\big(\hat{\mathbf{X}}_1\big) \neq \mathrm{E}\big(\hat{\mathbf{X}}_2\big) \; . \tag{3.86}$$

This in turn leads to a F-Test, refer to Niemeier (2008, p. 440). It is also possible to equivalently reformulate the above hypothesis in its implicit form, where the unknowns of the two epochs are the same

$$\hat{\mathbf{X}} = \hat{\mathbf{X}}_1 = \hat{\mathbf{X}}_2 \; . \tag{3.87}$$

If we fail to reject H_0 in favour of H_A, we can start to look for the cause by means of a localisation strategy as follows. In an iterative process, we start to remove only one unknown, say the dth, that corresponds to the two epochs in

$\hat{\mathbf{X}}_1$ as well as in $\hat{\mathbf{X}}_2$. Then, a least squares adjustment is performed where only the dth unknown is excluded. After each adjustment, a test statistic can be computed for each case. This process is repeated one by one for all unknowns. In the last step, we look for the smallest test statistic and its associated removed unknown. The reason why we seek for the smallest value is that it is often the case a large test statistic rejects the null hypothesis. In case the F-Test still rejects the H_0 in favour of H_A, we have to repeat the process over again with the cut down vector of unknowns. Using this strategy we can the significant temporal changes in an object.

4 Variational Calculus

I am pleased to see that we have differences. May we together become greater than the sum of both of us.

– Surak, Star Trek episode "The Savage Curtain" (1969)

Different types of differential equations can be solved approximately by means of the finite element method is presented in Sec. 2.6. The finite element method methodology as a mere recipe without asking why this method works in the first place is followed. The "test functions" and "variational formulation" are expressions that are simply accepted, although they appear obscure. The finite element method might be developed and motivated from mechanics but at some point it grows away from the physics and becomes a mathematical tool for pragmatic reason. Similarly, over time the least squares adjustment becomes limited in its application due to practical reason. The similarity between the method of least squares and finite element method is mentioned by many geodesists, e.g. (Jäger 1988), (Bahndorf 1991), (Singer 1995), (Milev 2001) or (Lienhart 2007). Analogies were drawn by components comparison between both methods, for example, the system of linear equations of the finite element method in Eq. (2.248) and of the least squares adjustment in Eq. (3.43) shares the same algebraic structure. But, this kind of comparison still lacks of in-depth examination. Joachim Boljen has made a more detailed comparison of the two methods and, for unfortunate reasons, has published it as a well-hidden chapter in (Boljen 1993). A very unusual statement in his work indicates that his research on this topic might contradicted the doctrine of his former superior. In order to avoid controversy, he might be forced to release his publications on this subject under meaningless titles. For that reason, other researchers are having hard time to find his works and his groundwork on this matter of the relationship between least squares adjustment and finite element method vanishes from the geodetic community. Due to the recent rediscovery of the well-hidden collection of his studies, one realises that scientific effort is more than doubly wasted: Boljen's groundwork and the researchers after him who have to redo this all again. The aim of this chapter is to catch up and continue this topic, which Boljen did not pursue further, in order to deepen the understanding of adjustment theory.

The notions of both methods are inherently different. While the finite element method solves certain classes of problems described by a system of elliptic partial differential equations, the method of least squares solves another class of problems formulated as an overdetermined system of equations. The contribution of this chapter is to show that both methods follow the same methodological steps developed by Lagrange and Euler already in 1755, see the correspondences between them in (Lagrange 1892). Therefore, a brief introduction to the variational calculus is given. It is particularly important to pay attention to the ability of the variational calculus to reformulate a given problem. There are three representations to describe a single problem, namely *strong*, *variational* and *extremal formulation*. This will explain why many methods have very similar traits. This is examined in more detail in the following using examples. The well-known Gauss-Markov model is derived by using variational calculus in its discrete and continuous version. Then, both the finite element method and the so-called "least squares" finite element method are derived with the aid of variational calculus with familiar notations in geodesy respectively adjustment calculation. The given examples should clarify that both methods, the method of least squares and the finite element method, are not different in terms of their methodical approach. In the end of this chapter a detailed summary is given. The relationship of both methods and the significance of variational calculus in adjustment theory are discussed. Also, possible cross-connections to other methods are also briefly outlined.

4.1 A Brief History of Variational Calculus

The origin of variational calculus can be traced back to the *Brachistochrone problem*. According to the *Webster's Revised Unabridged Dictionary* (1913), *Brachystochrone* is "a curve, in which a body, starting from a given point, and descending solely by the force of gravity, will reach another given point in a shorter time than it could by any other path." As reported by Funk (1962, p. 614), this mathematical challenge has already been studied by Galileo in 1638. He thought that an arc of a circle would be the fastest path, but it turns out that this is not the case, see Galilei (1891, Theorem 22, Propos. 36). In 1696 Johann Bernoulli called upon the mathematical community to solve this problem. His brother Jacob Bernoulli, Newton, Leibniz and many more participated this challenge.

Euler (1744) presented a systematic approach that allows him to advance from solving certain special cases such as the Brachistochrone problem to discussing more general classes of maximisation / minimisation problems, also known as *variational problems*. But Euler was dissatisfied, because his solution relies heavily on geometric considerations, which later became the *method of finite differences*. In 1755 a young prodigy with the name Lagrange sent a letter to Euler to present his idea of "*variation*". By this method, Lagrange reaches the same solution as Euler without requiring geometric considerations. Even though, the expression *calculus of variation* is coined by Lagrange's concept of disturbance "*variation*", this term is widely popularized by Euler. The variational calculus has great influences on different scientific fields. An in-depth overview about the history of variational calculus can be found in Gander and Wanner (2012). The basic idea of the variation calculus is discussed in the next section in the form of a small exercise.

4.2 Extremal, Variational and Strong Formulation of a Problem

Based on the following "standard" exercise in calculus of variation, the three different formulations of one and the same problem can be understood. Suppose a task demands to find the two times differentiable function $y = y(x)$ of the variable x, where the scalar valued quantity J is maximal or minimal respectively extremal. It is assumed that by means of the *Lagrangian density functional* Z that the following formulation of the quantity J can be used to describe appropriately the task

$$J = \int_a^b Z \,\mathrm{d}x = \int_a^b Z(x, y, y') \,\mathrm{d}x \;\rightarrow\; \text{extremal}\,, \tag{4.1}$$

where the boundary conditions, $y(x = a) = y_a$ and $y(x = b) = y_b$, are given and $y' = \frac{\mathrm{d}y}{\mathrm{d}x}$. In calculus of variations, the above formulation is considered to be a principle, a *variational principle* to be precise, which is believed that a certain class of processes follows. For example, the Fermat's principle also known as the *principle of least time* postulates that a ray of light traversed between two points in the least amount of time. In this case, J is the total traverse time that has to be minimal. The path between this two points is described by the function y. The density functional Z represents the obstacles such as different media that lie between the two points. The path y has to be determined. Another example is the aforementioned Brachistochrone problem. A curve y of fastest descent of a particle has to be determined. Therefore, the total descending time J has to be minimal. The gravity that the particle is subjected to as well as the consideration of kinetic energy are expressed by the density functional Z. The variational principle in Eq. (4.1) is a formulation that is valid and applicable for a specific class of problems. In dependence of a given problem the formulation in Eq. (4.1) might be insufficient. In this case, the variational principle has to be extended. Nevertheless, in general a variational principle formulates mathematically a given problem in form as a extremal postulation. Therefore, we can refer variational principles as *extremal formulations* of problems.

The objective is to find the curve y where the extremal formulation of a specific problem in Eq. (4.1) is maximal or minimal. As mentioned in the brief history of calculus of variations, it was Lagrange who found a non-geometrical approach to determine the curve y. The main difficulty is, simply put, to find the derivative of J with respect to y so that it can be set to zero to find the optimal curve y. To overcome this issue, Lagrange varied

around the optimal solution y with a disturbance η in Eq. (4.1) to obtain a non-optimal J. It reads

$$J = \int_a^b Z\big(x, y+\eta, y'+\eta'\big)\,\mathrm{d}x\,. \tag{4.2}$$

Furthermore, he decomposed η into two parts

$$\eta = \varepsilon\delta y\,, \tag{4.3}$$

where $\delta y = \delta y\big(x\big)$ is any function of variable x and the small parameter ε is a scalar value quantity independent of variable x. Inserting Eq. (4.3) into Eq. (4.2), it reads

$$J = \int_a^b Z\big(x, y+\varepsilon\delta y, y'+\varepsilon\delta y'\big)\,\mathrm{d}x\,. \tag{4.4}$$

The function δy is arbitrary in the sense that this function is freely selectable. As a result of this, the arbitrary function δy operates as a given quantity. However, the following constraint applies to this function δy. Since the starting and end points of the curve y are fixed, all possible disturbed curves $y+\eta$ must also pass through these two points. Thus, the disturbance η has to vanish at $x=a$ and at $x=b$. To achieve this, it must hold for

$$\delta y\Big|_{x=a} = \delta y\Big|_{x=b} = 0\,. \tag{4.5}$$

The small parameter ε is used to regulate the perturbation η. In case that $\varepsilon = 0$, J is optimal, since η vanishes and y is the optimal solution. Any other values for ε, J becomes non-optimal. Since the optimal solution y and the arbitrary function are both treated as given, the extremal form $J = J\big(\varepsilon\big)$ becomes a function which depends only on the one single small parameter ε. For $\varepsilon = 0$, J has the optimal value, therefore its first (directional) derivative has to vanish respectively it must hold for

$$\frac{\mathrm{d}J}{\mathrm{d}\varepsilon}\bigg|_{\varepsilon=0} \overset{!}{=} 0\,. \tag{4.6}$$

Inserting Eq. (4.4) into the above equation leads to

$$\frac{\mathrm{d}J}{\mathrm{d}\varepsilon}\bigg|_{\varepsilon=0} = \int_a^b \frac{\mathrm{d}Z}{\mathrm{d}\varepsilon}\bigg|_{\varepsilon=0}\mathrm{d}x\,. \tag{4.7}$$

The total differential $\mathrm{d}Z$ in the above equation reads

$$\mathrm{d}Z = \frac{\partial Z}{\partial x}\,\mathrm{d}x + \frac{\partial Z}{\partial\big(y+\varepsilon\delta y\big)}\,\mathrm{d}\big(y+\varepsilon\delta y\big) + \frac{\partial Z}{\partial\big(y'+\varepsilon\delta y'\big)}\,\mathrm{d}\big(y'+\varepsilon\delta y'\big)\,. \tag{4.8}$$

This in turn yields

$$\begin{aligned}\frac{\mathrm{d}Z}{\mathrm{d}\varepsilon} &= \frac{\partial Z}{\partial x}\underbrace{\frac{\mathrm{d}x}{\mathrm{d}\varepsilon}}_{=0} + \frac{\partial Z}{\partial\big(y+\varepsilon\delta y\big)}\underbrace{\frac{\mathrm{d}\big(y+\varepsilon\delta y\big)}{\mathrm{d}\varepsilon}}_{=\delta y} + \frac{\partial Z}{\partial\big(y'+\varepsilon\delta y'\big)}\underbrace{\frac{\mathrm{d}\big(y'+\varepsilon\delta y'\big)}{\mathrm{d}\varepsilon}}_{=\delta y'} \\ &= \frac{\partial Z}{\partial\big(y+\varepsilon\delta y\big)}\delta y + \frac{\partial Z}{\partial\big(y'+\varepsilon\delta y'\big)}\delta y'\,.\end{aligned} \tag{4.9}$$

When the disturbance is set to zero, i. e. $\varepsilon = 0$, it reads

$$\frac{\mathrm{d}Z}{\mathrm{d}\varepsilon}\bigg|_{\varepsilon=0} = \frac{\partial Z}{\partial y}\delta y + \frac{\partial Z}{\partial y'}\delta y'\,. \tag{4.10}$$

The second expression on the right-hand side in the preceding equation can be rewritten by means of the product rule as

$$\frac{\mathrm{d}}{\mathrm{d}x}\bigg(\frac{\partial Z}{\partial y'}\delta y\bigg) = \frac{\mathrm{d}}{\mathrm{d}x}\bigg(\frac{\partial Z}{\partial y'}\bigg)\delta y + \frac{\partial Z}{\partial y'}\delta y'\,. \tag{4.11}$$

Therefore, Eq. (4.10) can be rewritten as

$$\left.\frac{\mathrm{d}Z}{\mathrm{d}\varepsilon}\right|_{\varepsilon=0} = \frac{\partial Z}{\partial y}\delta y - \frac{\mathrm{d}}{\mathrm{d}x}\left(\frac{\partial Z}{\partial y'}\right)\delta y + \frac{\mathrm{d}}{\mathrm{d}x}\left(\frac{\partial Z}{\partial y'}\delta y\right). \tag{4.12}$$

Inserting the equation above into Eq. (4.7) yields

$$\left.\frac{\mathrm{d}J}{\mathrm{d}\varepsilon}\right|_{\varepsilon=0} = \int_a^b \left(\frac{\partial Z}{\partial y}\delta y - \frac{\mathrm{d}}{\mathrm{d}x}\left(\frac{\partial Z}{\partial y'}\right)\delta y\right)\mathrm{d}x + \int_a^b \frac{\mathrm{d}}{\mathrm{d}x}\left(\frac{\partial Z}{\partial y'}\delta y\right)\mathrm{d}x\,. \tag{4.13}$$

Due to Eq. (4.5), in the preceding equation the second term on the right-hand side vanished

$$\int_a^b \frac{\mathrm{d}}{\mathrm{d}x}\left(\frac{\partial Z}{\partial y'}\delta y\right)\mathrm{d}x = \left.\frac{\partial Z}{\partial y'}\right|_{x=b}\underbrace{\left.\delta y\right|_{x=b}}_{=0} - \left.\frac{\partial Z}{\partial y'}\right|_{x=a}\underbrace{\left.\delta y\right|_{x=a}}_{=0} = 0\,. \tag{4.14}$$

Finally, the following expression

$$\left.\frac{\mathrm{d}J}{\mathrm{d}\varepsilon}\right|_{\varepsilon=0} = \int_a^b \left(\frac{\partial Z}{\partial y} - \frac{\mathrm{d}}{\mathrm{d}x}\left(\frac{\partial Z}{\partial y'}\right)\right)\delta y\,\mathrm{d}x = 0\,. \tag{4.15}$$

is obtained. Since the above expression

$$\int_a^b \left(\frac{\partial Z}{\partial y} - \frac{\mathrm{d}}{\mathrm{d}x}\left(\frac{\partial Z}{\partial y'}\right)\right)\delta y\,\mathrm{d}x = 0 \tag{4.16}$$

is derived from the idea of LAGRANGE's variation, it is referred to as the *variational formulation*. This form plays an important role in the numerical computation for the finite element method as well as for the least squares adjustment as it shall be seen later. Since this formulation is often used to determine various approximate solutions, equation Eq. (4.16) is also known as the *weak* formulation.

In a nonchalant way, LAGRANGE concluded that from Eq. (4.16)

$$\frac{\partial Z}{\partial y} - \frac{\mathrm{d}}{\mathrm{d}x}\left(\frac{\partial Z}{\partial y'}\right) = 0 \tag{4.17}$$

must hold. This conclusion can be made due to the so-called *fundamental lemma of calculation of variations* that was not known to him at that time. According to this lemma, the arbitrary function δy can be anything due to its arbitrariness and the only way to ensure that the variational formulation in Eq. (4.16) is fulfilled for any arbitrary function δy is to force the expression in the parenthesis in Eq. (4.16) to be always zero. This leads to the equation in Eq. (4.17) that is known as the *Euler-Lagrange equation*. It can be solved analytically to determine the optimal curve y. Since an approximate solution is unable to satisfy Eq. (4.17) respectively only the exact one can fulfil, equation Eq. (4.17) is also referred to as the *strong formulation*.

What insights can be learnt from this exercise in calculus of variation? A given problem can be formulated in three different ways: extremal, variational and strong form. Moreover, these three formulations can be converted among each other. In this particular exercise a specified problem is restated from the extremal form in Eq. (4.1) to the variational form in Eq. (4.16) to the strong form in Eq. (4.17). It is also possible start at any form and converting to another one. Then, each formulation can be served as an entry point to various methods in order to solve the problem. Some main aspects of the three different formulations are presented as follows.

extremal form A problem is stated as a certain value J that has to be minimal or maximal. This value J may be scaled and shifted by a constant factor and a fixed offset without changing the problem statement. Therefore, the extremal formulation is not unique in that sense that J may take different extremal forms, but they may all describe the same problem. Some examples of extremal formulated problems are: The aforementioned Brachistochrone problem where the total descending time has to be minimal, maximising profits or minimising losses in economics,

in optics the principle of least time states that a ray of light prefers a path to travel from one point to another at least amount of time, in least squares adjustment the sum of weighted squared residuals has to be minimised and many more.

variational form This formulation is seemingly an intermediate state in the exercise of calculus of variation. But by far, this form serves as the most interesting entry point for many different numerical methods. If one looks closely, a simplified depiction of the variational form in Eq. (4.16) has this outline $\int fg = 0$. In a vector interpretation, this expression can be seen as a dot product between f and g. Therefore, it demands that f is orthogonal to g respectively it requests the perpendicular distance of f to g to be minimal. If f can be seen as some sort of measure on how well some solutions can fulfil f (also known as *residual*), the variational formulation can be used to minimize f in order to determine some optimal solution. Since f can be non-zero in the variational formulation, this implies that f can accept an approximate solution. Due to this reason, the variational formulation is considered less restrictive and this non-strictness property is often described as "weak". Therefore, the variational formulation is also known as the *weak formulation*. In this particular exercise, this form is derived from the extremal formulation, but it is also possible to reach the variational form from the strong formulation in Eq. (4.17) by multiplying it by an arbitrary function δy and integrating it over the domain of interest. This approach is for example often used in finite element method. And one may notice that the function δy is none other than the so-called *test function* in finite element method. It is important to note that for numerical analysis the function δy has to be specified and at the same time this function has to fulfil certain compatibility aspects in order to obtain computable results. Furthermore, one needs to state a certain *trial function* respectively *ansatz function* for y.

strong form In the exercise this formulation is extracted from variational form. If the simplified depiction of the variation formulation $\int fg = 0$ is re-examined, one notices that the strong form is $f = 0$. This implies that in the strong formulation the solution has to satisfy f completely. Only the exact solution can fulfil this requirement. This strictness is described as "strong". One may realize that in the exercise in calculus of variation the strong formulation is a differential equation. By thinking ahead, the strong formulation can be any kind of equation. As long as it can be assumed that a system of (differential) equations is being able to describe a given problem properly enough, an exact solution of the problem can be obtained by solving the equations. In case an exact solution is unobtainable, one can still try to approximate the solution by reformulating the strong formulation into its variational form. Furthermore, in comparison to other formulations, the strong formulation of a given problem has an exclusive characteristic when this formulation is represented independently of a particular system of coordinates. Aforementioned, an extremal formulation can be scaled and shifted without changing the problem statement. Therefore, it is possible to have different in fact infinite amount of extremal formulations that are describing the same problem. In contrast, a modification of the strong formulation leads to a different problem description and vice versa. In other words, a given problem is clearly assigned to one single representation in the strong form. This implies that there is only one theory of anything. Some examples of strong formulated problems are: equations of elastodynamics in mechanics in Eq. (2.161), the Lamé-Navier equations in Eq. (2.162), the Euler-Bernoulli beam equation in Eq. (2.182), heat equation in Eq. (2.206) in thermodynamics, Maxwell's equations in electrodynamics and even overdetermined system of equations in least squares adjustment.

The questions "Where to begin?" or "Which order one must follows to obtain a solution?" is unnecessary. All three formulations exist side-by-side. An expedient procedure results rather from an abstract comprehension of a given problem and one's intention.

In conclusion, a problem can be formulated in three different ways: As an *extremal formulation* where one has to look for an extremal value J to determine an optimal solution, as a *variational*, respectively, *weak formulation* where a numerical method is applied to compute an approximate solution and as a *strong formulation* where one has to find an analytical solution.

4.3 Calculus of Variations and Least Squares Adjustment

In least squares adjustment, the sum of weighted squared residuals is postulated to be minimal. Using variational calculus, the very same normal equations from adjustment calculation can be obtained from this postulation. For the continuous function, the minimization of the integrated squared residual is postulated. A normal equation system can also be determined by means of variational calculus.

The method of least squares in context of variational calculus

The least squares adjustment can be seen as a variational principle. For the sake of clarity, the solution of the linear Gauss-Markov model is derived. Consider the following overdetermined system of equations

$$\mathbf{L} = \boldsymbol{\Phi}\,, \tag{4.18}$$

where $\boldsymbol{\Phi} = \boldsymbol{\Phi}\big(\mathbf{X}\big)$ is a vector of functions of unknown parameters $\mathbf{X}$ and $\mathbf{L}$ containing the observations. Dealing with such an overdetermined equation system in which the observations in $\mathbf{L}$ are subjected to random errors, Eq. (4.18) is generally impossible to solve. For a specific case where Eq. (4.18) can be fulfilled, it is when the true observation vector is given $\mathbf{L} = \tilde{\mathbf{L}}$ and $\boldsymbol{\Phi} = \boldsymbol{\Phi}\big(\tilde{\mathbf{X}}\big)$ is a function of the true parameters $\tilde{\mathbf{X}}$. For any other $\mathbf{X}$, the difference between $\mathbf{L}$ and $\boldsymbol{\Phi}$ can be expressed by introducing the vector of residuals

$$\mathbf{v} = \boldsymbol{\Phi} - \mathbf{L}\,. \tag{4.19}$$

The aim is to find the adjusted parameters $\mathbf{X} = \hat{\mathbf{X}}$ where the sum of the weighted squared residuals is minimized

$$\Omega = \mathbf{v}^{\mathsf{T}}\mathbf{P}\mathbf{v} \;\rightarrow\; \text{minimal}\,, \tag{4.20}$$

where $\mathbf{P}$ is the weight matrix of the observations. The above expression is an extremal formulation, cf. Eq. (4.1). Substituting $\mathbf{v}$ in Eq. (4.20) with Eq. (4.19) leads to

$$\begin{aligned}\Omega = \mathbf{v}^{\mathsf{T}}\mathbf{P}\mathbf{v} &= \big(\boldsymbol{\Phi} - \mathbf{L}\big)^{\mathsf{T}}\mathbf{P}\big(\boldsymbol{\Phi} - \mathbf{L}\big) = \big(\boldsymbol{\Phi}^{\mathsf{T}} - \mathbf{L}^{\mathsf{T}}\big)\big(\mathbf{P}\boldsymbol{\Phi} - \mathbf{P}\mathbf{L}\big) = \\ &= \boldsymbol{\Phi}^{\mathsf{T}}\mathbf{P}\boldsymbol{\Phi} - \boldsymbol{\Phi}^{\mathsf{T}}\mathbf{P}\mathbf{L} - \underbrace{\mathbf{L}^{\mathsf{T}}\mathbf{P}\boldsymbol{\Phi}}_{=\left(\boldsymbol{\Phi}^{\mathsf{T}}\mathbf{P}\mathbf{L}\right)^{\mathsf{T}}=\boldsymbol{\Phi}^{\mathsf{T}}\mathbf{P}\mathbf{L}} + \mathbf{L}^{\mathsf{T}}\mathbf{P}\mathbf{L} = \boldsymbol{\Phi}^{\mathsf{T}}\mathbf{P}\boldsymbol{\Phi} - 2\boldsymbol{\Phi}^{\mathsf{T}}\mathbf{P}\mathbf{L} + \mathbf{L}^{\mathsf{T}}\mathbf{P}\mathbf{L}\,.\end{aligned} \tag{4.21}$$

Then, the idea of Lagrange is applied: $\boldsymbol{\Phi} = \boldsymbol{\Phi}\big(\hat{\mathbf{X}}\big)$ is varied by adding the disturbance vector

$$\boldsymbol{\eta} = \varepsilon\delta\boldsymbol{\Phi}\,, \tag{4.22}$$

where ε is the small parameter and $\delta\boldsymbol{\Phi} = \delta\boldsymbol{\Phi}\big(\mathbf{Y}\big)$ is the vector of test functions of an arbitrary set of parameters $\mathbf{Y}$. It reads

$$\begin{aligned}\Omega &= \big(\boldsymbol{\Phi} + \varepsilon\delta\boldsymbol{\Phi}\big)^{\mathsf{T}}\mathbf{P}\big(\boldsymbol{\Phi} + \varepsilon\delta\boldsymbol{\Phi}\big) - 2\big(\boldsymbol{\Phi} + \varepsilon\delta\boldsymbol{\Phi}\big)^{\mathsf{T}}\mathbf{P}\mathbf{L} + \mathbf{L}^{\mathsf{T}}\mathbf{P}\mathbf{L} \\ &= \big(\boldsymbol{\Phi}^{\mathsf{T}} + \varepsilon\delta\boldsymbol{\Phi}^{\mathsf{T}}\big)\big(\mathbf{P}\boldsymbol{\Phi} + \varepsilon\mathbf{P}\delta\boldsymbol{\Phi}\big) - 2\big(\boldsymbol{\Phi}^{\mathsf{T}} + \varepsilon\delta\boldsymbol{\Phi}^{\mathsf{T}}\big)\mathbf{P}\mathbf{L} + \mathbf{L}^{\mathsf{T}}\mathbf{P}\mathbf{L} \\ &= \boldsymbol{\Phi}^{\mathsf{T}}\mathbf{P}\boldsymbol{\Phi} + \varepsilon\boldsymbol{\Phi}^{\mathsf{T}}\mathbf{P}\delta\boldsymbol{\Phi} + \varepsilon\delta\boldsymbol{\Phi}^{\mathsf{T}}\mathbf{P}\boldsymbol{\Phi} + \varepsilon^2\delta\boldsymbol{\Phi}^{\mathsf{T}}\mathbf{P}\delta\boldsymbol{\Phi} - 2\boldsymbol{\Phi}^{\mathsf{T}}\mathbf{P}\mathbf{L} - 2\varepsilon\delta\boldsymbol{\Phi}^{\mathsf{T}}\mathbf{P}\mathbf{L} + \mathbf{L}^{\mathsf{T}}\mathbf{P}\mathbf{L}\,,\end{aligned} \tag{4.23}$$

cf. Eq. (4.4). In case that $\varepsilon = 0$, Ω is minimal, since $\boldsymbol{\eta}$ vanishes and $\boldsymbol{\Phi} = \boldsymbol{\Phi}\big(\hat{\mathbf{X}}\big)$ is the adjusted solution. Any other values for ε, Ω becomes non-minimal. The essence of the Lagrange's method is that all unknown parameters $\mathbf{X}$ can be varied simultaneously by a single small parameter ε to find the adjusted parameters. This in turn yields $\Omega = \Omega\big(\varepsilon\big)$ that solely depends on ε. Therefore, Ω is minimal when its directional derivative vanishes at $\varepsilon = 0$

$$\left.\frac{\mathrm{d}\Omega}{\mathrm{d}\varepsilon}\right|_{\varepsilon=0} \overset{!}{=} 0\,. \tag{4.24}$$

The left-hand side of above equation reads

$$\begin{aligned}\left.\frac{\mathrm{d}\Omega}{\mathrm{d}\varepsilon}\right|_{\varepsilon=0} &= \left(\boldsymbol{\Phi}^{\mathsf{T}}\mathbf{P}\delta\boldsymbol{\Phi} + \delta\boldsymbol{\Phi}^{\mathsf{T}}\mathbf{P}\boldsymbol{\Phi} + \varepsilon\delta\boldsymbol{\Phi}^{\mathsf{T}}\mathbf{P}\delta\boldsymbol{\Phi} - 2\delta\boldsymbol{\Phi}^{\mathsf{T}}\mathbf{P}\mathbf{L}\right)\Big|_{\varepsilon=0} \\ &= \boldsymbol{\Phi}^{\mathsf{T}}\mathbf{P}\delta\boldsymbol{\Phi} + \underbrace{\delta\boldsymbol{\Phi}^{\mathsf{T}}\mathbf{P}\boldsymbol{\Phi}}_{=\left(\boldsymbol{\Phi}^{\mathsf{T}}\mathbf{P}\delta\boldsymbol{\Phi}\right)^{\mathsf{T}}=\boldsymbol{\Phi}^{\mathsf{T}}\mathbf{P}\delta\boldsymbol{\Phi}} - 2\delta\boldsymbol{\Phi}^{\mathsf{T}}\mathbf{P}\mathbf{L} \\ &= 2\boldsymbol{\Phi}^{\mathsf{T}}\mathbf{P}\delta\boldsymbol{\Phi} - 2\underbrace{\delta\boldsymbol{\Phi}^{\mathsf{T}}\mathbf{P}\mathbf{L}}_{=\left(\mathbf{L}^{\mathsf{T}}\mathbf{P}\delta\boldsymbol{\Phi}\right)^{\mathsf{T}}=\mathbf{L}^{\mathsf{T}}\mathbf{P}\delta\boldsymbol{\Phi}}\end{aligned}$$

$$= 2\boldsymbol{\Phi}^{\mathsf{T}}\mathbf{P}\delta\boldsymbol{\Phi} - 2\mathbf{L}^{\mathsf{T}}\mathbf{P}\delta\boldsymbol{\Phi}\,. \tag{4.25}$$

The variational formulation is obtained by setting the above equation to zero

$$\left(\boldsymbol{\Phi}^{\mathsf{T}}\mathbf{P} - \mathbf{L}^{\mathsf{T}}\mathbf{P}\right)\delta\boldsymbol{\Phi} = 0\,, \tag{4.26}$$

cf. Eq. (4.16). The fundamental lemma of calculation of variations is applied above as in Eq. (4.16) to Eq. (4.17) in order to obtain

$$\boldsymbol{\Phi}^{\mathsf{T}}\mathbf{P} - \mathbf{L}^{\mathsf{T}}\mathbf{P} = 0\,. \tag{4.27}$$

The strong formulation results by equating the coefficients with respect to $\mathbf{P}$ and transposing the equation

$$\boldsymbol{\Phi}^{\mathsf{T}}\mathbf{P} = \mathbf{L}^{\mathsf{T}}\mathbf{P} \;\rightarrow\; \boldsymbol{\Phi}^{\mathsf{T}} = \mathbf{L}^{\mathsf{T}} \;\rightarrow\; \boldsymbol{\Phi} = \mathbf{L}\,. \tag{4.28}$$

The strong formulation is the overdetermined system of equations before the vector of residuals $\mathbf{v}$ is introduced. One notices again that the strong formulation can be fulfilled only by the true solution $\boldsymbol{\Phi} = \boldsymbol{\Phi}\left(\tilde{\mathbf{X}}\right)$ where $\Omega = 0$ and there is usually no guarantee for the existence of this analytical solution.

Aforesaid, the variational formulation serves for many numerical methods as an entry point, therefore Eq. (4.26) is used to obtain the solution of the Gauss-Markov model. For the simplicity, a linear functional model

$$\boldsymbol{\Phi} = \mathbf{A}\mathbf{X} \tag{4.29}$$

with design matrix $\mathbf{A}$ containing its coefficients is assumed. To obtain numerical results, the vector of test functions is chosen to share the same algebraic structure as the functional model $\boldsymbol{\Phi}$. This choice is a characteristic that least squares adjustment and finite element method have in common. Thus, both contain the design matrix $\mathbf{A}$ and the test functions reads

$$\delta\boldsymbol{\Phi} = \mathbf{A}\mathbf{Y}\,. \tag{4.30}$$

The arbitrariness of $\delta\boldsymbol{\Phi}$ ensures that the parameters in the vector $\mathbf{Y}$ can take any values. The variational formulation Eq. (4.26) can be written as

$$\begin{aligned}\left(\hat{\mathbf{X}}^{\mathsf{T}}\mathbf{A}^{\mathsf{T}}\mathbf{P} - \mathbf{L}^{\mathsf{T}}\mathbf{P}\right)\mathbf{A}\mathbf{Y} &= 0\\ \hat{\mathbf{X}}^{\mathsf{T}}\mathbf{A}^{\mathsf{T}}\mathbf{P}\mathbf{A}\mathbf{Y} &= \mathbf{L}^{\mathsf{T}}\mathbf{P}\mathbf{A}\mathbf{Y}\,.\end{aligned} \tag{4.31}$$

Equating coefficients with respect to $\mathbf{Y}$ yields

$$\hat{\mathbf{X}}^{\mathsf{T}}\mathbf{A}^{\mathsf{T}}\mathbf{P}\mathbf{A} = \mathbf{L}^{\mathsf{T}}\mathbf{P}\mathbf{A}\,. \tag{4.32}$$

Finally, the last step is to transpose the above equation, we obtain the normal equations as in Eq. (3.41)

$$\mathbf{A}^{\mathsf{T}}\mathbf{P}\mathbf{A}\hat{\mathbf{X}} = \mathbf{A}^{\mathsf{T}}\mathbf{P}\mathbf{L}\,.$$

Four conclusions can be drawn from this:

1. It is possible to derive the solution of the linear Gauss-Markov model by using variational calculus.
2. In adjustment calculation, the optimal parameters are obtained by differentiating the objective function Ω with respect to the unknown parameters $\mathbf{X}$. In variational calculus, the same optimal parameters result by differentiating the objective function Ω with respect to the small parameter ε. This implies that

$$\left.\frac{\mathrm{d}\Omega}{\mathrm{d}\varepsilon}\right|_{\varepsilon=0} \equiv \frac{\mathrm{d}\Omega}{\mathrm{d}\mathbf{X}} \tag{4.33}$$

must hold. In this regard, one can conclude that it is more elegant to differentiate the objective function Ω with respect to the *one* small parameter ε than to numerous unknown parameters $\mathbf{X}$.

3. The starting point of the least squares adjustment is the overdetermined system of linear equations in Eq. (4.18). Or, equivalently, Eq. (4.28) can be considered as the starting point. One can multiply Eq. (4.28) with the vector of test functions $\delta\mathbf{\Phi}$ in order to reach the variational formulation in Eq. (4.26). From here the normal equations can be obtained, see Eq. (4.31). By doing this way, one can reach the normal equations "faster", as the way to get there is shorter, i. e. from Eq. (4.28) to Eq. (4.26), than from Eq. (4.18) to Eq. (4.26). In conclusion, multiplying the strong formulation (as in Eq. (4.18) or Eq. (4.28)) with the vector of test functions $\delta\mathbf{\Phi}$ has the same effect as to introducing the residuals $\mathbf{v}$ as in Eq. (4.19). This "inverse" usage of variational calculus is mainly carried out in the finite element method.

4. Assume that the starting point is the strong formulation in Eq. (4.28). And the aim is to determine the target function Ω. Therefore, the trace of backwards application of the variational calculus is being followed, i. e. from Eq. (4.28) to Eq. (4.21). One can observe that the term $\mathbf{L}^\mathsf{T}\mathbf{P}\mathbf{L}$ of the objective function in Eq. (4.21) is a scalar constant. A modification of this term into

$$\Omega = \mathbf{\Phi}^\mathsf{T}\mathbf{P}\mathbf{\Phi} - 2\mathbf{\Phi}^\mathsf{T}\mathbf{P}\mathbf{L} + c\,, \tag{4.34}$$

where c is of any constant, the resulting parameters $\mathbf{X}$ remain unaffected, since the constant c vanishes by the derivation in Eq. (4.24). This example shows that the extremal formulation is not unique. By changing the constant c, the objective function Ω can take different forms, but they all describe the same problem. And that $c = \mathbf{L}^\mathsf{T}\mathbf{P}\mathbf{L}$ respectively $\Omega = \mathbf{v}^\mathsf{T}\mathbf{P}\mathbf{v}$ is a special case. In adjustment calculation, this fact is overlooked due to the introduction of residuals $\mathbf{v}$ instead of using the test functions $\delta\mathbf{\Phi}$.

Continuous Least Squares Adjustment

The adjustment calculation usually deals with problems involving discrete observations $\mathbf{L}$. By means of the variational calculation, the handling of continuous observation function L can also be taken into account (cf. Burden and Faires 2011, Sec. 8.2). Consider the following equation

$$L = \Phi\,, \tag{4.35}$$

where $L = L(x)$ is the "given" observation function and $\Phi = \Phi(x)$ is the "wanted" trial function. Both functions depend on the variable x. In general, the above equation is impossible to satisfy as it attempts to describe a continuous observation signal L by an idealized function Φ with adjustable unknown parameters. The trial function Φ approximates the observation function L. The difference between the two functions creates a residual function

$$v = \Phi - L\,, \tag{4.36}$$

where $v = v(x)$ depends also on the variable x. The aim is to minimize the integrated squared residuals

$$\Omega = \int_a^b v^2\,\mathrm{d}x = \int_a^b (\Phi - L)^2\,\mathrm{d}x \;\rightarrow\; \text{minimal}\,, \tag{4.37}$$

where the integration limits are a and b. A weight function $P = P(x)$ can be introduced for the objective function Ω by dividing Eq. (4.35) by a variance function $\sigma = \sigma(x)$, where $P = \frac{1}{\sigma^2}$. For the sake of clarity, this is omitted by $\sigma = 1$. The above expression is an extremal formulation, cf. Eq. (4.1). Using the Lagrange's method, Φ is perturbed with the disturbance function $\eta = \eta(x)$ which is decomposed into two parts

$$\eta = \varepsilon\delta\Phi\,, \tag{4.38}$$

where $\delta\Phi = \delta\Phi(x)$ is the test function and ε is the small parameter. The non-optimal Ω reads

$$\Omega = \int_a^b (\Phi + \eta - L)^2\,\mathrm{d}x = \int_a^b (\Phi + \varepsilon\delta\Phi - L)^2\,\mathrm{d}x\,, \tag{4.39}$$

cf. Eq. (4.4). The target function Ω becomes minimal when its directional derivative vanishes and where the disturbance is eliminated by setting $\varepsilon = 0$

$$\begin{aligned}\left.\frac{\mathrm{d}\Omega}{\mathrm{d}\varepsilon}\right|_{\varepsilon=0} &\stackrel{!}{=} 0\\ &= \int_a^b \frac{\mathrm{d}}{\mathrm{d}\varepsilon}\big(\Phi + \varepsilon\delta\Phi - L\big)^2\,\mathrm{d}x\Big|_{\varepsilon=0} = \int_a^b 2\big(\Phi + \varepsilon\delta\Phi - L\big)\delta\Phi\,\mathrm{d}x\Big|_{\varepsilon=0} = \int_a^b 2\big(\Phi - L\big)\delta\Phi\,\mathrm{d}x\,. \end{aligned} \tag{4.40}$$

The variational formulation is therefore

$$\int_a^b \big(\Phi - L\big)\delta\Phi\,\mathrm{d}x = 0\,, \tag{4.41}$$

cf. Eq. (4.16). The fundamental lemma of calculation of variations is applied above as in Eq. (4.16) to Eq. (4.17) in order to obtain the strong formulation

$$\Phi - L = 0\,, \tag{4.42}$$

which is to be expected.

The variational formulation in Eq. (4.41) is used to compute the solution of the continuous Gauss-Markov model. Also, for the simplicity, a trial function

$$\Phi = \sum_{i=0}^{N-1} c_i X_i \tag{4.43}$$

is used, which is a linear combination of a fixed number N of given basis functions $X_i = X_i\left(x\right)$ with unknown scalar valued parameters c_i. To obtain computable results, the test function $\delta\Phi$ is chosen to share the same structure as the trial function Φ. Thus, the test function reads

$$\delta\Phi = \sum_{j=0}^{N-1} b_j X_j\,. \tag{4.44}$$

The parameters b_j can take any values, therefore the arbitrariness of $\delta\Phi$ is ensured. Inserting Eqs. (4.43) and (4.44) into Eq. (4.41), the variational formulation in Eq. (4.41) can be rewritten as

$$\begin{aligned}\int_a^b \Phi\delta\Phi\,\mathrm{d}x &= \int_a^b L\delta\Phi\,\mathrm{d}x\\ \int_a^b \left(\sum_{i=0}^{N-1} c_i X_i\right)\left(\sum_{j=0}^{N-1} b_j X_j\right)\mathrm{d}x &= \int_a^b L\left(\sum_{j=0}^{N-1} b_j X_j\right)\mathrm{d}x\\ \sum_{j=0}^{N-1}\sum_{i=0}^{N-1} c_i \int_a^b X_i X_j\,\mathrm{d}x\, b_j &= \sum_{j=0}^{N-1}\int_a^b L X_j\,\mathrm{d}x\, b_j\,. \end{aligned} \tag{4.45}$$

From here it is advisable to switch to matrix notation, as the unknowns c_i are to be determined. It reads

$$\mathbf{X}^\mathsf{T}\mathbf{N}\mathbf{b} = \mathbf{n}^\mathsf{T}\mathbf{b}\,, \tag{4.46}$$

where

$$\mathbf{X}^\mathsf{T} = \begin{bmatrix} c_0 & c_1 & \dots & c_i & \dots & c_{N-1}\end{bmatrix}\,,$$

$$
\mathbf{N} = \begin{bmatrix} \int_a^b X_0 X_0 \,\mathrm{d}x & \cdots & \int_a^b X_0 X_j \,\mathrm{d}x & \cdots & \int_a^b X_1 X_{N-1} \,\mathrm{d}x \\ \vdots & \ddots & \vdots & \ddots & \vdots \\ \int_a^b X_i X_0 \,\mathrm{d}x & \cdots & \int_a^b X_i X_j \,\mathrm{d}x & \cdots & \int_a^b X_i X_{N-1} \,\mathrm{d}x \\ \vdots & \ddots & \vdots & \ddots & \vdots \\ \int_a^b X_{N-1} X_0 \,\mathrm{d}x & \cdots & \int_a^b X_{N-1} X_j \,\mathrm{d}x & \cdots & \int_a^b X_{N-1} X_{N-1} \,\mathrm{d}x \end{bmatrix},
$$

$$
\mathbf{n}^\mathsf{T} = \begin{bmatrix} \int_a^b L X_0 \,\mathrm{d}x & \int_a^b L X_1 \,\mathrm{d}x & \cdots & \int_a^b L X_j \,\mathrm{d}x & \cdots & \int_a^b L X_{N-1} \,\mathrm{d}x \end{bmatrix},
$$

$$
\mathbf{b} = \begin{bmatrix} b_0 & b_1 & \dots & b_j & \dots & b_{N-1} \end{bmatrix}^\mathsf{T}.
$$

By equating the coefficients with respect to $\mathbf{b}$ followed by a transposition, the above equation can be rewritten as

$$
\mathbf{X}^\mathsf{T}\mathbf{N} = \mathbf{n}^\mathsf{T} \text{ respectively } \mathbf{N}\mathbf{X} = \mathbf{n}\,. \tag{4.47}
$$

The normal equations for the continuous Gauss-Markov model is obtained. The normal matrix $\mathbf{N}$ is square and symmetrical due to the choice of the compatible test function $\delta\Phi$ in regard to the test function Φ. Non-compatible test function would lead to non-squared that leads to unsolvable normal equations.

Example: Fourier series

The continuous Gauss-Markov model is applied, for example, in Fourier series, where an (observation) signal L of length T is represented approximately as the sum of a finite but fixed number N of complex exponentials, or respectively of sine / cosine functions. In this case, the integral interval is from $a = 0$ to $b = T$, where the length T of the signal L is given. The following trial and test function are used

$$
\Phi = \sum_{k=-N}^{N} c_k \exp\bigl(\jmath k\omega x\bigr) \text{ and } \delta\Phi = \sum_{l=-N}^{N} b_l \exp\bigl(\jmath l\omega x\bigr)\,, \tag{4.48}
$$

where $\omega = \frac{2\pi}{T}$ is the fundamental frequency, $\jmath$ is the imaginary unit (lateral unit), c_k are unknown scalar complex valued parameters and b_l are the coefficients of the test function. Using the results from Eq. (4.47) and the following orthogonal relationship

$$
\int_0^T \exp\bigl(\jmath k\omega x\bigr) \exp\bigl(\jmath l\omega x\bigr) \,\mathrm{d}x = \begin{cases} \bigl[\frac{1}{\jmath(k+l)\omega} \exp\bigl(\jmath(k+l)\omega x\bigr)\bigr]_0^T = 0 & \text{if } k+l \neq 0\,, \\ \bigl[x\bigr]_0^T = T & \text{if } k+l = 0\,, \end{cases} \tag{4.49}
$$

the normal equation system reads as

$$
\begin{bmatrix} & & & T \\ & & \iddots & \\ & T & & \\ \iddots & & & \\ T & & & \end{bmatrix} \begin{bmatrix} c_{-N} \\ \vdots \\ c_0 \\ \vdots \\ c_N \end{bmatrix} = \begin{bmatrix} \int_0^T L \exp(-\jmath N\omega x) \,\mathrm{d}x \\ \vdots \\ \int_0^T L \exp(\jmath 0\omega x) \,\mathrm{d}x \\ \vdots \\ \int_0^T L \exp(\jmath N\omega x) \,\mathrm{d}x \end{bmatrix}. \tag{4.50}
$$

Respectively, the above equation can be rewritten as

$$
c_k = \frac{1}{T} \int_0^T L \exp(-\jmath k\omega x) \,\mathrm{d}x\,. \tag{4.51}
$$

From here, it leads inevitably to Fourier Analysis.

4.4 Calculus of Variations and Finite Element Method

In contrary to least squares adjustment, the finite element method is used to approximate the solution of differential equations. That is, instead of dealing with (algebraic) equations as in Eq. (4.18) and in Eq. (4.35), differential equations, for example, such as

$$\nabla^2 \boldsymbol{\Phi} = \mathbf{L} \tag{4.52}$$

are solved where ∇^2 is the vector Laplacian operator. This equation is known as Poisson equation. Elastostatic equations such as the in Lamé-Navier equations in Eq. (2.162) and the Euler-Bernoulli beam equation in Eq. (2.182) are considered as Poisson-type equations. For the sake of better understanding, a one-dimensional case as follows is considered

$$\frac{\mathrm{d}^2 \Phi}{\mathrm{d}x^2} = L\,, \tag{4.53}$$

where $\Phi = \Phi\big(x\big)$ and $L = L\big(x\big)$ are functions of the variable x and the boundary conditions for $\Phi_a = \Phi\big(x = a\big)$ and $\Phi_b = \Phi\big(x = b\big)$ are given. From perspective of variational calculus, the Poisson equation represents the Euler-Lagrange equation respectively strong formulation. A numerical solution can be obtained by progressing backwards in the calculus of variations by starting from the strong formulation.

Ritz-Galerkin Method

To obtain the variational form of the Poisson equation, Eq. (4.53) is multiplied by the test function $\delta\Phi$ and is integrated over the whole interval. It reads

$$\int_a^b \frac{\mathrm{d}^2 \Phi}{\mathrm{d}x^2} \delta\Phi \,\mathrm{d}x = \int_a^b L \delta\Phi \,\mathrm{d}x\,. \tag{4.54}$$

By means of the product rule, the expression on the left-hand side can be rewritten as

$$\frac{\mathrm{d}}{\mathrm{d}x}\left(\frac{\mathrm{d}\Phi}{\mathrm{d}x}\delta\Phi\right) = \frac{\mathrm{d}^2\Phi}{\mathrm{d}x^2}\delta\Phi + \frac{\mathrm{d}\Phi}{\mathrm{d}x}\frac{\mathrm{d}\delta\Phi}{\mathrm{d}x}\,. \tag{4.55}$$

Substituting the above equation in Eq. (4.54) yields

$$\int_a^b \frac{\mathrm{d}}{\mathrm{d}x}\left(\frac{\mathrm{d}\Phi}{\mathrm{d}x}\delta\Phi\right)\mathrm{d}x - \int_a^b \frac{\mathrm{d}\Phi}{\mathrm{d}x}\frac{\mathrm{d}\delta\Phi}{\mathrm{d}x}\,\mathrm{d}x = \int_a^b L\delta\Phi\,\mathrm{d}x\,. \tag{4.56}$$

The first expression on the left-hand side vanishes due to the disappearing of the test function on the boundaries $x = a$ and $x = b$, see Eq. (4.5),

$$\int_a^b \frac{\mathrm{d}}{\mathrm{d}x}\left(\frac{\mathrm{d}\Phi}{\mathrm{d}x}\delta\Phi\right)\mathrm{d}x = \frac{\mathrm{d}\Phi}{\mathrm{d}x}\bigg|_{x=b}\underbrace{\delta\Phi\big|_{x=b}}_{=0} - \frac{\mathrm{d}\Phi}{\mathrm{d}x}\bigg|_{x=a}\underbrace{\delta\Phi\big|_{x=a}}_{=0} = 0\,. \tag{4.57}$$

Thus, the variational form of the one-dimensional Poisson equation reads

$$\int_a^b \Phi'\delta\Phi'\,\mathrm{d}x = -\int_a^b L\delta\Phi\,\mathrm{d}x\,, \tag{4.58}$$

where $\Phi' = \frac{\mathrm{d}\Phi}{\mathrm{d}x}$ and $\delta\Phi' = \frac{\mathrm{d}\delta\Phi}{\mathrm{d}x}$. Next, Φ is represented approximately as the sum of a set of basis functions

$$\Phi = \sum_{i=1}^{N} u_i X_i\,, \tag{4.59}$$

where u_i are scalar valued coefficients of the basis functions $X_i = X_i(x)$. The derivative order of the variational formulation in Eq. (4.58) specifies that the basis functions X_i must be at least once differentiable. The corresponding test function has to be arbitrary, but for numerical computation it has to be compatible. Hence, the test function consists of the same set of basis functions as the trial function

$$\delta\Phi = \sum_{j=1}^{N} w_j X_j \,, \tag{4.60}$$

where w_j are arbitrary scalar valued coefficients. Substituting the functions Φ and $\delta\Phi$ in Eq. (4.58), it reads

$$\begin{aligned} \int_a^b \left(\sum_{i=1}^{N} u_i X_i'\right)\left(\sum_{j=1}^{N} w_j X_j'\right) \mathrm{d}x &= -\int_a^b L\left(\sum_{j=1}^{N} w_j X_j\right) \mathrm{d}x \\ \sum_{j=1}^{N}\sum_{i=1}^{N} u_i \int_a^b X_i' X_j' \,\mathrm{d}x\, w_j &= -\sum_{j=1}^{N} \int_a^b L X_j \,\mathrm{d}x\, w_j \,, \end{aligned} \tag{4.61}$$

where $X_i' = \frac{\mathrm{d}X_i}{\mathrm{d}x}$. It is advisable to switch to matrix notation, as the unknown u_i are to be determined. It yields

$$\mathbf{u}^\mathsf{T}\mathbf{K}\mathbf{w} = \mathbf{f}^\mathsf{T}\mathbf{w} \,, \tag{4.62}$$

where

$$\begin{aligned} \mathbf{u}^\mathsf{T} &= \begin{bmatrix} u_1 & u_2 & \dots & u_i & \dots & u_N \end{bmatrix} \,, \\ \mathbf{K} &= \begin{bmatrix} \int_a^b X_1' X_1' \,\mathrm{d}x & \cdots & \int_a^b X_1' X_j' \,\mathrm{d}x & \cdots & \int_a^b X_1' X_N' \,\mathrm{d}x \\ \vdots & \ddots & \vdots & \ddots & \vdots \\ \int_a^b X_i' X_1' \,\mathrm{d}x & \cdots & \int_a^b X_i' X_j' \,\mathrm{d}x & \cdots & \int_a^b X_i' X_N' \,\mathrm{d}x \\ \vdots & \ddots & \vdots & \ddots & \vdots \\ \int_a^b X_N' X_1' \,\mathrm{d}x & \cdots & \int_a^b X_N' X_j' \,\mathrm{d}x & \cdots & \int_a^b X_N' X_N' \,\mathrm{d}x \end{bmatrix} \,, \\ \mathbf{f}^\mathsf{T} &= \begin{bmatrix} -\int_a^b L X_1 \,\mathrm{d}x & -\int_a^b L X_2 \,\mathrm{d}x & \cdots & -\int_a^b L X_j \,\mathrm{d}x & \cdots & -\int_a^b L X_N \,\mathrm{d}x \end{bmatrix} \,, \\ \mathbf{w}^\mathsf{T} &= \begin{bmatrix} w_1 & w_2 & \dots & w_j & \dots & w_N \end{bmatrix} \,. \end{aligned}$$

Equating the coefficients of the above equation with respect to $\mathbf{w}$ followed by a transposition yields the "classical" finite element method equation

$$\mathbf{u}^\mathsf{T}\mathbf{K} = \mathbf{f}^\mathsf{T} \text{ respectively } \mathbf{K}\mathbf{u} = \mathbf{f} \,. \tag{4.63}$$

$\mathbf{K}$ is the *coefficient matrix*, the vector $\mathbf{u}$ is referred to as *unknown solution vector* and $\mathbf{f}$ is the *right-hand side vector*. The coefficient matrix $\mathbf{K}$ is square and symmetric due to the compatibility of the chosen test function $\delta\Phi$ with respect to the approximate solution Φ. Non-compatible test function would lead to non-squared matrix that makes the finite element method equation unsolvable.

The question arises: What is the extremal formulation of the Poisson equation in conjunction with finite element method? In variational calculus, the Poisson equation in Eq. (4.53) is considered as the strong formulation. Therefore, it is seen as a Euler-Lagrange equation as stated in Eq. (4.17). Furthermore, the variational formulation of the Poisson equation in Eq. (4.58) contains Φ' and $\delta\Phi'$. Thus, it can be concluded that the Lagrangian density functional has the following dependency

$$Z = Z\left(x, \Phi, \Phi'\right) . \tag{4.64}$$

One notices that the above functional is exactly the same as discussed in Sec. 4.2 with the difference that y in Eq. (4.1) is replaced by Φ. Consequently, the POISSON equation in Eq. (4.53) has be to be equal to the strong formulation in Eq. (4.17)

$$\frac{\partial Z}{\partial \Phi} - \frac{\mathrm{d}}{\mathrm{d}x}\left(\frac{\partial Z}{\partial \Phi'}\right) = \Phi'' - L\,, \tag{4.65}$$

where $\Phi'' = \frac{\mathrm{d}^2\Phi}{\mathrm{d}x^2}$. The Lagrangian density functional Z has to be determined in order to reach the extremal formulation. By means of a well-educated guess, it is possible to write the following Lagrangian density functional that satisfies the above equation

$$Z = -\frac{1}{2}\Phi'\Phi' - L\Phi + C\,, \tag{4.66}$$

where $C = C\big(x\big)$ is an arbitrary function. As a result, the approximate finite element solution occurs when

$$J = \int_a^b \left(-\frac{1}{2}\Phi'\Phi' - L\Phi + C\right)\mathrm{d}x \;\rightarrow\; \text{extremal}\,. \tag{4.67}$$

The above objective function is the extremal formulation of the POISSON equation in conjunction with the finite element method. The determination of the objective function is unnecessary for the approximation of the solution of the POISSON equation. Therefore, the extremal formulation is usually ignored in the finite element method. An example as follows shows that the objective function can appear quite different for the same problem.

Least Squares Finite Element Method

In Eq. (4.67), we have the extremal formulation of the finite element method for the POISSON equation. However, there are other extremal formulations that can be obtained by using other trial and test functions. For the so-called *least squares finite element method* (BOCHEV and GUNZBURGER 2009), we use the following trial and test function

$$\Phi = \sum_{i=1}^{N} u_i X_i \text{ and } \delta\Phi'' = \sum_{j=1}^{N} w_j X_j''\,, \tag{4.68}$$

where $X'' = \frac{\mathrm{d}^2 X}{\mathrm{d}x^2}$. While the same trial function as in finite element method is used, this time a different test function is applied. It is to be noted that, in comparison with the RITZ-GALERKIN method, the least squares finite element method requires higher-order polynomial for the solution Φ as well as for the corresponding test function $\delta\Phi$, therefore the basis function X_i has to be at least two times differentiable. By multiplying the above test function with the POISSON equation in Eq. (4.53) followed by the integration over the whole interval yields another variational form for the POISSON equation

$$\int_a^b \Phi''\delta\Phi''\,\mathrm{d}x = \int_a^b L\delta\Phi''\,\mathrm{d}x\,. \tag{4.69}$$

We notice from the above equation that the test function $\delta\Phi''$ appears in the variational form. Therefore, the Lagrangian density functional Z has the following dependency

$$Z = Z\big(x, \Phi''\big)\,. \tag{4.70}$$

In order to determine the EULER-LAGRANGE equation as in Eq. (4.17) for the above density functional Z, the extremal value J as in Eq. (4.6) has to be found as follows

$$\begin{aligned}
&\left.\frac{\mathrm{d}J}{\mathrm{d}\varepsilon}\right|_{\varepsilon=0} \stackrel{!}{=} 0 \\
&\qquad = \int_a^b \frac{\mathrm{d}Z}{\mathrm{d}\varepsilon}\,\mathrm{d}x\bigg|_{\varepsilon=0} = \int_a^b \frac{\partial Z}{\partial x}\underbrace{\frac{\mathrm{d}x}{\mathrm{d}\varepsilon}}_{=0} + \frac{\partial Z}{\partial\big(\Phi'' + \varepsilon\delta\Phi''\big)}\underbrace{\frac{\mathrm{d}\big(\Phi'' + \varepsilon\delta\Phi''\big)}{\mathrm{d}\varepsilon}}_{=\delta\Phi''}\,\mathrm{d}x\bigg|_{\varepsilon=0} =
\end{aligned}$$

$$= \int_a^b \frac{\partial Z}{\partial\left(\Phi'' + \varepsilon\delta\Phi''\right)}\delta\Phi''\,\mathrm{d}x\bigg|_{\varepsilon=0} = \int_a^b \frac{\partial Z}{\partial\Phi''}\delta\Phi''\,\mathrm{d}x \stackrel{!}{=} 0\,. \tag{4.71}$$

By applying the fundamental lemma of calculation of variations to the above equation, the EULER-LAGRANGE equation for this case is obtained

$$\frac{\partial Z}{\partial\Phi''} = 0\,. \tag{4.72}$$

Equating both strong formulations, the above EULER-LAGRANGE equation and the POISSON equation in Eq. (4.53), it reads

$$\frac{\partial Z}{\partial\Phi''} = \Phi'' - L\,. \tag{4.73}$$

Hence, the Lagrangian density functional is

$$Z = \frac{1}{2}\Phi''\Phi'' - L\Phi'' + C\,, \tag{4.74}$$

where $C = C(x)$ is an arbitrary function. In a special case where $C = \frac{1}{2}LL$, the Lagrangian density functional becomes

$$Z = \frac{1}{2}\Phi''\Phi'' - L\Phi'' + \frac{1}{2}LL = \frac{1}{2}\left(\Phi'' - L\right)^2. \tag{4.75}$$

The extremal formulation of the POISSON equation for the "least squares" finite element method is

$$J = \int_a^b \frac{1}{2}\left(\Phi'' - L\right)^2 \mathrm{d}x \;\rightarrow\; \text{minimal}\,. \tag{4.76}$$

The same objective function as above can be determined if the residual function v is introduced to POISSON equation in Eq. (4.53) as

$$\frac{\mathrm{d}^2\Phi}{\mathrm{d}x^2} = L + v\,. \tag{4.77}$$

The same result as in Eq. (4.76) is obtained for minimizing the integrated squared residual function

$$J = \int_a^b \frac{1}{2}v^2\,\mathrm{d}x = \int_a^b \frac{1}{2}\left(\frac{\mathrm{d}^2\Phi}{\mathrm{d}x^2} - L\right)^2 \mathrm{d}x = \int_a^b \frac{1}{2}\left(\Phi'' - L\right)^2 \mathrm{d}x \;\rightarrow\; \text{minimal}\,. \tag{4.78}$$

Due to this similarity with the method of least squares, this approach to solve the POISSON's differential equation is called the *least squares* finite element method. One notices that both objective functions, in Eq. (4.67) and in Eq. (4.76), are fundamentally different. Although both extremal formulations are used to approximate solution for same strong formulation, the POISSON equation.

In conclusion, there is a unique strong formulation for a specific problem. But, different extremal formulations of the same strong formulation can be found. Consequently, there exists many variational formulations. This in turn leads to different approximate solutions with various qualities for a specific problem. For a unique numerical solution, however, an unambiguous extremal formulation (apart from scaling and shifting) must be established. This is accomplished by specifying the trial and test function, Φ and $\delta\Phi$.

4.5 Calculus of Variations in Adjustment Theory

A specific problem can take the form of one of many possible objective functions or as a unique system of (differential) equations. The variational calculus introduces how to classify the many possible representations of a specific problem into one of the three forms. And it introduces a procedural way to rewrite different formulations of a particular problem. In the long term, it should be shown that all methods can be classified in one way or another in

the scheme of variational calculation. In this dissertation, the least squares and finite element method are analysed in the context of the variational calculus.

The finite element method is used to approximate a solution of differential equations. While the least squares adjustment is applied for solving overdetermined system of algebraic equations. Both methods share the same challenge of not knowing the "true" solution. Even though a system of differential equations for a specific engineering problems can be formulated by means of, for example, continuum physics. But afterwards, there are generally two obstacles: Does a solution exist at all for the given differential equations? And, if it is the case, how do we get it? In fact, one may not even know if there is a solution at all. For example, the existence of an exact solution of the Navier-Stokes equation in fluid mechanics is still unknown, see (Fefferman 2000). Only for a limited case such as the one-dimensional Poisson equation respectively Euler-Bernoulli beam equation, it is possible to obtain close-form solution. But, these types of differential equations result from simplification of an engineering problem with debatable assumptions. In order to obtain quantitative results without any questionable simplifications, a numerical approximation technique such as the finite element method must be used. The differential equations are multiplied by the test function and integrated over the region of interest. This transforms the differential equations into their corresponding variational form. It is then possible to obtain numerical results. In practice, it usually remains unnoticed that the procedure of variational calculus is applied in reverse. In the context of variational calculus, the differential equations represent the strong formulation of the problem. Since their variational formulation ultimately leads to the approximate solution, it is understandable that their extremal formulation becomes irrelevant in the finite element method. There are other numerical methods for solving differential equations such as the least squares finite element method. By using different trial and test functions, Φ and $\delta\Phi$, various numerical methods result. This approach is the so-called *method of weighted residuals*, see (B. Finlayson and Scriven 1966). The *residuals* refer to the discrepancy arising from the fact that any trial functions fails to satisfy the strong formulation. The *weight* referred to the possibility of using different test functions. And, the integrated *weighted residuals* lead to various variational formulations. These in turn lead to different approximate methods. Also, in a similar situation concerning the solutions of differential equations, overdetermined system of algebraic equations has no solution at all due to their discrepancies. In adjustment calculation, this deficiency can be eased by introducing residuals into the algebraic equations as an additive quantity to the observations. At the same time, the sum of weighted squared residuals must be minimal in order to obtain an adjusted solution. In the adjustment calculation, the variational calculus procedure is followed in a special way. The strong formulation is the overdetermined system of algebraic equations. Instead of following the variational calculus in reverse as in the finite element method, i. e. by multiplying the test functions with the strong formulation in order to obtain the variation formulation respectively the normal equations. A "detour" is made by introduction of residuals to the algebraic equations. And a "special" extremal formulation that the sum of weighted squared residuals has to be minimal is then postulated. The directional derivative respectively the derivation with respect to the unknowns of this objective function also leads to the normal equations. This target function is in so far "special" as other objective functions are also possible that result in exactly the same numerical solution. Other kinds of objective functions can be formulated by scaling and shifting. Ultimately, this special objective function is required for statistical evaluations. By using different trial and test functions, Φ and $\delta\Phi$, various analysis methods result. In particular, the Fourier series belongs to the problem domain, which can be expressed by an algebraic equation as strong formulation. The trial and test functions, Φ and $\delta\Phi$, are represented as the sum of a set of complex exponentials. In summary, it can be concluded that both the finite element method and the least squares adjustment follow the same variational calculus procedure. The normal equations of the least squares adjustment and the system of linear equations of the finite element method are similar insofar as both methods use their corresponding variational forms to calculate their respective numerical solutions. The differences are that both solve different types of equations in conjunction with different representations for the trial and test function. Hence, the relationship between finite element method and least squares adjustment can be associated by variational calculus.

A few final remarks are in order: First, variational calculus is to be considered as a universal procedure of the adjustment theory. Many methods can be explained by answering the following questions:

- What is the formulation of the problem and, if necessary, the conditions?
- Is it a continuous or discrete problem?
- Which trial function is used for the solution?

Therefore, variational calculus should be considered as a unifying method in the adjustment theory. An overview of the discussed methods is shown in Tab. 4.1 . Second, methods have been developed from different scientific fields to solve problems of their discipline. Accordingly, the methods are strongly motivated by the specific perspectives of the respective discipline. From an abstract perspective, i. e. the methods are presented without mechanical or geodetic accents, it becomes clear that the methods are actually identical. Therefore, the finite element method should be regarded as part of the adjustment theory rather than part of physics, because this method requires no physical justification. In addition, the adjustment theory should be understood as a method theory. Third, B. Finlayson and Scriven (1966) as well as B. A. Finlayson (1972) describe in their paper the method of weighted residuals. Their focus is on the different methods of solving differential equations numerically. The fact that the methods are also suitable for data analysis, i. e. algebraic equations can also be solved numerically with them, is ignored. As far as Boljen (1993) is concerned, in his work he presents a short treatment of the variational calculus. A comparison between the continuous and discrete version of least squares method are also shown. He realizes that what he considered as "finite element method" is a continuous problem. But if one takes a closer look at his extremal formulation, it turns out that this is least squares finite element method rather than Ritz-Galerkin finite element method. Also, Milev (2001) recognizes the analogies between the principle of virtual work from mechanics and the method of least squares in geodesy. But in his work he introduces the variational calculus by means of Lagrangian mechanics for non-expert in mechanics. Through this representation, the methodological similarities between the two methods are difficult to comprehend. A more detailed presentation of the variational calculus and the abstraction of important elements of it were absent in the work of the above-mentioned authors.

Table 4.1: An overview of the discussed methods. Gauss-Markov model (GMM), continuous Gauss-Markov model (cGMM), finite element method (FEM), least squares finite element method (LSFEM)

	DGMM	CGMM	FEM	LSFEM
Strong Form	$\boldsymbol{\Phi} = \mathbf{L}$	$\Phi = L$	$\Phi'' = L$	$\Phi'' = L$
Variational Form	$\left(\boldsymbol{\Phi}^\mathsf{T}\mathbf{P} - \mathbf{L}^\mathsf{T}\mathbf{P}\right)\delta\boldsymbol{\Phi} = 0$	$\int\left(\Phi - L\right)\delta\Phi \,\mathrm{d}x = 0$	$\int\left(\Phi'\delta\Phi' + L\delta\Phi\right)\mathrm{d}x = 0$	$\int\left(\Phi'' - L\right)\delta\Phi'' \,\mathrm{d}x = 0$
possible Extremal Form	$\Omega = \left(\boldsymbol{\Phi} - \mathbf{L}\right)^\mathsf{T}\mathbf{P}\left(\boldsymbol{\Phi} - \mathbf{L}\right)$	$\Omega = \int\left(\Phi - L\right)^2 \mathrm{d}x$	$J = \int\left(-\frac{1}{2}\Phi'\Phi' - L\Phi + C\right)\mathrm{d}x$	$J = \int \frac{1}{2}\left(\Phi'' - L\right)^2 \mathrm{d}x$
Trial Function	$\boldsymbol{\Phi} = \mathbf{AX}$	$\Phi = \sum_i c_i X_i$	$\Phi = \sum_i c_i X_i$	$\Phi = \sum_i c_i X_i$
Test Function	$\delta\boldsymbol{\Phi} = \mathbf{AY}$	$\delta\Phi = \sum_j b_j X_j$	$\delta\Phi = \sum_j b_j X_j$	$\delta\Phi'' = \sum_j b_j X_j''$

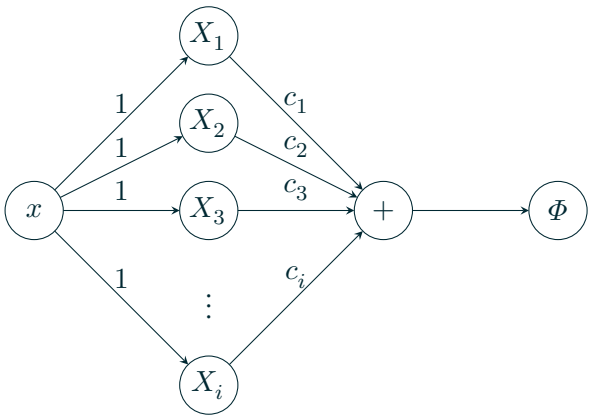


Figure 4.1: The representation of the trial function $\Phi = \sum_i c_i X_i$ as a neuron network.

4.6 A first step towards a unified method

The studies in this chapter show that although many methods originate from different disciplines, they can still be considered identical in terms of variational calculus. Observe an extremal formulation similar to Eq. (4.1), say, a scalar valued quantity J is a functional of the function y. The quantity J becomes stationary when the optimal solution $\hat{y}$ is used, and to find this function $\hat{y}$ is the target. There are many algorithms that can be used to find the solution. Provided that the gradient of J with respect to the unknowns is available, then it is possible, for example, to use the *gradient descent* to find the optimal solution. In this context, it is worth mentioning that according to Rojas (1996) the trial function in Eq. (4.43) can be represented as a *neuron network* as depicted in Fig. 4.1. Determining the coefficients of this trial function using gradient descent is the simplest form of *machine learning*. There are other iterative algorithms that require no gradient of J, for example, the *evolution strategy*, see (Rechenberg 1994). As has already been discussed in detail, the variational formulation is the starting point for many methods. As shown in Eq. (4.51), the entire *Fourier analysis* can be justified from this equation. And based on this, the *Laplace Transformation* can be established. From here, it leads inevitably to *signal processing*. The *finite element method* also has related methods such as spectral finite element method, finite volume method, boundary element method. There are also methods to solve a limited number of strongly formulated problems directly, such as *separation of variables*. As shown, many methods can be assigned in the schema of the variational calculus. However, there are certain problem classes, such as inverse problems, where a single use of a particular method fails to produce the desired result. This requires a consecutive use of different methods to solve these kinds of problems. And that leads to the so-called "integrated analysis". One such procedure is the so-called *Measurement- and Model-based Structural analysis* (MeMoS), in which the finite element method and the method of least squares are combined directly and consecutively in order to detect and to locate damage in structures, see (Neitzel et al. 2014).

5 Measurement- and Model-based Structural Analysis

> I haven't faced death. I've cheated death. I've tricked my way out of death and patted myself on the back for my ingenuity; I know nothing.
>
> – Admiral James Tiberius "Jim" Kirk,
> Star Trek II: The Wrath of Khan (1982)

One major ambition in *Structural Health Monitoring* (SHM) is to develop the ability to detect, localize and identify damage as well as to predict the lifespan of civil structures. This would allow well-informed decision on whether to repair or to demolish these structures. The monitoring of civil engineering structures is based on the evaluation of spatially and temporally distributed hybrid measurements. These can be acquired using, for example, total stations, levelling instruments, inclinometers, fibre optic sensors, strain gauges, terrestrial laser scanning or global navigation satellite system. However, to allow for an integrated evaluation of the examined structure, a new concept that include physical models needs to be developed.

Engineering problems are often solved using the finite element method (FEM). The result is suggestively validated by an overlay comparison with interpolation with the discrete measurements, see for example Kottner et al. (2014) and Yang et al. (2014). The results based solely on this comparison can be misinterpreted. In contrast, an integrated evaluation takes into account both the physical modelling and the measurements. This combined evaluation has not been implemented yet due to the common subdivision of engineering sciences into two groups: the modelling or experimental factions. This separation is clearly seen in commercial finite element method software packages: they do not provide any interoperability with measurement and model data. In recent years, some effort has been undertaken to overcome this obstacle, see for example Bucher et al. (1995). Since the commercial finite element method software packages do not allow any access to the model data, they have to be treated as a black-box.

The determination of material parameters from measurements is not only important in materials science, its application in monitoring of civil infrastructures is also utmost significant. In materials science, test apparatuses such as tensile testing machine are used to determine material properties of particular specimens. By taking this thought one step further, a civil engineering structure can be considered as a large and complex sample and its characteristics can be monitored. Structural changes due to ageing, degradation or damaging processes are expressed by altering material parameters. An additional challenge is that in contrary to materials science, an engineering structure "specimen" is produced in such a way that a complex physical model is required in conjunction with the measurements in order to examine the specimen's material characteristics.

Many algorithms for computing material parameters from measurements are available in the literature, see for example Kauer (2001), Balaraman et al. (2006), Zhang et al. (2011), and Hassaballah et al. (2013). Essentially, however, they are the same, since this approach uses an *optimiser* to iteratively tune the parameters until the computed results of the finite element method are in accordance with the measurements, see Fig. 5.1. For example, adaptive Kalman filtering is an optimiser in Eichhorn (2005) and Schmalz et al. (2010). Lienhart (2007) calibrates his physical model by means of *condition equations* in conjunction with the least squares adjustment. And Sterthaus (2008, p. 89) has recognized that the optimizer can be replaced by any optimization methods. The main issue is that this algorithm contains inaccessible program parts with respect to the finite element method. Due to these restrictions, we are hindered to comprehend the inner process of the programs. Consequently, the question arises as to how we can be sure that the result from this algorithm is reliable. In addition, the optimizers often require numerical values from the partial derivatives such as the Jacobian matrix. Without direct access to the finite element data, the optimization calculation can be unnecessarily prolonged. Furthermore, such an evaluation allows only limited statistical analysis of the results. But for monitoring purposes a rigorous statistical analysis is in fact essential and therefore it is highly desired.

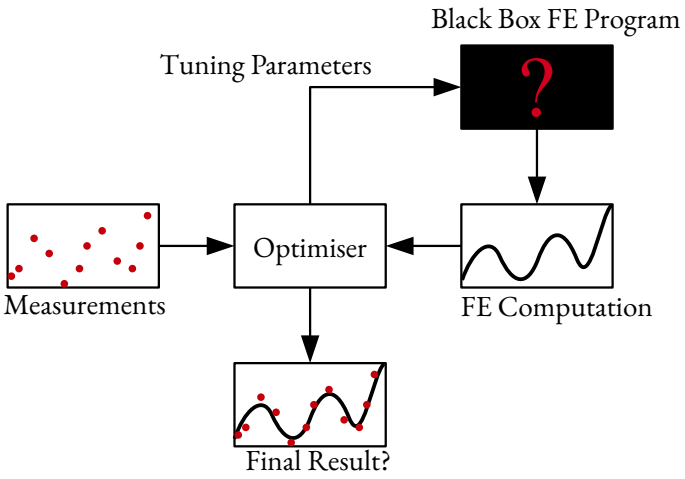


Figure 5.1: Basic principle of the approaches for material parameter determination of complex samples as proposed by Eichhorn (2005) and Lienhart (2007)

In contrast to this debatable approach, we follow a rigorous and direct method. The main idea of this integrated analysis, first proposed in Neitzel et al. (2014), is that it uses the sophistication of the continuum mechanics as well as of the adjustment calculation from geodesy – "best of both worlds". Hereby, it is necessary to understand every aspect of the process: From modelling part by means of continuum mechanics, numerical approximation by finite element method, computation of material parameters from measurements by least squares adjustment as well as applying statistical test to check the results. Every step is performed in a transparent approach without using "black-boxed" software. This leads us to an interesting aspect: It allows us to associate the finite element nodes in Eq. (2.248) with the vector of observations in Eq. (3.1) for hybrid measurements

$$\mathbf{L} \equiv \mathbf{u}\,. \tag{5.1}$$

As a consequence, we can invert the finite element method procedure by integrating a finite element model into the least squares adjustment and thus allows us to evaluate a physical model and measurements in a combined analysis. This enables us to calculate the material parameters directly from measured field. And provide us the possibility to perform a detailed analysis of the results using statistical tests.

The application of this method is called the *Measurement- and Model-based Structural Analysis* (MeMoS). We utilize it to examine the following aspects concerning structural health monitoring:

- What are the optimal measurement set-ups for structural health monitoring?
- How can damages of a structure be detected and localised?
- How can material parameters of a structure be determined from measured field quantities?
- How can a geometrical complex structure be represented with a simplified but equivalent object?
- How can the Measurement- and Model-based Structure Analysis be circumstantiated by an experimental validation?

5.1 On Optimal Measurement Set-Ups for Material Parameter Determination

The word *monitoring* in structural health monitoring brings up several frequently ignored questions: What measurands and sensor precision are needed to monitor a given structure? Where are the optimal sensor placements? How many sensors are necessary? How to analyse spatially distributed hybrid measurements? Or, in short: What is the sensor configuration best suited for structural health monitoring? If these questions are not explicitly addressed,

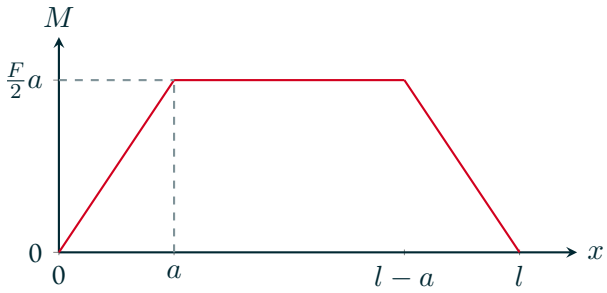


Figure 5.2: The bending moment M

the usefulness of the measurement data for an evaluation is left to coincidence. Therefore, a *measuring strategy* respectively a *sensitivity analysis* is strongly desired. To develop a monitoring strategy, an integrated evaluation via a finite element approach which combines spatially distributed hybrid measurements with mechanical structural modelling is proposed. Together with the method of least squares adjustment and Monte Carlo algorithm, this will open up the possibility to simulate different kinds of measuring strategies and to choose the most appropriate one.

The introduced approach is illustrated on the example of a statically bended EULER-BERNOULLI beam as shown in Sec. 2.5.2. We demonstrate on this numerical example how an integrated analysis can be applied to determine the optimal measurement set-up for material parameter determination. For this, we create a finite element model of a *four-point bending test apparatus*. Based on this model, we generate synthetic measurements of displacement, inclination and strain observations for predefined measuring points. Then, a *Monte Carlo simulation* (MCS) is performed to analyse the dependence of estimated parameters at the location of the measuring point as well as on the stochastic properties of the measurements.

This section is partly published in WEISBRICH et al. (2014) and in BECKER et al. (2015)

5.1.1 Four-Point Bending Test Apparatus

The EULER-BERNOULLI beam equation in Eq. (2.182) can be rewritten as

$$\frac{\mathrm{d}^2 u}{\mathrm{d}x^2} = -\frac{M}{EI}\,, \tag{5.2}$$

where I_{22} and x_1 are redefined as I and x. Due to the semi-inverse method shown in Eq. (2.167), we know that the displacement u only depends on x. Hence, we can write $\frac{\mathrm{d}^2 u}{\mathrm{d}x^2} = \frac{\partial^2 u}{\partial x^2}$. For our numerical example, the specimen has a total length of l and has a rectangular cross section of width B and height H. Moreover, the specimen is clamped at the position $x = 0$ with a fixed bearing and at $x = l$ with a moveable bearing. For a four-point bending test, forces of equal strength $F/2$ are applied to the beam specimen at the positions $x = a$ and $x = l - a$. Under these requirements and according to Eq. (2.181), the course of the internal bending moment M reads as

$$M = \begin{cases} \frac{F}{2}x & \text{for } 0 \le x \le a\,, \\ \frac{F}{2}a & \text{for } a \le x \le l-a\,, \\ \frac{F}{2}(l-x) & \text{for } l-a \le x \le l \end{cases} \tag{5.3}$$

and is shown in Fig. 5.2. Since the beam specimen has a rectangular cross section over its entire length, the area moment of inertia is a given constant scalar value of

$$I = \frac{BH^3}{12}\,. \tag{5.4}$$

Furthermore the specimen is clamped on its both ends with bearings. This leads to the following DIRICHLET boundary conditions

$$u(x=0) = u(x=l) = 0\,. \tag{5.5}$$

For given bending moment M, area moment of inertia I and DIRICHLET boundary conditions, the EULER-BERNOULLI beam equation describes the "indirect" relationship between the field quantity displacement u and the material parameter elastic modulus E. In contrast, the solution of the beam differential equation expresses "directly" the displacement u as a function of elastic modulus E in form of an algebraic equation.

5.1.2 Measurands Identification

A physical model can be used to identify what measurands are appropriate for the material parameter determination. In our case the EULER-BERNOULLI beam model is utilized to find suitable measurands to evaluate the elastic modulus E of a beam specimen.

According to GERE and GOODNO (2013, pp. 418–431) as well as to W. H. MÜLLER and FERBER (2005, p. 139 ff), the second spatial derivative of the displacement u, i. e. the beam equation itself, is closely related to the longitudinal strain

$$\varepsilon_{11} = \varepsilon = -e_{\mathrm{u}} \frac{\mathrm{d}^2 u}{\mathrm{d}x^2} = e_{\mathrm{u}} \frac{M}{EI}\,, \tag{5.6}$$

where $e_{\mathrm{u}} = \frac{H}{2}$ is the orthogonal distance between the neutral surface and the bottom surface of the beam. The slope of the deflection $\tan(\alpha)$ is described by the first spatial derivative of the deflection u, i. e. the infinitesimal change of the deflection $\mathrm{d}u$ in relation to infinitesimal step in position $\mathrm{d}x$. And the slope is obtained by integrating the beam equation, we have

$$\tan(\alpha) = \frac{\mathrm{d}u}{\mathrm{d}x} = -\int_0^l \frac{M}{EI}\,\mathrm{d}x + C\,, \tag{5.7}$$

where C is the constant of integration and is determined by the boundary and transition conditions. The inclination α is computed by taking the arctangent of the above equation. The deflection u is computed by integrating the beam equation two times. This in turn yields

$$u = -\int_0^l \int_0^l \frac{M}{EI}\,\mathrm{d}x + Cx + D\,, \tag{5.8}$$

where C and D are the constants of integration that is determined by the boundary and transition conditions.

In conclusion, within the EULER-BERNOULLI beam model the displacement and tilt sensors as well as strain gauges are best suited to determine the elastic modulus E of a beam specimen. Sensors for the force F, the force application position a, the DIRICHLET boundary conditions as well as the specimen initial geometry can also be considered.

5.1.3 The Exact Solution of the Beam Differential Equation

The functional model of least squares adjustment can be based on the exact as well as on the approximate solution of differential equations. For the four-point bending test set-up, the course of the longitudinal strain ε, of the tangent of the inclination $\tan(\alpha)$ and of the displacement u can be determined analytically from the Eqs. (5.6) to (5.8) under the requirements of the bending moment, the area moment of inertia and the boundary conditions in Eqs. (5.3) to (5.5). The exact solution of the beam differential equation reads

$$\varepsilon = \begin{cases} e_{\mathrm{u}} k x & \text{for } 0 \le x \le a\,, \\ e_{\mathrm{u}} k a & \text{for } a \le x \le l-a\,, \\ e_{\mathrm{u}} k (l-x) & \text{for } l-a \le x \le l\,, \end{cases} \tag{5.9}$$

$$\tan(\alpha) = \begin{cases} -\frac{1}{2} k x^2 + C_1 & \text{for } 0 \le x \le a\,, \\ -kax + C_2 & \text{for } a \le x \le l-a\,, \\ \frac{1}{2} k x^2 - klx + C_3 & \text{for } l-a \le x \le l\,, \end{cases} \tag{5.10}$$

$$u = \begin{cases} -\frac{1}{6} k x^3 + C_1 x & \text{for } 0 \le x \le a\,, \\ -\frac{1}{2} kax^2 + C_2 x + D_2 & \text{for } a \le x \le l-a\,, \\ \frac{1}{6} k x^3 - \frac{1}{2} klx^2 + C_3 x + D_3 & \text{for } l-a \le x \le l\,, \end{cases} \tag{5.11}$$

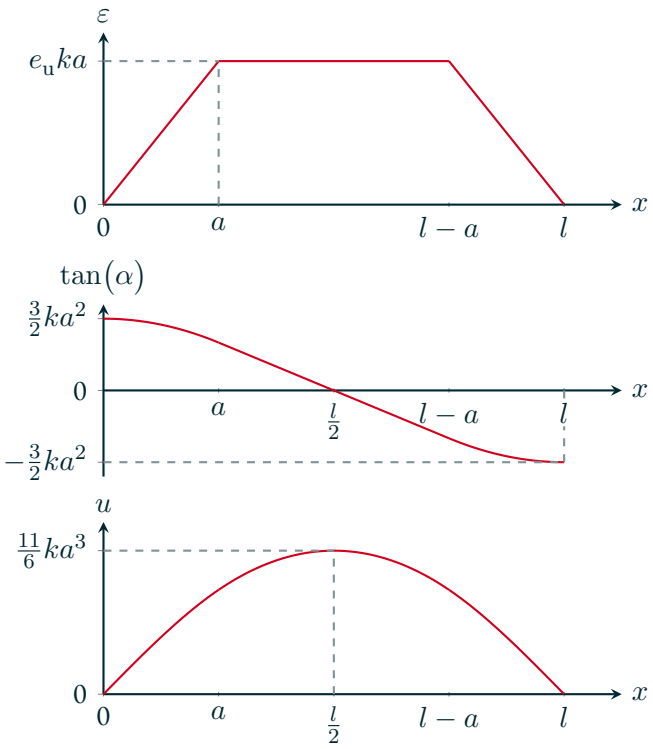


Figure 5.3: The exact solution of the beam differential equation, from top to bottom: strain ε, tangent of the inclination $\tan(\alpha)$, displacement u

where $k = \frac{F/2}{EI}$, $C_1 = \frac{1}{2}ka(l-a)$, $C_2 = \frac{1}{2}kal$, $C_3 = \frac{1}{2}k(l-a)^2 + \frac{1}{2}kal$, $D_2 = -\frac{1}{6}ka^3$ and $D_3 = -\frac{1}{2}kal^2 - \frac{1}{2}kl(l-a)^2 + \frac{1}{3}kl^3$ and is shown in Fig. 5.3. The above equations form the basis to analyse spatially distributed hybrid measurements. If measurements of the field quantities strain ε, tilt $\tan(\alpha)$ and deflection u are available as observations, it is possible to determine the unknown elastic material parameter E by means of the mechanical model described in Eqs. (5.9) to (5.11) and least squares adjustment. This common evaluation of hybrid measurements and physical model is referred as the *integrated analysis*. It is to be noted that our interest lies in the relationship between field quantities and material parameters, hence we consider the force F, the force application position a, the DIRICHLET boundary conditions and the area moment of inertia I as error-free.

It is not always possible that an exact solution can be determined for given differential equations and given boundary conditions. In this case, numerical methods such as finite element method are introduced. In Sec. 2.6.9, the solution of the beam equation is approximated with aid of finite element method. Non-linear elements are usually used in consideration of improving the numerical approximation results. But, in regard of integrated analysis of hybrid measurements, for each element a polynomial of order 5 is required. As mentioned in Sec. 2.6.9, each node contains the numerical value of the displacement, of its first and second derivatives. From Eqs. (5.6) to (5.8), we know that these values represent the deflection, inclination and strain. From Eqs. (2.270) and (2.271), the approximate solution of the beam differential equations via finite element method reads as follows

$$\mathbf{u}^\star = \mathbf{K}^{-1}\mathbf{f}\,. \tag{5.12}$$

Moreover, the load vector $\mathbf{f}$, assembled from Eq. (2.265), contains the unknown elastic material parameter E and it can be recast as

$$\mathbf{f} = \mathbf{b}\frac{1}{E}\,. \tag{5.13}$$

As a result, Eq. (5.12) can be reformulate as

$$\mathbf{u}^\star = \mathbf{K}^{-1}\mathbf{b}\frac{1}{E}\,, \tag{5.14}$$

Table 5.1: Specification of the four-point bending set-up and beam specimen for the finite element modelling.

beam length l	7.25 m	beam elastic modulus E	70 GPa
beam width B	0.20 m	load F	7460 N
beam height H	0.37 m	loading position a	2.42 m
number of equidistantly discretised finite elements n			725

For the evaluation in least squares adjustment, it is helpful to use the component notation for the above equation

$$u_o^\star = \sum_{m=1}^{3n} \kappa_{om} b_m \frac{1}{E} \,, \tag{5.15}$$

where κ_{om} is the entry of the inverted stiffness matrix $\mathbf{K}^{-1}$. The above equation is the approximate solution of the beam differential equation and it can be utilized to formulate the functional model. In a same manner as analytical solution, if measurements of the field quantities strain $u_\nu'' = -\frac{\varepsilon_\nu}{e_u}$, tilt $u_\nu' = \tan(\alpha_\nu)$ and deflection u_ν are available as observations at the node position ν, we are able to determine the unknown elastic material parameter E by means of least squares adjustment. As before, the force F, the force application position a, and the area moment of inertia I is considered to be error-free, hence the vector b_m is a fixed value. Likewise, the DIRICHLET boundary conditions as well as the finite element discretisation are also regarded as fixed, thus κ_{om} is error-free. Then, Eq. (5.15) can be expressed as

$$u_o^\star = \underbrace{\sum_{j=1}^{3n} \kappa_{om} b_m}_{=A_o} \underbrace{\frac{1}{E}}_{=X} = A_o X \,. \tag{5.16}$$

The above relation is used to formulate the function model.

5.1.4 Sensor Precision Modelling and Synthetic Measurements

The stochastic property of sensor precision can be modelled as a normal distributed noise. In our analysis, we assume that the noises are normal distributed and be therefore characterised by standard deviations. Within a deterministic model, computed values are considered to be true. In regard of the association of the numerical computed values and observations in Eq. (5.1), by adding noises to the computed values allows us to generate *synthetic measurements*.

The finite element solution $u_o^\star$ of the beam differential equation in Eq. (5.16) can be computed deterministically for a fixed specification listed in Tab. 5.1. The conversion of the numerical solution into tilt and strain is performed by means of Eqs. (5.6) and (5.7), we obtain

$$\begin{aligned}
u_o^\star \quad &\text{for } o = 1, \ldots, n \quad &\rightarrow \quad u_\nu \quad &\rightarrow \quad u_\nu \\
u_o^\star \quad &\text{for } o = n+1, \ldots, 2n \quad &\rightarrow \quad u_\nu' \quad &\rightarrow \quad \alpha_\nu \\
u_o^\star \quad &\text{for } o = 2n+1, \ldots, 3n \quad &\rightarrow \quad u_\nu'' \quad &\rightarrow \quad \varepsilon_\nu
\end{aligned} \,,$$

for $\nu = 1, \ldots, n$. Based on this solution, a random normal distributed noise is added in accordance to the assumed sensor precision. This in turn yields the synthetic measurement for the displacement, inclination and strain as follows

$$l_{o,u} = u_\nu + u_{\nu,\text{noise}} \,,\; l_{o,\alpha} = \alpha_\nu + \alpha_{\nu,\text{noise}} \,,\; l_{o,\varepsilon} = \varepsilon_\nu + \varepsilon_{\nu,\text{noise}} \,, \tag{5.17}$$

where $u_{\nu,\text{noise}} \sim \mathcal{N}(0, \sigma_u^2)$, $\alpha_{\nu,\text{noise}} \sim \mathcal{N}(0, \sigma_\alpha^2)$, $\varepsilon_{\nu,\text{noise}} \sim \mathcal{N}(0, \sigma_\varepsilon^2)$ respectively $l_{o,u} \sim \mathcal{N}(u_\nu, \sigma_u^2)$, $l_{o,\alpha} \sim \mathcal{N}(\alpha_\nu, \sigma_\alpha^2)$, $l_{o,\varepsilon} \sim \mathcal{N}(\varepsilon_\nu, \sigma_\varepsilon^2)$ and σ_u^2, σ_α^2, σ_ε^2 are the variances of the displacement, tilt and strain sensors. The vector of synthetic observations $\mathbf{L}$ is assembled based on Eq. (5.17).

5.1.5 Sensitivity Analysis

The *sensitivity analysis* examines the influence of sensor precision and sensor position on the unknown parameters. The sensitivity of the elastic modulus with respect to the following sets of predefined sensor precision as well as the sensor position is evaluated. The standard deviations for the displacement are

$$\sigma_u = 10^{-1}\,\mathrm{mm}, 10^{-2}\,\mathrm{mm}, 10^{-3}\,\mathrm{mm}\,, \tag{5.18}$$

for the inclination are

$$\sigma_\alpha = 1\,\mathrm{mgon}, 10^{-1}\,\mathrm{mgon}, 10^{-2}\,\mathrm{mgon} \tag{5.19}$$

and for the strain are

$$\sigma_\varepsilon = 10\,\mu\mathrm{strain}, 1\,\mu\mathrm{strain}, 10^{-1}\,\mu\mathrm{strain}\,. \tag{5.20}$$

The vector of synthetic observation $\mathbf{L}$ is assembled from Eq. (5.17). The corresponding functional model is based on the relationship in Eq. (5.16). The sets of predefined sensor precision in Eqs. (5.18) to (5.20) are used to formulate the stochastic model for the observations.

The index o is uniquely assigned to a measurand and a measuring position. For each index o, 1000 Monte Carlo Simulations were carried out. In each Monte Carlo simulation, a synthetic measurement l_o is generated. Upon this observation, the adjusted elastic parameter $\hat{E}$ and its standard deviation $\sigma_{\hat{E}}$ are obtained by means of least squares adjustment.

The results of the sensitivity examination are shown in Figs. 5.4 to 5.7. They show pretty much the expected conclusion. Nevertheless, Fig. 5.4 is chosen to use as an example to clarify the meaning of the results. The red line represents a displacement sensor with an precision of $\sigma_u = 10^{-1}\,\mathrm{mm}$. At the node position $\nu = 350$ the standard deviation of the estimated elastic modulus is around $\sigma_{\hat{E}} = 10\,\mathrm{GPa}$. The adjusted elastic modulus $\hat{E}$ estimated from a displacement measurement at this node position is around $\hat{E} = 70\,\mathrm{GPa}$ with a standard deviation of $\sigma_{\hat{E}} = 10\,\mathrm{GPa}$. The estimated parameter may be inexact due to the low precision of the sensor. The "spikes" near both ends of the specimen show very high standard deviations. Evaluations of the measurements in this particular area result in unusable estimation of the elastic modulus. This is due to the small displacements near at both ends that are smaller than the precision of the sensor. The tilt and strain sensor examinations in Figs. 5.5 and 5.6 are repeated with same results.

Fig. 5.7 shows the impact of the precision of the estimated elastic modulus $\sigma_{\hat{E}}$ depending on the number of sensors. The precision can be raised by increasing the number of sensors. But at certain amount, the gain of sensor precision declines. Then, economical aspects has to be considered to evaluate the benefit of precision improvement.

From this examination, we come to the conclusion that a sensor has to be placed at a certain spot where the impact is greater than its standard deviation. Without this numerical examination and just by applying common sense and experience to this, we will come to this wisdom, too. But, how does one figure out where the structural impact is the greatest in advance? Beside engineering hunch, a model-based approach can provide prior knowledge. It is therefore highly desirable to incorporate methods of modelling in measuring tasks. Even we should not underestimate the engineering intuition, but from a rational standpoint a well-developed model is more comprehensible.

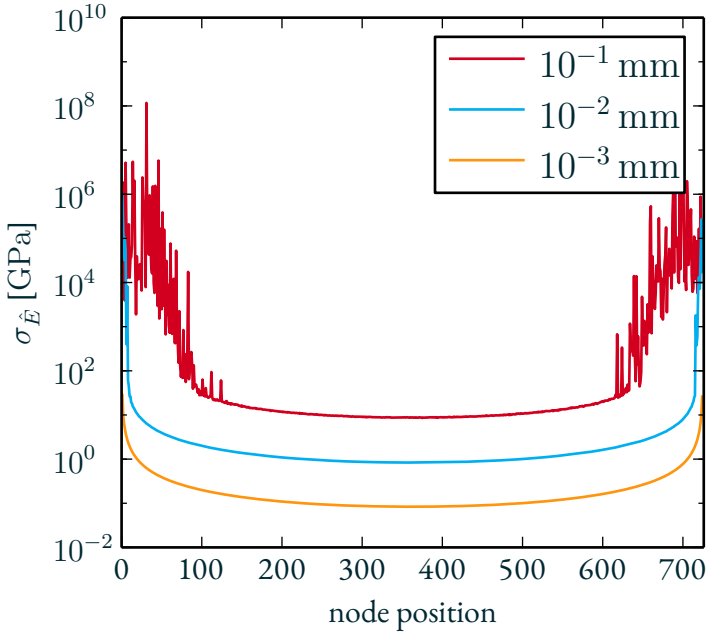


Figure 5.4: Precision of the estimated elastic modulus $\sigma_{\hat{E}}$ depending on sensor position and three different precisions of a displacement sensor

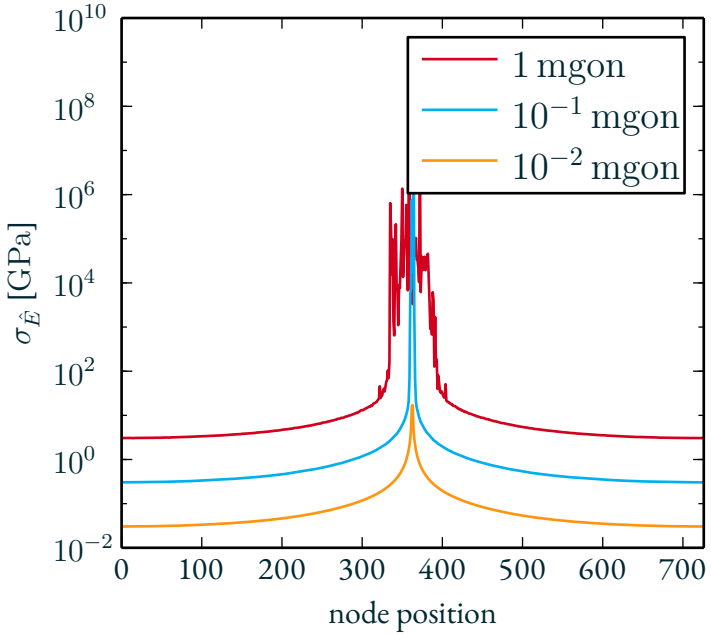


Figure 5.5: Precision of the estimated elastic modulus $\sigma_{\hat{E}}$ depending on sensor position and three different precisions of a tilt sensor

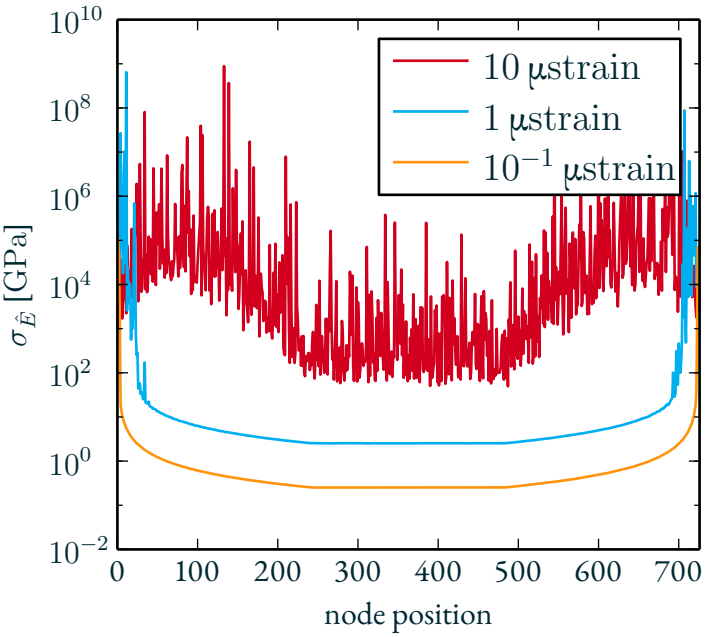


Figure 5.6: Precision of the estimated elastic modulus $\sigma_{\hat{E}}$ depending on sensor position and three different precisions of a strain sensor

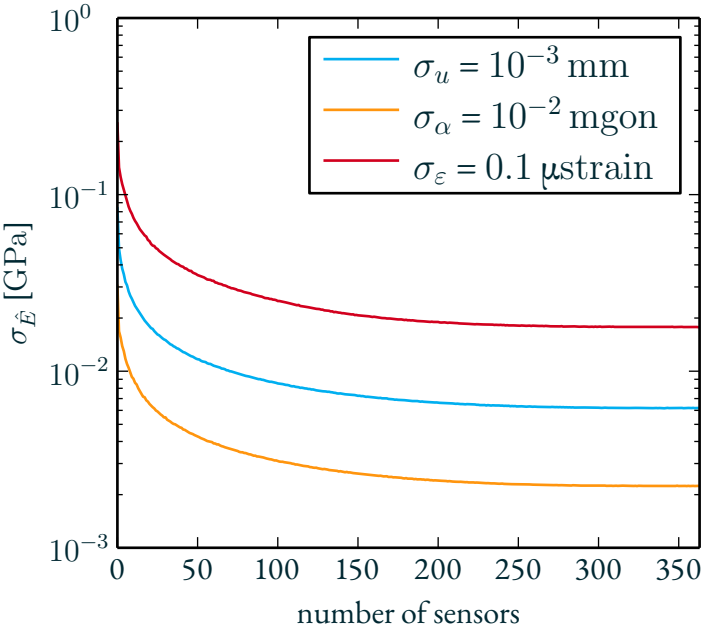


Figure 5.7: Precision of the estimated elastic modulus $\sigma_{\hat{E}}$ depending on number of sensors with fixed precision

5.2 Damage Detection and Localisation within a slender beam

The issues of detection and localisation of damage within a slender beam is being studied. In order to simulate the beam damage caused by material degradation, in the finite element model we decrease systematically the elastic modulus of a group of finite elements. Since YOUNG's modulus and the area moment of inertia are coupled multiplicatively as EI in Eq. (2.265). Therefore, it is indistinguishable, whether one or other has caused the material degradation within the beam theory. Thus, the area moment of inertia has to be assumed to be a constant throughout the whole beam, see Fig. 5.8.

This section is partly published in WU et al. (2014) and in BECKER et al. (2015).

The specification that is listed in Tab. 5.1 is used. The displacement, the inclination and the strain are calculated accordingly to Eq. (5.12) and in case each finite element has different elastic modulus the right-hand side load vector has to be reformulated as follows

$$u_o^\star = \sum_{m=1}^{3n} \kappa_{om} f_m = \sum_{m=1}^{3n} \kappa_{om} \left(\sum_{\zeta=1}^{N} \frac{1}{{}^{\zeta}EI} {}^{\zeta}b_m \right). \tag{5.21}$$

For the numerical simulation and examination, the amount of simulated damage can be induced by decreasing the elastic modulus values ${}^{\zeta}X = \frac{1}{{}^{\zeta}E}$ for a specific element or predefined group of elements. As before, synthetic measurements were generated by adding normal distributed noise in accordance to the assumed sensor precision to the computed values $u_o^\star$. The functional model is

$$l_o^\star = \sum_{m=1}^{3n} \kappa_{om} f_m = \sum_{\zeta=1}^{N} \underbrace{\sum_{m=1}^{3n} \kappa_{om} \frac{1}{I} {}^{\zeta}b_m}_{={}^{\zeta}A_o} {}^{\zeta}X = \sum_{\zeta=1}^{N} {}^{\zeta}A_o {}^{\zeta}X \tag{5.22}$$

or respectively in matrix notation

$$\mathbf{L} = \mathbf{K}^{-1}\mathbf{f} = \mathbf{K}^{-1} \left(\sum_{\zeta=1}^{N} \frac{1}{{}^{\zeta}EI} {}^{\zeta}\mathbf{b} \right) = \sum_{\zeta=1}^{N} \Big(\underbrace{\mathbf{K}^{-1} \frac{1}{I} {}^{\zeta}\mathbf{b}}_{={}^{\zeta}\mathbf{A}} {}^{\zeta}X \Big) = \sum_{\zeta=1}^{N} {}^{\zeta}\mathbf{A} {}^{\zeta}X = \mathbf{A}\mathbf{X}\,, \tag{5.23}$$

where the length of the vector ${}^{\zeta}\mathbf{A}$ is $3n$, the shape of the design matrix $\mathbf{A}$ is $3n \times N$ and the size of the vector of unknowns $\mathbf{X}$ is N. The issue about this functional model is that it requires all nodes have to be observed. Otherwise, an under-determined system of equations appears. To overcome this problem, the concept of *observed unknowns* (KRAUS 1996, pp. 38–42) is used that one may facilitate additional a priori informations to the system. Manufacturer information can be considered as a priori knowledge as an example. Here, the Tab. 5.1 is used as an a priori information to describe the undamaged state of the beam specimen. This approach has two positive characteristics: Firstly, using this method results in an overdetermined system that can be treated with least squares adjustment.

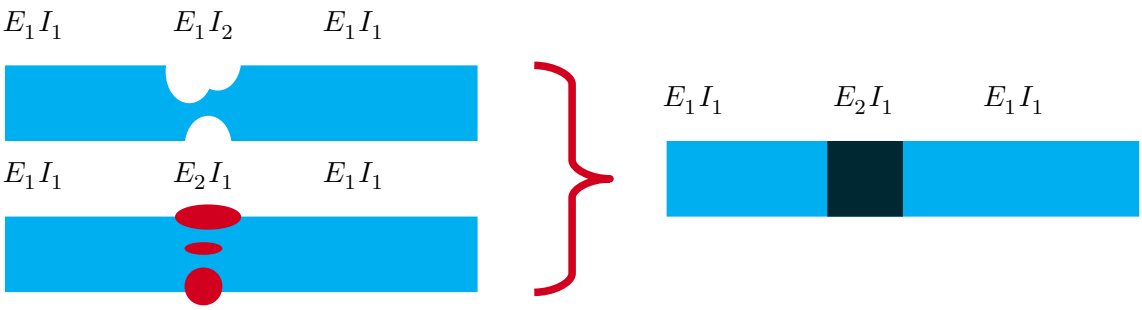


Figure 5.8: Beam defects due to geometric changes or material changes (left) are simulated by material degradation (right)

Table 5.2: Synthetic measurements on beam specimen

measure	sensor precision	positions
displacement	$\sigma_u = 10^{-3}\,\mathrm{mm}$	2.43 m, 3.64 m, 4.85 m
inclination	$\sigma_\alpha = 10^{-2}\,\mathrm{mgon}$	0.02 m, 7.24 m
strain	$\sigma_\varepsilon = 10^{-1}\,\mu\mathrm{strain}$	2.41 m, 3.62 m, 4.83 m

Secondly, the observed quantities and a priori information are fused into one system, we can stochastically test this arrangement how well they agree. The statistical significance test of the agreement and, in case of disagreement, a following localisation of the cause are known as *deformation analysis*.

Aforementioned, we facilitate the "elastic" moduli $X_0 = \frac{1}{E_0}$ and its standard deviation $\sigma_{X_0} = \frac{1}{E_0^2}\sigma_{E_0}$ of the undamaged beam state as a priori information. From the sensitivity examination of Sec. 5.1.5, Fig. 5.7 shows that a determination of the elastic modulus from the undamaged state of the beam yields an elasticity value of $E_0 = 70\,\mathrm{GPa}$ with an average standard deviation of $\sigma_{E_0} = 400\,\mathrm{MPa}$ for up to ten sensors of different types. Therefore, for this examination, it can be specified that every element of an undamaged beam have the same elastic modulus ${}^{\zeta}l_{\text{apriori}} = X_0$ with standard deviation σ_{X_0}. The a priori functional model reads

$$ {}^{\zeta}l_{\text{apriori}} = {}^{\zeta}X \text{ respectively } \mathbf{L}_{\text{apriori}} = \mathbf{I}\mathbf{X}\,, \tag{5.24} $$

where $\mathbf{I}$ is the identity matrix. The total system consists of the a priori functional model in Eq. (5.24) and the "a posteriori" functional model in Eq. (5.23) reads

$$ \underbrace{\begin{bmatrix}\mathbf{L}\\ \mathbf{L}_{\text{apriori}}\end{bmatrix}}_{=\bar{\mathbf{L}}} = \underbrace{\begin{bmatrix}\mathbf{A}\\ \mathbf{I}\end{bmatrix}}_{=\bar{\mathbf{A}}}\mathbf{X} \text{ respectively } \bar{\mathbf{L}} = \bar{\mathbf{A}}\mathbf{X}\,. \tag{5.25} $$

A deformation analysis of the total system is performed in two steps: Firstly, a global test is conducted in order to determine the significance of change between the two beam states. The null hypothesis H_0 assumes that both states of the beam is equal, see Eq. (3.68). And the corresponding alternative Hypothesis H_A states that both beam conditions are significant different. Eq. (3.70) is used as H_A. Secondly, in case the beam states has been significantly changed, i. e., rejection of H_0 with favour to H_A, the one observed unknown elastic modulus in $\mathbf{L}_{\text{apriori}}$ that caused the significant difference has to be localised. This is carried out as follows: We start by removing one observed unknown ${}^{d}l_{\text{apriori}}$ in $\mathbf{L}_{\text{apriori}}$ from the total system in Eq. (5.25). Then, least squares adjustment is performed afterwards. It yields a target function in which the d^{th} observed unknown is removed ("$\backslash d$") from the total system in Eq. (5.25)

$$ \Omega_{\backslash d} = \left(\mathbf{v}^{\mathsf{T}}\mathbf{P}\mathbf{v}\right)\Big|_{\backslash d}\,. \tag{5.26} $$

This process has to be repeated one by one for all observed unknowns listed in $\mathbf{L}_{\text{apriori}}$. The smallest target value from all $\Omega_{\backslash d}$ yields the location of the damaged elements. By removing the influence of certain damaged element from the a priori information, the significance change between the two beam state can be weakened. This also implies that damage occur at this specific location. Therefore, the deformation analysis can be used to detect and localise damage.

Various damage scenarios are introduced in order to examine this approach. Since there are many possibilities to damage the beam, we restrict ourself to only induce degradation between the beam position 2.77 m and 3.07 m. Furthermore, we limited ourself to two possible variations: The number of effected finite elements can be increased from 3 to 30 with step size of 3. The elastic modulus values of the effected finite elements can be decreased from 70 GPa to 15 GPa with step size of 2.5 GPa. Thus, in total we tested 230 possible scenarios, see Fig. 5.9. For each combination, 1000 Monte Carlo Simulations were performed.

The results of the examination is shown in Figs. 5.10 and 5.11. For a better understanding of the illustrations, an example is carried out in the following. Eight synthetic measurements at predefined positions were generated based on Tabs. 5.1 and 5.2. Furthermore, we decreased the elastic modulus of twelve elements to 60 GPa, i. e., beam damage is induced between 2.77 m and 2.89 m. According to the result in Fig. 5.10, the damage detection

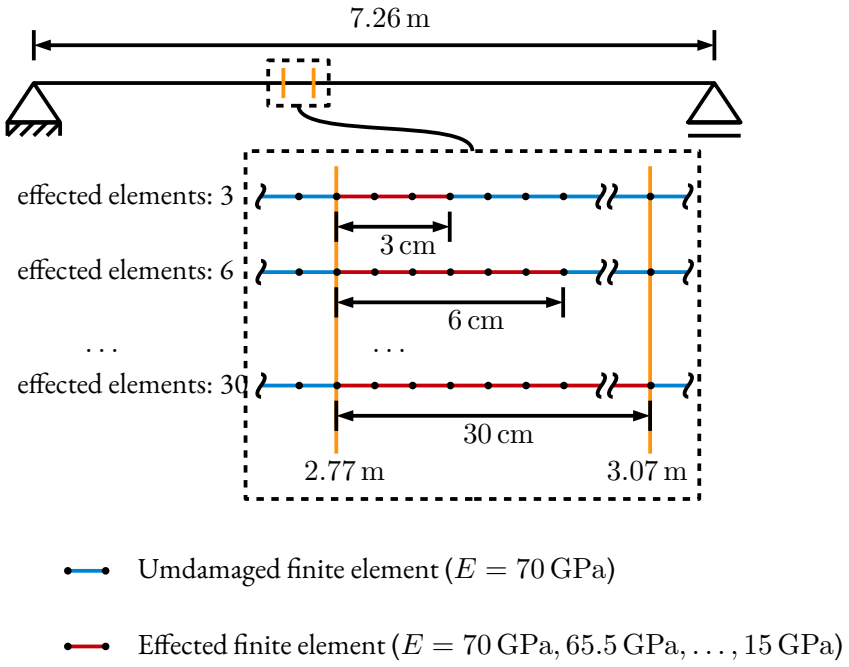


Figure 5.9: Examination of predefined damage scenarios

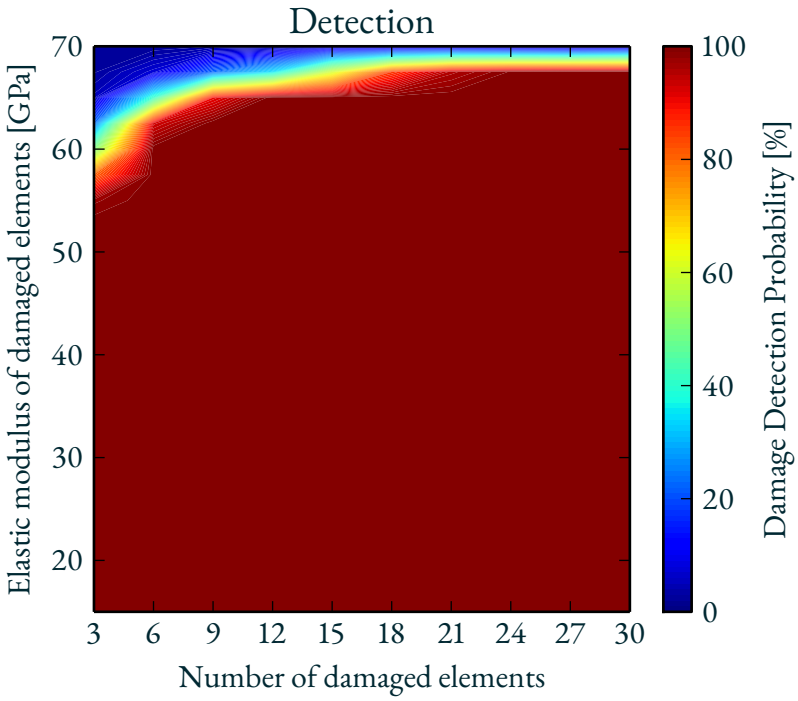


Figure 5.10: Damage detection depending on material degradation (change of elastic modulus) and number of damaged elements

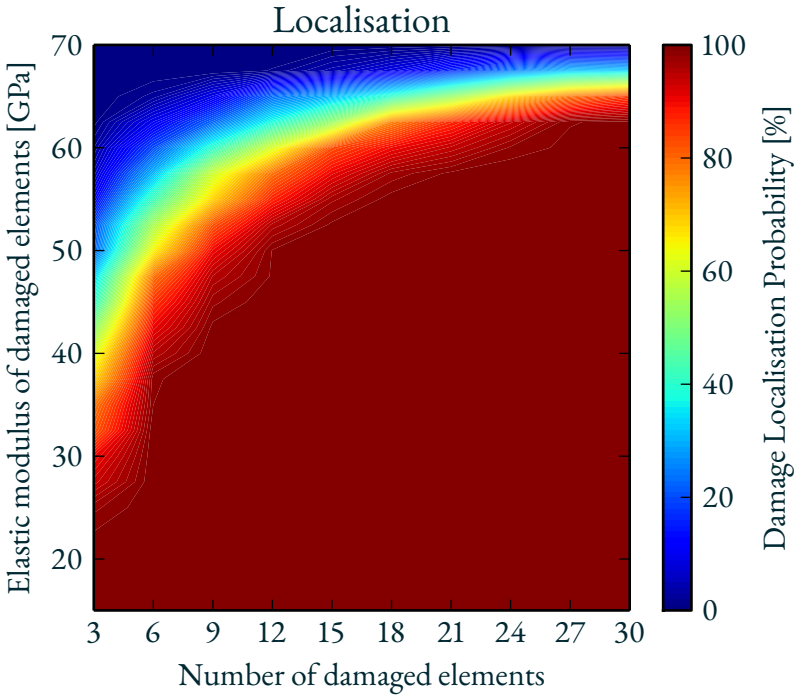


Figure 5.11: Damage localisation depending on material degradation (change of elastic modulus) and number of damaged elements

probability is 100 %. However, even we expanded the range to 17 cm, i. e., between 2.50 m and 3.06 m, the result in Fig. 5.11 shows that out of 1000 MCS, only approximately 500 Monte Carlo Simulations could localise the damage correctly.

In this examination it was shown that this approach is promising in regard of the damage detection and localisation. As depicted in Figs. 5.10 and 5.11, the rate of detection is more successful than the localisation rate. Even though, the success rate of damage localisation can be further improved by enhancing numerically the sensor precision in this analysis. But for achieving more realistic results, the assumed precision sensors are based on the current available sensor market.

5.3 A Four-Point Bending Test Apparatus for Measurement- and Model-based Structural Analysis

To examine the capability to detect and localise damage using the presented Measurement- and Model-based Structural Analysis, a four-point bending test apparatus for an aluminium beam specimen is built for this purpose. In contrary to the numerical preliminary examinations, the inclination and strain measurements were omitted for cost reasons. This is regrettable because, as the results in Figs. 5.4 to 5.6 show, the sensor types offer different precision in determining the elastic parameter in dependence of the applied position. While the tilt sensors are suitable for determining the elastic modulus of the beam near the bearings, the displacement and strain sensors are appropriate for evaluating the centric region of the beam. Since only the displacement measurements are available, damage in the region at both ends of the beam may not be detected.

Specimen and experimental set-up

The specimen is a 1.5 m long slender aluminium beam with a square cross-section of 35 mm by 35 mm, see Fig. 5.12. The beam was designed with small indentations. They ensure that the applied and reactive forces always act in the same place on the beam specimen. On both ends of the lower side of the beam, there are indentations for the bearings. The notches are located 1 cm from the outer edge of the beam. The bearings consist of a metal chamfer strip glued to a wooden structure. An aluminium profile was used to connect the bearing to the tripod.



Figure 5.12: A six-point bending test apparatus for an aluminium beam specimen. This test device was partly enhanced by scrap such as lead battery, dumbbell, plastic box.

The tripod was placed on top of a metal star. To prevent the tripod from slipping, the tripod spider was glued to the floor with double-sided adhesive tape. In addition, weights were placed on the stand spider. On the upper side of the beam there are four indentations for attaching weights. Damage is caused by drilling and sawing the beam.

Measurement system

Photogrammetry is used to measure the deformation of the beam. In order to track the local displacements, in total 34 round target stickers are applied on the surface of the beam (31 markers) as well as on the tripod (three markers). The evaluation software has been developed by the Institute of Geodesy and Geoinformation Science at the Technische Universität Berlin to determine the position of the markers. Accordingly, the camera calibration and distortion corrections was carried out by them.

Calibration of the reference state

In order to adjust the elastic modulus of an undamaged slender beam, twelve experiments were conducted. The properties of target position measurements are listed in Tab. 5.3. In each experiment, the deformation behaviour of the beam is examined in either unloaded or loaded state. For each beam state, n_{photo} images are taken at short intervals. The exposure time was also taken into account when determining the intervals. A total of 12 by 300 observations are obtained for each of the 31 markers. In order to reduce the computational effort, the median $\mathbf{p}_s$ of n_{photo} coordinate measurements in x- and y-direction is used in each state s as an observation for each marker. The reason for using the median instead of the mean value is that the distribution of the coordinates has no concentric form. In addition, the median is comparatively more robust against outliers than the mean value. The displacement vector computed from the corresponding unloaded and loaded states in y-direction serves as observations for the calibration and it reads

$$\begin{aligned}\mathbf{L} &= \begin{bmatrix} \mathbf{p}_1^y - \mathbf{p}_0^y & \mathbf{p}_3^y - \mathbf{p}_2^y & \mathbf{p}_5^y - \mathbf{p}_4^y & \mathbf{p}_7^y - \mathbf{p}_6^y & \mathbf{p}_9^y - \mathbf{p}_8^y & \mathbf{p}_{11}^y - \mathbf{p}_{10}^y \end{bmatrix}^{\mathsf{T}} \\ &= \begin{bmatrix} \mathbf{u}_0 & \mathbf{u}_1 & \mathbf{u}_2 & \mathbf{u}_3 & \mathbf{u}_4 & \mathbf{u}_5 \end{bmatrix}^{\mathsf{T}} . \end{aligned} \tag{5.27}$$

The finite element model for a slender beam was discussed in Sec. 2.6.9 and Secs. 5.1 and 5.2. However, in this case, some small adaptations have to be made. Firstly, the beam consists of 36 non-equidistant elements respectively

Table 5.3: For each state s, weights (m_1, m_2, m_3) were attached to the undamaged beam specimen and n_{photo} images were taken.

s	n_{photo}	m_1 [kg]	m_2 [kg]	m_3 [kg]	designation
0	300	0.0	0.0	0.0	exp_0_0
1	300	0.0	3.565	0.0	exp_1_1
2	300	0.0	0.0	0.0	exp_2_0
3	300	0.0	7.12	0.0	exp_3_1
4	300	0.0	0.0	0.0	exp_4_0
5	300	0.0	10.668	0.0	exp_5_1
6	300	0.0	0.0	0.0	exp_6_0
7	300	0.0	17.825	0.0	exp_7_1
8	300	0.0	0.0	0.0	exp_8_0
9	300	0.649	3.563	1.279	exp_9_1
10	300	0.0	0.0	0.0	exp_10_0
11	300	1.269	7.139	0.660	exp_11_1

37 nodes. The total number of nodes comprises the 31 markers and six force application points. Secondly, it was observed that the bearings were subsiding. Therefore, a slight extension based on Eq. (5.23) has to be made in order to take the DIRICHLET boundary conditions as additional unknowns into account. The extended version of Eq. (5.23) reads

$$\begin{bmatrix} \mathbf{K} & \mathbf{C}^{\mathsf{T}} \\ \mathbf{C} & \mathbf{0} \end{bmatrix} \mathbf{u} = \begin{bmatrix} \mathbf{b} & \mathbf{0} \\ \mathbf{0} & \mathbf{I} \end{bmatrix} \begin{bmatrix} \mathbf{X} \\ \mathbf{u}_0 \end{bmatrix} , \tag{5.28}$$

where $\mathbf{K}$ is the singular stiffness matrix, $\mathbf{C}$ is the constraint matrix, $\mathbf{b}$ is the load matrix, $\mathbf{X}$ is the vector of unknowns and $\mathbf{u}_0$ contains the DIRICHLET boundary conditions as unknown parameters. This in turn yields

$$\mathbf{u} = \begin{bmatrix} \mathbf{K} & \mathbf{C}^{\mathsf{T}} \\ \mathbf{C} & \mathbf{0} \end{bmatrix}^{-1} \begin{bmatrix} \mathbf{b} & \mathbf{0} \\ \mathbf{0} & \mathbf{I} \end{bmatrix} \begin{bmatrix} \mathbf{X} \\ \mathbf{u}_0 \end{bmatrix} = \begin{bmatrix} \mathbf{A} & \mathbf{U} \end{bmatrix} \begin{bmatrix} \mathbf{X} \\ \mathbf{u}_0 \end{bmatrix} , \tag{5.29}$$

where upon closer examination the design matrix $\mathbf{A}$ is the same as in Eq. (5.23) and the matrix $\mathbf{U}$ acts as a kind of linear correction resulting from the non-trivial boundary conditions. The functional model is based on the above equation.

The variance-covariance matrix of the marker position observations $\mathbf{\Sigma_{pp}}$ is determined by the measurements of the entire experiment. In total, 12 measurement series were carried out on the undamaged beam (see Tab. 5.3) and 43 series of measurements on various damaged beam (see Tab. 5.4). The vectors $\mathbf{x}_s^M$ and $\mathbf{y}_s^M$ of length n_{photo} contain the x- respectively y-coordinates of a marker M in state s. The residual vectors $\mathbf{v}_{x_s}{}^M$ and $\mathbf{v}_{y_s}{}^M$ are computed as

$$\mathbf{v}_{x_s}{}^M = \mathbf{x}_s^M - \bar{\mathbf{x}}_s^M \text{ and } \mathbf{v}_{y_s}{}^M = \mathbf{y}_s^M - \bar{\mathbf{y}}_s^M , \tag{5.30}$$

where $\bar{\mathbf{x}}_s^M$ and $\bar{\mathbf{y}}_s^M$ are the median of $\mathbf{x}_s^M$ respectively $\mathbf{y}_s^M$. The residual matrix of the marker position for all marker in all states is assembled as

$$\mathbf{v_p} = \begin{bmatrix} \mathbf{v}_{x_s}{}^M & \mathbf{v}_{y_s}{}^M \end{bmatrix} . \tag{5.31}$$

The variance-covariance matrix of the marker position observations reads

$$\mathbf{\Sigma_{pp}} = \frac{\mathbf{v_p^{\mathsf{T}} v_p}}{412080 - 1870} . \tag{5.32}$$

Since the precision of targets position measurements is considered to be equal for all states and is uncorrelated between states, the variance-covariance matrix for the displacements reads

$$\mathbf{\Sigma_{LL}} = \begin{bmatrix} \mathbf{I} & -\mathbf{I} \end{bmatrix} \begin{bmatrix} \mathbf{\Sigma_{pp}} & \mathbf{0} \\ \mathbf{0} & \mathbf{\Sigma_{pp}} \end{bmatrix} \begin{bmatrix} \mathbf{I} \\ -\mathbf{I} \end{bmatrix} = \mathbf{\Sigma_{pp}} + \mathbf{\Sigma_{pp}} = 2\mathbf{\Sigma_{pp}} . \tag{5.33}$$

Therefore, the variance-covariance matrix of the displacement in 2D reads

$$\mathbf{\Sigma_{LL}} = 2\mathbf{\Sigma_{pp}} = \begin{bmatrix} 5.047 \cdot 10^{-5} & 8.204 \cdot 10^{-6} \\ 8.204 \cdot 10^{-6} & 7.233 \cdot 10^{-5} \end{bmatrix} \mathrm{mm}^2 \,. \tag{5.34}$$

Accordingly, the standard deviation of the displacement in y-direction is

$$\sigma_{l_y} = \sigma_u = 0.009\,\mathrm{mm}\,. \tag{5.35}$$

Since the functional and stochastic models are available, the elastic modulus of the undamaged beam can be adjusted from all twelve experiments respectively six displacement observations. It was specified that all finite elements have the same YOUNG's modulus. Therefore, in a first step, one elastic parameter and six by two unknown DIRICHLET boundary conditions were determined. In a second step, the adjusted DIRICHLET boundary conditions are fixed and at the same time the modulus of elasticity is re-adjusted. The adjusted elastic modulus is

$$\hat{E} = 67.397\,\mathrm{GPa} \text{ with } \sigma_{\hat{E}} = 0.062\,\mathrm{GPa} \tag{5.36}$$

and corresponds to that of aluminium. Moreover, the adjusted results are also shown in Fig. 5.13. The bending lines are shown in top left corner ($\mathbf{u}_1$ blue, $\mathbf{u}_2$ red, $\mathbf{u}_3$ yellow, $\mathbf{u}_4$ green, $\mathbf{u}_5$ brown, $\mathbf{u}_6$ light blue). The measured displacements are marked as a black star. Correspondingly, the residuals are shown in top right corner. In some cases, it is advantageous to have all residuals in one representation which is shown in the middle of the figure. Both red vertical bars represent the removed outliers. They were detected using standardised residuals which is shown in bottom of the figure.

Damage detection and localisation

In the same way as in Sec. 5.2, the presented approach is followed in order to detect and localise damage. However, to avoid long computation time, in case where the global test failed to reject the null hypothesis, the standardised residuals NV_ζ of the observed unknown elastic parameters are evaluated. Aforementioned, the finite element discretization of the beam specimen is determined in dependence on the attached markers as well as the application points of the forces and bearings. Thus, the finite element model of the beam consists of 36 non-equidistant elements. Considering the two boundary conditions and a linear interpolation of the elastic parameter of each element, a total of 39 unknowns result. An incorrect adjustment of the boundary conditions as unknowns can occur as the elastic parameters of the elements attempt to compensate for the effects of yielding bearings. To counter this effect, the following approach is proposed. In a first step, all elements share the same elastic modulus. In other words, one YOUNG's modulus and two boundary conditions have to be determined from the displacement observations. Then, in the second step, the adjusted boundary conditions are used as fixed values, while the 36 elastic parameters are determined from the displacement observations.

The beam was gradually damaged at a fixed position, see Fig. 5.14. The edge-to-edge length of the beam is 1500 mm. As shown, the damage was caused at approximately 383 mm, measured from the right edge. The beam length in the finite element model is 1480 mm which corresponds to the distance between the bearings. Thus, the damage position is at approximate 1107 mm. The damage has been successively increased, see Tab. 5.4. First, the beam was drilled through with a radius of 4 mm. Six different load experiments were then carried out (exp4mm). The damage was not detected in five out of six cases. And the localization of the fault failed where an alleged damage was detected. The borehole is then extended to a radius of 8 mm. Four stress tests were carried out here (exp8mm). Again, three out of four cases the damage undetectable. The beam was then further damaged. The borehole was extended to 10 mm radius (exp10mm), then two more holes were drilled with 10 mm radius each (exp3L), and damage was further increased (exp3L2). Again, no damage was noticeably detected. Then, the beam was sawed (exp_Y, exp_K). Here, it was observed that if the attached weights were large enough, the damage was detected but the localisation of the damage failed. Ultimately, the damage was large enough (exp_Z), so that the damage could be detected and localized repeatedly. The complete process is shown in the Tab. 5.5.

Some examples of the results from the evaluation are discussed. Attention should be paid to the residuals. Fig. 5.15 shows the evaluation of displacement measurements $\mathbf{u}_4$. In this case, no damage is detected and the beam was actually undamaged. In Fig. 5.16, however, the displacement measurements $\mathbf{u}_3$ evaluation lead to false damage

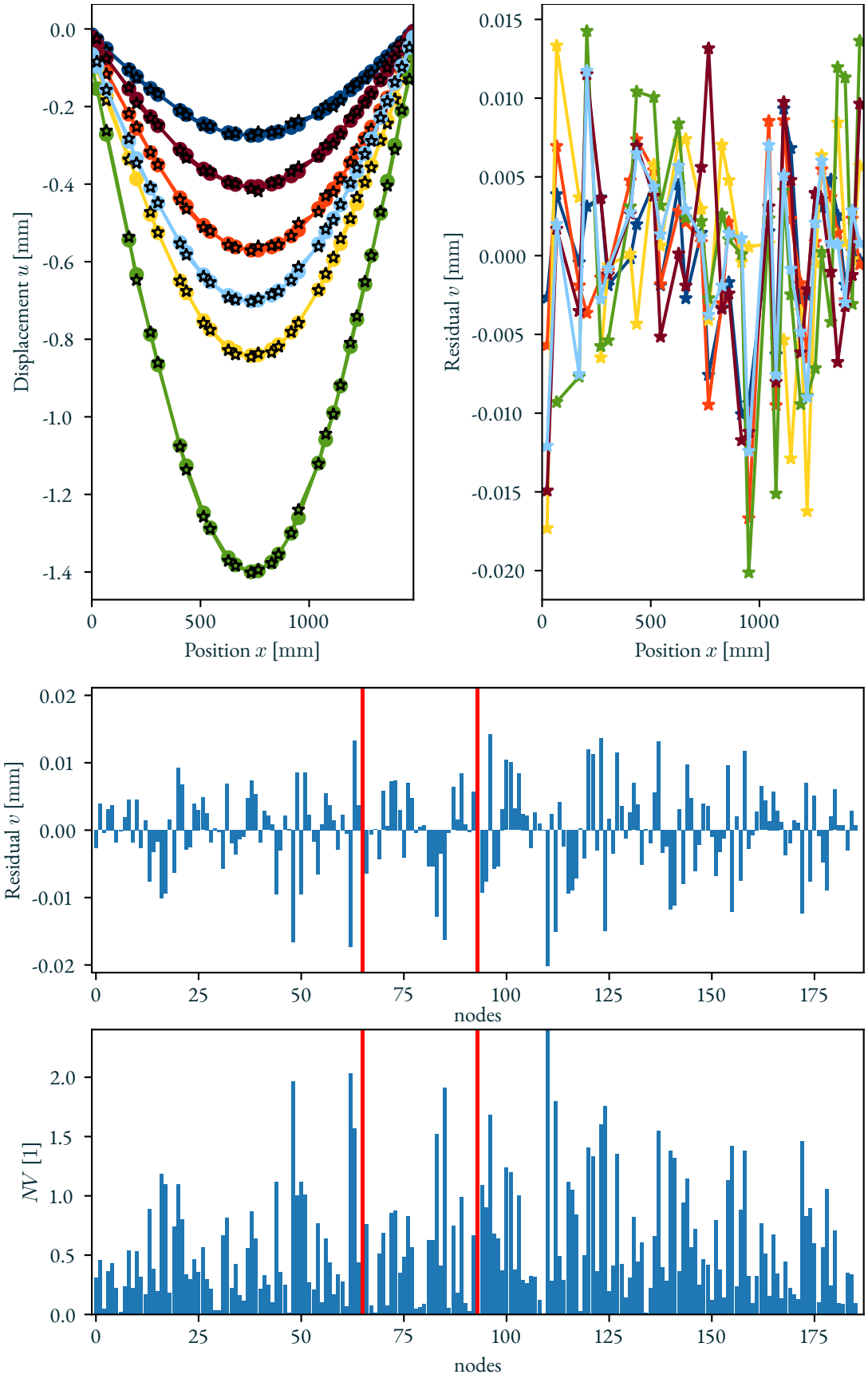


Figure 5.13: Deflection lines of the undamaged beam subjected to various external forces and the measured displacement from photogrammetry (top left), the corresponding residuals (top right), the complete residuals in one representation (middle) and the corresponding standardised residuals (bottom)

Table 5.4: For each state s, weights (m_1, m_2, m_3) were attached to the damaged beam specimen and n_{photo} images were taken.

s	n_{photo}	m_1 [kg]	m_2 [kg]	m_3 [kg]	designation
12	300	0.0	0.0	0.0	exp4mm_0_0
13	300	0.0	17.819	0.0	exp4mm_1_1
14	294	0.0	0.0	0.0	exp4mm_2_0
15	300	0.0	3.563	0.0	exp4mm_3_1
16	300	0.0	0.0	0.0	exp4mm_4_0
17	300	0.0	7.134	0.0	exp4mm_5_1
18	298	0.0	0.0	0.0	exp4mm_6_0
19	300	0.0	3.564	0.0	exp4mm_7_1
20	300	0.0	0.0	0.0	exp4mm_8_0
21	300	0.0	7.135	0.0	exp4mm_9_1
22	300	0.0	0.0	0.0	exp4mm_10_0
23	289	0.0	17.817	0.0	exp4mm_11_1
24	300	0.0	0.0	0.0	exp8mm_0_0
25	300	0.0	17.82	0.0	exp8mm_1_1
26	150	0.0	0.0	0.0	exp8mm_2_0
27	150	0.0	10.709	0.0	exp8mm_3_1
28	150	0.0	0.0	0.0	exp8mm_4_0
29	150	0.0	3.593	0.0	exp8mm_5_1
30	150	0.0	0.0	0.0	exp8mm_4_0
31	150	0.0	3.593	0.0	exp8mm_6_1
32	150	0.0	0.0	0.0	exp10mm_0_0
33	150	0.0	3.569	0.0	exp10mm_1_1
34	150	0.0	0.0	0.0	exp3L_0_0
35	150	0.0	3.578	0.0	exp3L_1_1
36	150	0.0	0.0	0.0	exp3L2_0_0
37	150	0.0	3.545	0.0	exp3L2_1_1
38	150	0.0	7.121	0.0	exp3L2_2_1
39	150	0.0	10.698	0.0	exp3L2_3_1
40	150	0.0	0.0	0.0	exp_Y_0_0
41	150	0.0	3.546	0.0	exp_Y_1_1
42	150	0.0	7.125	0.0	exp_Y_2_1
43	150	0.0	10.703	0.0	exp_Y_3_1
44	150	0.0	14.248	0.0	exp_Y_4_1
45	150	0.0	0.0	0.0	exp_K_0_0
46	150	0.0	7.114	0.0	exp_K_1_1
47	139	0.0	0.0	0.0	exp_Z_0_0
48	150	0.0	10.695	0.0	exp_Z_1_1
49	150	0.0	0.0	0.0	exp_Z_2_0
50	150	0.0	3.561	0.0	exp_Z_3_1
51	150	0.0	7.128	0.0	exp_Z_4_1
52	150	0.0	10.69	0.0	exp_Z_5_1
53	150	0.0	14.241	0.0	exp_Z_6_1
54	150	0.0	17.808	0.0	exp_Z_7_1

Table 5.5: The measurement data designation indicates whether the beam is actually damaged or undamaged, the displacement measurements set $\mathbf{u}_i$ from state s^0 to s, the theoretical reference standard deviation σ_0, the empirical reference standard deviation s_0, the test statistic χ^2_r, the threshold value for all cases $\chi^2_{r,1-\alpha} = 44.985$ for redundancy $r = 31$ and error probability $\alpha = 5\,\%$, if it holds $p : \chi^2_r > \chi^2_{r,1-\alpha}$ then reject H_0 in favour of H_A, the allegedly damaged finite element ζ respectively ${}^{\zeta}\hat{E}$, the ratio $r_{el} = \frac{{}^{22}\hat{E}}{\hat{E}}$ between the damaged and undamaged finite element, ${}^{22}\hat{E}$ and $\hat{E}$, the total attached weights m

designation	$\mathbf{u}_i$	s	s^0	σ_0 [10^{-3}]	s_0 [10^{-3}]	χ^2_r	p	ζ	${}^{22}\hat{E}$ [GPa]	r_{el} [%]	m [kg]
exp	0	1	0	5.742	3.416	10.973	false				3.565
	1	3	2	5.742	3.775	13.395	false				7.120
	2	5	4	5.742	6.585	40.768	false				10.668
	3	7	6	5.742	7.465	52.399	true	7			17.825
	4	9	8	5.742	4.535	19.337	false				5.491
	5	11	10	5.742	3.828	13.778	false				9.068
exp4mm	6	13	12	5.742	5.586	29.331	false				17.819
	7	15	14	5.742	3.878	14.136	false				3.563
	8	17	16	5.742	4.872	22.316	false				7.134
	9	19	18	5.742	3.904	14.328	false				3.564
	10	21	20	5.742	5.015	23.645	false				7.135
	11	23	22	5.742	7.344	50.713	true	8			17.818
exp8mm	12	25	24	5.742	10.003	94.065	true	10			17.820
	13	27	26	5.742	6.883	44.542	false				10.709
	14	29	28	5.742	3.778	13.421	false				3.593
	15	31	30	5.742	3.345	10.517	false				3.593
exp10mm	16	33	32	5.742	2.732	7.017	false				3.569
exp3L	17	35	34	5.742	6.695	42.145	false				3.578
exp3L2	18	37	36	5.742	3.304	10.261	false				3.545
	19	38	36	5.742	5.991	33.744	false				7.121
	20	39	36	5.742	8.281	64.466	true	11			10.698
exp_Y	21	41	40	5.742	4.295	17.347	false				3.546
	22	42	40	5.742	6.412	38.652	false				7.125
	23	43	40	5.742	8.187	63.009	true	11			10.703
	24	44	40	5.742	16.087	243.297	true	12			14.248
exp_K	25	46	45	5.742	12.526	147.514	true	15			7.114
exp_Z	26	48	47	5.742	53.867	2727.981	true	22	67.348	99.93	10.695
	27	50	49	5.742	17.065	273.799	true	22	67.392	99.99	3.561
	28	51	49	5.742	34.300	1106.085	true	22	67.376	99.97	7.128
	29	52	49	5.742	53.330	2673.953	true	22	67.348	99.93	10.690
	30	53	49	5.742	68.296	4385.298	true	22	67.313	99.88	14.241
	31	54	49	5.742	86.981	7112.952	true	22	67.264	99.80	17.808

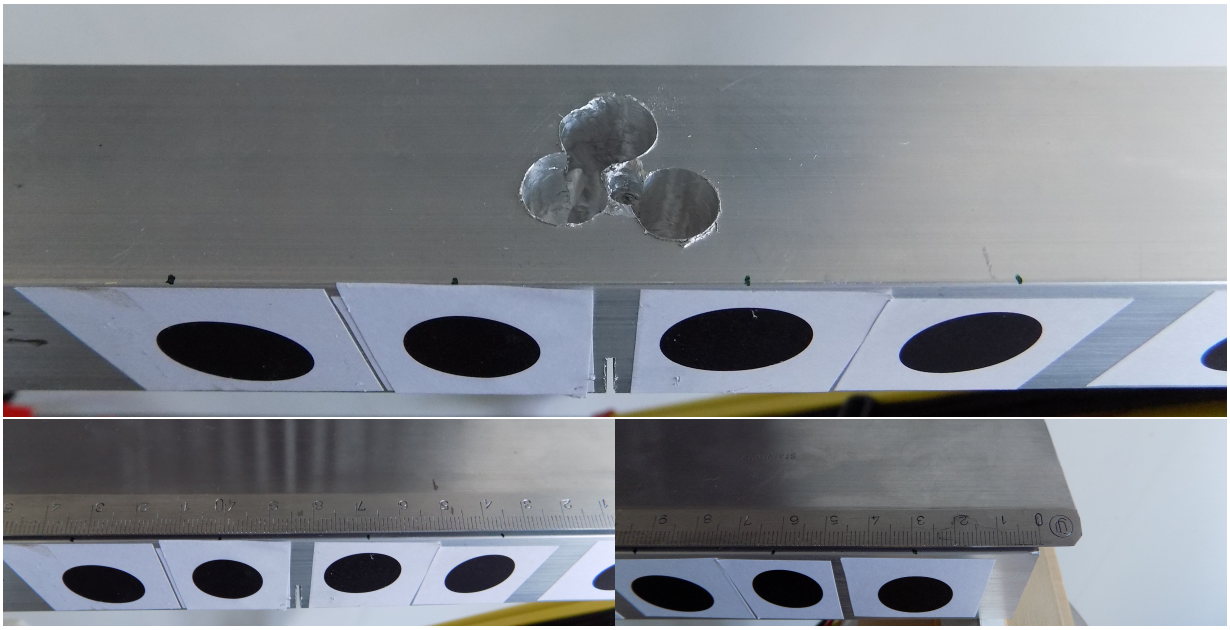


Figure 5.14: The position where damage is induced.

detection. In Fig. 5.17, the beam was actually damaged, but no damage was detected for the displacement measurements $\mathbf{u}_{21}$. In Fig. 5.18, the evaluation of the displacement measurements $\mathbf{u}_{25}$ leads to positive damage detection, but the damage is located incorrectly as seen in Fig. 5.19. Finally, consistent results can be obtained for the analysis of measurement series $\mathbf{u}_{26}$ to $\mathbf{u}_{31}$. In these cases, the damage to the beam was large enough so that, regardless of the applied forces, the global test was always positive and the location of the damage was always confined in the same place. For the measurements $\mathbf{u}_{27}$ in Fig. 5.20 approximately three and a half kilograms of weight were attached to the beam. The localization of the damage pointed to the element node $\zeta = 22$, see Fig. 5.21. For the measurement series $\mathbf{u}_{31}$ in Fig. 5.22, approximately 18 kilograms were placed on the beam. As seen in Fig. 5.23, the element node $\zeta = 22$ is also the location of damage.

Aforementioned, the damage position is at approximate $1107\,\mathrm{mm}$. Thus, it affects the element node $\zeta = 24$ which is at $1112\,\mathrm{mm}$. However, according to the performed analysis, the damage is located at the element node $\zeta = 22$ which is at $990\,\mathrm{mm}$. This results in an error estimate of $117\,\mathrm{mm}$ ($= 1107\,\mathrm{mm} - 990\,\mathrm{mm}$). In relation to the total length of $1480\,\mathrm{mm}$, the mislocalization is less than 8 percent, ($\frac{117\,\mathrm{mm}}{1480\,\mathrm{mm}} \approx 0.079$).

Conclusion

By means of a beam bending experiment, the evaluation has shown that the Measurement- and Model-based Structural Analysis is capable of detecting and locating damage. However, the likelihood of localizing damage is hampered by systematic influences. Here, in this particular case, it was observed that ambient light affected the photogrammetric system. Ambient light changes, for example, due to the influence of clouds. As a result, the pixels on the images change their contrasts and thus influencing the adjusting circular position of the marker. It is also inevitable that the markers will become soiled over time. This also impacts an apparent change in the marker position. Subsiding tripods and bearings was also unhelpful in reducing systematic influences during evaluation. The maximum deflection was approximately $1.4\,\mathrm{mm}$ and due to the subsiding of roughly $0.1\,\mathrm{mm}$, the elastic parameter was missing $3\,\mathrm{GPa}$ at the end of the adjustment. In order to counteract the subsidence, on the one hand the finite element model had to be extended, on the other hand the attached weight should not become too large. Since the beam was very stiff and it was not possible to attach too much weight, the deflection became too small. But it was necessary that the deflection had to be large enough to overcome the noise and systematic influences of photogrammetry. In the end, there was no other choice but to increase the damage to the beam. This made it possible to achieve consistent damage detection and localisation.

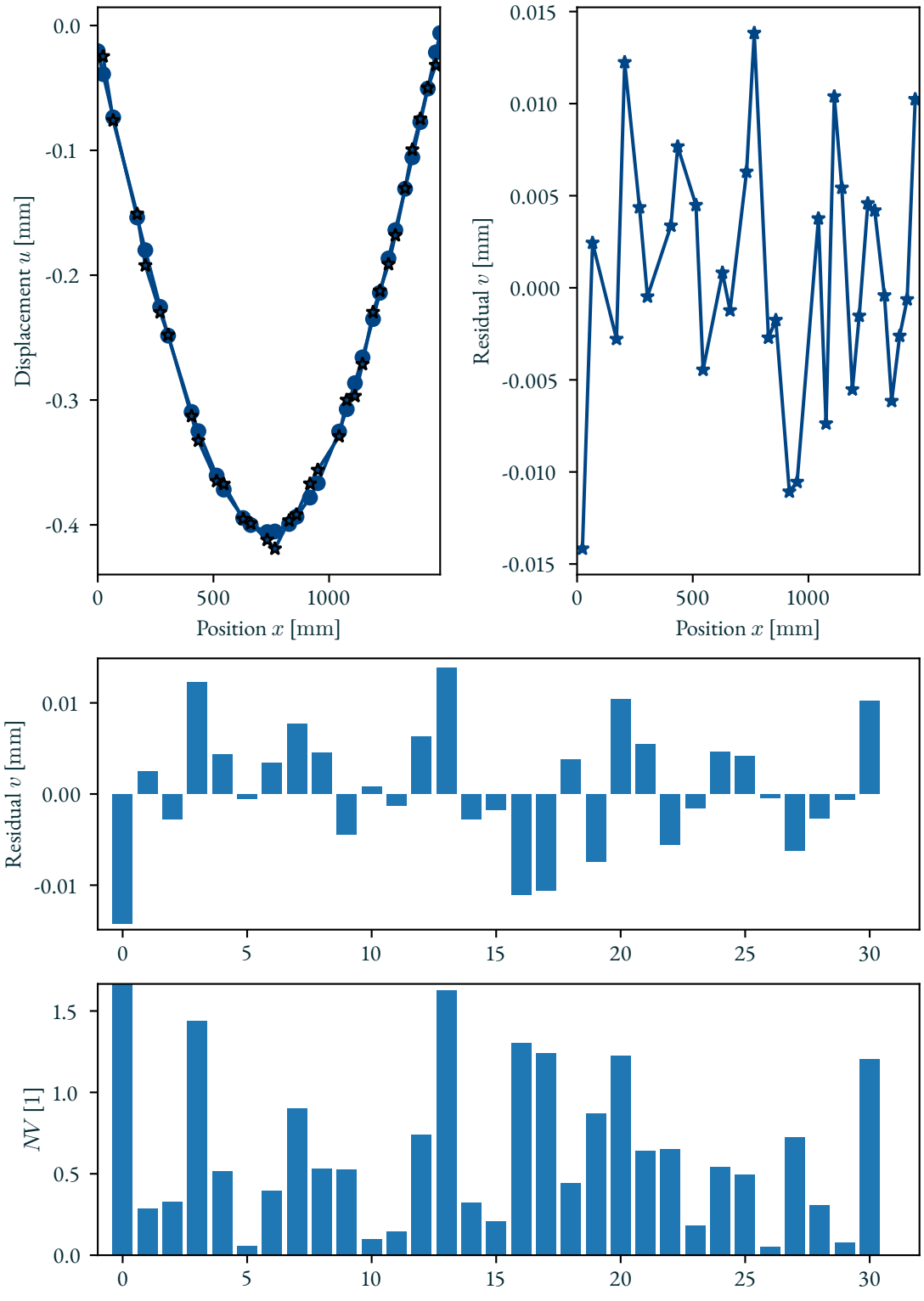


Figure 5.15: Undamaged beam subjected to external weight of 5.491 kg, adjusted deflection line and measured displacement $\mathbf{u}_4$ (top left), the corresponding residuals as line representation (top right), the corresponding residuals as bar representation (middle), and the standardised residuals of the displacement observations (bottom); no damage detected

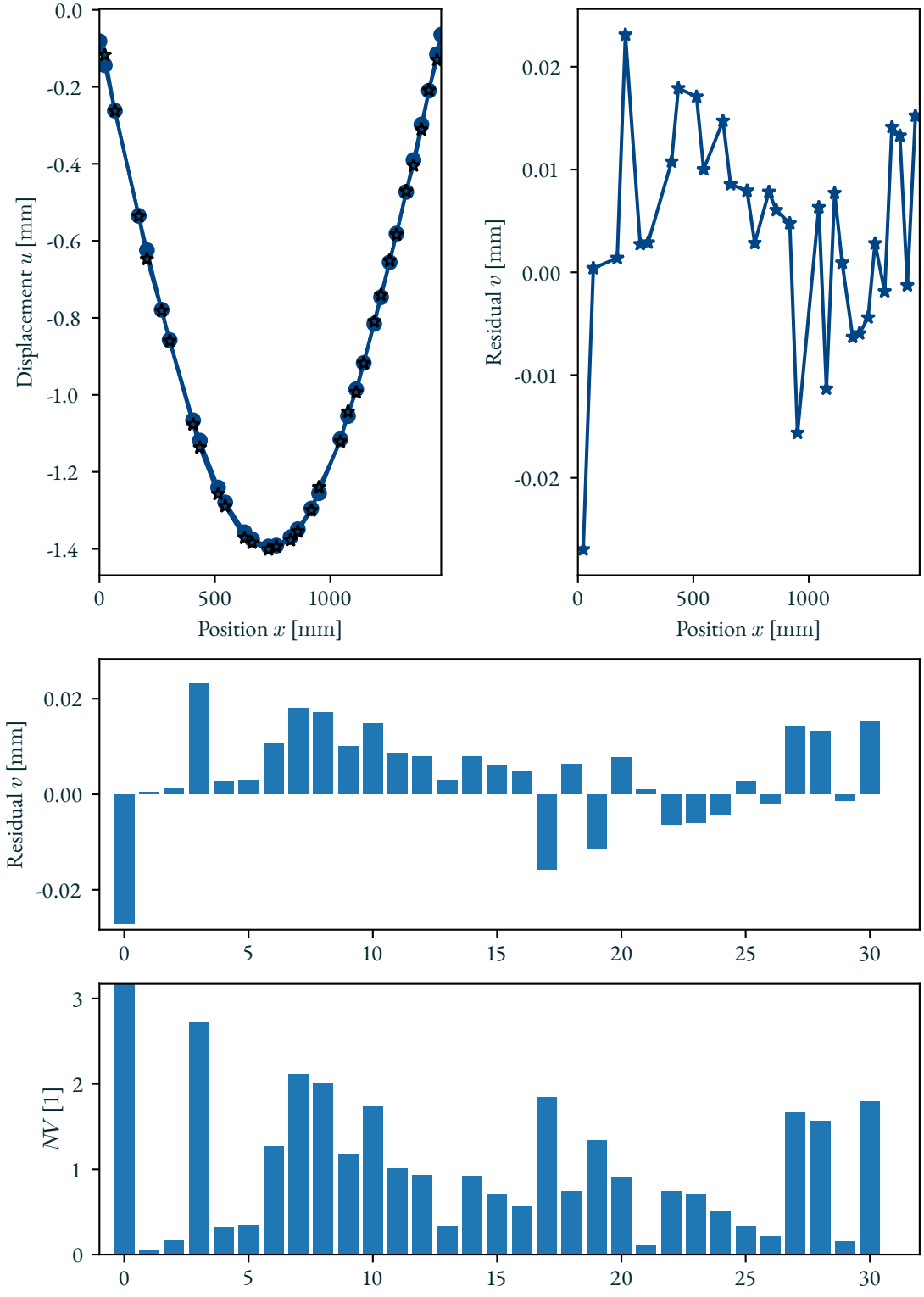


Figure 5.16: Undamaged beam subjected to external weight of 17.825 kg, adjusted deflection line and measured displacement $\mathbf{u}_3$ (top left), the corresponding residuals as line representation (top right), the corresponding residuals as bar representation (middle), and the standardised residuals of the displacement observations (bottom); damage detected, false alarm

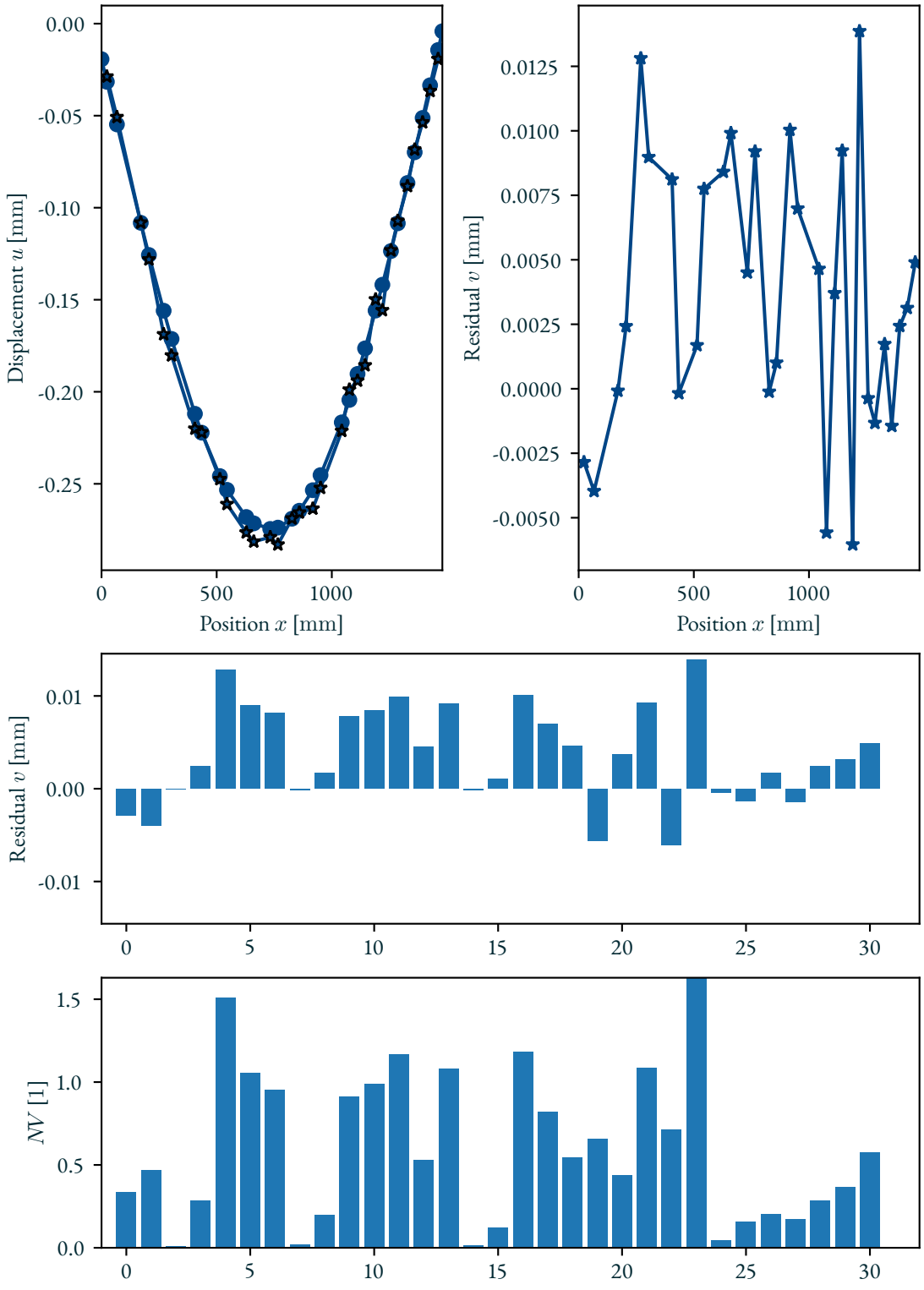


Figure 5.17: Damaged beam subjected to external weight of 3.546 kg, adjusted deflection line and measured displacement $\mathbf{u}_{21}$ (top left), the corresponding residuals as line representation (top right), the corresponding residuals as bar representation (middle), and the standardised residuals of the displacement observations (bottom); no damage detected

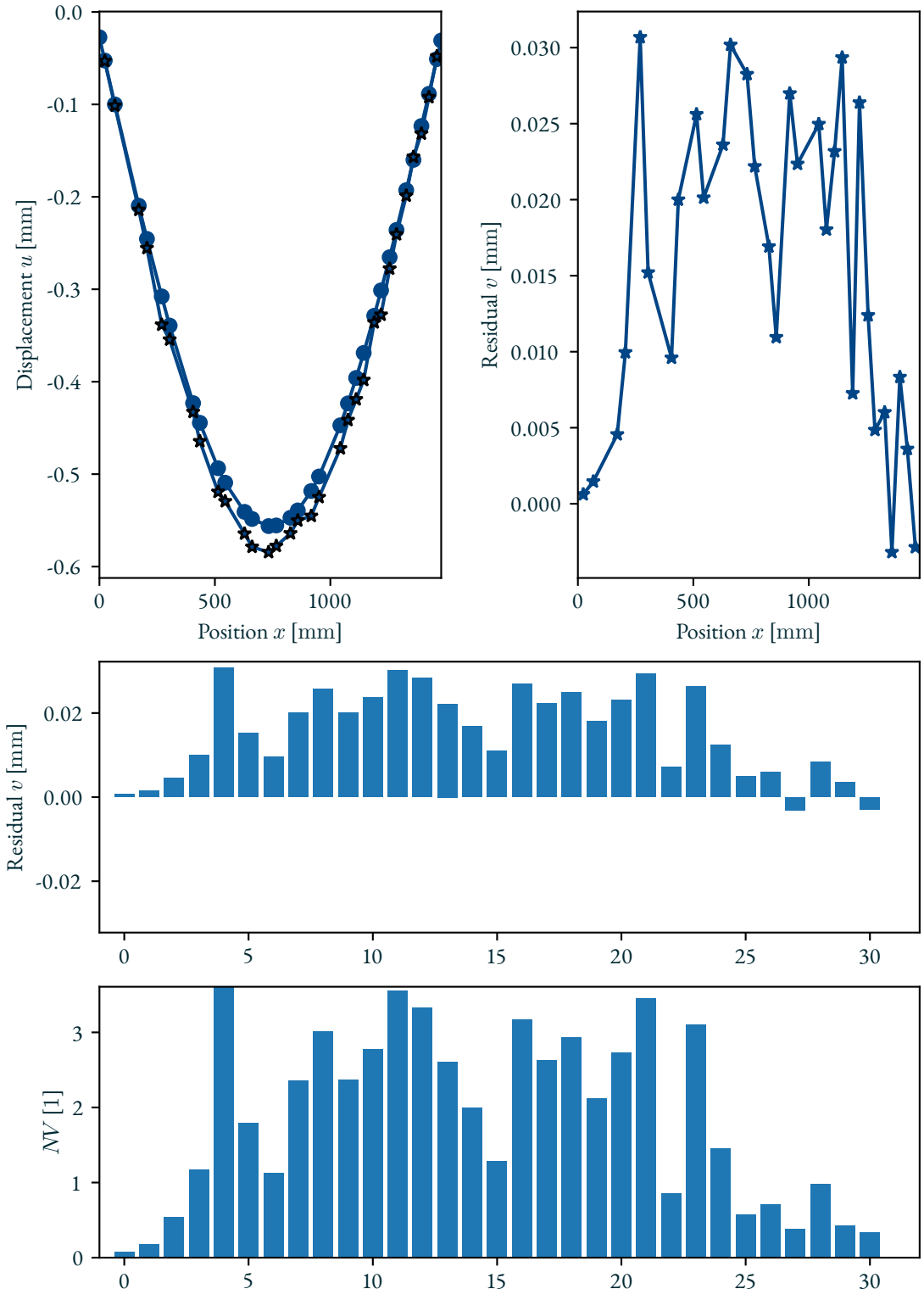


Figure 5.18: Damaged beam subjected to external weight of 7.114 kg, adjusted deflection line and measured displacement $\mathbf{u}_{25}$ (top left), the corresponding residuals as line representation (top right), the corresponding residuals as bar representation (middle), and the standardised residuals of the displacement observations (bottom); damage detected

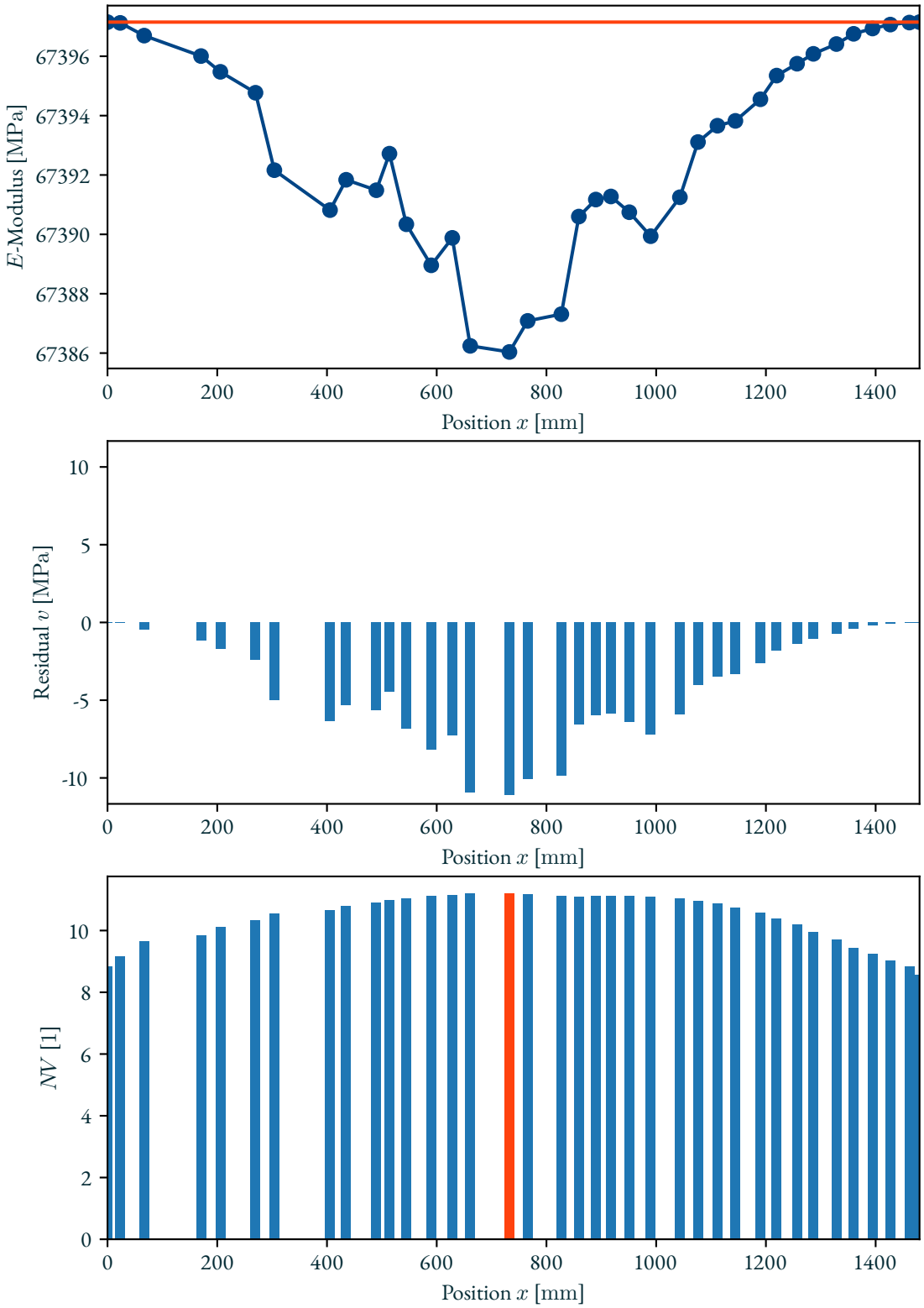


Figure 5.19: Damaged beam subjected to external weight of 7.114 kg, displacement measurements $\mathbf{u}_{25}$; elastic moduli of the beam (top), the residuals of the observed unknowns (middle), the standardised residuals of the observed unknowns (bottom); damage localisation at element node $\zeta = 15$

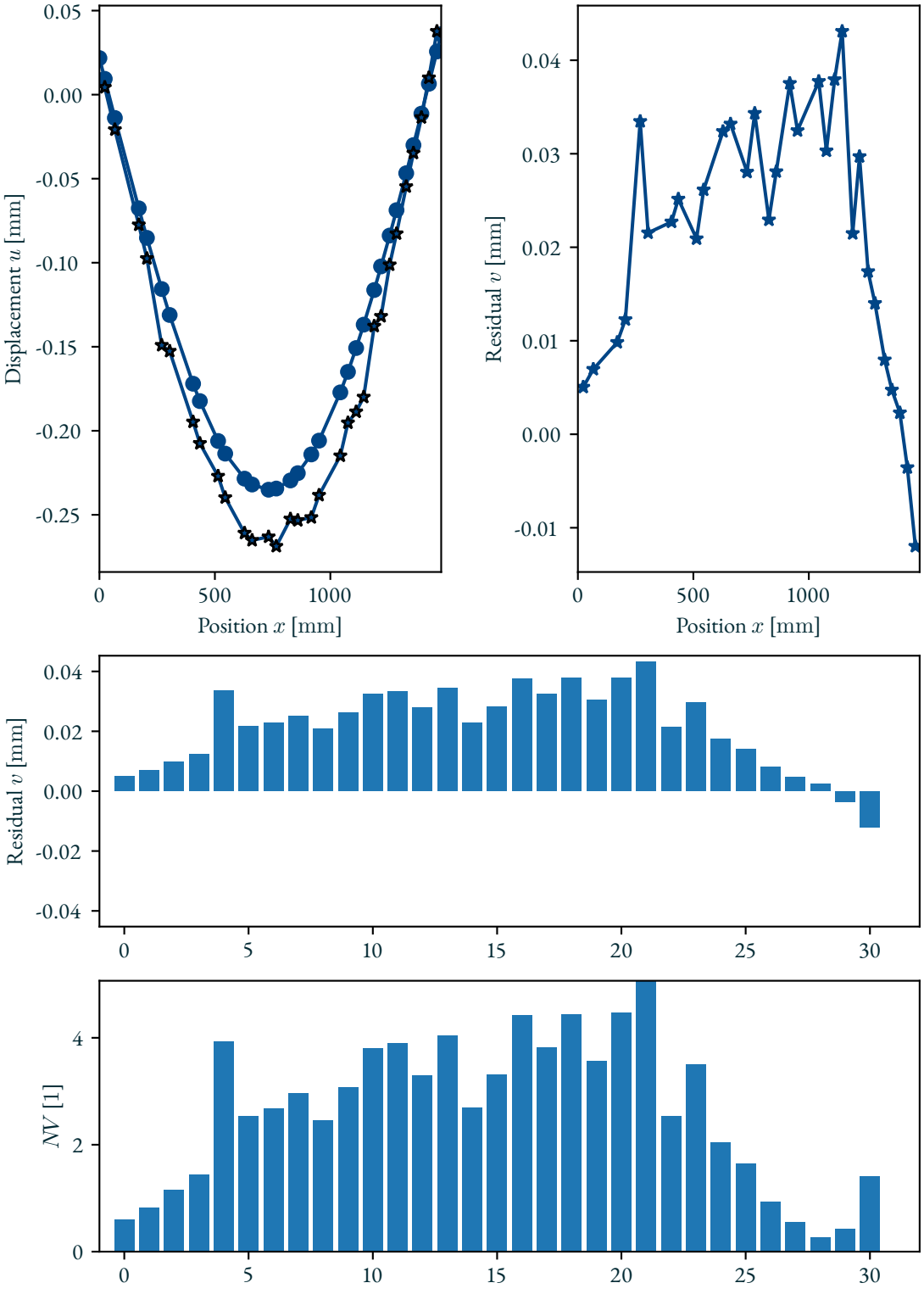


Figure 5.20: Damaged beam subjected to external weight of 3.561 kg, adjusted deflection line and measured displacement $\mathbf{u}_{27}$ (top left), the corresponding residuals as line representation (top right), the corresponding residuals as bar representation (middle), and the standardised residuals of the displacement observations (bottom); damage detected

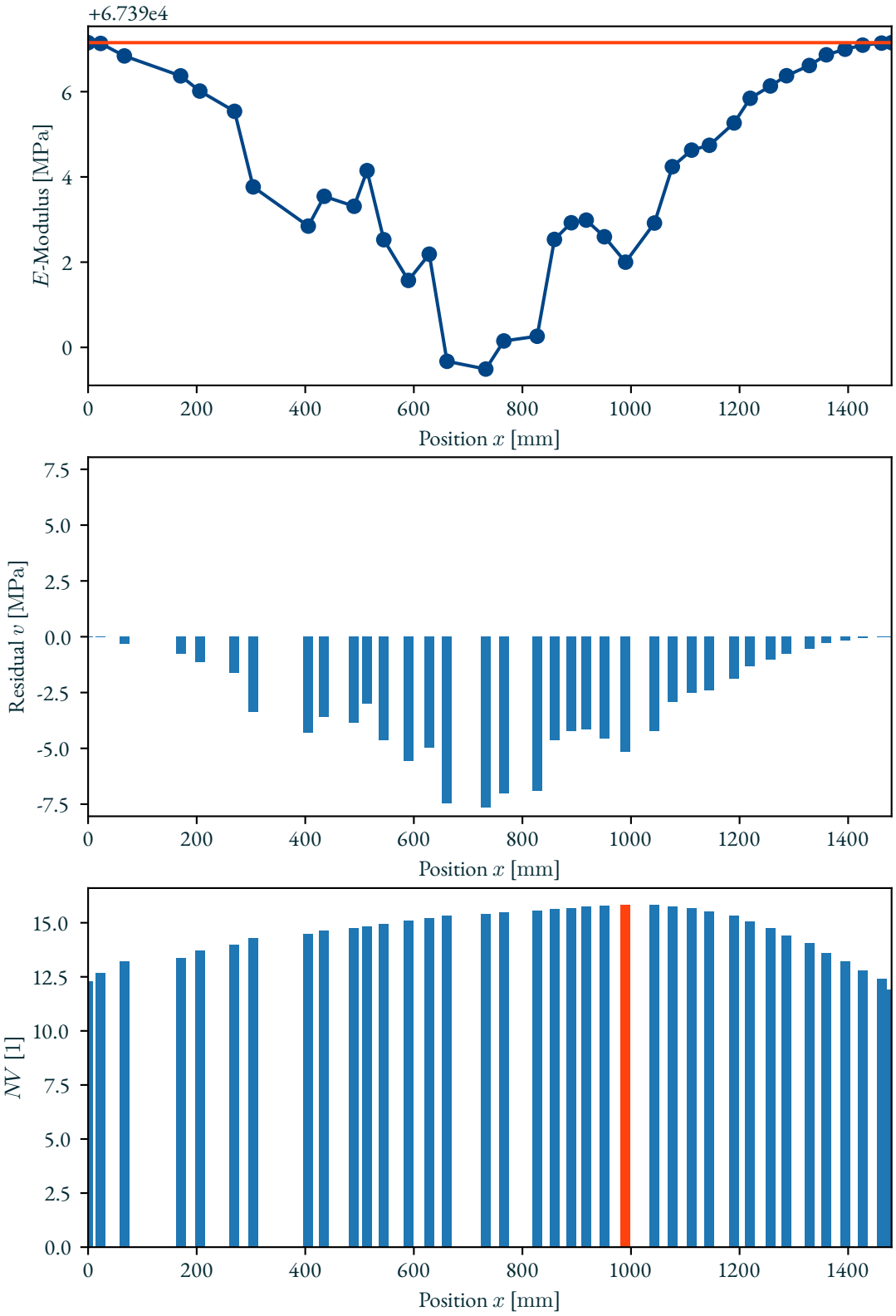


Figure 5.21: Damaged beam subjected to external weight of 3.561 kg, displacement measurements $\mathbf{u}_{27}$; elastic moduli of the beam (top), the residuals of the observed unknowns (middle), the standardised residuals of the observed unknowns (bottom); damage localisation at element node $\zeta = 22$

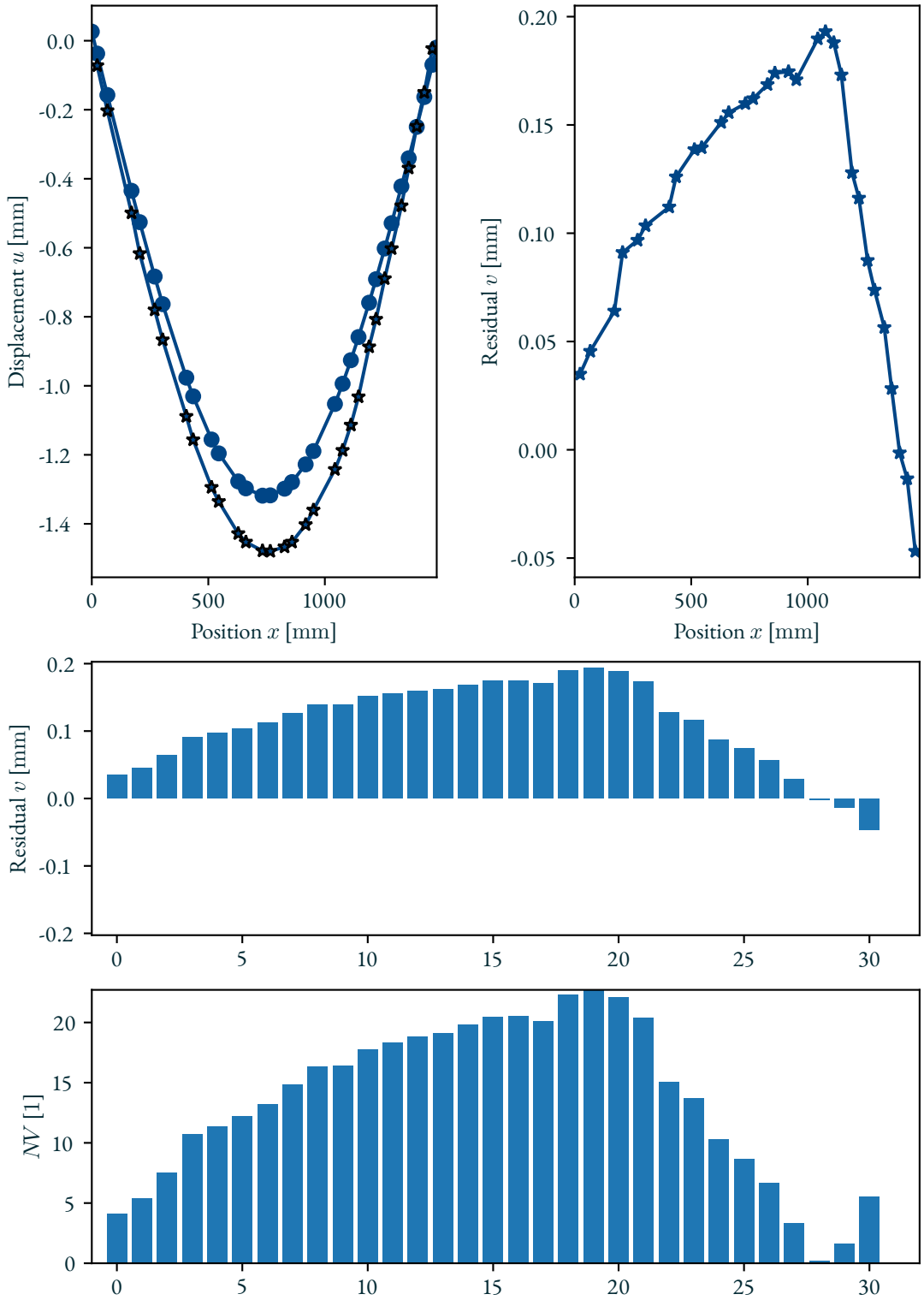


Figure 5.22: Damaged beam subjected to external weight of 17.808 kg, adjusted deflection line and measured displacement $\mathbf{u}_{31}$ (top left), the corresponding residuals as line representation (top right), the corresponding residuals as bar representation (middle), and the standardised residuals of the displacement observations (bottom); damage detected

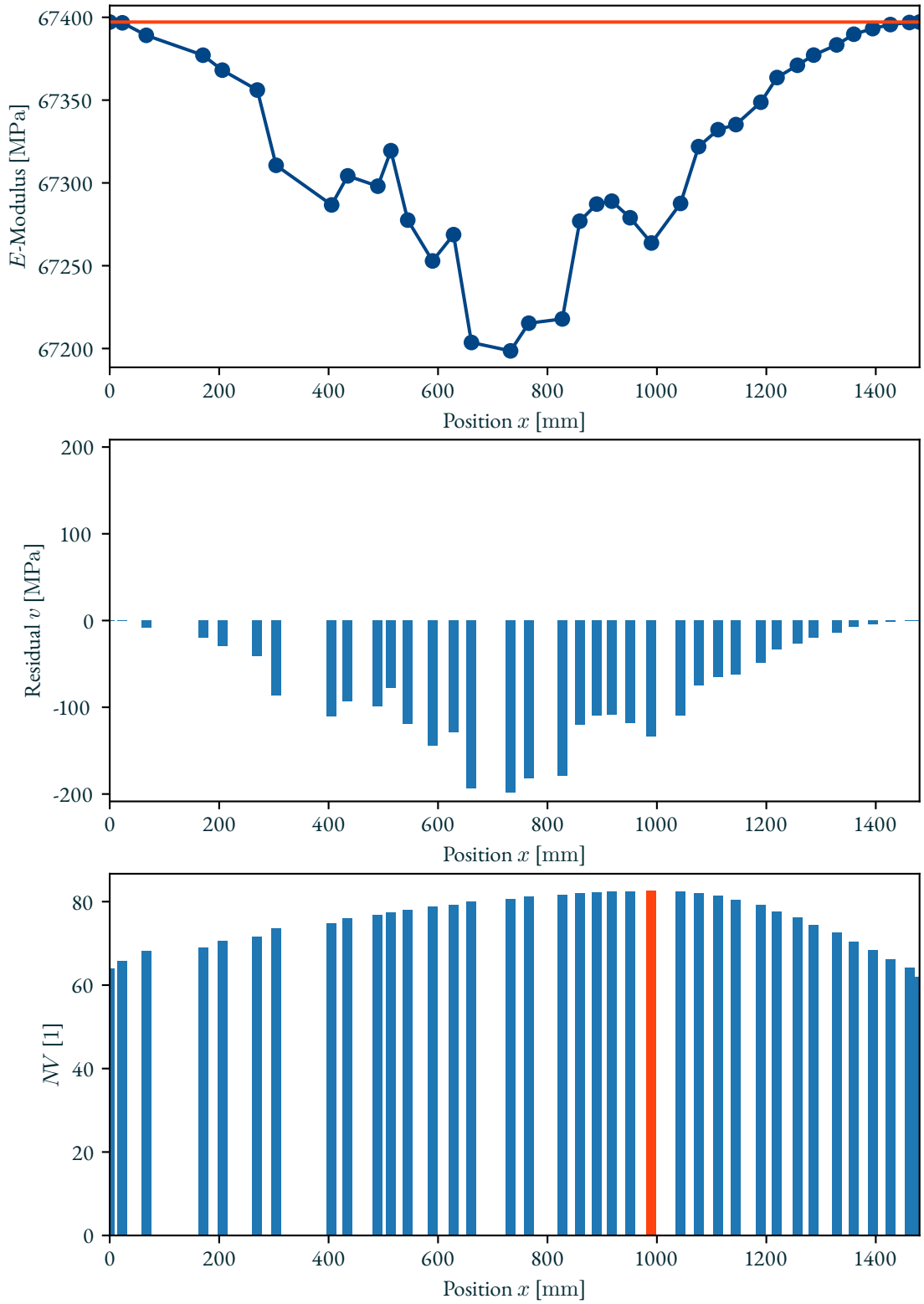


Figure 5.23: Damaged beam subjected to external weight of 17.808 kg, displacement measurements $\mathbf{u}_{31}$; elastic moduli of the beam (top), the residuals of the observed unknowns (middle), the standardised residuals of the observed unknowns (bottom); damage localisation at element node $\zeta = 22$

5.4 Adjustment of Material Parameters from Displacement Field Measurement

The determination of material parameters from displacement field measurement is being examined for linear elastic solid. A frequently used approach to compute material constants can be found in many studies. Even though they presented the approach in many variations, but in the end they are essentially based on the same algorithm: Parameters are iteratively tuned until the computed results are in accordance with the measurements. The main drawback of this approach is that mainly commercial software is used that hinders us to investigate its inner evaluation process. This leads to the question, how the results from this commercial software can be trusted. On the contrary to these debatable approaches, a method is presented that inverts the procedure of finite element method by using the most general model for a least squares adjustment – the Gauss-Helmert Model.

This section is partly published in Wu et al. (2016).

The integration of finite element method into the least squares adjustment is further extended for a joint evaluation of an elastostatic model and displacement field measurement. For linear solids which obey the Hooke's law, the material parameters determination from measurements is being examined. Aforementioned, many algorithms for computing material parameters from measurements are given in the literature. But essentially they are the same. This approach tunes iteratively the parameters until the computed finite element method results are in accordance with the measurements, see Fig. 5.1. The main issue is that this algorithm contains inaccessible program parts. Due to these restrictions, we are hindered to comprehend the inner process of the programs. Consequently, the question arises as to how we can be sure that the result from this algorithm is reliable. In contrast to this debatable approach, we follow a rigorous and direct method. Hereby, it is necessary to understand every aspect of the process: From modelling part by means of continuum mechanics, numerical approximation by finite element method and computation of material parameters from measurements by least squares adjustment. The "classical" finite element method procedure starts with known material constants and ends up with computed fields such as displacement or temperature field. We present a method to invert the finite element method procedure using the most general model for a least squares adjustment – the Gauss-Helmert Model. From measured displacement field, the material parameters are directly calculated.

The focus is to show the basic concept of this integrated analysis, therefore we conveniently limit the example to a simplified case. Firstly, we examine a linear elastic isotropic solid. In Voigt's notation (Zienkiewicz et al. 2013, p. 23), the stiffness tensor in matrix notion in Eq. (2.142) reads

$$\mathbf{C} = \begin{bmatrix} \lambda+2\mu & \lambda & \lambda & & & \\ & \lambda+2\mu & \lambda & & & \\ & & \lambda+2\mu & & & \\ & & & \mu & & \\ & & & & \mu & \\ \text{symmetrical} & & & & & \mu \end{bmatrix} = \begin{bmatrix} C_{11} & C_{12} & C_{12} & & & \\ & C_{11} & C_{12} & & & \\ & & C_{11} & & & \\ & & & C_{44} & & \\ & & & & C_{44} & \\ \text{symmetrical} & & & & & C_{44} \end{bmatrix},$$

where the Lamé constants are re-expressed as $C_{11} = \lambda + 2\mu$, $C_{12} = \lambda$ and $C_{44} = \mu$. Secondly, we consider an elastostatic case and where the body forces such as gravity force are neglected. Applying the finite element method leads to

$$\int C_{ijkl} \frac{\partial \delta u_i}{\partial x_j} \frac{\partial u_k}{\partial x_l} \,\mathrm{d}V = \int \delta u_i t_i \,\mathrm{d}A \;\Rightarrow\; \left(C_{11}\mathbf{K}^{11} + C_{12}\mathbf{K}^{12} + C_{44}\mathbf{K}^{44}\right)\mathbf{u} = \mathbf{f}\,, \tag{5.37}$$

where $\mathbf{K}^{11}$, $\mathbf{K}^{12}$, $\mathbf{K}^{44}$ are the stiffness matrices given by the initial geometry of the solid, the load vector $\mathbf{f}$ given by the known applied surface forces t_i and $\mathbf{u}$ is the measured displacement field vector. Lastly, we assume that the displacement field vector $\mathbf{u}$ can be completely measured with the same precision for all values. Thus, the associated weight matrix $\mathbf{P}$ is the identity matrix. The stiffness matrices $\mathbf{K}^{11}$, $\mathbf{K}^{12}$, $\mathbf{K}^{44}$ and the load vector $\mathbf{f}$ are considered

as error-free. The aim is to determine the material constants C_{11}, C_{12} and C_{44} from the observed displacement field $\mathbf{u}$.

In adjustment theory, this is a non-linear adjustment problem and it is known as *adjustment with condition equations*. It can be solved with Gauss-Helmert Model after linearisation. The functional relationship based on Eq. (5.37) reads

$$\left(C_{11}\mathbf{K}^{11} + C_{12}\mathbf{K}^{12} + C_{44}\mathbf{K}^{44}\right)\left(\mathbf{u}+\mathbf{v}\right) = \mathbf{f}\,, \tag{5.38}$$

where the vector of residuals $\mathbf{v}$ is introduced for the observed displacement field $\mathbf{u}$. For the condition equations, we write

$$\boldsymbol{\Psi} = \left(C_{11}\mathbf{K}^{11} + C_{12}\mathbf{K}^{12} + C_{44}\mathbf{K}^{44}\right)\left(\mathbf{u}+\mathbf{v}\right) - \mathbf{f} = \mathbf{0}\,. \tag{5.39}$$

The design matrices $\mathbf{A}$ and $\mathbf{B}$ are obtained as follows

$$\mathbf{B} = \left.\frac{\partial \boldsymbol{\Psi}}{\partial \mathbf{v}}\right|_{\substack{\mathbf{v}=\mathbf{v}^0 \\ \hat{\mathbf{X}}=\hat{\mathbf{X}}^0}} = C_{11}^0\mathbf{K}^{11} + C_{12}^0\mathbf{K}^{12} + C_{44}^0\mathbf{K}^{44} \tag{5.40}$$

and

$$\mathbf{A} = \left.\frac{\partial \boldsymbol{\Psi}}{\partial \hat{\mathbf{X}}}\right|_{\substack{\mathbf{v}=\mathbf{v}^0 \\ \hat{\mathbf{X}}=\hat{\mathbf{X}}^0}} = \begin{bmatrix}\mathbf{K}^{11}\left(\mathbf{u}+\mathbf{v}^0\right) & \mathbf{K}^{12}\left(\mathbf{u}+\mathbf{v}^0\right) & \mathbf{K}^{44}\left(\mathbf{u}+\mathbf{v}^0\right)\end{bmatrix}\,, \tag{5.41}$$

where the starting values for the vector of residuals is $\mathbf{v}^0$ and for the vector of unknowns is

$$\hat{\mathbf{X}}^0 = \begin{bmatrix}C_{11}^0 & C_{12}^0 & C_{44}^0\end{bmatrix}\,. \tag{5.42}$$

For the vector of misclosures $\mathbf{w}$, we have

$$\mathbf{w} = -\mathbf{B}\mathbf{v}^0 + \boldsymbol{\Psi}^0 = C_{11}\mathbf{K}^{11}\mathbf{u} + C_{12}\mathbf{K}^{12}\mathbf{u} + C_{44}\mathbf{K}^{44}\mathbf{u} - \mathbf{f}\,. \tag{5.43}$$

Solving Eq. (3.24) iteratively by means of the above design matrices, $\mathbf{A}$ and $\mathbf{B}$, and vector of misclosures $\mathbf{w}$ until a break-off condition is met, we obtain the wanted unknown material parameters.

An application example may provide some insight to this presented method. Without loss of generality, we discretised a aluminium solid cube with the side length of 40 mm into 20250 tetrahedrons with 4096 nodes. The simulated displacement field $\mathbf{u}_{\text{sim}}$ is generated by means of Eq. (5.37)

$$\mathbf{u}_{\text{sim}} = \left(C_{11}\mathbf{K}^{11} + C_{12}\mathbf{K}^{12} + C_{44}\mathbf{K}^{44}\right)^{-1}\mathbf{f}\,, \tag{5.44}$$

where the stiffness matrices $\mathbf{K}^{11}$, $\mathbf{K}^{12}$ and $\mathbf{K}^{44}$ are determined by the geometrical and discretisation specification of the cube as well as fixed boundary conditions. The applied force vector $\mathbf{f}$ is predefined. The elastic parameters for aluminium are

$$C_{11} = 1.025\cdot 10^5\,\text{MPa}\,,\; C_{12} = 5.281\cdot 10^4\,\text{MPa}\,\text{and}\,C_{44} = 2.584\cdot 10^4\,\text{MPa}\,. \tag{5.45}$$

Then, the simulated displacement field $\mathbf{u}_{\text{sim}}$ is used as observed quantities

$$\mathbf{u} = \mathbf{u}_{\text{sim}}\,, \tag{5.46}$$

without adding measurement noise for the sake of simplicity. Poor starting values were used for test purposes. The initial elastic parameters are chosen one order of magnitude smaller than the true values

$$C_{11}^0 = 1.0\cdot 10^4\,\text{MPa}\,,\; C_{12}^0 = 5.0\cdot 10^3\,\text{MPa}\,,\; C_{44}^0 = 2.0\cdot 10^3\,\text{MPa}$$

and the vector of residuals also contains poor initial values

$$\mathbf{v}^0 = \begin{bmatrix}1 & 1 & \cdots & 1\end{bmatrix}^{\mathsf{T}}\,,$$

nevertheless the solution converges stably to the true values as in Eq. (5.45) after 18 iterations.

In this numerical analysis, the determination of material parameters is conducted rigorously with least squares adjustment in combination with the deterministic elastostatic model. This opens the possibility of assessments for material constants and their stochastic properties with statistic tests. The characteristic of measurements is that only a small sample information of the complete body is captured. An important aspect to follow is how to recover material parameters with "incomplete" information which is often the case with measurements. This examination is performed with an illustrative example in the next section.

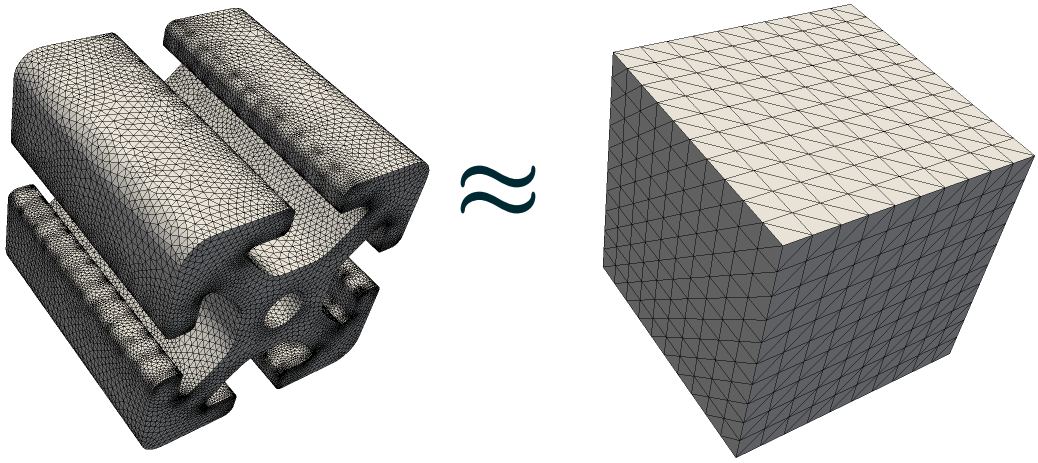


Figure 5.24: Aluminium profile with a geometrical complex inner structure can be substituted by an approximate model

5.5 Approximate Model for Geometrical Complex Structures

Many engineering structures are nowadays made of composite materials or metal foam. These modern engineering materials contain very complex inner geometry. To simulate the deformational behaviour of these structures often requires a high number of discretisation elements. This in turn yields a very large system of linear equations that are extremely time and memory consuming or practically impossible to solve. It is therefore desirable to find an approach to overcome this obstacle. A numerical method is proposed to find an approximate substitute model for geometrical complex structures.

This section is partly published in Wu et al. (2017).

Aluminium profiles such as shown in Fig. 5.24 (left) are often used to construct frames for carrying loads. Prediction of the deformational behaviour of a construction built from aluminium profiles is often computed in finite element method. Due to the aluminium profiles' complex formed cross section and its size in proportion to the structure, an extremely high number of discretisation points is required. This leads to various computational problems and ridiculous requirements such as a very long calculation time as well as an extreme computer memory demand. Therefore, it is highly desired to find a substitute model as shown in Fig. 5.24 (right) that can be easily discretised and thus needs less memory and computational time.

A cubic segment of the aluminium profile is substituted by a solid cubic body. The complex inner geometry as well as the material properties (Aluminium: $E = 66.6\,\mathrm{GPa}$, $\mu = 0.34$) are given. As shown in Fig. 5.24, the aim is to find an approximate model, which indicates very similar deformational behaviour as the aluminium profile. The approximate model is a solid cube and has the dimension as external dimension of the complex profile. While the complex structured aluminium profile is made of linear elastic isotropic material (two parameters), the approximate model has to be made of an anisotropic linear elastic material in order to pay for its geometrical simplicity. In other words, the challenge is to find the material constants of an anisotropic solid cube that deforms approximately in the same way as the geometrical complex profile made of isotropic material. Both bodies are subjected to the same external loads.

The aim is to find the set of elastic parameters for the substitute model that mimics approximately the deformational behaviour of the original finite element model. The unknown elastic parameters of the anisotropic linear elastic material can be estimated by means of least squares adjustment. Via finite element method the complete deformation field of the original body can be computed, and we are using this field to determine the substitute model's elastic parameters. But we limit ourselves that we can only observe, respectively only use, the displacement field on the surface. However, a comparison between both models in Figs. 5.25 (a) and 5.25 (b) shows that the surface nodes of them are fundamentally different: Firstly, generally the surface nodes of the substitute model and the original model do not coincide. But, it is possible to interpolate the vector value within the original finite element model for the substitute model. Secondly, some surface nodes that exist on the substitute model do not exist on the

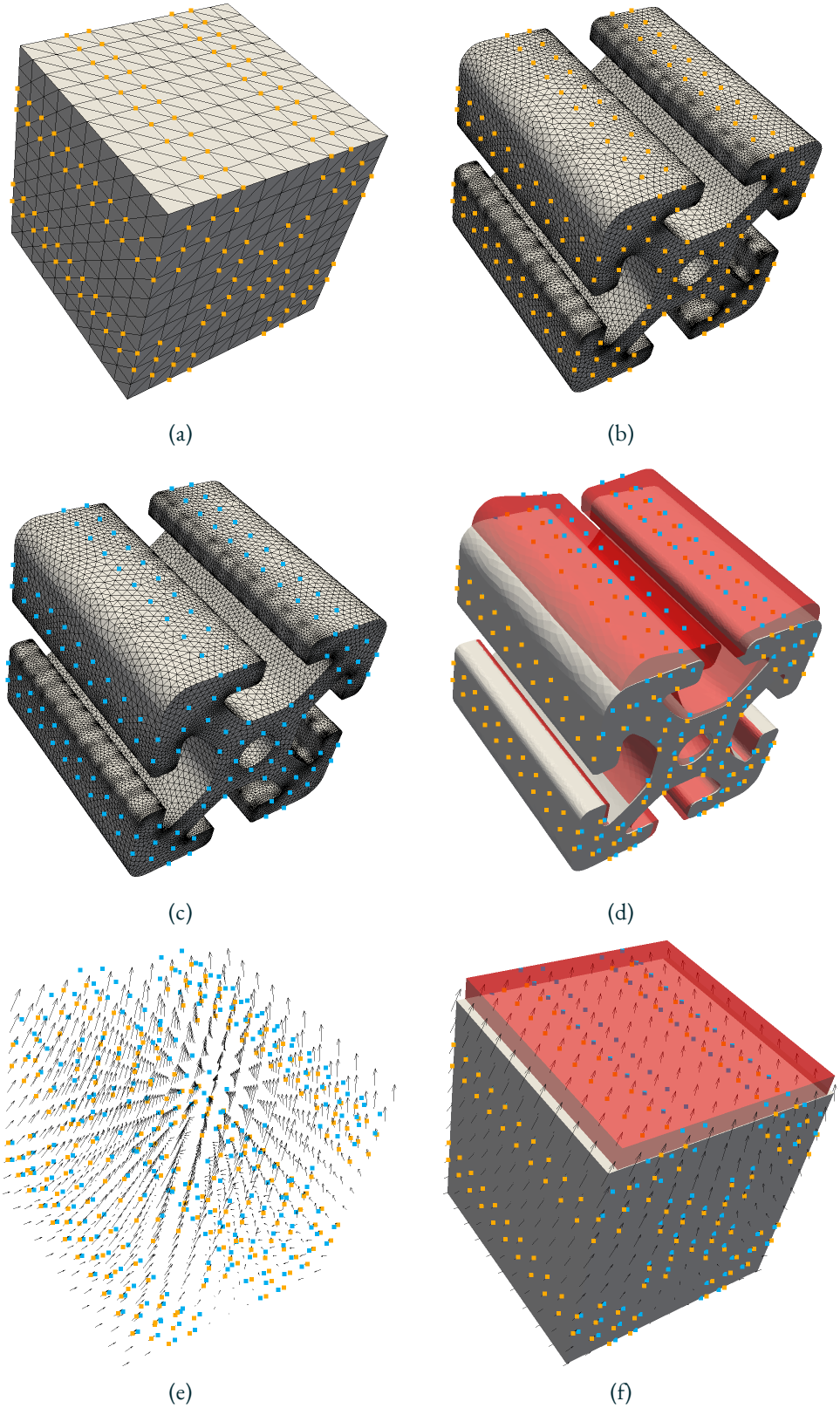


Figure 5.25: (a) Undeformed substitute model; (b) Undeformed original model; (c) Deformed original model; (d) Overlay comparison between the undeformed (grey) and deformed (red transparent) body of the original model; (e) Displacement field; (f) Overlay comparison between the undeformed (grey) and deformed (red transparent) body of the substitute model

original model ("gaps"). In this case, vector values of these surface nodes are treated as additional unknowns. Same goes for the nodes within the body of the substitute model. Thus, the yellow dots in Figs. 5.25 (a) and 5.25 (b) show the surface nodes that exist in the substitute model as well as exist in or are interpolated from the original finite element model. When a predefined force is applied to the original finite element model in Fig. 5.25 (b), the model will be deformed as shown in Fig. 5.25 (c). Accordantly, as shown in Fig. 5.25 (d), the yellow dots in the undeformed state will move to their new destination in the deformed state that are marked as blue dots. The displacement of the nodes from the undeformed to the deformed state (respectively yellow dots to blue dots) yields the displacement field in Fig. 5.25 (e). The aim is to determine the anisotropic linear elastic parameters of the substitute model subjected to the same predefined force, where the substitute model will yield approximately the same displacement field as the original body; see Fig. 5.25 (f).

Under predefined loading set-up, the displacement field $\mathbf{u}$ of a cubic segment of the aluminium profile can be computed by means of the finite element method according to Eq. (5.37) as follows

$$\mathbf{u} = \left(C_{11}\mathbf{K}^{11} + C_{12}\mathbf{K}^{12} + C_{44}\mathbf{K}^{44}\right)^{-1}\mathbf{f} \tag{5.47}$$

where $\mathbf{K}$ is the stiffness matrix that is determined by the complex inner geometry of the aluminium profile segment, the elastic constants C_{11}, C_{12} and C_{44} are computed from the YOUNG's modulus and POISSON's ratio, E and μ, for aluminium and $\mathbf{f}$ is the load vector which is computed from the given external loads.

Anisotropic linear elastic materials can have up to 21 parameters. Therefore, we obtain a system of linear equations from the finite element method for the anisotropic substitute cube as follows

$$\left(\sum_{k=1}^{21} C_k \mathbf{K}^k\right)\mathbf{u}^\star = \mathbf{f}\,, \tag{5.48}$$

where C_k are the elastic parameters and $\mathbf{K}^k$ are the stiffness matrices of the substitute body. The determination of the 21 material constants from displacement field is a non-linear adjustment problem that can be solved with GAUSS-HELMERT Model after linearisation. Aforementioned, non-existing and non-observable nodes have to be treated as additional unknowns. Therefore, some adaptation has to be made in regard to the vector of misclosures $\mathbf{w}$ and the design matrices $\mathbf{A}$ and $\mathbf{B}$ in the adjustment.

Eq. (5.47) is used to compute the "observable" displacement field of the original aluminium segment. Unfortunately, due to the "empty gaps" in the aluminium profile, some displacements are non-existent or are non-observable in point of view of the approximate model. The required but absent part of displacement field becomes additional "virtual" displacement field in the approximate model. In other words, in Eq. (5.48) the "unobservable" displacement field turns into additional unknowns. As a consequence, the vector of unknowns contains the 21 elastic parameters as well as the virtual displacement field. Furthermore, we required that the observable displacement field nodes can be obtained only on the surface of the aluminium beam. The virtual displacement nodes as well as nodes within the aluminium body are considered as unobservable nodes, and they will be estimated based on the observable displacement nodes.

In order to determine the design matrices $\mathbf{A}$ and $\mathbf{B}$, it is necessary to assemble the observed and unobserved stiffness matrices, $\mathbf{K}^k_{\text{obs}}$ and $\mathbf{K}^k_{\text{virtual}}$, based on corresponding columns in the stiffness matrices $\mathbf{K}_k$ in Eq. (5.48). The design matrix $\mathbf{A}$ consists of two parts

$$\mathbf{A} = \begin{bmatrix}\mathbf{A}_\mathbf{C} & \mathbf{A}_\mathbf{u}\end{bmatrix}\,, \tag{5.49}$$

where

$$\mathbf{A}_\mathbf{C} = \begin{bmatrix}\mathbf{K}_1\mathbf{u}^\star & \mathbf{K}_2\mathbf{u}^\star & \dots & \mathbf{K}_{21}\mathbf{u}^\star\end{bmatrix} \tag{5.50}$$

and

$$\mathbf{A}_\mathbf{u} = \sum_{k=1}^{21} C_k \mathbf{K}^k_{\text{virtual}}\,. \tag{5.51}$$

The vector $\mathbf{u}^\star$ contains the virtual displacement $\mathbf{u}_{\text{virtual}}$ as well as observable displacement plus their corresponding residuals, $\mathbf{u}_{\text{obs}} + \mathbf{v}$. The matrix $\mathbf{B}$ is computed as

$$\mathbf{B} = \sum_{k=1}^{21} C_k \mathbf{K}^k_{\text{obs}}\,. \tag{5.52}$$

The vector of misclosures reads

$$\mathbf{w} = -\mathbf{B}\mathbf{v} + \left(\sum_{k=1}^{21} C_k \mathbf{K}^k\right)\mathbf{u}^\star - \mathbf{f}\,. \tag{5.53}$$

Anisotropic linear elastic materials can have up to 21 parameters. Due to symmetric considerations of the cubic segment of the aluminium profile, it is possible to reduce the number of elastic parameters to six parameters and therefore the HOOKE's law in Voigt's matrix notation becomes

$$\begin{bmatrix}\sigma_{11}\\ \sigma_{22}\\ \sigma_{33}\\ \sigma_{23}\\ \sigma_{13}\\ \sigma_{12}\end{bmatrix} = \begin{bmatrix} ① & ⑤ & ⑥ & & & \\ & ① & ⑥ & & & \\ & & ② & & & \\ & & & ③ & & \\ & & & & ③ & \\ \text{symmetrical} & & & & & ④ \end{bmatrix} \begin{bmatrix}\varepsilon_{11}\\ \varepsilon_{22}\\ \varepsilon_{33}\\ 2\varepsilon_{23}\\ 2\varepsilon_{13}\\ 2\varepsilon_{12}\end{bmatrix} \tag{5.54}$$

The above six parameters are determined by the simultaneous evaluation of seven different displacement fields. Figs. 5.26 to 5.32 show that these seven displacement fields were obtained by seven independent experiments. In Figs. 5.26 to 5.28, three (inverted) compression testings were performed in order to determine how a sample changes in response to an external load. A compression test is depicted in FLÜGGE (1975, p. 171). A cubic segment of the original aluminium profile is inserted in a rigid die. One surface of the sample is loaded by external force while the other five sample sides are fixed due to the undeformable virtual die. This test set-up causes the induced normal stress to change solely its associated normal strain. The other strain components vanish. For example, when normal stress σ_{11} is induced in Fig. 5.26, only the normal strain ε_{11} results. Therefore, the elastic modulus ① in Eq. (5.54) can be computed as the ratio of normal stress and normal strain $① = \frac{\sigma_{11}}{\varepsilon_{11}}$. The same goes for the cases of σ_{22} and ε_{22} for modulus ①, and σ_{33} and ε_{33} for modulus ②. In this approximation, "inverted" compression tests were performed. The specimen is pulled instead of compressed. Other than that, the boundary conditions remains the same. In Figs. 5.29 to 5.31, three simple shear testings were conducted. One expects that, when a sample is sheared, the surface subjected to the shear force subsides perpendicular to the shear force direction. However, this is not the case for this test, since this results in a shear strain as well as an unwanted normal strain. A simple shear test prevent during the shear test the formation of normal strain in a sample through an appropriate set-up, see for example Fig. 5.31. The simple shear simulation set-up is implemented through suitable boundary conditions. This in turn enables us to determine the elastic parameters ③ or ④. Finally, in Fig. 5.32, an uniaxial tensile testing is carried out. This allows us to compute the elastic modulus ①, ②, ⑤ and ⑥. The adjusted elastic parameter yields

$$\mathbf{C} = \begin{bmatrix} 12.951 & 10.575 & 7.012 & & & \\ 10.575 & 12.951 & 7.012 & & & \\ 7.012 & 7.012 & 47.107 & & & \\ & & & 10.210 & & \\ & & & & 10.210 & \\ & & & & & 6.129 \end{bmatrix} \text{GPa}\,. \tag{5.55}$$

In order to verify the computed six parameters in Eq. (5.55) for the substitute model, in Fig. 5.33 a comparison were made between an original aluminium profile beam (grey) and a beam made out of the anisotropic material (red, transparent) with the adjusted parameters. Both beams have the same length, either $l = 1520\,\text{mm}$ (Fig. 5.34) or $l = 700\,\text{mm}$ (Fig. 5.35). Three different forces are applied: $F = 50\,\text{N}$ (blue), $F = 500\,\text{N}$ (yellow) and $F = 5000\,\text{N}$ (red). Three different test set-ups are used: Three-point bending test, one and double-sided cantilever test. Thus, in total 18 tests were performed. In each test, the maximum deflection values of the substitute $\max|\mathbf{u}_{\text{subs}}|$ and the original beam $\max|\mathbf{u}_{\text{orig}}|$ are evaluated by means of the relative error that is defined as follows

$$e_{\text{rel}} = \frac{\max|\mathbf{u}_{\text{subs}}| - \max|\mathbf{u}_{\text{orig}}|}{\max|\mathbf{u}_{\text{orig}}|} 100\,\%\,. \tag{5.56}$$

The relative error e_{rel} are shown in Figs. 5.34 and 5.35. More detailed results are listed in Tab. 5.6. One can observe that for all cases, except for one case, the relative errors e_{rel} are less than one percent. The relative error for that one case is around $2.7\,\%$. Since a linear elastostatic model was implemented, the different amount of the forces

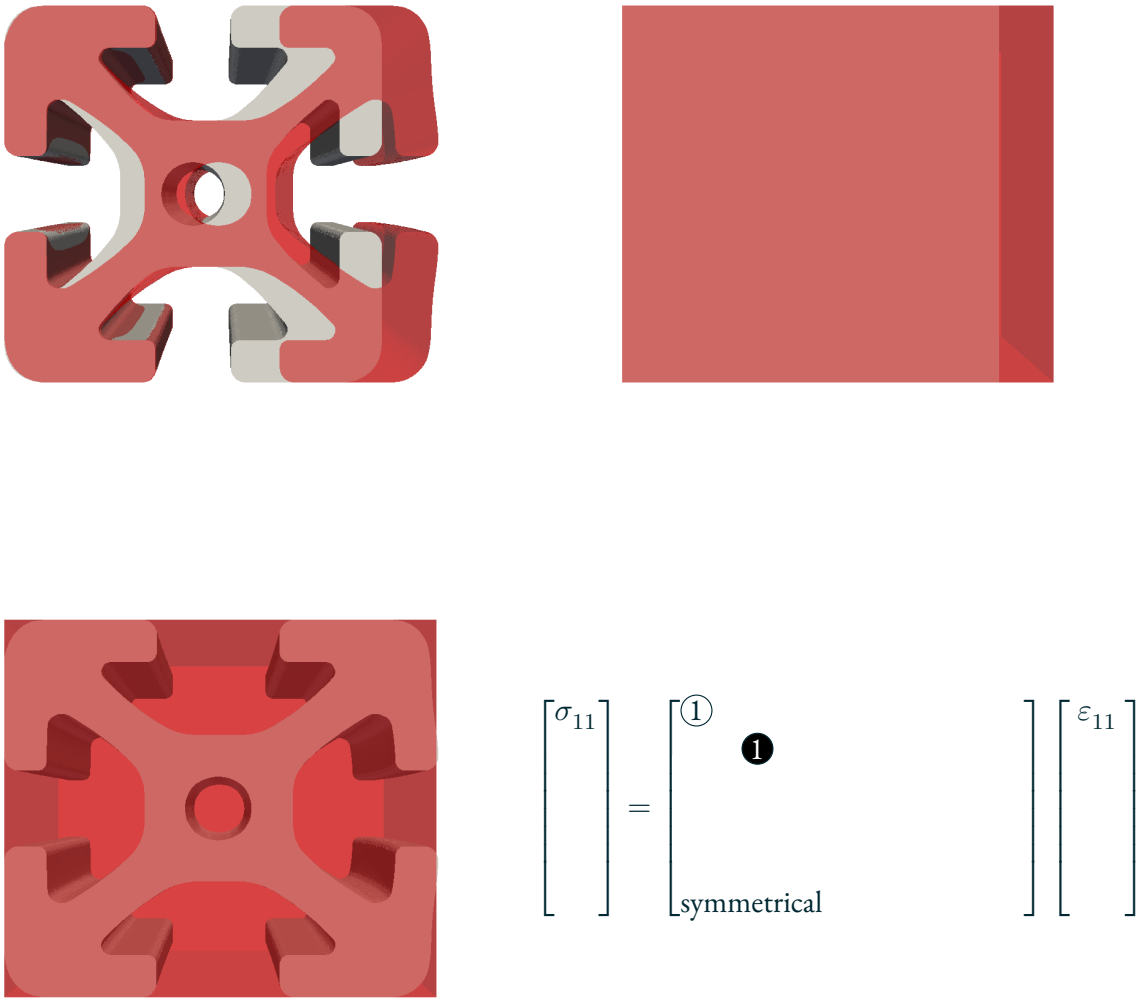


Figure 5.26: An "inverted" compression test in x_1-axis direction on the surface normal in x_1-axis direction; *top left* A normal stress σ_{11} is applied to the original sample; *top right* A normal stress σ_{11} is applied to the substitute sample; *bottom left* An overlay comparison between the original and substitute samples in a deformed state; *bottom right* Parameter ① and also due to symmetry considerations parameter ❶ can be determined in this test

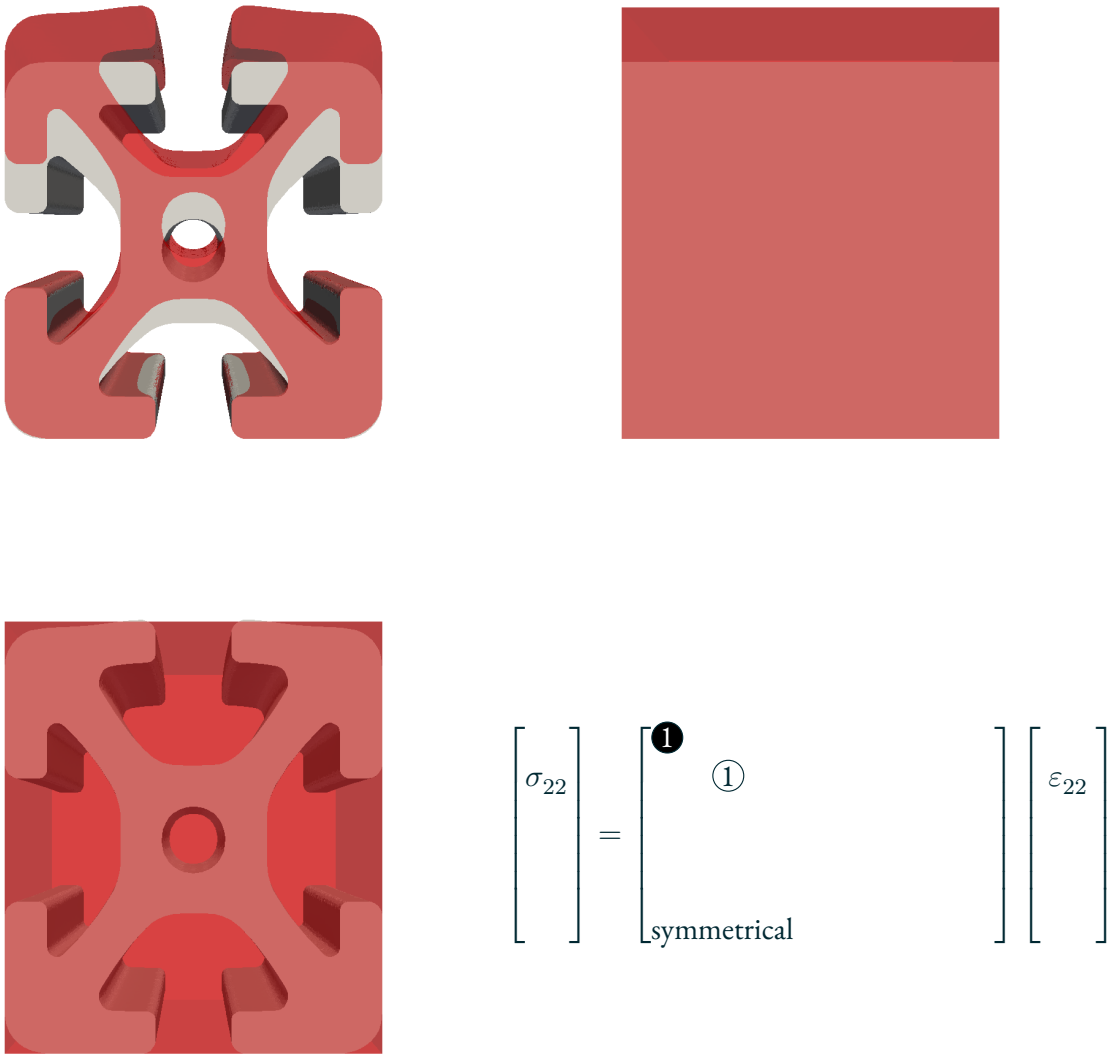


Figure 5.27: An "inverted" compression test in x_2-axis direction on the surface normal in x_2-axis direction; *top left* A normal stress σ_{22} is applied to the original sample; *top right* A normal stress σ_{22} is applied to the substitute sample; *bottom left* An overlay comparison between the original and substitute samples in a deformed state; *bottom right* Parameter ① and also due to symmetry considerations parameter ❶ can be determined in this test

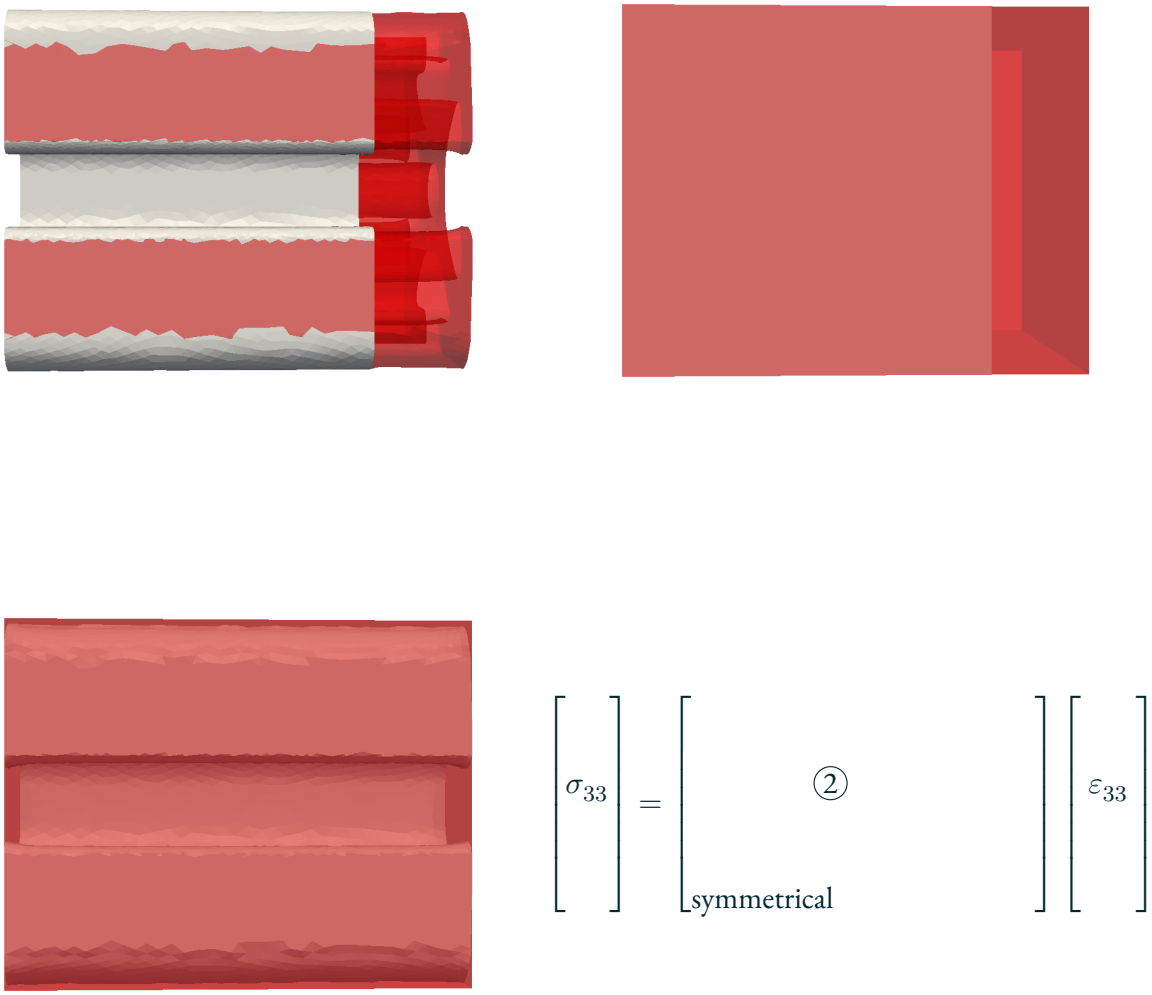


Figure 5.28: An "inverted" compression test in x_3-axis direction on the surface normal in x_3-axis direction; *top left* A normal stress σ_{33} is applied to the original sample; *top right* A normal stress σ_{33} is applied to the substitute sample; *bottom left* An overlay comparison between the original and substitute samples in a deformed state; *bottom right* Parameter ② can be determined in this test

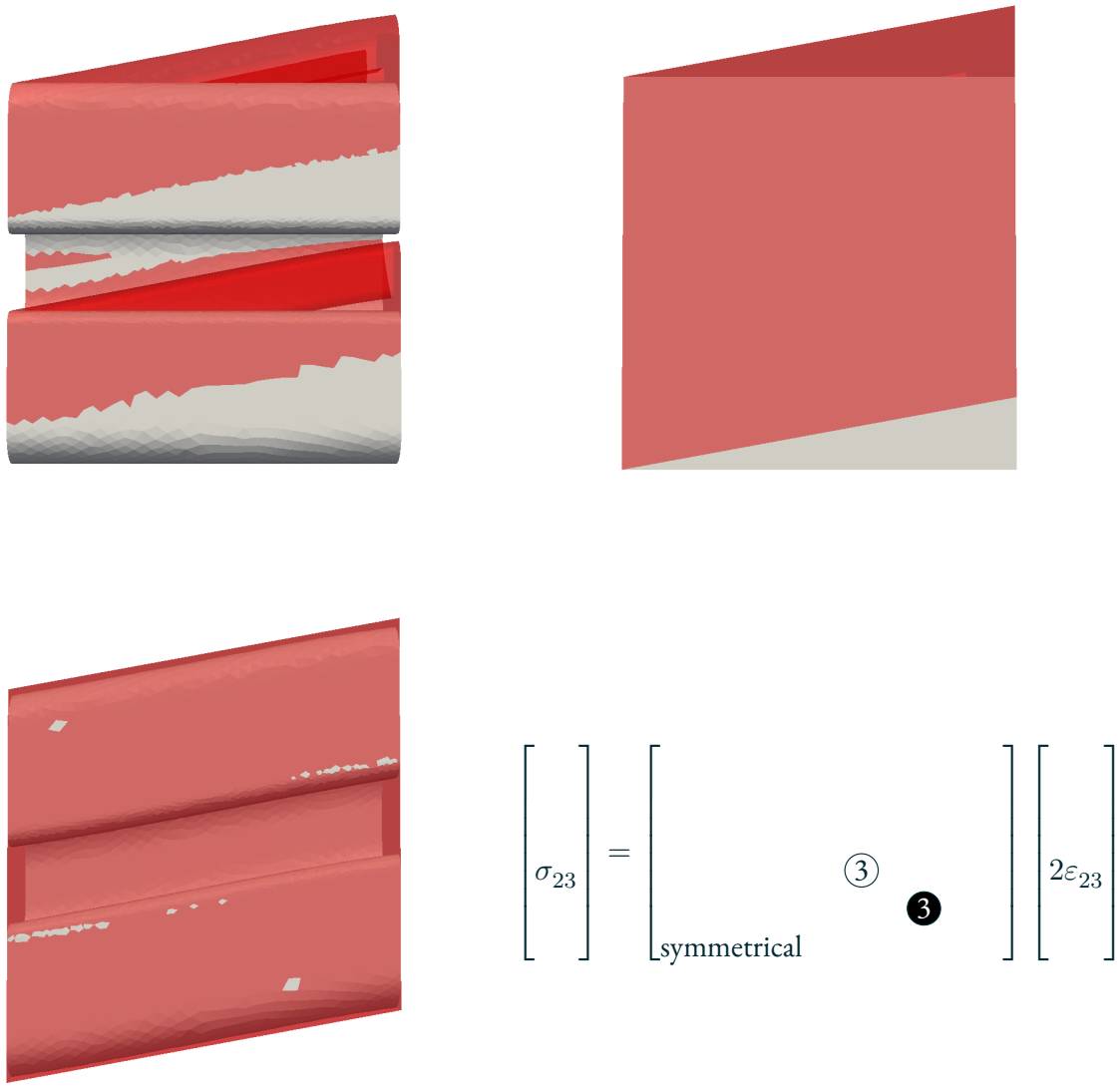


Figure 5.29: A simple shear test in x_2-axis direction on the surface normal in x_3-axis direction; *top left* A shear stress σ_{23} is applied to the original sample; *top right* A shear stress σ_{23} is applied to the substitute sample; *bottom left* An overlay comparison between the original and substitute samples in a deformed state; *bottom right* Parameter ③ and also due to symmetry considerations parameter ❸ can be determined in this test

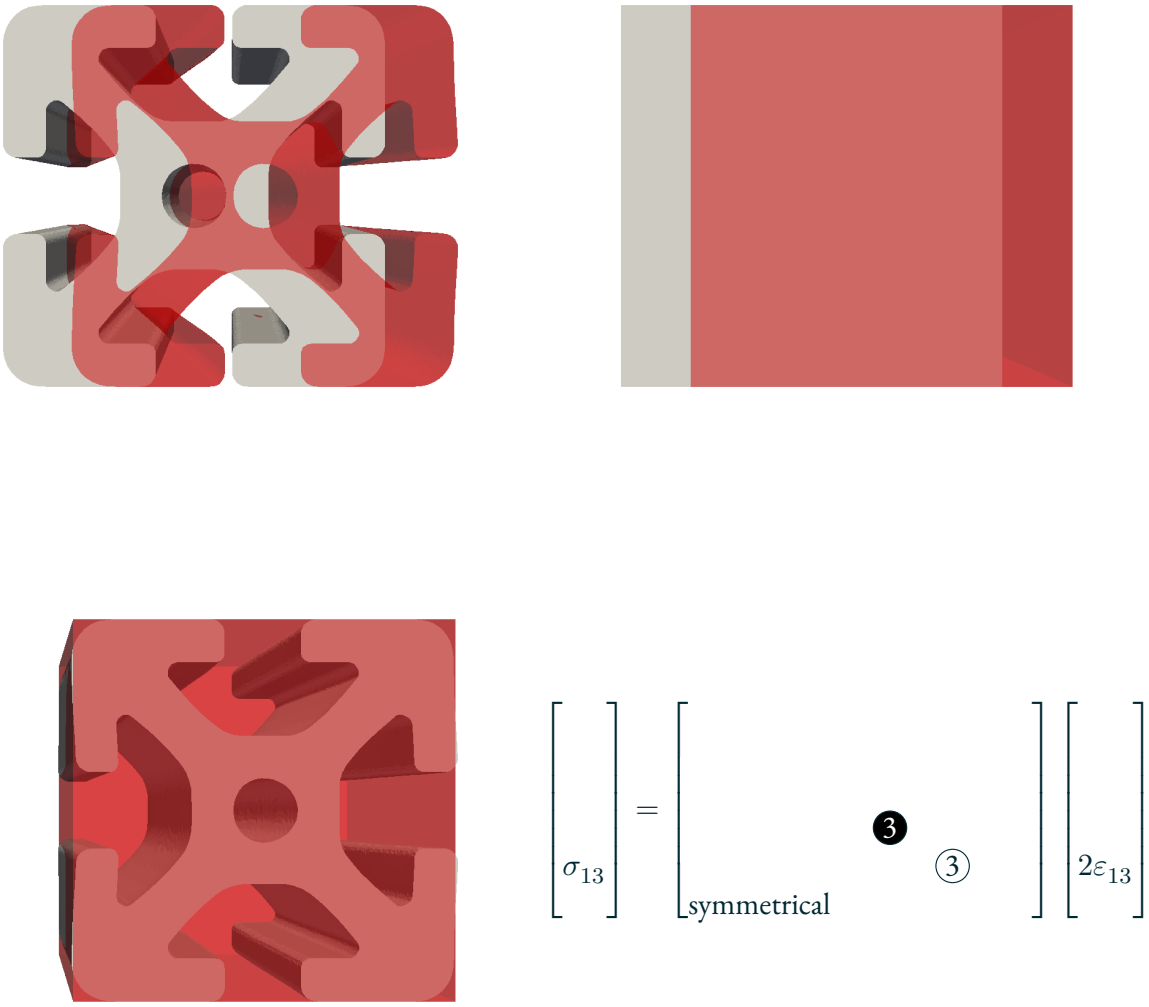


Figure 5.30: A simple shear test in x_1-axis direction on the surface normal in x_3-axis direction; *top left* A shear stress σ_{13} is applied to the original sample; *top right* A shear stress σ_{13} is applied to the substitute sample; *bottom left* An overlay comparison between the original and substitute samples in a deformed state; *bottom right* Parameter ③ and also due to symmetry considerations parameter ❸ can be determined in this test

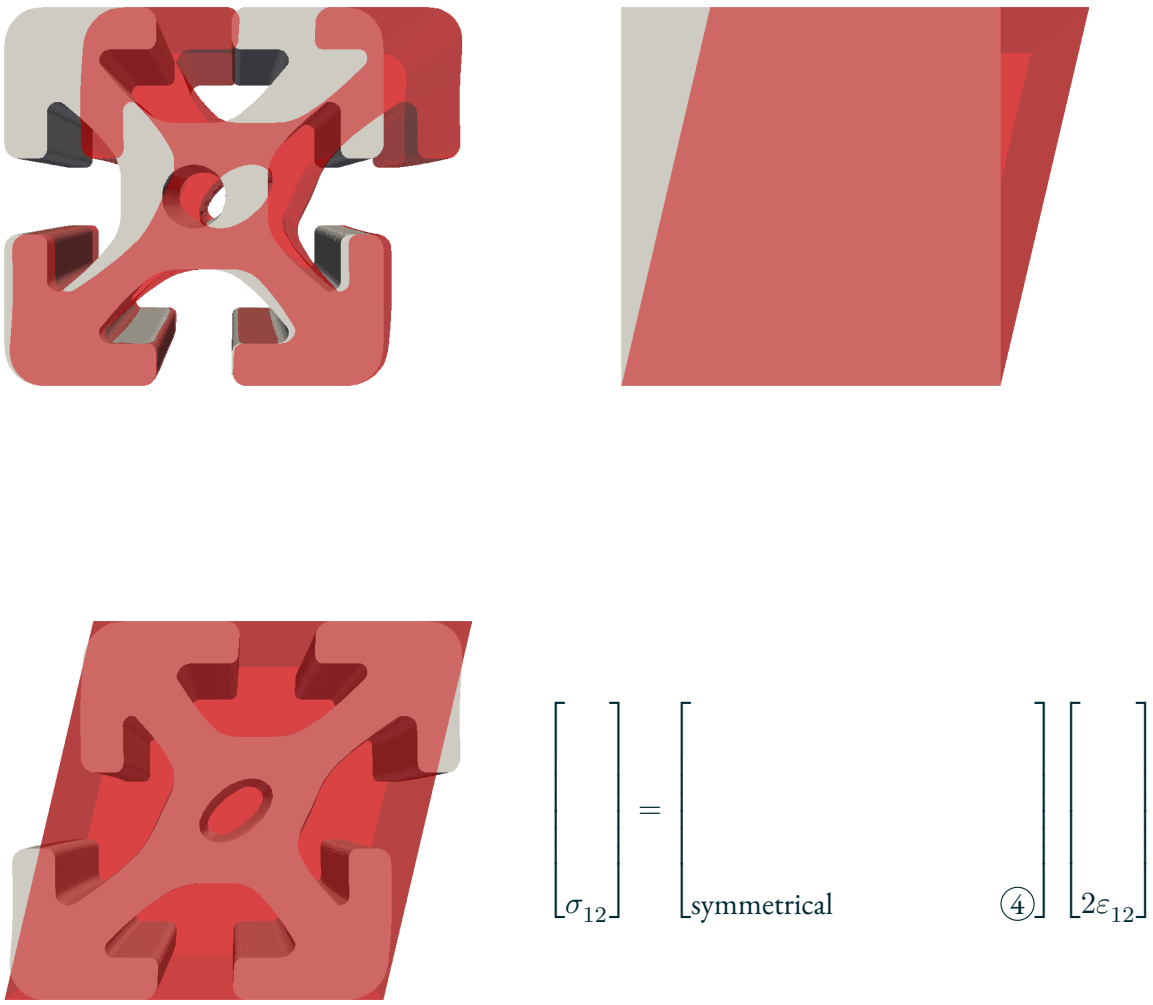


Figure 5.31: A simple shear test in x_1-axis direction on the surface normal in x_2-axis direction; *top left* A shear stress σ_{12} is applied to the original sample; *top right* A shear stress σ_{12} is applied to the substitute sample; *bottom left* An overlay comparison between the original and substitute samples in a deformed state; *bottom right* Parameter ④ can be determined in this test

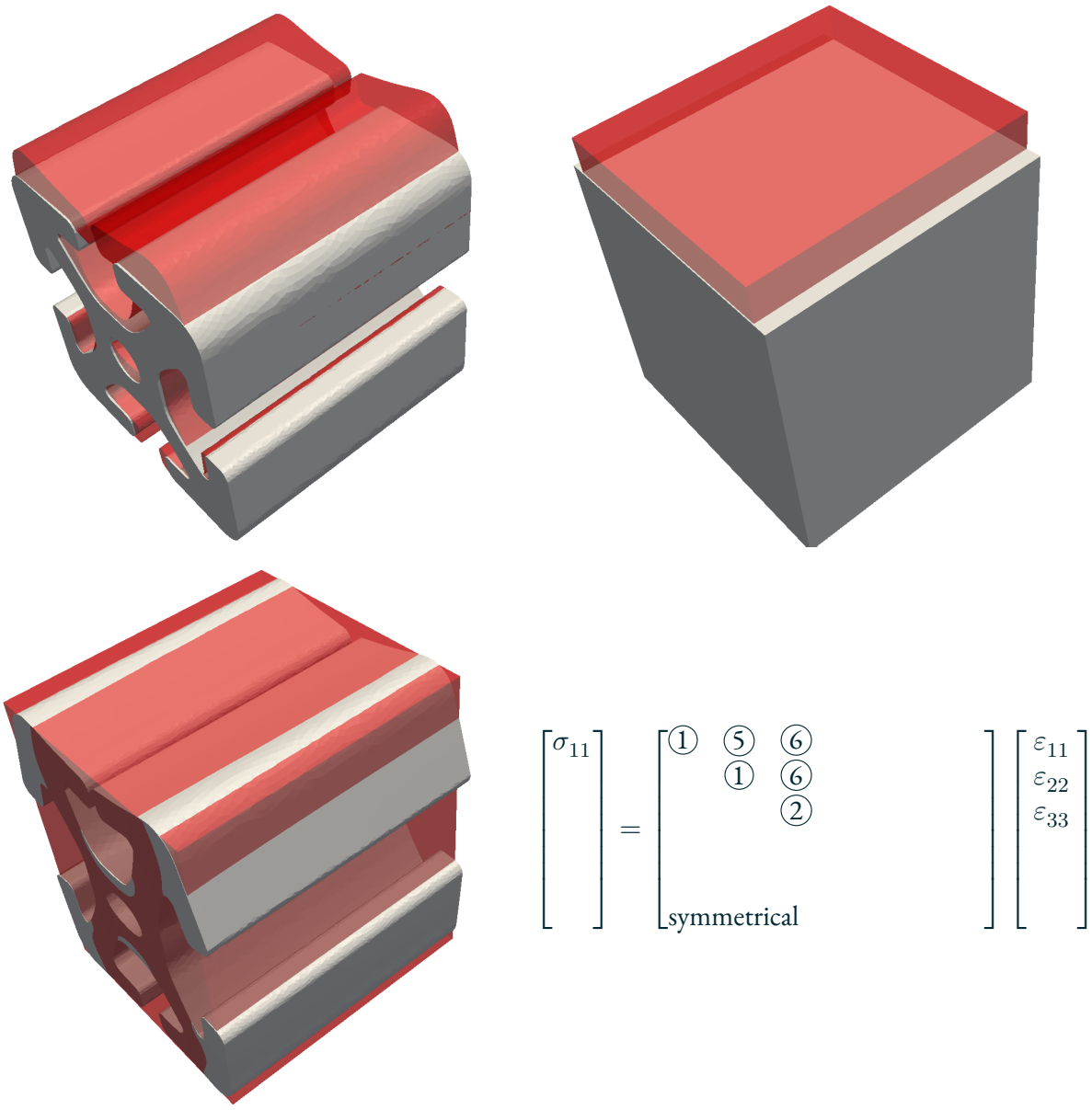


Figure 5.32: An uniaxial tensile test in x_1-axis direction on the surface normal in x_1-axis direction; *top left* A normal stress σ_{11} is applied to the original sample; *top right* A normal stress σ_{11} is applied to the substitute sample; *bottom left* An overlay comparison between the original and substitute samples in a deformed state; *bottom right* Parameters ①, ②, ⑤ and ⑥ can be determined in this test

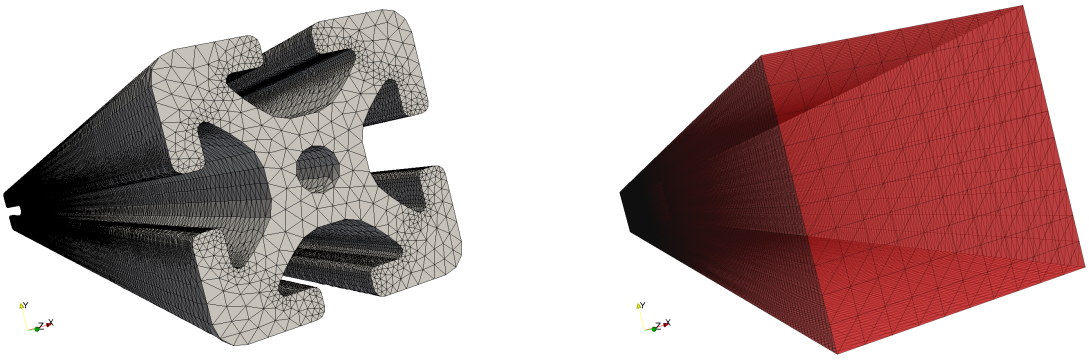
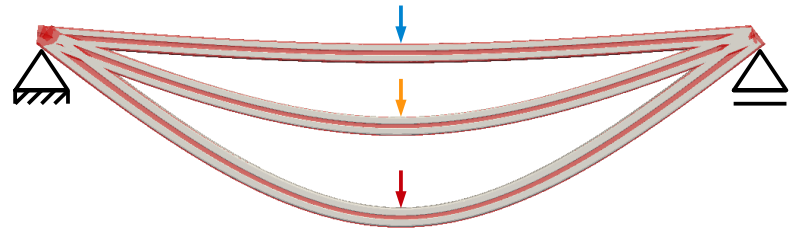
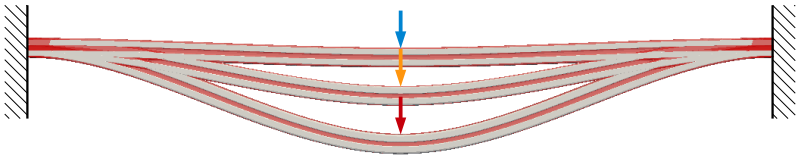


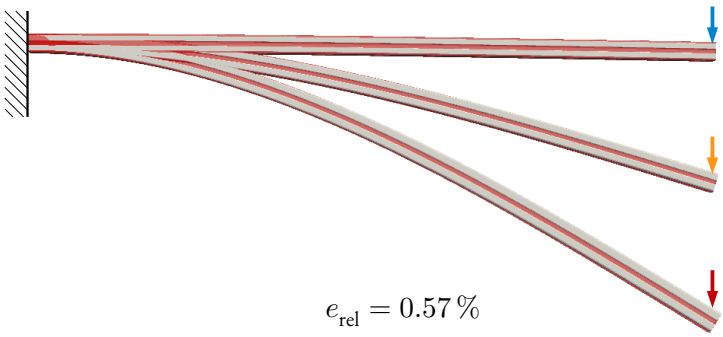
Figure 5.33: For the verification of the adjusted elastic parameters, a comparison between a original aluminium beam with a substitute beam is being made



$e_{\text{rel}} = 0.33\,\%$



$e_{\text{rel}} = 0.25\,\%$



$e_{\text{rel}} = 0.57\,\%$

Figure 5.34: Overlay comparison between original aluminium (grey) beam and substitute beam (red, transparent); length of the beams: 1520 mm; Three test set-ups: *top* Three-point bending test, *middle* one sided cantilever test and *bottom* double sided cantilever test; Three different forces: 50 N (blue), 500 N (yellow) and 5000 N (red)

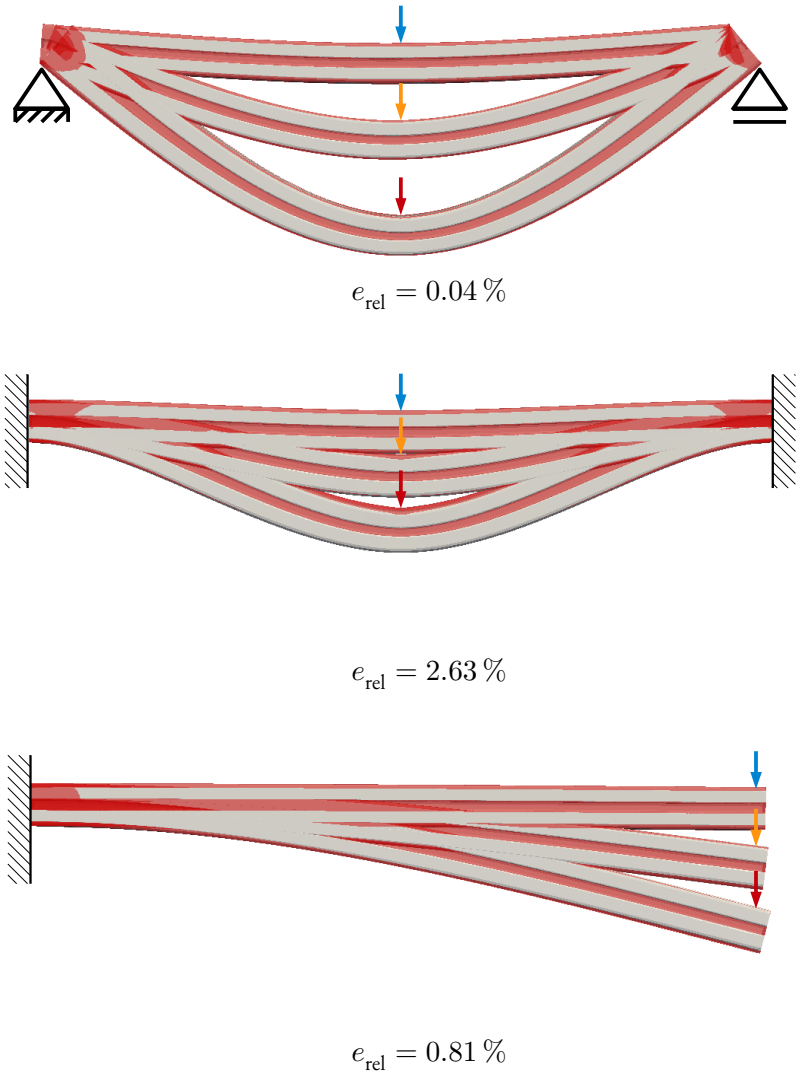


Figure 5.35: Overlay comparison between original aluminium (grey) beam and substitute beam (red, transparent); length of the beams: 700 mm; Three test set-ups: *top* Three-point bending test, *middle* one sided cantilever test and *bottom* double sided cantilever test; Three different forces: 50 N (blue), 500 N (yellow) and 5000 N (red)

Table 5.6: Results of original and substitute beams that are subjected to three-point bending tests (TP), double sided cantilever tests (DC) and single sided cantilever tests (SC) and the total computational time (TCT)

	Forces $[\mathrm{N}]$	$\max \lvert\mathbf{u}_{\mathrm{subs}}\rvert\ [\mathrm{mm}]$	$\max \lvert\mathbf{u}_{\mathrm{orig}}\rvert\ [\mathrm{mm}]$	$e_{\mathrm{rel}}\ [\%]$
		beam length $l = 1520\,\mathrm{mm}$		
TP	50	0.3894	0.3881	0.3319
	500	3.894	3.881	0.3319
	5000	38.94	38.81	0.3319
DC	50	0.098 26	0.098 51	0.2524
	500	0.9826	0.9851	0.2524
	5000	9.826	9.851	0.2524
SC	50	6.181	6.146	0.5667
	500	61.81	61.46	0.5667
	5000	618.1	614.6	0.5667
TCT $[\mathrm{s}]$		75	11246	
		beam length $l = 700\,\mathrm{mm}$		
TP	50	0.039 09	0.039 07	0.0438
	500	0.3909	0.3907	0.0438
	5000	3.909	3.907	0.0438
DC	50	0.010 29	0.010 57	2.6324
	500	0.1029	0.1057	2.6324
	5000	1.029	1.057	2.6324
SC	50	0.606 41	0.6015	0.8137
	500	6.0641	6.015	0.8137
	5000	60.641	60.15	0.8137
TCT $[\mathrm{s}]$		67	3878	

that are applied to the beams are irrelevant for relative error. The linearity elasticity assured that the ratio of the applied force and the displacement is always constant, e. g., double amount of applied forces yields double amount of displacement. This homogenisation process accelerates the computational time and cuts down the memory usage immensely. In the presented case, finite element simulations for the original beam took roughly in total 4 hours and 12 minutes (11 246 s + 3878 s), while for substitute beam it was just in total two-and-a-half minutes (75 s + 67 s). Nevertheless, "*all that glitters is not gold*", there are some disadvantages accompanying this approach. Firstly, a lot of considerations has to be made in order to figure out the "right" experiments. In our case, it was seven independent experiments: three compression testings, three shear testings and one uniaxial tensile testing. When other thinkable testing set-ups are added to the evaluation, they distorted the set of parameters and led to wrong verification results. For example, in a simple shear test, applying a shear stress σ_{32} on to the original aluminium beam segment leads to a deformation that is different from when applying a shear stress σ_{23}. In point of view of the substitute model the original body in general behaves non-linear. It is therefore impossible to mimic non-linear behaviour in linear elastostatic model even all 21 constants are used in order to fit this task. In order to induce approximately linear behaviour, one has to apply as little as possible amount of forces during the experiments. Furthermore, test set-ups that induce non-linear behaviour has to be discarded. Secondly, the finite element mesh composition of the substitute body is able to influence the adjustment of the parameters, especially the elastic parameter ⑤ and ⑥. When the mesh formation is changed, we obtained another set of parameter. Thus, the adjusted set of elastic parameters are only valid for a specific pre-defined mesh arrangement. Lastly, the Gauss-Helmert Model is more general than the Gauss-Markov Model. But, from a numerical point of view the Gauss-Markov Model is more numerically stable than Gauss-Helmert Model when it comes to dealing with inverting large matrices. It is therefore desirable to reformulate this class of problem that is suitable for an Gauss-Markov Model approach.

5.6 A Small Scale Test Bridge for Measurement- and Model-based Structural Analysis

In order to further examine the capability of Measurement- and Model-based Structural Analysis to detect and locate damage on complex structures, a small-scale truss bridge model (1520 mm × 720 mm × 720 mm) made of aluminium profiles is built as a test specimen for this purpose. This test bridge is named *Variationsbrücke*. As the two numerical preliminary examinations in Secs. 5.4 and 5.5 show, the determination of the material parameters of linear-elastic bodies is naturally related to the displacement field measurement by the elastostatic equation in Eq. (2.162). To what extent the inclination and strain field measurements can be considered in the elastostatic equation is tricky to answer. First, it would be necessary to determine how inclination and strain variables are expressed in the elastostatic equation as in Sec. 5.1.2. Then, a special non-linear finite element has to be developed based on this identification similar to Sec. 2.6.9. Afterwards, it can be answered to what extent which advantages can be achieved with hybrid measurements. However, this would go beyond the scope of this dissertation. Therefore, only the displacement field measurement with linear finite element is considered, since the emphasis lies in the complex geometric modelling.

Specimen structure and experimental set-up

The truss frame of the test bridge is made of aluminium profiles with a sophisticated design of the cross-sectional area. In comparison, with solid profiles, only a fraction of the material is needed to produce the profiles, while their bending resistance decreases slightly. The truss frame of the test bridge is made of aluminium profiles with a sophisticated design of the cross-sectional area. In comparison, with solid profiles, only a fraction of the material is needed to produce the profiles, while their bending resistance decreases slightly. The profiles are built into a truss frame by connecting them by means of fastening sets made of steel. The bridge model is mounted on four steel bearings which each of them consist of a cylinder arranged between two plates. Fixed bearings are made by holding onto one end of the bridge. The bridge is subjected by an external load by placing a heavy object beneath it. At the same time, measurements can be conducted below the bridge. Therefore, the bridge specimen is elevated by attaching it on a pedestal with four columns. Damages can be induced by loosening the fastening pieces. The set-up is shown in Fig. 5.36.



Figure 5.36: The bridge specimen on the pedestal, approximately 2147.6 N was applied

Available measurement equipments

Terrestrial laser scanning records the distances and measurement orientations of any points of an area or of an object of interest from a fixed observation point. The observable space is a truncated sphere. The recorded data contains the coordinates of the measured points which form a so-called point cloud. Point clouds of different observation points can be assembled using a certain algorithm to reconstruct the discrete surface information of an object of interest. Then, this data can be processed further for a solid modelling. From here, a finite element discretisation can be carried out for the reference state of an object of interest.

Photogrammetry is applied to take measurements from photographs. The absolute positions of surface markers on an object of interest in each photo are determined. The evaluation of photos taken from two different states results the displacement of markers, i.e. the position change of a specific marker between the reference and current states.

Load cell is used to measure force. When a force is applied on a load cell, certain structures within the cell deform. And this deformation is captured by strain gauges. The force can in turn be determined by the calibrated strain gauges.

Capturing the reference state geometry

A real object and its computer aided design model can differ in size. Therefore, it is desired to measure the object rather than to trust the technical drawings. One possibility to capture the dimension of an object of interest is using terrestrial laser scanning to scan it. The main problem is how to convert the data points from laser scanner in such a way that it can be used in a finite element simulation. Although success is not always guaranteed, a practical procedure is presented as follows. After the scans are performed and the point clouds of the object are registered, a discrete surface representation of the object in form as a point cloud is obtained. From this data points, a computer aided design model is generated. And this solid model can be further processed in a finite element mesh generator.

The aluminium bridge specimen had to be pre-treated with an anti-reflective spray in order to be scanned by the terrestrial laser scanner. In addition, the grooves of the aluminium profiles had to be covered with a thin film because the laser beam is obstructed when it reaches the areas around the grooves. At ten different positions, the laser scans were performed. The post-processing of the point clouds was done by commercial software. It converts the complete scan of the object into a file format which could be further processed by an automatic tetrahedral mesh generator for the finite element evaluation.

Because the scan quality was unfortunately unsatisfactory for further processing, (see Fig. 5.37), it was decided to use the computer aided design model instead. They are several reasons why the terrestrial laser scanning lost its scan quality. Terrestrial laser scanning is usually applied for objects that are much larger than the bridge model specimen. In addition, it was scanned in a confined space in close proximity to the specimen object, since large room was not available at that time. Another aspect was that due to the cramped room not all areas of the bridge could be recorded. The missing areas was artificially fixed in a post-processing.

Measurement of displacements

Round target stickers applied on surface of the bridge specimen were used to track local displacements. By means of a commercial photogrammetry system (GOM Correlate), many photos of the bridge specimen can be taken from different viewing points and angles. And in a post-processing procedure, the coordinates of the markers were determined. The positions of the marker points were determined for different load and damage states of the bridge model.

The experiment was conducted for five different states: (1) Undamaged and unloaded, (2) undamaged and loaded, (3) damage level 1 and loaded, (4) damage level 2 and loaded, (5) damage level 3 and loaded. The different stages are shown in Fig. 5.37. In the first damage level three screws are loosened as indicated by the red spheres. In the second stage, three additional screws are released in addition to the first one (red and yellow spheres). In damage level 3, in total ten screws are removed. (red, yellow and blue spheres). In Fig. 5.38 shows the first damage stage as an example. The displacements of the bridge specimen are determined with respect to the undamaged and unloaded state (1).

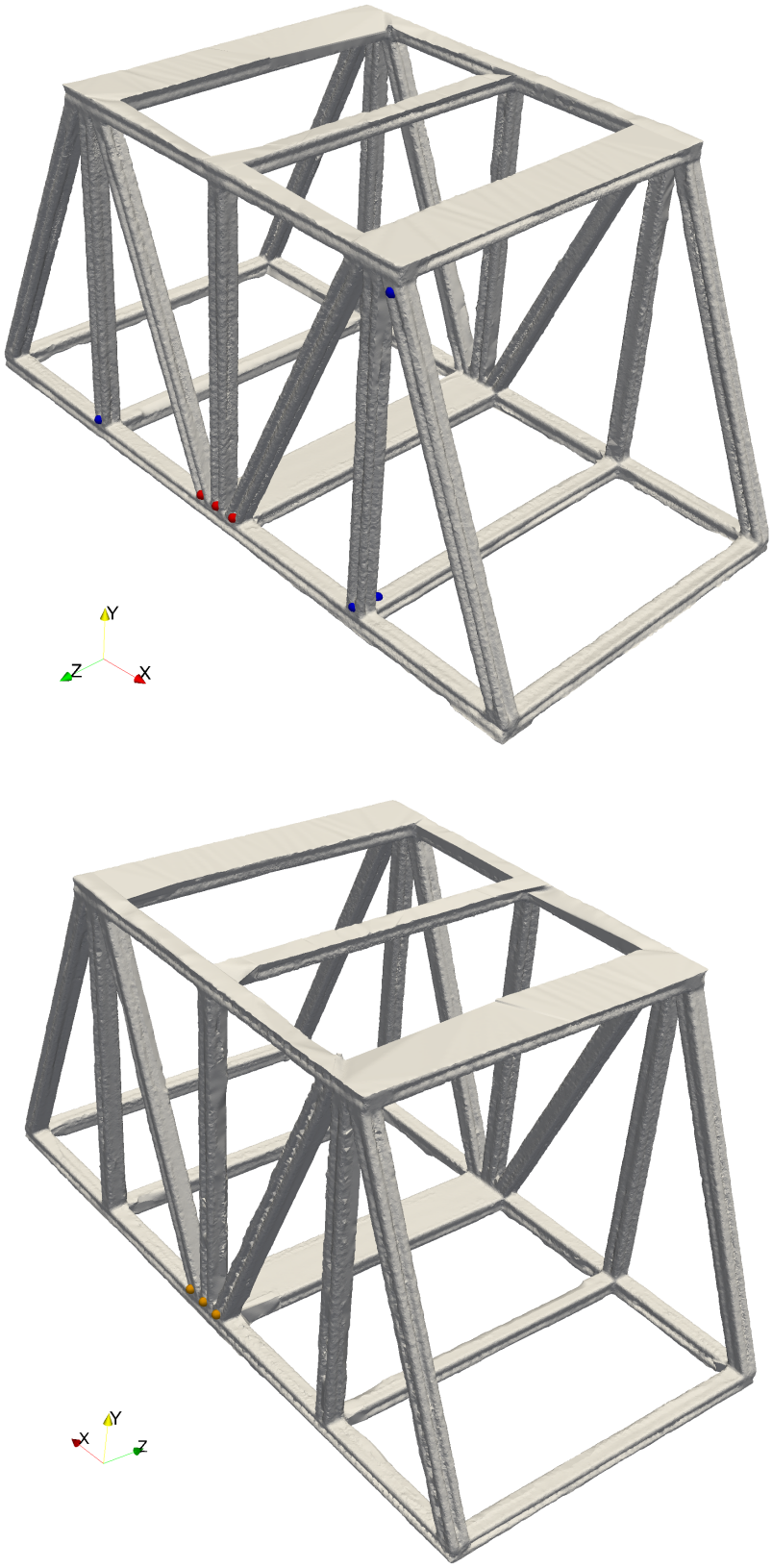


Figure 5.37: Terrestrial laser scanning of the bridge model, the coloured spheres indicate where screws are loosened to cause damage, damage level 1: red spheres, damage level 2: red and yellow spheres, damage level 3: red, yellow and blue spheres

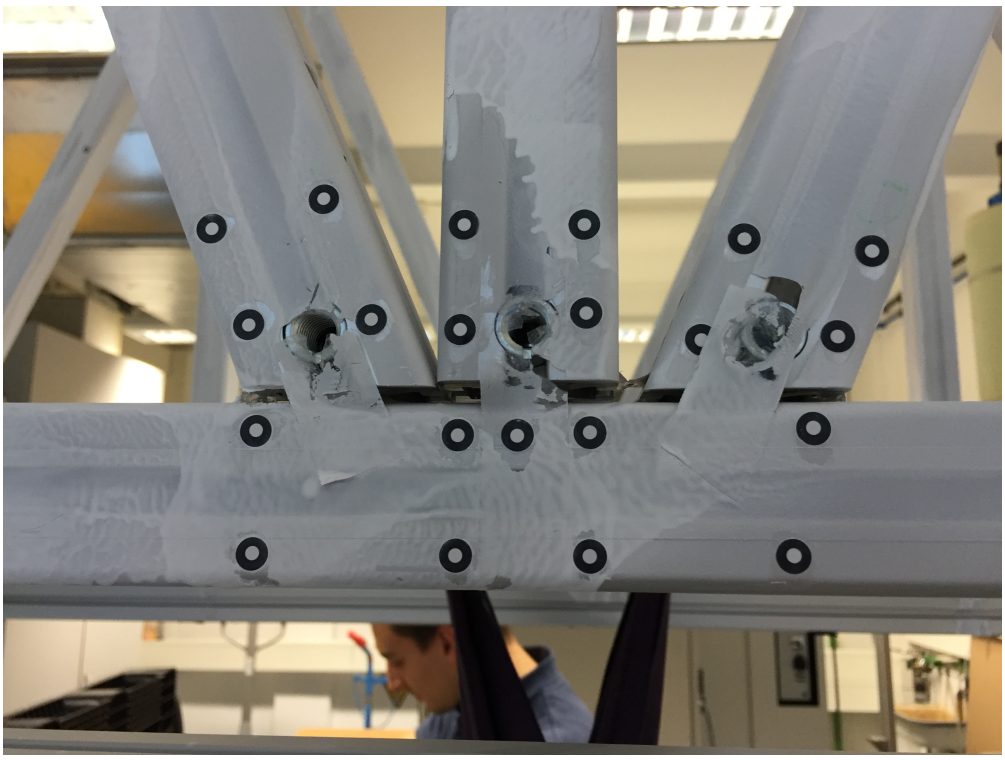


Figure 5.38: Screws are released to induce artificial damages to the bridge model

In addition, marker stickers were also applied to the pedestal. Since the targets are fixed on the pedestal during the entire experiment, the standard deviation of the displacement observations can be determined from this.

Calibration of the reference state

The approximate substitute model from Sec. 5.5 is used to describe the aluminium profiles of the bridge specimen since a finite element discretisation of the complete body would be infeasible. These aluminium profiles are longitudinal objects with a very detailed cross section. This requires a finite element discretisation with impracticable element quantity. This in turn requires large amounts of computer memory that is not available. The connection parts are not further examined and are therefore ignored. Consequently, the bridge specimen is fully characterised by six material constants. The aluminium profiles are designed in such a way that the main load is distributed best along the x_1-axis direction. This is also noticeable that material constant ② has the largest value in comparison with other material parameters. For that reason, it is assumed that changes or damages in the bridge specimen has the great impact on parameter ②. As mentioned above, truss-like or bridge-like structures is designed in such a way that they are subjected to specific loads. Other loading modes never occur in practice or are difficult realise, thus it is impossible to determine the remaining material constants ①, ③, ④, ⑤, ⑥. These parameters are considered to be fixed and are given in Eq. (5.55). For the reference state of the bridge model, the six unknown material parameters and their stochastic properties are determined from the displacements from state (1) to (2).

Direction dependence of the stiffness tensor

As shown in Fig. 5.39, the bridge specimen consists of aluminium profiles with five different types of spatial orientation. The various kinds of profiles are marked accordingly with 1000, 2000, 3000, 4000, 5000. The steel plates are marked with 0. Thus, the stiffness tensor has to be rotated accordantly for each type of the aluminium profiles. Rotation matrices for the x_1-, x_2- and x_3-axis reads

$$\mathbf{R}_1 = \begin{bmatrix} 1 & 0 & 0 \\ 0 & \cos(\theta_1) & \sin(\theta_1) \\ 0 & -\sin(\theta_1) & \cos(\theta_1) \end{bmatrix}, \tag{5.57}$$

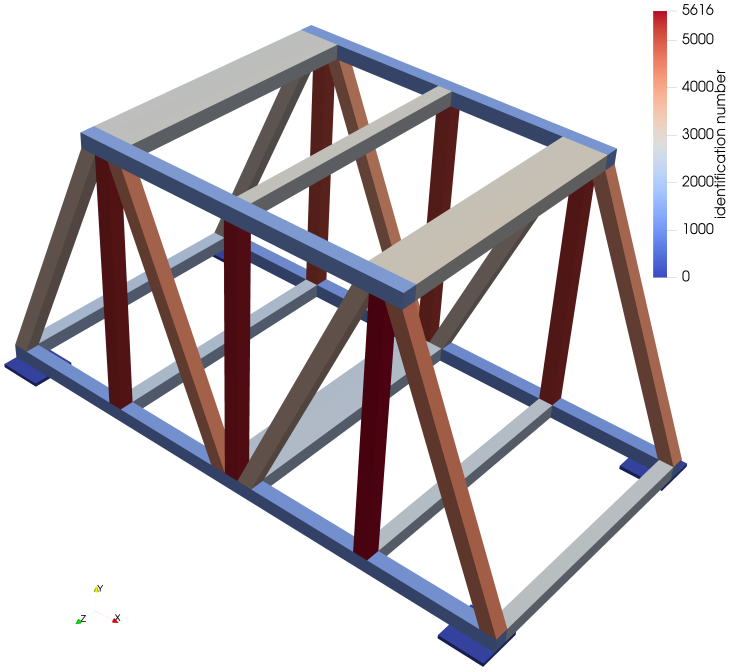


Figure 5.39: The stiffness tensor has to be rotated in accordance to the different spatial orientations of the profiles

$$\mathbf{R}_2 = \begin{bmatrix} \cos(\theta_2) & 0 & -\sin(\theta_2) \\ 0 & 1 & 0 \\ \sin(\theta_2) & 0 & \cos(\theta_2) \end{bmatrix} , \tag{5.58}$$

$$\mathbf{R}_3 = \begin{bmatrix} \cos(\theta_3) & \sin(\theta_3) & 0 \\ -\sin(\theta_3) & \cos(\theta_3) & 0 \\ 0 & 0 & 1 \end{bmatrix} . \tag{5.59}$$

It should be noted that the above rotation matrices are used to rotate the observer coordinate system inherent in the stiffness tensor. Accordingly, attention must be paid to the signs before sinus functions. Consequently, the rotation matrix is

$$\mathbf{R} = \mathbf{R}_3 \mathbf{R}_2 \mathbf{R}_1 . \tag{5.60}$$

The stiffness tensor in Eq. (2.136) can be rotated by the above rotational matrix in index notation as follows

$$C^{\star}_{mnop} = R_{mi} R_{nj} R_{ok} R_{pl} C_{ijkl} , \tag{5.61}$$

where $C^{\star}_{mnop}$ is the rotated stiffness in accordance with the rotational matrix $\mathbf{R}$ respectively R_{xy} in index notation. The different spatial orientations for aluminium profiles are listed in Tab. 5.7.

The opportunity to use the GAUSS-MARKOV model instead of the GAUSS-HELMERT model

Under predefined experiment conditions described above, the system of normal equations from the finite element model reads

$$(\mathbf{K}_0 + ②\mathbf{K})\mathbf{u} = \mathbf{f} , \tag{5.62}$$

where the stiffness matrix $\mathbf{K}_0$ contains the fixed parameters ①, ③ to ⑥ and their related geometrical considerations as well as the aspects of the steel plates of the bridge specimen, the stiffness matrix $\mathbf{K}$ comprises geometrical information related to the unknown parameter ②, the displacement vector $\mathbf{u}$, NEUMANN boundary conditions

Table 5.7: Different spatial orientations of the aluminium profile

profile type	θ_1	θ_2	θ_3
1000	0°	90°	0°
2000	0°	0°	0°
3000	0°	90°	66.37°
4000	0°	90°	−66.37°
5000	0°	90°	90°

leads to the load vector $\mathbf{f}$ and the DIRICHLET boundary conditions are incorporated by removing the corresponding rows and column of above equation. From here on it is possible to follow the approach presented in Sec. 5.5, where the GAUSS-HELMERT model of the adjustment calculation is used to determine the unknown parameters. However, for this particular case, using this approach the computational effort becomes too high, therefore the GAUSS-MARKOV model is more desired. The functional model based on above equation reads

$$\mathbf{L} + \mathbf{v} = \left(\mathbf{K}_0 + \textcircled{2}\mathbf{K}\right)^{-1}\mathbf{f}\,, \tag{5.63}$$

where $\mathbf{L}$ contains the displacement observations. The equation above corresponds to Eq. (3.33). The design matrix base on Eq. (3.35) for this case is

$$\mathbf{A} = \frac{\partial}{\partial \textcircled{2}}\left(\mathbf{K}_0 + \textcircled{2}\mathbf{K}\right)^{-1}\Big|_{\textcircled{2}=\textcircled{2}^0}\mathbf{f} = -\left(\mathbf{K}_0 + \textcircled{2}^0\mathbf{K}\right)^{-1}\mathbf{K}\left(\mathbf{K}_0 + \textcircled{2}^0\mathbf{K}\right)^{-1}\mathbf{f}\,, \tag{5.64}$$

where $\textcircled{2}^0$ is the starting value for the parameter $\textcircled{2}$ and the *derivative of inverse matrix* with respect to $\textcircled{2}$ is applied.

Determination of the variance-covariance matrix of the displacements

Since it can be assumed that the 125 target makers on the pedestal columns are fixed during the entire experiment, the variance-covariance matrix of the displacements is determined by them. Their spatial positions were determined by a commercial photogrammetric system and can be stored for example as a matrix for further processing. A matrix $\mathbf{p}_s$ with the dimension of 125 by 3 contains the spatial positions of all target stickers in all three axis for each state s, e. g.,

$$\mathbf{p}_1 = \begin{bmatrix} 356.688 & 32.306 & 779.825 \\ 356.993 & 7.190 & 779.857 \\ 370.367 & 32.055 & 779.856 \\ \vdots & \vdots & \vdots \\ 1520.121 & 7.184 & 377.294 \\ 1520.270 & 6.914 & 631.517 \\ 1520.272 & 6.496 & 598.470 \end{bmatrix} \text{mm}\,. \tag{5.65}$$

The matrix $\bar{\mathbf{p}}$ containing the mean values of $\mathbf{p}_s$ for five states reads

$$\bar{\mathbf{p}} = \frac{\sum_{s=1}^{5}\mathbf{p}_s}{5}\,. \tag{5.66}$$

The matrix of residuals can be computed as

$$\mathbf{v}_\mathbf{p} = \begin{bmatrix} \mathbf{p}_1 - \bar{\mathbf{p}} \\ \mathbf{p}_2 - \bar{\mathbf{p}} \\ \mathbf{p}_3 - \bar{\mathbf{p}} \\ \mathbf{p}_4 - \bar{\mathbf{p}} \\ \mathbf{p}_5 - \bar{\mathbf{p}} \end{bmatrix}\,. \tag{5.67}$$

The variance-covariance matrix of the position measurements of the targets is

$$\mathbf{\Sigma_{pp}} = \frac{\mathbf{v_p^T v_p}}{500}\,. \tag{5.68}$$

Some remarks are in order: Five states and 125 target points yield in total 625 observations per axis. And in Eq. (5.66) 125 mean values were calculated for each axis. Therefore, we have "$625 - 125 = 500$" in the denominator of above equation. The displacements of two different states, here in particular from (1) to (2), serve as observations and their vector is computed as

$$\mathbf{L} = \mathbf{p}_2 - \mathbf{p}_1\,. \tag{5.69}$$

Since the precision of targets position measurements is considered to be the same for all states and is uncorrelated between states, as in Eq. (5.33) the variance-covariance matrix for the displacements is $\mathbf{\Sigma_{LL}} = 2\mathbf{\Sigma_{pp}}$. The consideration of all target markers on the pedestal that are fixed for all states yields the following covariance-covariance matrix for the displacement measurements

$$\mathbf{\Sigma_{LL}} = \begin{bmatrix} 2.827 \cdot 10^{-4} & -8.700 \cdot 10^{-6} & -3.825 \cdot 10^{-5} \\ -8.700 \cdot 10^{-6} & 8.491 \cdot 10^{-5} & 3.003 \cdot 10^{-6} \\ -3.825 \cdot 10^{-5} & 3.002 \cdot 10^{-6} & 1.630 \cdot 10^{-4} \end{bmatrix} \mathrm{mm}^2\,. \tag{5.70}$$

The square root of the diagonal components of above matrix leads to the standard deviation of the displacement measurement in x_1-, x_2- and x_3-axis direction

$$\sigma_{l_{x_1}} = 0.017\,\mathrm{mm}\,,\ \sigma_{l_{x_2}} = 0.01\,\mathrm{mm}\,,\ \sigma_{l_{x_3}} = 0.013\,\mathrm{mm}\,. \tag{5.71}$$

The precision of this photogrammetric system applied for this particular case is roughly estimated to be one hundredth of a millimetre.

The standardised observation for removing observations with a low signal-to-noise ratio

The bridge-like design of the specimen is constructed in such a way that it hardly deforms at maximal available load. Consequently, if displacement measurements are carried out at certain areas where no deformation actually occurs, only measuring noise is obtained. Observations with a low signal-to-noise ratio must be removed because they can distort the adjustment result and destabilize the numerical calculation. Normally the t-test can be used to eliminate the observations with a low signal-to-noise ratio. It is examined how the observations differ significantly from the expected value 0. In this case, the null and alternative hypothesis read

$$H_0 : \mathrm{E}(l_i) = 0 \text{ and } H_A : \mathrm{E}(l_i) \neq 0 \tag{5.72}$$

The corresponding test statics is

$$T_t = \frac{|l_i|}{\sigma_{l_i}}\,. \tag{5.73}$$

The threshold for a one sample t-test for degrees of freedom $r = 1$ and error probability of $\alpha = 5\,\%$ is

$$t_{r,1-\alpha} = 6.313\,. \tag{5.74}$$

On the bridge model 531 markers were applied. Thus, in total there were 1593 displacement measurements. By using the t-test, approximately $72\,\%$ of all measurements are eliminated. The numerical preliminary examinations have shown that the removal of the observations by the t-test might be too stringent. Some measurements with a low signal-to-noise ratio can still have sufficient information substance. Therefore, a lower threshold value is desired and an alternative way is suggested. To distinguish from the t-test, a measure that is similar to the standardised residual in Eq. (3.77) is introduced: The *standardised observation* is defined as

$$NL_i = \frac{|l_i|}{\sigma_{l_i}}\,. \tag{5.75}$$

Any measurement l_i in the vector of observations $\mathbf{L}$ are kept if its standardised observation $NL_i > 4$. In other words, only measurements that are clearly larger than their standard deviation are considered to adjust the unknowns. This eliminates approximately $57\,\%$ of the measurements.

Compensation for the imperfections of the functional model

Now that both the functional model and the stochastic model are available, the unknown parameter ② can be calibrated from the relevant displacement measurements for the undamaged case respectively from state (1) to (2). The starting value $②^0 = 47.107\,\mathrm{GPa}$ as in Eq. (5.55). In the first run to adjust the parameter, it turned out that the stochastic model was chosen too optimistically. The empirical reference standard deviation is much larger than the theoretical reference standard deviation. This does not imply that the measurement precision of the photogrammetry is poorer than expected. Instead, this indicates that significant physical effects were unconsidered by the functional model. This imperfection leads to systematic errors and thus to a seemingly incorrect stochastic model. Since there are no more resources available, it is impossible to produce an alternative test bridge or to improve the current experiment design. An extension of the physical model to take account of the systematic effects such as residual stress is also unsuitable, since this leads to additional material parameters that are difficult to determine with the available measurement equipments. A rather questionable approach is needed to overcome this obstacle: The stochastic model is forced to compensate for the imperfections of the functional model. To achieve this, the *variance component estimation* (Niemeier 2008, pp. 318–325) is applied. However, the ability to interpret the results might be lost. The practical approach of the variance component estimation is to adapt the precision of each observation group in such a way that the ratio of the empirical reference standard deviation s_0 and the theoretical reference standard deviation σ_0 becomes 1. This affects two aspects: Firstly, here, the stochastic model was chosen too optimistic. After applying the variance component estimation, the stochastic model will become pessimistic. Therefore, the sensitivity of the global test is influenced by this and thus the ability to detect damage is reduced. Secondly, the variances of the residuals $\sigma^2_{v_i}$ might be also affected and there might be a possibility that the standardised residuals yield incorrect results for localising damage. However, it can be shown that for this special case, the standardised residuals are scaled by a constant factor. This aspect will be discussed later.

The variance component estimation

The variance component estimation for one observation group is performed as follows. In the first step, the theoretical reference variance is decomposed by two factors

$$\sigma_0^2 = \breve{\alpha}_0^2 \breve{\sigma}_0^2\,, \tag{5.76}$$

where both $\breve{\alpha}_0^2$ and $\breve{\sigma}_0^2$ are usually set to one. But, in this special case, $\breve{\sigma}_0^2 = 4$ is assumed. As shown in the small auxiliary calculation above, a multiplying factor does not affect the adjusted results. From a numerical point of view, the value 4 for $\breve{\sigma}_0^2$ is the smallest number that leads to computational stability. Then the adjustment is carried out as usual. The empirical reference variance s_0^2 obtained is then used for $\breve{\alpha}_0^2$ for the second iteration. It means that $\breve{\alpha}_0^2 = s_0^2$ and $\breve{\sigma}_0^2 = 1$, then adjustment is carried out iteratively until the empirical reference variance s_0^2 becomes one. In this case, the variance component estimation was done in one iteration and $\breve{\alpha}_0^2$ converges roughly to 106.9. The covariance-covariance matrix for the displacement measurements in Eq. (5.70) is multiplied by $\breve{\alpha}_0^2$. This yields the compensated variance-covariance matrix of the observations

$$\mathbf{\Sigma_{LL}} = \begin{bmatrix} 3.022 \cdot 10^{-2} & -9.301 \cdot 10^{-4} & -4.089 \cdot 10^{-3} \\ -9.301 \cdot 10^{-4} & 9.077 \cdot 10^{-3} & 3.210 \cdot 10^{-4} \\ -4.089 \cdot 10^{-3} & 3.210 \cdot 10^{-4} & 1.742 \cdot 10^{-2} \end{bmatrix} \mathrm{mm}^2\,. \tag{5.77}$$

The square root of the diagonal components of above matrix leads to the standard deviation of the displacement measurement in x_1-, x_2- and x_3-axis direction

$$\sigma_{l_{x_1}} = 0.174\,\mathrm{mm}\,,\ \sigma_{l_{x_2}} = 0.095\,\mathrm{mm}\,,\ \sigma_{l_{x_3}} = 0.132\,\mathrm{mm}\,. \tag{5.78}$$

The calibration results

The final calibration process can be followed in Tab. 5.8. The adjusted parameter reads

$$\hat{②} = 29.4\,\mathrm{GPa} \text{ with } \sigma_{\hat{②}} = 0.848\,\mathrm{GPa}\,. \tag{5.79}$$

Table 5.8: Calibration process of the reference state

Iteration	Ω [1]	$\Delta\hat{\mathbf{X}}$ [MPa]	② [MPa]
0			47 107.0
1	3.257 038 942 56	−27 020.097 972 1	20 086.902 027 9
2	3.265 676 997 55	6285.492 226 57	26 372.394 254 5
3	3.248 321 912 14	2694.703 956 08	29 067.098 210 6
4	3.247 204 759 65	337.128 837 339	29 404.227 047 9
5	3.247 193 446 82	8.920 068 169 87	29 413.147 116 1
6	3.247 193 456 55	0.136 655 264 999	29 413.283 771 4
7	3.247 193 456 82	0.002 053 851 658 2	29 413.285 825 2
8	3.247 193 456 77	$3.061\,910\,297\,83 \cdot 10^{-5}$	29 413.285 855 8
9	3.247 193 456 84	$8.387\,416\,078 \cdot 10^{-7}$	29 413.285 856 7

The resulting parameter is smaller than expected and the reasons for this can only be assumed. Aluminium profiles of the specimen are impossible to be produced perfectly. During the assembly we noticed that some parts were too short. Consequently, it was unavoidable to cause residual stresses in the specimen during assembling. Furthermore, the fastening sets were ignored in the modelling and also holes has to be drilled for them. This could also weaken the structure. The substitute model is just an approximation of the original specimen structure. That also caused errors in the evaluation. Especially, material parameters that are indeterminable from the current experimental set-up have to be fixed. How precise the measuring systems worked can also be questioned here. In addition, the condition number of the stiffness matrix $\mathbf{K}_0 + ②\mathbf{K}$ in Eq. (5.64) is about 10^8 to 10^9. This indicates that the problem is inherently poorly conditioned. Consequently, a deviating Jacobian matrix results in the design matrix $\mathbf{A}$ in Eq. (5.64). This would explain why the target function value Ω in Tab. 5.8 increased in the iteration step from 1 to 2 and from 6 to 7. However, the deviation of the Jacobian matrix can be regarded as marginal since $\Delta\hat{\mathbf{X}}$ still converges stably towards numerical zero. In addition, this influence is negligible in so far as it influences the adjustment result from the eighth digit onwards. Nevertheless, this calibrated result in Eq. (5.79) is used as observed unknowns and their standard deviations for damage detection and localization in the following section.

Damage detection and localisation

To detect and localise damage, the approach presented in Sec. 5.2 is followed. But, some modifications must be made due to practical considerations. The bridge specimen's approximate finite element model consists of 545495 elements. To reduce the computational time, an alternative finite element model is grouped into 598 chunks. For each of these chunks ζ, a separate set of unknown material parameters ${}^{\zeta}②$ is introduced into the adjustment as observed unknowns. The individual parameters can grouped as a vector of unknowns

$$\mathbf{X} = \begin{bmatrix} {}^{1}② & {}^{2}② & \dots & {}^{\zeta}② & \dots & {}^{598}② \end{bmatrix}^{\mathsf{T}} . \tag{5.80}$$

We obtain a system of linear equations from the finite element method as follows

$$\left(\mathbf{K}_0 + \sum_{\zeta=1}^{598} {}^{\zeta}②\,{}^{\zeta}\mathbf{K}\right)\mathbf{u} = \mathbf{f} . \tag{5.81}$$

For the same reason as before, the Gauss-Markov model of the adjustment calculation is applied to determine the unknowns. The functional model based on above equation reads

$$\mathbf{L} + \mathbf{v} = \left(\mathbf{K}_0 + \sum_{\zeta=1}^{598} {}^{\zeta}②\,{}^{\zeta}\mathbf{K}\right)^{-1}\mathbf{f} . \tag{5.82}$$

The Eq. (5.25) in Sec. 5.2 applied for this non-linear case reads

$$\begin{bmatrix} \mathbf{L}_i \\ \mathbf{L}_{\text{apriori}} \end{bmatrix} - \begin{bmatrix} \mathbf{u}^0 \\ \mathbf{X}^0 \end{bmatrix} = \underbrace{\begin{bmatrix} \mathbf{A} \\ \mathbf{I} \end{bmatrix}}_{=\bar{\mathbf{A}}} \Delta\hat{\mathbf{X}} . \tag{5.83}$$

$\mathbf{L}_i$ is the vector of displacement observations for the set i. The different sets of displacement measurements are: $\mathbf{L}_1$ from state (1) to (2), $\mathbf{L}_2$ from state (1) to (3), $\mathbf{L}_3$ from state (1) to (4) and $\mathbf{L}_4$ from state (1) to (5). The computed displacements $\mathbf{u}^0$ can be obtained by using Eq. (5.81)

$$\mathbf{u}^0 = \left(\mathbf{K}_0 + \sum_{\zeta=1}^{598} {}^{\zeta}\textcircled{2}^0 {}^{\zeta}\mathbf{K}\right)^{-1} \mathbf{f}\,, \tag{5.84}$$

where ${}^{\zeta}\textcircled{2}^0$ is the starting value for the parameter ${}^{\zeta}\textcircled{2}$ and the associating stiffness matrices ${}^{\zeta}\mathbf{K}$. As previously, the *derivative of inverse matrix* with respect to the unknowns ${}^{\zeta}\textcircled{2}$ is applied to determine the design matrix

$$\mathbf{A} = \begin{bmatrix} {}^{1}\mathbf{A} & {}^{2}\mathbf{A} & \cdots & {}^{\zeta}\mathbf{A} & \cdots & {}^{598}\mathbf{A} \end{bmatrix}\,, \tag{5.85}$$

where

$$\begin{aligned} {}^{\zeta}\mathbf{A} &= \frac{\partial}{\partial {}^{\zeta}\textcircled{2}} \left(\mathbf{K}_0 + \sum_{\zeta=1}^{598} {}^{\zeta}\textcircled{2} {}^{\zeta}\mathbf{K}\right)^{-1} \Bigg|_{{}^{\zeta}\textcircled{2}={}^{\zeta}\textcircled{2}^0} \mathbf{f} \\ &= -\left(\mathbf{K}_0 + \sum_{\zeta=1}^{598} {}^{\zeta}\textcircled{2}^0 {}^{\zeta}\mathbf{K}\right)^{-1} {}^{\zeta}\mathbf{K} \left(\mathbf{K}_0 + \sum_{\zeta=1}^{598} {}^{\zeta}\textcircled{2}^0 {}^{\zeta}\mathbf{K}\right)^{-1} \mathbf{f}\,. \end{aligned} \tag{5.86}$$

The vector of observed unknowns is based on Eq. (5.79) and reads

$$\mathbf{L}_{\text{apriori}} = 29.4\,\text{GPa}\,\mathbf{1}\,, \tag{5.87}$$

where $\mathbf{1} = \begin{bmatrix} 1 & 1 & \cdots & 1 \end{bmatrix}^{\mathsf{T}}$ is the *vector of ones*. The stochastic model is premised on the results of Eq. (5.71) as well as Eq. (5.79) and it becomes possible to state the variance-covariance matrix of the observations as

$$\mathbf{\Sigma}_{\mathbf{LL}} = \begin{bmatrix} \underline{\mathbf{\Sigma}}_{\mathbf{LL}} & \mathbf{0} \\ \mathbf{0} & \underline{\mathbf{\Sigma}}_{\mathbf{XX}} \end{bmatrix} = \sigma_0^2 \begin{bmatrix} \underline{\mathbf{Q}}_{\mathbf{LL}} & \mathbf{0} \\ \mathbf{0} & \underline{\mathbf{Q}}_{\mathbf{XX}} \end{bmatrix} = \sigma_0^2 \mathbf{Q}_{\mathbf{LL}}\,, \tag{5.88}$$

where the variance-covariance matrix $\underline{\mathbf{\Sigma}}_{\mathbf{LL}}$ is assembled from Eq. (5.77) and

$$\underline{\mathbf{\Sigma}}_{\mathbf{XX}} = \left(0.848\,\text{GPa}\right)^2 \mathbf{I}\,. \tag{5.89}$$

is based on Eq. (5.79). Aforementioned, $\breve{\sigma}_0^2 = 4$ was assumed and $\breve{\alpha}_0^2 = 106.9$ is obtained by variance component estimation for single observation group. For this special case, the standardised residuals are scaled by a constant factor $\breve{\alpha}_0^2$. This can be shown by means of the propagation of $\mathbf{\Sigma}_{\mathbf{LL}}$ in Eq. (5.88) to variance-covariance matrix of the residuals $\mathbf{\Sigma}_{\mathbf{vv}}$ in Eq. (3.61). For Gauss-Markov model, Eq. (3.61) can be rewritten as

$$\mathbf{Q}_{\mathbf{vv}} = \mathbf{A}\left(-\mathbf{A}^{\mathsf{T}}\mathbf{Q}_{\mathbf{LL}}^{-1}\mathbf{A}\right)^{-1}\mathbf{A}^{\mathsf{T}} + \mathbf{Q}_{\mathbf{LL}} = \mathbf{Q}_{\mathbf{LL}} - \mathbf{A}\left(\mathbf{A}^{\mathsf{T}}\mathbf{Q}_{\mathbf{LL}}^{-1}\mathbf{A}\right)^{-1}\mathbf{A}^{\mathsf{T}}\,. \tag{5.90}$$

Inserting $\bar{\mathbf{A}}^{\mathsf{T}} = \begin{bmatrix} \mathbf{A} & \mathbf{I} \end{bmatrix}$ from Eq. (5.83) and $\mathbf{Q}_{\mathbf{LL}}$ from Eq. (5.88) into above equation, the following expression is obtained

$$\mathbf{Q}_{\mathbf{vv}} = \begin{bmatrix} -\mathbf{A}(\underline{\mathbf{Q}}_{\mathbf{XX}}^{-1} + \mathbf{A}^{\mathsf{T}}\underline{\mathbf{Q}}_{\mathbf{LL}}^{-1}\mathbf{A})^{-1}\mathbf{A}^{\mathsf{T}} + \underline{\mathbf{Q}}_{\mathbf{LL}} & -\mathbf{A}(\underline{\mathbf{Q}}_{\mathbf{XX}}^{-1} + \mathbf{A}^{\mathsf{T}}\underline{\mathbf{Q}}_{\mathbf{LL}}^{-1}\mathbf{A})^{-1} \\ -(\underline{\mathbf{Q}}_{\mathbf{XX}}^{-1} + \mathbf{A}^{\mathsf{T}}\underline{\mathbf{Q}}_{\mathbf{LL}}^{-1}\mathbf{A})^{-1}\mathbf{A}^{\mathsf{T}} & -(\underline{\mathbf{Q}}_{\mathbf{XX}}^{-1} + \mathbf{A}^{\mathsf{T}}\underline{\mathbf{Q}}_{\mathbf{LL}}^{-1}\mathbf{A})^{-1} + \underline{\mathbf{Q}}_{\mathbf{XX}} \end{bmatrix}\,. \tag{5.91}$$

The focus is on the lower right corner of the above matrix, from which the standardized residuals of the parameter NV_ζ are calculated. It reads

$$\mathbf{Q}_{\mathbf{vv}}^{\zeta\zeta} = \underline{\mathbf{Q}}_{\mathbf{XX}} - (\underline{\mathbf{Q}}_{\mathbf{XX}}^{-1} + \mathbf{A}^{\mathsf{T}}\underline{\mathbf{Q}}_{\mathbf{LL}}^{-1}\mathbf{A})^{-1}\,. \tag{5.92}$$

The second addend of the above expression can be rewritten by means of the *inverse of a sum of matrices* (Henderson and Searle 1981) as

$$(\underline{\mathbf{Q}}_{\mathbf{XX}}^{-1} + \mathbf{A}^{\mathsf{T}}\underline{\mathbf{Q}}_{\mathbf{LL}}^{-1}\mathbf{A})^{-1} = \underline{\mathbf{Q}}_{\mathbf{XX}} - \underline{\mathbf{Q}}_{\mathbf{XX}}\mathbf{A}^{\mathsf{T}}(\underline{\mathbf{Q}}_{\mathbf{LL}} + \mathbf{A}\underline{\mathbf{Q}}_{\mathbf{XX}}\mathbf{A}^{\mathsf{T}})^{-1}\mathbf{A}\underline{\mathbf{Q}}_{\mathbf{XX}}\,. \tag{5.93}$$

Table 5.9: Global test for different displacement measurements sets $\mathbf{L}_i$, the theoretical reference standard deviation σ_0, the empirical reference standard deviation s_0, the total redundancy r, test statistic χ^2_r, threshold value $\chi^2_{r,1-\alpha}$, if it holds $\chi^2_r > \chi^2_{r,1-\alpha}$ then reject H_0 in favour of H_A

$\mathbf{L}_i$	σ_0	s_0	r	χ^2_r	$\chi^2_{r,1-\alpha}$	$\chi^2_r > \chi^2_{r,1-\alpha}$
1	442.8	220.9	688	171.2	750.1	False
2	442.8	557.9	1007	1598.4	1081.9	True
3	442.8	1049.6	1095	6151.7	1173.1	True
4	442.8	3116.6	1233	61 073.0	1315.8	True

The lower right corner of $\mathbf{Q}_{\mathbf{vv}}$ yields

$$\mathbf{Q}^{\zeta\zeta}_{\mathbf{vv}} = \underline{\mathbf{Q}}_{\mathbf{XX}}\mathbf{A}^\mathsf{T}\left(\underline{\mathbf{Q}}_{\mathbf{LL}} + \mathbf{A}\underline{\mathbf{Q}}_{\mathbf{XX}}\mathbf{A}^\mathsf{T}\right)^{-1}\mathbf{A}\underline{\mathbf{Q}}_{\mathbf{XX}}\,. \tag{5.94}$$

From numerical examination of this case, it holds $\underline{\mathbf{Q}}_{\mathbf{LL}} \gg \mathbf{A}\underline{\mathbf{Q}}_{\mathbf{XX}}\mathbf{A}^\mathsf{T}$, therefore

$$\mathbf{Q}^{\zeta\zeta}_{\mathbf{vv}} \approx \underline{\mathbf{Q}}_{\mathbf{XX}}\mathbf{A}^\mathsf{T}\underline{\mathbf{Q}}^{-1}_{\mathbf{LL}}\mathbf{A}\underline{\mathbf{Q}}_{\mathbf{XX}}\,. \tag{5.95}$$

It can be seen that if $\underline{\mathbf{Q}}_{\mathbf{LL}}$ is multiplied by a factor $\breve{\alpha}^2_0$, $\underline{\mathbf{Q}}_{\mathbf{LL}} \to \breve{\alpha}^2_0\underline{\mathbf{Q}}_{\mathbf{LL}}$, the lower right corner of $\mathbf{Q}_{\mathbf{vv}}$ becomes

$$\mathbf{Q}^{\zeta\zeta}_{\mathbf{vv}} \approx \underline{\mathbf{Q}}_{\mathbf{XX}}\mathbf{A}^\mathsf{T}\left(\breve{\alpha}^2_0\underline{\mathbf{Q}}_{\mathbf{LL}}\right)^{-1}\mathbf{A}\underline{\mathbf{Q}}_{\mathbf{XX}} = \frac{1}{\breve{\alpha}^2_0}\underline{\mathbf{Q}}_{\mathbf{XX}}\mathbf{A}^\mathsf{T}\underline{\mathbf{Q}}^{-1}_{\mathbf{LL}}\mathbf{A}\underline{\mathbf{Q}}_{\mathbf{XX}}\,. \tag{5.96}$$

In conclusion, the standardised residuals of the observed unknowns NV_ζ are scaled by the factor $\breve{\alpha}^2_0$. Although the compensated variance-covariance matrix of the observations in Eq. (5.77) is enlarged by more than 100 times in comparison to Eq. (5.70), it can be expected that qualitatively the same standardised residuals of the observed unknowns NV_ζ are obtained. Please note that this is a special case.

Now that all necessary quantities are available for computing Eq. (5.83), after the adjustment it is possible to perform a global test respectively χ^2-test as in Sec. 3.3.2 to detect damage. In all displacements sets, the error probability α of 5 % is chosen as proposed by many. This choice has no explanation, see (Neitzel 2004, pp. 92–93) for further details. An overview of all χ^2-tests is listed in Tab. 5.9. The displacement measurements $\mathbf{L}_1$ is used to calibrate the reference state finite element model in Eq. (5.79) and as expected if $\mathbf{L}_1$ is reused to adjust the elastic parameters in Eq. (5.25) and subsequently performing the global test, we fail to reject the null hypothesis that no damage has occurred. Furthermore, when the other displacement measurements $\mathbf{L}_2$, $\mathbf{L}_3$ and $\mathbf{L}_4$ are evaluated, we reject the null hypothesis in favour of the alternative hypothesis. This indicates that damages are detected for the corresponding cases. The theoretical reference standard deviation $\sigma_0 = 442.8$ in Tab. 5.9 is determined by taking the mean value of the trace of the variance-covariance matrix $\mathbf{\Sigma}_{\mathbf{LL}}$ in Eq. (5.88).

To localise the damage, it was proposed in Sec. 5.2 to evaluate the target function $\Omega_{\setminus\zeta}$ as in Eq. (5.26) by releasing consecutively the unknown parameters ζ from their associating observed unknowns. The smallest value of all $\Omega_{\setminus\zeta}$ reveals the position of damage. Since this method is an iterative approach, it requires an unfeasible computational time. Therefore, instead following the proposed approach, the standardised residuals NV_ζ of the observed unknowns are evaluated for the cases where the null hypothesis is rejected in the global test ($\mathbf{L}_2$, $\mathbf{L}_3$ and $\mathbf{L}_4$). The observed unknowns $\mathbf{L}_{\text{apriori}}$ in Eq. (5.87) contain elastic parameters of the bridge in the reference state. After the adjustment, the corresponding vector of residuals is obtained that in a way corrects the parameters of the reference state with respect to the current observations. And the largest standardised residual will lead to the location of the damage. Even though this approach is an approximation in comparison to the rigorous proposed method in Sec. 5.2, experience has shown that this simplified procedure corresponds well with the rigorous counterpart.

The standardised residuals of the observed unknowns NV_ζ for the displacement measurements $\mathbf{L}_2$ are shown in Fig. 5.40. For this case, the three screws were loosened to induce artificial damage to the bridge specimen, see Fig. 5.37 (red spheres) and Fig. 5.38. One would expect that a concentrated accumulation of high standardised residuals values would gather around the damaged area. Unfortunately, that is not the case. But, it can be observed in Fig. 5.40 (top) that high standardised residuals are distributed on the side, where the screws are released,

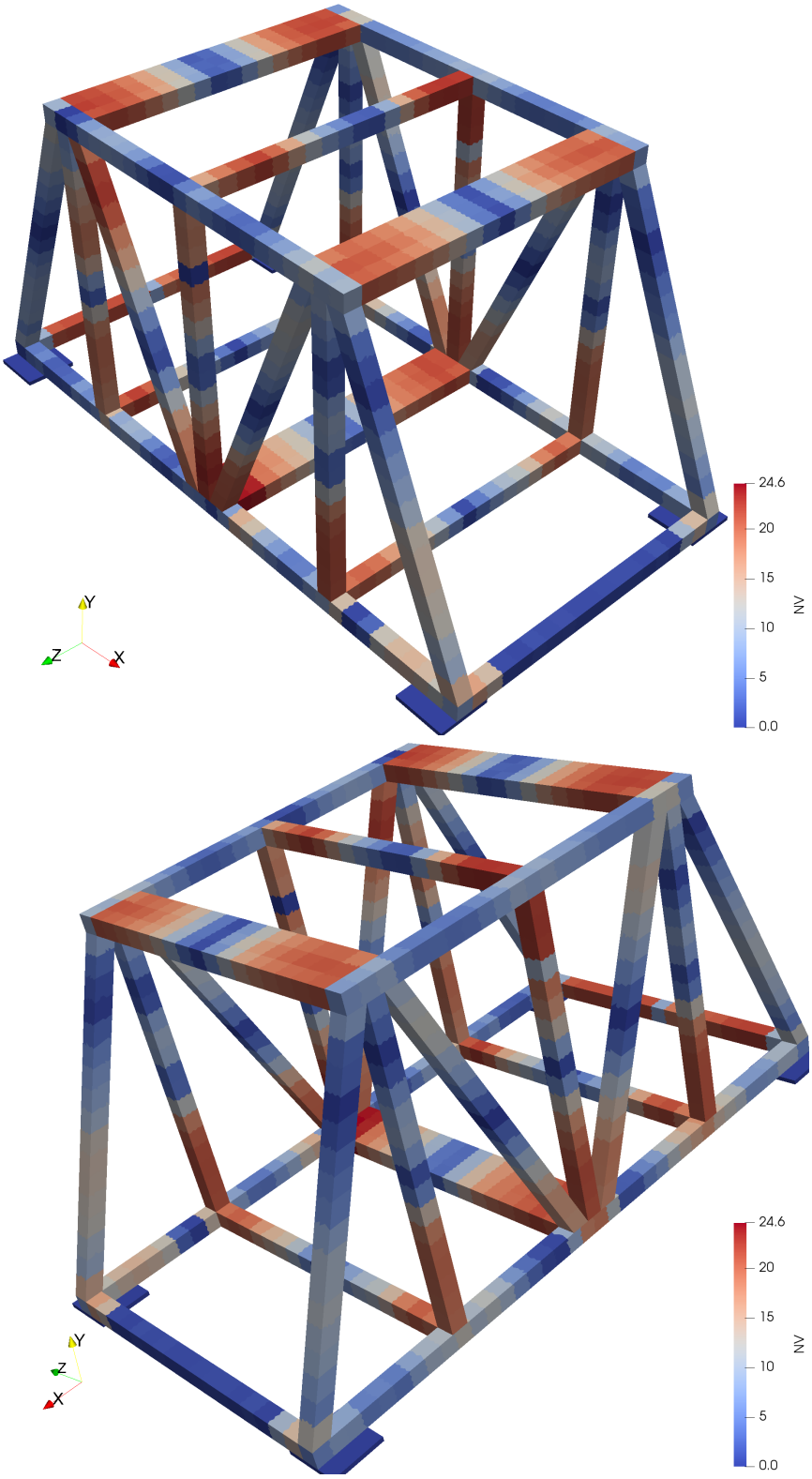


Figure 5.40: The standardised residuals of the observed unknowns NV_ζ for 598 chunks of the bridge specimen's finite element model by evaluation of the displacement measurements $\mathbf{L}_2$, two different perspectives of the bridge specimen (top and bottom)

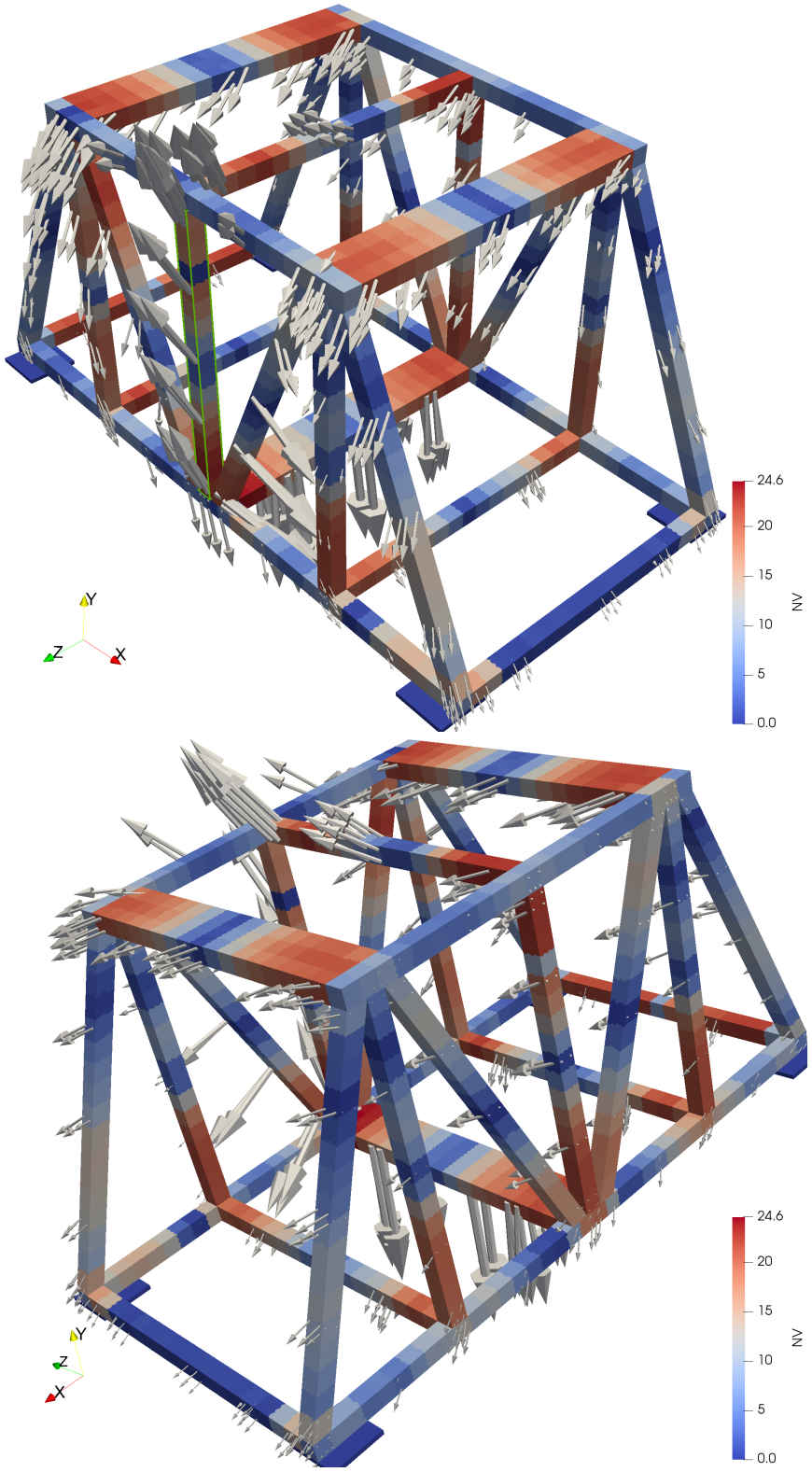


Figure 5.41: The standardised residuals of the observed unknowns NV_ζ by evaluation of the displacement measurements $\mathbf{L}_2$ including the observed displacement vectors magnified 500 times, a profile is highlighted in green that indicates an additional displacement field induced by residual stress

compared to the opposite side in Fig. 5.40 (bottom). To further examine the results, it is helpful to include the displacement measurements $\mathbf{L}_2$. In Fig. 5.41, the displacement vectors are also plotted with 500 times magnification. In addition, a vertical profile is highlighted in green. One can observe that the displacements of this profile is facing towards the positive y-direction. If the bridge specimen is under external load, it is expected that the displacements are more likely to point in the opposite direction. This behaviour could be explained that the residual stress is involved. It was actually the case that during the experiment three screws had to be loosened and a slight upward movement of the specimen was observed at that moment. The released residual stress causes an additional displacement field that overlaps with the load induced displacements. However, the total displacement fields are evaluated to adjust the unknown parameters. Therefore, the adjusted parameters can be distorted by the residual stress field. The damage becomes difficult to locate due to systematic influences that has not been taken into account by the physical model.

In Fig. 5.42, the standardised residuals based on the evaluation of the displacement measurements $\mathbf{L}_3$ is shown. This time three screws on each side are removed (in total six), see Fig. 5.37 (red and yellow spheres). One notices that the residual stress on one side of the frame is much larger than the other. It might be explained that some profiles were actually shorter than ordered on that side. The connection parts have to be modified and these profiles were put in place with a lot of strength. Comparing this evaluation of the displacement measurements $\mathbf{L}_3$ with $\mathbf{L}_2$, the standardised residuals indicate how the residual stress redistributes an additional displacement field that is induced by releasing the screws.

The displacements measurements $\mathbf{L}_4$ capture the bridge specimen, where all ten screws are removed, see Fig. 5.37 (red, yellow and blue spheres). Since on one side more screws are loosened (red and blue spheres) than on the other side (yellow spheres), it is to be expected that one side with the most of the removed screws has the largest displacement field. This in turn yields large standardises residuals. Fig. 5.43 shows the results of the evaluation of the displacement measurements $\mathbf{L}_4$ and it can be observed on this particular side in Fig. 5.43 (top) of the specimen that a distribution of large standardised residuals can be found.

Conclusion – Variationsbrücke

The ability of the presented Measurement- and Model-based Structural Analysis to detect and localise damage of a real complex structured bridge specimen is examined. The experiments were carried out under non-laboratory conditions. In particular, due to time pressure, the bridge model was produced with undesirable properties such as residual stress. To make this more difficult, the bridge model consists of profiles with complex geometric inner structures. This geometrical property leads to difficulties in finite element meshing. Even if the meshing worked, it would lead to numerical instability. To overcome this difficulty, a substitute model was applied. Even this alternative model works to some extent, this was not derived rigorously from continuum mechanics. Furthermore, the intrinsic reason why a bridge is designed as it is, is because the bridge shape provides the greatest resistance to deformation. But, at the same time, the deformation must be large enough to be measured by the sensors. Getting these two requirements together was one of the difficulties. The maximum displacement for $\mathbf{L}_1$ is $0.145\,\mathrm{mm}$, for $\mathbf{L}_2$ $0.495\,\mathrm{mm}$, for $\mathbf{L}_3$ $0.957\,\mathrm{mm}$ and for $\mathbf{L}_4$ $4.478\,\mathrm{mm}$, while the precision of photogrammetry is one hundredth of a millimetre. Since the available laboratory space was small, it was impossible to design the length of the bridge much longer. Nevertheless, this experiment shows that the presented anlysis is at some extent in accordance with the results of the preliminary numerical examinations in Sec. 5.2. The preliminary examinations show that the probability of detecting damage is higher than localising damage with fixed measuring precision, see Fig. 5.10 and Fig. 5.11. This also applies for this experiment. The global test is very well suited to determine whether there is any damage at all. The localization of individual damages with the help of the local test is in general possible, but in practice it is made difficult by the influence of systematic errors (e.g. non-modelled properties of the mechanical model). However, MeMoS can indicate the area of damage, even if it is not able to pinpoint the exact location of the damage in the examinations carried out. Therefore, it is desirable to conduct another experiment while keeping the systematic influences as small as possible.

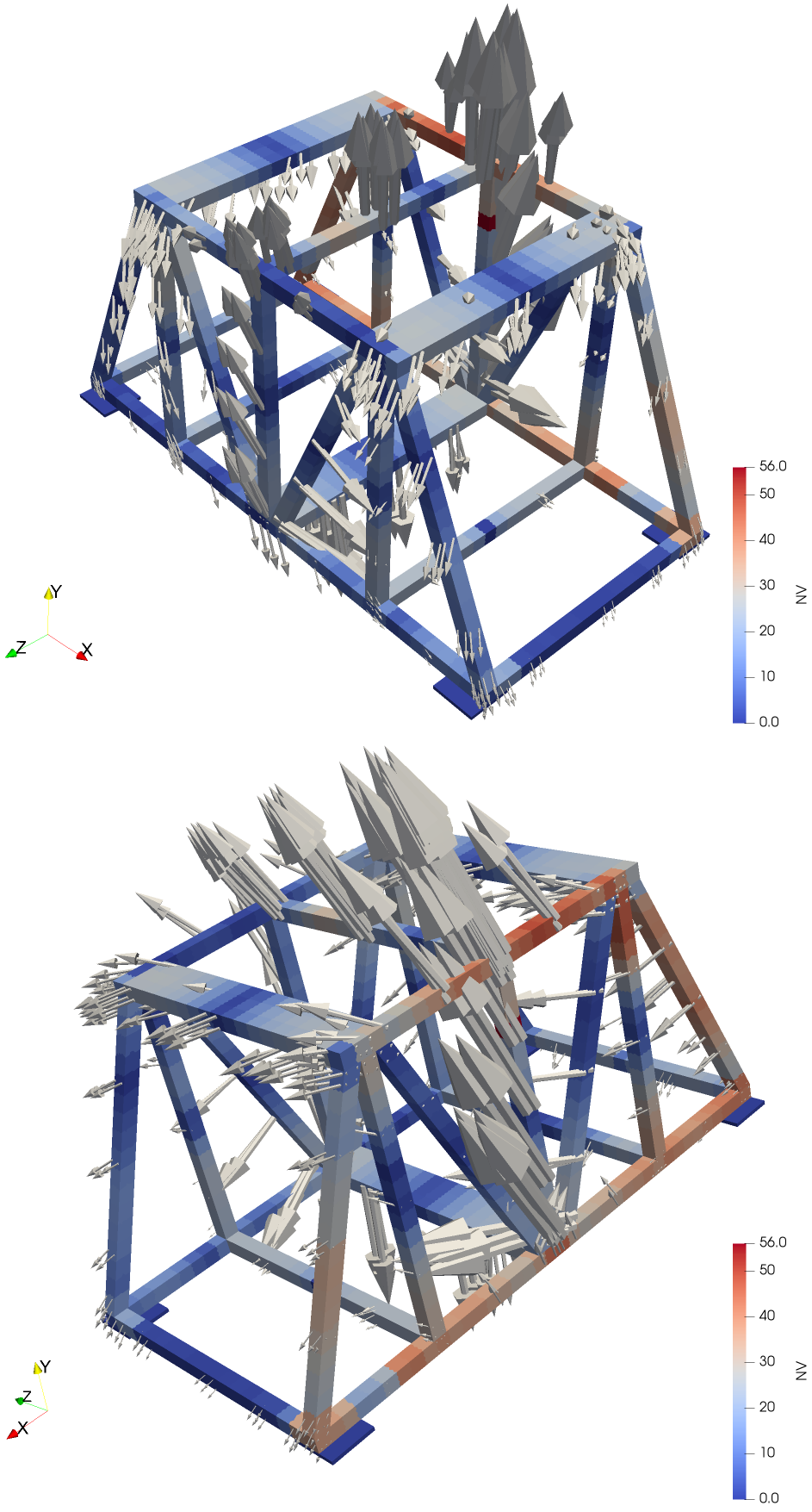


Figure 5.42: The standardised residuals of the observed unknowns NV_ζ by evaluation of the displacement measurements $\mathbf{L}_3$ including the observed displacement vectors magnified 500 times

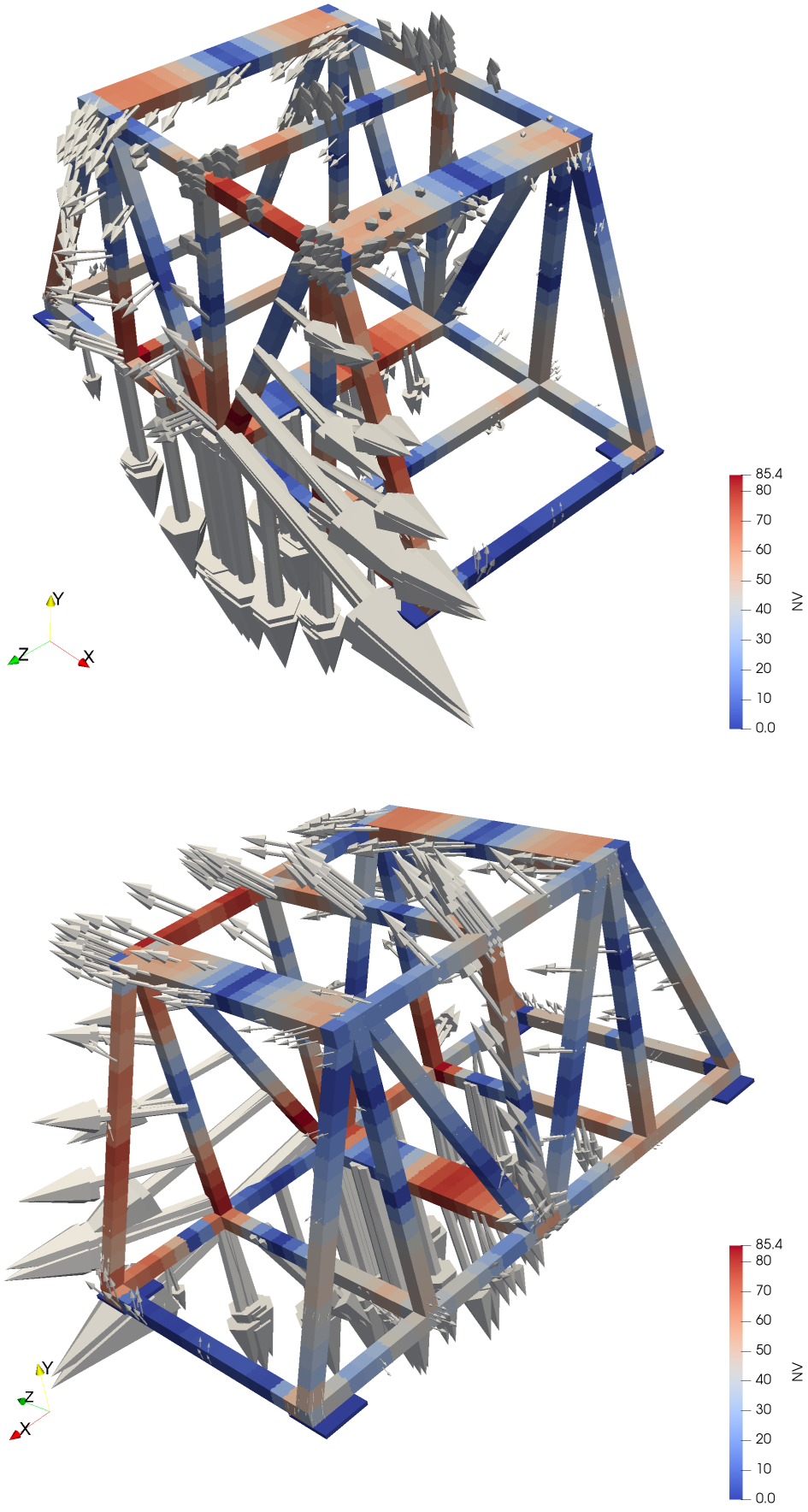


Figure 5.43: The standardised residuals of the observed unknowns NV_ζ by evaluation of the displacement measurements $\mathbf{L}_4$ including the observed displacement vectors magnified 500 times

6 Epilogue

If I'm not back in five minutes… just wait longer.

– Ace Ventura, Ace Ventura: Pet Detective (1994)

Concluding Review

The idea that led to Measurement- and Model-based Structural Analysis was the collaboration of two different engineering sciences, geodesy and continuum physics. It was recognized that there are knowledge gaps on both sides and that the gap could be partially closed by the knowledge of the other field of expertise. This led to a lively cooperation with the realisation that although both disciplines dealt with different tasks with different topics, they solve problems using essentially identical methods. It is the *Variational Calculus* that connects both disciplines. The calculus of variations, founded almost 300 years ago by Lagrange and Euler, influenced both disciplines in many ways. In mechanics, it led to the development of the *principle of virtual displacements*, of the *Lagrangian mechanics*, of the *finite element method* and many more. As can be read in Dunnington et al. (2004, p. 11 ff), Gauss was influenced by the work of Lagrange and Euler. It should not be proven that he has taken up the calculus of variations for the development of the least squares method. Nevertheless, based on the generalization of the adjustment calculation by Helmert (1872, p. 173 ff), it can be seen that his *correlates* are nothing more than the *Lagrange multiplier*. Because of this compatibility, it can be seen how inherently different methods are related. There are many other methods that have been developed for different reasons, motivations and out of different perspectives independent of the calculus of variations. Nevertheless, the calculus of variations can help to understand both old and newly developed methods. And it is precisely this understanding that leads to appreciation and ultimately to new possibilities and to maturity.

By means of two experiments, the Measurement- and Model-based Structural Analysis shows its promising capability for damage detection and localization. This capability was achieved thanks to the cooperation of two different fields of expertise. A physical model of the samples is expressed in the form of differential equations and boundary conditions using continuum mechanics. In this way, the material parameters could be considered as a possible parameter for the assessment of damage. Furthermore, displacements and their derivatives, inclinations and strains were identified as possible measurands. And it could also be decided which quantity could be seen as fixed values. Using the finite element method, the differential equations and boundary conditions could be transformed into a system of linear equations on which the functional model of the least squares method can be based. The adjustment calculation offers the possibility to determine unknown parameters from the observations and to evaluate the results stochastically, whereby statistical global and local tests could be used to detect and localize damage.

Scientific and Technological Contribution

By examining the variational calculus in the work, it became clear that the finite element method and the least squares method is one single method. The only difference is that both methods solve different problems. The finite element method solves special types of partial differential equations with corresponding boundary conditions, while the least squares method solves overdetermined systems of equations. In Boljen (1993), this insight was already given, but the presentation was incomplete. In the interest of completion, it was shown in this work that the same problem can be formulated in three variants (strong, weak and extremal formulation) and that they can be reformulated among one another. It was also shown that both methods lead to a weak solution of their corresponding problem. The term "weak" refers to the approximate respectively most probable property of the solution.

Weak solutions are unable to solve the strongly formulated problem. The exact or analytical solution of the partial differential is generally unknown, but applying finite element method, an approximate solution can be obtained. Similarly, there is in general no solution for an overdetermined system of equations, but the most probable solution is obtained by using the least squares method. It should also be noted that the viewpoint of variational calculus is by no means limited to the two methods. The different solution methods emerge when the following questions are determined:

- Is it a continuous or discrete problem?
- What is the formulation of the problem and, if necessary, the conditions?
- Which trial function is used for the solution?
- Which test function is used for the solution?

The study of the variational calculus led to the realisation that many methods are principally the same. Old, new and unknown methods from other disciplines may be more accessible if the variational calculus is used as some sort of "template". In this work, we have shown how the finite element method and the least squares method fit into the scheme of the variational calculus. This insight is intended to expand the adjustment theory and is thus the scientific contribution to the geodetic community.

For the development of this Measurement- and Model-based Structural Analysis, the finite element method and the method of least squares is combined. Equations of system of linear equations from the finite element method were selected depending on the observations, and they are inserted directly into the least squares method. As a result, the finite element method calculation procedure is inverted. For arbitrarily shaped bodies, the elastic parameters can be determined directly from the measured displacement fields. This also offers the ability to compute directly the stochastic properties of the material constants. In addition, this has the advantage that the linear elasticity can be exploited to calculate the gradient of the target function or the Jacobian directly. While the other approach with the outer loop around the finite element method, the individual columns of the Jacobian must be costly calculated from the objective function. The following aspects could be examined with Measurement- and Model-based Structural Analysis:

- *Determination of an optimal measurement set-ups.* The test structures "Variationsbrücke" and an aluminium beam are characterised using elastostatic equations or the Euler-Bernoulli beam theory. From this, the elastic parameters are considered suitable for damage evaluation. Also, the displacement fields respectively the displacement, inclination and strain have been found to be possible measurands. The capability to directly calculate the stochastic properties of the material constants allows a numerical preliminary examination of displacement, inclination and strain sensors. It was shown how the precision of the sensors, the placement of the sensors and the number of sensors impacted the parameters. The optimal measurement set-ups can then be determined from these results.
- *Finding a geometrically simple substitute model for a geometric complex body.* If the complexity of the body exceeds a certain limit, a finite element meshing of the body is no longer possible due to the memory limit. By using Measurement- and Model-based Structural Analysis, a substitute model can be determined. The geometric simpler substitute model deforms like the geometrically more complex original under the same conditions. A representative part of the geometrically complex body made of isotropic linear elastic material is cut out. Then, the deformation behaviour of this part is calculated by the finite element method. The resulting displacement field is then evaluated. Using the Measurement- and Model-based Structural Analysis, the elastic parameters of the substitute part made of anisotropic linear elastic material are determined. This allows a substitute model to be derived.
- *Detect and localise damage.* The undamaged state of the test structure is defined as reference state. In this state, the test structure consists of finite elements that share the same elastic parameter. This is then used as observed unknowns to allow a comparison between the reference and a current state of the test structure. The χ^2-test respectively the global test jointly evaluates all residuals of the observations to detect significant changes between the states of the test structure. If this is the case, damage is detected. Only then the individual finite elements are then checked iteratively by releasing them individually and evaluating the target

function. The minimum value of all possible target function values indicates the position of the damaged elements. In order to circumvent the iterative calculation, the standardised residuals can be used to estimate the location of the damaged elements.

Two experiments were carried out to validate the ability of Measurement- and Model-based Structural Analysis to detect and locate damage. In both experiments, photogrammetry was used to determine the displacement field. The following test structures were built:

- *"Variationsbrücke".* A truss consisting of special construction profiles made of aluminium. Artificial damages were caused by loosening screws. Damage could be detected, but the localization was unsuccessful. It is suspected that due to production errors, the profiles did not meet the required length. Residual stress was inadvertently generated during assembly. The standardized residuals in the results probably indicate the released residual stresses.

- *Aluminium beam.* Because the results of the previous experiment were unsatisfactory, a bending test experiment was carried out. In spite of subsiding bearings, damage could be detected and localized to a certain extent. Still, it was unable to pinpoint the absolute correct location, but it indicates approximately the damaged area in consistent manner. It should be noted that the residuals of the displacement observations shows more precise position of the damage than the standardised residuals.

As noticed, due to the time constraints some big leaps had to be made in the development of Measurement- and Model-based Structural Analysis. Although at that time, the theoretical works were unfinished, it was already insisted on planning the experiment. Due to the great pressure from the boss and from a very eager colleague, it was decided to build the aluminium truss as a test structure. The result was anything but exhilarating. Nonetheless, this has led to some new techniques and insights such as the substitute model, the introduction of standardised observations to circumvent the determination of the optimal measurement set-up for photogrammetry, the linear relationship between the standardized residuals and the cofactor matrix of observations, and consequently this has led to the second experiment and to the extension of stiffness matrix to determine the boundary condition as unknowns. The Measurement- and Model-based Structural Analysis is by definition a diagnostic method suitable for monitoring tasks. But, the experiments show that Measurement- and Model-based Structural Analysis is still premature. Nevertheless, the establishment of the fundamentals of Measurement and Model-based Structural Analysis is the technological contribution for structural health monitoring.

Improvement Suggestions and Further Research

The weak link of Measurement- and Model-based Structural Analysis is the physical modelling of the specimen and its external influences. Either the condition can be adapted so that a simplified physical model is sufficient to describe the specimen, or the physical model must be enhanced. For the latter, the following points might of interest for a geodetic re-evaluation:

- *Kinematics*. A reassessment of the motion description from a geodesist's point of view could bring new insights, see Sec. 2.2.

- *Material laws.* The more complex the physical processes, the more complex the material equations are. Together with geodesists, the material equations can be examined for their numerical and stochastic properties. It is then possible to formulate new equations, whereby their parameters can be determined with numeric stability.

- *Vibrations.* The vibration behaviour of a test bridge is to be examined. It is helpful to use the elastodynamic equations derived in Sec. 2.5.1 as well as their numerical treatment with finite element method in Sec. 2.6.

- *Hybrid measurements.* Although different types of observation were also treated theoretically, see Sec. 5.1, only the displacement in the experimental examinations could be measured in this dissertation. In further work, hybrid measurements should be studied.

As already mentioned at the beginning, the procedure of the variational calculus could be a universal entry point for many methods. It could be lucrative for adjustment theory to examine the following points:

- *Examination of known methods.* FOURIER-Analysis and LAPLACE transform, for example, are well-known. It can be shown that with a small amount of preliminary information, such as problem description and solution approach, it is possible to reach the known methods from the variational calculus procedure.
- *Examination of different solution representations.* The solution function is often expressed as an infinite series. The most popular representation is the power series. By omitting some summands, other types of infinite series are formed. The relationship between different series should be examined, for example, the LAURENT series and CHEBYSHEV polynomials. The development of new series should also be studied, for example, Wavelets or neuronal networks.
- *Examination of popular methods.* From completely unfamiliar procedures of popular applications, it should be shown that they follow the same scheme. By means of simple examples, it should show how to encrypt and decrypt a number, how to adjust the parameters of a neuronal networks by GAUSS-MARKOV model, etc.

Bibliography

Uuuuuuuuuur Ahhhrrrrrr Uhrrrrrrr Ahhhhhhrrrrr
Aaaaaarhg…

– Chewbacca, Star Wars franchise

Abali, B. E. (2014): Thermodynamically compatible modeling, determination of material. parameters, and numerical analysis of nonliear rheological materials. epubli GmbH.

Abali, B. E. (2017): Computational Reality: Solving Nonlinear and Coupled Problems in Continuum Mechanics. Springer Nature Singapore Pte Ltd.

Altenbach, H., Maugin, G., and Erofeev, V. (2011): Mechanics of Generalized Continua. Advanced Structured Materials. Springer Berlin Heidelberg.

Baarda, W. (1968): A testing procedure for use in geodetic networks. Rijkscommissie voor Geodesie.

Bahndorf, J. (1991): Zur Systematisierung der Seilnetzberechnung und zur Optimierung von Seilnetzen. German. Deutsche Geodätische Kommission, Reihe C, Nr. 373, München.

Balaraman, K., Mukherjee, S., Chawla, A., and Malhotra, R. (2006): Inverse Finite Element Characterization of Soft Tissues Using Impact Experiments and Taguchi Methods. Tech. rep. SAE Technical Paper.

Becker, T., Weisbrich, S., Wu, C.-C., and Neitzel, F. (2015): Advances in structural monitoring by an integrated analysis of sensor measurements and 3D building model. Ed. by M. Breunig, M. Al-Doori, E. Butwilowski, P. Kuper, J. Benner, and K. Haefele. bookpartcollection.

Bochev, P. B. and Gunzburger, M. D. (2009): Least-Squares Finite Element Methods. Springer.

Boljen, J. (1993): "Eine Verallgemeinerung der Ausgleichung nach der Methode der kleinsten Quadrate". German. In: *Ausgewählte Kapitel der Landes- und Ingenieurvermessung*. Wissenschaftliche Arbeiten der Fachrichtung Vermessungswesen der Universität Hannover, pp. 192–236.

Brandes, K., Neitzel, F., Weisbrich, S., and Daum, W. (2012): "Lagrange-Multiplikatoren (LM) der Ausgleichungsrechnung als Indikator für Strukturschäden". German. In: *tm-Technisches Messen* 79.7–8, pp. 348–358.

Brincker, R. and Ventura, C. E. (2015): Introduction to Operational Modal Analysis. Wiley.

Bronshtein, I., Semendyayev, K., Musiol, G., and Mühlig, H. (2007): Handbook of Mathematics. Springer Berlin Heidelberg.

Bucher, C., Schorling, Y., and Wall, W. (1995): "SLang–the Structural Language, a tool for computational stochastic structural analysis". In: *Engineering Mechanics, Proceedings of the 10th Conference*. Ed. by S. Sture. ASCE, pp. 1123–1126.

Burden, R. L. and Faires, J. D. (2011): Numerical Analysis. 9th. BROOKS/COLE CENGAGE Learning.

Chadwick, P., Vianello, M., and Cowin, S. C. (2001): "A new proof that the number of linear elastic symmetries is eight". In: *Journal of the Mechanics and Physics of Solids* 49.11, pp. 2471–2492.

Chesnais, C., Boutin, C., and Hans, S. (2011): "Structural dynamics and generalized continua". In: *Mechanics of Generalized Continua*. Springer, pp. 57–76.

Chrzanowski, A., Chen, Y. Q., Szostak-Chrzanowski, A., and Secord, J. M. (1990): "Combination of Geometrical Analysis with Physical Interpretation for the Enhancement of Deformation Modeling". In: *Proceedings of FIG XVIX Congress of Engineering Surveys, Commission 6*. Helsinki, pp. 326–341.

Cosserat, E. and Cosserat, F. (1909): Théorie des Corps Déformables. French.

Czichos, H. (2013): Handbook of Technical Diagnostics. Fundamentals and Application to Structures and Systems. Ed. by H. Czichos. Springer-Verlag Berlin Heidelberg. Chap. Principles, Concepts and Assessment of Structural Health Monitoring.

Dasgupta, B. (2006): Applied Mathematical Methods. Dorling Kindersley.

Daum, W. (2013): Handbook of Technical Diagnostics. Fundamentals and Application to Structures and Systems. Ed. by H. Czichos. Springer-Verlag Berlin Heidelberg. Chap. Principles, Concepts and Assessment of Structural Health Monitoring, pp. 413–424.

Deb, D. (2006): Finite Element Methods : Concepts and Applications in Geomechanics. PHI Learning Pvt. Ltd.

DIN 18709 (1995): Concepts, abbreviations and symbols in surveying. DIN. Beuth Verlag GmbH.

Dunnington, G., Gray, J., and Dohse, F. (2004): Carl Friedrich Gauss: Titan of Science. MAA spectrum. Mathematical Association of America.

Eckart, C. (1940): "The thermodynamics of irreversible processes. I. The simple fluid". In: *Physical Review* 58.3, p. 267.

Eichhorn, A. (2005): Ein Beitrag zur Identifikation von dynamischen Strukturmodellen mit Methoden der adaptiven Kalman-Filterung. German. Deutsche Geodätische Kommission, Reihe C, Nr. 585, München.

Eisenberg, M. A. and Malvern, L. E. (1973): "On finite element integration in natural co-ordinates". In: *International Journal for Numerical Methods in Engineering* 7.4, pp. 574–575.

Eringen, A. C. (2012): Microcontinuum field theories: I. Foundations and Solids. Springer Science & Business Media.

Euler, L. (1744): *Opera Omnia*. Vol. 24: Methodus inveniendi lineas curvas maximi minimive proprietate gaudentes, sive solutio problematis isoperimetrici latissimo sensu accepti. Latin. Ser. I. Eneström no. 65. Lausannae & Genevae: apud Marcum-Michaelem Bousquet et socios.

Farrar, C. R. and Worden, K. (2013): Structural Health Monitoring: A Machine Learning Perspective. Wiley.

Fefferman, C. L. (2000): "Existence and smoothness of the Navier-Stokes equation". In: *The Millennium Prize Problems*. American Mathematical Society, pp. 57–67.

Finlayson, B. and Scriven, L. (1966): "The Method of Weighted Residuals—a review". In: *Applied Mechanics Reviews* 19.9, pp. 735–748.

Finlayson, B. A. (1972): The Method of Weighted Residuals and Variational Principles: With Application in Fluid Mechanics, Heat and Mass Transfer. Vol. 87. Mathematics in Science and Engineering. Academic Press.

Flügge, W. (1975): Viscoelasticity. Springer Berlin Heidelberg.

Funk, P. (1962): Variationsrechnung und ihre Anwendung in Physik und Technik. German. Vol. 94. Die Grundlehren der mathematischen Wissenschaften, In Einzeldarstellungen mit besonderer Berücksichtigung der Anwendungsgebiete. Berlin, Heidelberg: Springer.

Galerkin, B. G. (1915): "Series solution of some problems of elastic equilibrium of rods and plates". In: *Vestnik inzhenerov i tekhnikov* 19.7, pp. 897–908.

Galilei, G. (1891): Unterredungen und mathematische Demonstration über zwei neue Wissenszweige, die Mechanik und die Fallgesetze betreffend: Dritter und vierter Tag mit 90 Figuren im Text: aus dem italienischen und lateinischen übersetzt und herausgegeben von Arthur von Göttingen. German. Leipzig: Verlag von Wilhelm Engelmann.

Gander, M. J. and Wanner, G. (2012): "From Euler, Ritz, and Galerkin to Modern Computing". In: *SIAM Review* 54.4, pp. 627–666.

Gere, J. M. and Goodno, B. J. (2013): Mechanics of Materials, SI Edition. 8th. Cengage Learning.

Ghilani, C. D. (2010): Adjustment Computations: Spatial Data Analysis. Fifth Edition. Wiley.

Girifalco, L. (2000): Statistical Mechanics of Solids. Monographs on the Physics and Chemistry of Materials. Oxford University Press, USA.

Grafarend, E. (1984): "Variance-covariance component estimation of Helmert type in the Gauss-Helmert model". In: *Zeitschrift für Vermessungswesen* 109, pp. 34–44.

Gross, D., Hauger, W., Schröder, J., Wall, W. A., and Bonet, J. (2011): Engineering Mechanics 2: Mechanics of Materials. Springer Berlin Heidelberg.

Gross, D., Hauger, W., Schröder, J., Wall, W. A., and Rajapakse, N. (2009): Engineering Mechanics 1: Statics. Springer.

Grote, K.-H. and Antonsson, E. K. (2009): Springer Handbook of Mechanical Engineering. Springer Handbook of Mechanical Engineering Bd. 10. Springer.

Hassaballah, A. I., Hassan, M. A., Mardi, A. N., and Hamdi, M. (2013): "An inverse finite element method for determining the tissue compressibility of human left ventricular wall during the cardiac cycle". In: *PLoS ONE* 8.12.

Haupt, P. (2010): Continuum Mechanics and Theory of Materials. Springer Berlin Heidelberg.

Helmert, F. R. (1872): Die ausgleichungsrechnung nach der methode der kleinsten quadrate. B. G. Teubner.

Henderson, H. V. and Searle, S. R. (1981): "On Deriving the Inverse of a Sum of Matrices". In: *SIAM Review* 23.1, pp. 53–60.

Hetnarski, R. B. and Eslami, M. R. (2009): Thermal Stresses – Advanced Theory and Applications. Solid Mechanics and Its Applications. Springer Netherlands.

Heunecke, O., Kuhlmann, H., Welsch, W., Eichhorn, A., and Neuner, H. (2013): Handbuch Ingenieurgeodäsie: Auswertung geodätischer überwachungsmessungen. German. 2nd ed. Handbuch Ingenieurgeodäsie. Wichmann.

Irgens, F. (2008): Continuum Mechanics. Springer Berlin Heidelberg.

ISO 13372:2012 (2012): Condition monitoring and diagnostics of machines — Vocabulary. ISO. Beuth Verlag GmbH.

Jäger, R. (1988): Analyse und Optimierung geodätischer Netze nach spektralen Kriterien und mechanischen Analogien. German. Deutsche Geodätische Kommission, Reihe C, Nr. 516, München.

Kauer, M. (2001): Inverse finite element characterization of soft tissues with aspiration experiments. Dissertation ETH Zürich.

Kottner, R., Kocób, J., Kroupa, T., and Krystek, J. (2014): "Characterization of Cork/Rubber Composite and modeling of observed mechanical behavior". In: *31th Danubia-Adria Symposium Proceedings*. VDI Verein Deutscher Ingenieure e. V., pp. 187–188.

Kraus, K. (1996): Photogrammetrie: Verfeinerte Methoden und Anwendungen. German. Vol. 2. Dümmler / Bonn.

Lagrange, J. (1892): Œuvres de Lagrange: Correspondance de Lagrange avec Condorcet, Laplace, Euler et divers savants publiée et annotée par Ludovic Lalanne. French. Ed. by J.-A. Serret and G. Darboux. Œuvres de Lagrange. Gauthier-Villars.

Lenzmann, L. and Lenzmann, E. (2004): "Strenge Auswertung des nichtlinearen Gauß-Helmert-Modells". In: *AVN* 111, pp. 68–73.

Lienhart, W. (2007): Analysis of inhomogeneous structural monitoring data. Shaker Verlag.

Liu, I.-S. (2002): Continuum Mechanics. Springer Berlin Heidelberg.

Mikhail, E. M. and Ackermann, F. (1976): Observations and least squares. IEP series in civil engineering. IEP.

Mikhail, E. M. and Gracie, G. (1981): Analysis and adjustment of survey measurements. Van Nostrand Reinhold Co.

Milev, I. (2001): Integrierte Modelle zur Physikalischen Interpretation Geodätischer Deformationsuntersuchungen. German. Deutsche Geodätische Kommission, Reihe C, Nr. 540, München.

Müller, I. (1973): Thermodynamik. German. Bertelsmann-Universitätsverlag.

Müller, I. (2007): A History of Thermodynamics: The Doctrine of Energy and Entropy. Springer Berlin Heidelberg.

Müller, I. and Müller, W. H. (2008): Fundamentals of Thermodynamics and Applications. Springer.

Müller, W. H. (2014): An Expedition to Continuum Theory. Springer.

Müller, W. H. and Ferber, F. (2005): Technische Mechanik für Ingenieure. German. 2., verbesserte Auflage. Fachbuchverlag Leipzig im Carl Hanser Verlag.

Narasimhan, T. N. (1999): "Fourier's heat conduction equation: History, influence, and connections". In: *Reviews of Geophysics* 37.1, pp. 151–172.

Neitzel, F. (2004): Identifizierung konsistenter Datengruppen am Beispiel der Kongruenzuntersuchung geodätischer Netze. German. Deutsche Geodätische Kommission, Reihe C, Nr. 565, München.

Neitzel, F., Weisbrich, S., and Wu, C.-C. (2014): "Integration der Finite-Elemente-Methode in die Ausgleichungsrechnung zur Parameteridentifikation". German. In: *Ingenieurvermessung 14. Beiträge zum 17. Internationalen Ingenieursvermessungskurs Zürich, 2014*. 17. Internationalen Ingenieursvermessungskurs (Jan. 14–17, 2014). Ed. by A. Wieser. Wichmann Verlag, pp. 301–310.

Neuser, D. A. (1992): Curve and Surface Design. Ed. by H. Hagen. Society for Industrial and Applied Mathematics. Chap. Curve and Surface Interpolation Using Quintic Weighted Tau-Splines, pp. 55–86.

Niemeier, W. (1979): Zur Kongruenz mehrfach beobachteter geodätischer Netze. Fachrichtung Vermessungswesen: Wissenschaftliche Arbeiten der Fachrichtung Vermessungswesen der Universität Hannover. Universität Hannover.

Niemeier, W. (2008): Ausgleichungsrechnung: Statistische Auswertemethoden. German. 2., überarb. und erw. Aufl. De Gruyter Lehrbuch. Berlin [u.a.]: De Gruyter.

Nuzzo, R. (2014): "Statistical errors". In: *Nature* 506.7487, pp. 150–152.

Rechenberg, I. (1994): Evolutionsstrategie '94. German. Vol. 1. Werkstatt Bionik und Evolutionstechnik. Stuttgart: Frommann-Holzboog.

Ritz, W. (1908): "über eine neue Methode zur Lösung gewisser Variationsprobleme der mathematischen Physik". German. In: *J. Reine Angew. Math.* 135, pp. 1–61.

Ritz, W. (1909): "Theorie der Transversalschwingungen einer quadratischen Platte mit freien Rändern". German. In: *Annalen der Physik* 28, Nr. 4, pp. 737–786.

Rojas, R. (1996): Neural Networks: A Systematic Introduction. Springer Berlin Heidelberg.

Schmalz, T., Buhl, V., and Eichhorn, A. (2010): "An adaptive Kalman-filtering approach for the calibration of finite difference models of mass movements". In: *Journal of Applied Geodesy* 4.3, pp. 127–135.

Serway, R. and Jewett, J. (2008): PHYSICS for Scientists and Engineers with Modern Physics. 7th ed. Thomson Brooks/Cole.

Singer, P. (1995): Die Berechnung von Minimalflächen, Seifenblasen, Membrane und Pneus aus geodätischer Sicht. German. Deutsche Geodätische Kommission, Reihe C, Nr. 448, München.

Sterthaus, J. (2008): Parameteridentifikation an metallischen Werkstoffen basierend auf numerischen Simulationen und instrumentierter Eindringprüfung. German. Cuvillier Verlag.

Stojanović, R. (1972): "A continuum-mechanical approach to the mechanics of rock masses". In: *Rock mechanics* 4.1, pp. 45–58.

Strang, G. and Fix, G. J. (2008): An analysis of the finite element method. 2nd ed. Wellesley, MA: Wellesley-Cambridge.

Szabó, I. (1966): Einführung in die Technische Mechanik: Nach Vorlesungen. 7th ed. Springer Berlin Heidelberg.

Tadmor, E., Miller, R., and Elliott, R. (2012): Continuum Mechanics and Thermodynamics: From Fundamental Concepts to Governing Equations. Continuum Mechanics and Thermodynamics: From Fundamental Concepts to Governing Equations. Cambridge University Press.

Teunissen, P. (2000): Adjustment Theory: An Introduction. Series on mathematical geodesy and positioning. Delft University Press.

Warner, M. and Terentjev, E. M. (2003): Liquid crystal elastomers. Vol. 120. Oxford University Press.

Webster, N. (1913): Webster's Revised Unabridged Dictionary. Springfield, MA: C. & G. Merriam Co.

Weisbrich, S., Wu, C.-C., and Neitzel, F. (2014): "On optimal measurement set-ups for parameter identification from an integrated structural analysis of hybrid measurements and finite element model". In: *XIVth Bilateral Czech/German Symposium 'Experimental methods and numerical simulation in engineering science'*. Ed. by R. Harte, pp. 46–47.

Welsch, W. M. (1986): "Some aspects of the analysis of geodetic strain observations in kinematic models". In: *Tectonophysics* 130.1-4, pp. 437–458.

Welsch, W. M. and Heunecke, O. (2001): "Models and terminology for the analysis of geodetic monitoring observations". In: *Proc. 10th Int. FIG-Symp. Deformation Measurements*, pp. 390–412.

Wenzel, H. and Pichler, D. (2005): Ambient Vibration Monitoring. Wiley.

Worden, K., Farrar, C. R., Manson, G., and Park, G. (2007): "The fundamental axioms of structural health monitoring". In: *Proceedings of the Royal Society of London A: Mathematical, Physical and Engineering Sciences*. Vol. 463. 2082. The Royal Society, pp. 1639–1664.

Wu, C.-C., Weisbrich, S., and Neitzel, F. (2014): "Integrated structural analysis of hybrid measurement and finite element method for damage detection within a slender beam". In: *31st Danubia-Adria Symposium on advances in experimental mechanics (Proceedings)*, pp. 191–192.

Wu, C.-C., Weisbrich, S., and Neitzel, F. (2016): "Inverse finite element adjustment of material parameters from integrated analysis of displacement field measurement". In: *Materials Today: Proceedings* 3.4. Ed. by G. Nicoletto, S. D. Pastrama, and I. Emri, pp. 1211–1215.

Wu, C.-C., Weisbrich, S., and Neitzel, F. (2017): "Approximate model for geometrical complex structures". In: *Materials Today: Proceedings* 4.5, Part 1. Ed. by I. Emri, pp. 5995–6000.

Yamaguchi, H. (2008): Engineering Fluid Mechanics. Springer Netherlands.

Yang, H., Xu, X., and Neumann, I. (2014): "The Benefit of 3D Laser Scanning Technology in the Generation and Calibration of FEM Models for Health Assessment of Concrete Structures". In: *Sensors* 14.11, pp. 21889–21904.

Zhang, C., Bellet, M., Bobadilla, M., Shen, H., and Liu, B. (2011): "Inverse finite element modelling and identification of constitutive parameters of UHS steel based on Gleeble tensile tests at high temperature". In: *Inverse Problems in Science and Engineering* 19.4, pp. 485–508.

Zienkiewicz, O. C., Taylor, R. L., and Zhu, J. Z. (2013): The finite element method: Its basis and fundamentals, seventh edition. 7th ed. Kidlington, Oxford, UK and Waltham, MA: Butterworth-Heinemann.

A Source Codes

The source codes for Sec. 2.6 are given in this appendix.

Listing A.1: Generating the stiffness matrix ${}^{\zeta}\mathbf{K}$

```
from numpy import array, zeros
from numpy.linalg import det, inv

def K_sub(C, nu_1, nu_2, nu_3, nu_4):
    """ C is the stiffness tensor and
        nu_1, nu_2, nu_3, nu_4 are the vertex coordinates of the tetrahedron
    """

    """ For details see Eq. (2.223) """
    M = array([
    [     1.,      1.,      1.,      1.],
    [nu_1[0], nu_2[0], nu_3[0], nu_4[0]],
    [nu_1[1], nu_2[1], nu_3[1], nu_4[1]],
    [nu_1[2], nu_2[2], nu_3[2], nu_4[2]]
    ])

    """ The volume of a tetrahedron """
    V_sub = 1./6. * abs(det(M))

    """ The matrix on the right-hand side in Eq. (2.223) contains the derivatives """
    Partial_Xi = inv(M)[:,1:]

    """ Initiation of the stiffness matrix """
    k_sub = zeros((4,4,3,3))

    """ Computation of the stiffness matrix, for details see Eq. (2.226) """
    for m in xrange(4):
        for n in xrange(4):
            for i in xrange(3):
                for j in xrange(3):
                    for k in xrange(3):
                        for l in xrange(3):
                            k_sub[m,n,i,k] += C[i,j,k,l] * Partial_Xi[m,j] *
                                Partial_Xi[n,l]

    return k_sub * V_sub
```

Listing A.2: Computing the mass matrix ${}^{\zeta}\mathbf{M}$

```
from numpy import array, zeros, concatenate
from numpy.linalg import det
from scipy.special import p_roots

def M_sub(function, nu_1, nu_2, nu_3, nu_4, Gauss_Points):
    """ function is a user defined function,
        nu_1, nu_2, nu_3, nu_4 are the vertex coordinates of the tetrahedron and
        Gauss_Points are the number of sample points
    """

    """ The volume of a tetrahedron """
    V_sub = abs((1./6.) * det(array([nu_1-nu_4, nu_2-nu_4, nu_3-nu_4]).T))
```

```
    """ SciPy generates the sample points and weights for Gauss-Legendre quadrature
        """
    n, w = p_roots(Gauss_Points)

    """ Initiation of the dummy matrix """
    m = zeros((4,4))

    """ Computation of the mass matrix, for details see Eq. (2.233) """
    for p in xrange(Gauss_Points):
        for q in xrange(Gauss_Points):
            for r in xrange(Gauss_Points):
                a_3 = 1.
                xi_nu_3 = (1./2.)*(n[p]+1.)

                a_2 = 1. - xi_nu_3
                xi_nu_2 = (1./2.)*(a_2*n[q]+a_2)

                a_1 = 1. - xi_nu_3 - xi_nu_2
                xi_nu_1 = (1./2.)*(a_1*n[r]+a_1)

                xi_nu_4 = 1. - xi_nu_3 - xi_nu_2 - xi_nu_1

                x = xi_nu_1 * nu_1 + xi_nu_2 * nu_2 + xi_nu_3 * nu_3 + xi_nu_4 * nu_4

                f = function(x)

                m[0,0] += a_3*w[p] * a_2*w[q] * a_1*w[r] * xi_nu_1 * xi_nu_1 * f
                m[0,1] += a_3*w[p] * a_2*w[q] * a_1*w[r] * xi_nu_1 * xi_nu_2 * f
                m[0,2] += a_3*w[p] * a_2*w[q] * a_1*w[r] * xi_nu_1 * xi_nu_3 * f
                m[0,3] += a_3*w[p] * a_2*w[q] * a_1*w[r] * xi_nu_1 * xi_nu_4 * f

                m[1,0] += a_3*w[p] * a_2*w[q] * a_1*w[r] * xi_nu_2 * xi_nu_1 * f
                m[1,1] += a_3*w[p] * a_2*w[q] * a_1*w[r] * xi_nu_2 * xi_nu_2 * f
                m[1,2] += a_3*w[p] * a_2*w[q] * a_1*w[r] * xi_nu_2 * xi_nu_3 * f
                m[1,3] += a_3*w[p] * a_2*w[q] * a_1*w[r] * xi_nu_2 * xi_nu_4 * f

                m[2,0] += a_3*w[p] * a_2*w[q] * a_1*w[r] * xi_nu_3 * xi_nu_1 * f
                m[2,1] += a_3*w[p] * a_2*w[q] * a_1*w[r] * xi_nu_3 * xi_nu_2 * f
                m[2,2] += a_3*w[p] * a_2*w[q] * a_1*w[r] * xi_nu_3 * xi_nu_3 * f
                m[2,3] += a_3*w[p] * a_2*w[q] * a_1*w[r] * xi_nu_3 * xi_nu_4 * f

                m[3,0] += a_3*w[p] * a_2*w[q] * a_1*w[r] * xi_nu_4 * xi_nu_1 * f
                m[3,1] += a_3*w[p] * a_2*w[q] * a_1*w[r] * xi_nu_4 * xi_nu_2 * f
                m[3,2] += a_3*w[p] * a_2*w[q] * a_1*w[r] * xi_nu_4 * xi_nu_3 * f
                m[3,3] += a_3*w[p] * a_2*w[q] * a_1*w[r] * xi_nu_4 * xi_nu_4 * f

    line1 = array([m[0,0], 0., 0., m[0,1], 0., 0., m[0,2], 0., 0., m[0,3]])
    line2 = array([m[1,0], 0., 0., m[1,1], 0., 0., m[1,2], 0., 0., m[1,3]])
    line3 = array([m[2,0], 0., 0., m[2,1], 0., 0., m[2,2], 0., 0., m[2,3]])
    line4 = array([m[3,0], 0., 0., m[3,1], 0., 0., m[3,2], 0., 0., m[3,3]])

    tri_z = array([0., 0., 0.])

    m_sub = concatenate((
    line1, tri_z, line1, tri_z, line1, \
    line2, tri_z, line2, tri_z, line2, \
    line3, tri_z, line3, tri_z, line3, \
    line4, tri_z, line4, tri_z, line4, \
    )).reshape((12,12))

    return m_sub * (3./4.) * V_sub
```

Listing A.3: Computing the load vector for volume force integral ${}^{\zeta}\mathbf{f}_{f_i}^{\mathsf{T}}$

```
from numpy import array, zeros
from numpy.linalg import det
```

```
from scipy.special import p_roots

def f_v_sub(function, nu_1, nu_2, nu_3, nu_4, Gauss_Points):
    """ function is a user defined function,
        nu_1, nu_2, nu_3, nu_4 are the vertex coordinates of the tetrahedron and
        Gauss_Points are the number of sample points
    """

    """ The volume of a tetrahedron """
    V_sub = abs((1./6.) * det(array([nu_1-nu_4, nu_2-nu_4, nu_3-nu_4]).T))

    """ SciPy generates the sample points and weights for Gauss-Legendre quadrature
        """
    n, w = p_roots(Gauss_Points)

    """ Initiation of the volume load vector """
    f_sub = zeros(12)

    """ Computation of the volume load vector, for details see Eq. (2.239) """
    for p in xrange(Gauss_Points):
        for q in xrange(Gauss_Points):
            for r in xrange(Gauss_Points):
                a_3 = 1.
                xi_nu_3 = (1./2.)*(n[p]+1.)

                a_2 = 1. - xi_nu_3
                xi_nu_2 = (1./2.)*(a_2*n[q]+a_2)

                a_1 = 1. - xi_nu_3 - xi_nu_2
                xi_nu_1 = (1./2.)*(a_1*n[r]+a_1)

                xi_nu_4 = 1. - xi_nu_3 - xi_nu_2 - xi_nu_1

                x = xi_nu_1 * nu_1 + xi_nu_2 * nu_2 + xi_nu_3 * nu_3 + xi_nu_4 * nu_4

                f = function(x)

                f_sub[0:3]  += a_3*w[p] * a_2*w[q] * a_1*w[r] * xi_nu_1 * f
                f_sub[3:6]  += a_3*w[p] * a_2*w[q] * a_1*w[r] * xi_nu_2 * f
                f_sub[6:9]  += a_3*w[p] * a_2*w[q] * a_1*w[r] * xi_nu_3 * f
                f_sub[9:12] += a_3*w[p] * a_2*w[q] * a_1*w[r] * xi_nu_4 * f

    return f_sub * (3./4.) * V_sub
```

Listing A.4: Computing the load vector for surface force integral ${}^{\zeta}\mathbf{f}_{t_i}^{\mathsf{T}}$

```
from numpy import cross, zeros
from numpy.linalg import norm
from scipy.special import p_roots

def f_s_sub(function, nu_1, nu_2, nu_3, Gauss_Points):
    """ function is a user defined function,
        nu_1, nu_2, nu_3 are the vertex coordinates of the triangle and
        Gauss_Points are the number of sample points
    """

    """ The area of a triangle """
    A_sub = (1./2.) * norm(cross(nu_1-nu_3, nu_2-nu_3))

    """ SciPy generates the sample points and weights for Gauss-Legendre quadrature
        """
    n, w = p_roots(Gauss_Points)

    """ Initiation of the surface load vector """
    f_sub = zeros(9)
```

```
    """ Computation of the volume load vector, for details see Eq. (2.246) """
    for p in xrange(Gauss_Points):
        for q in xrange(Gauss_Points):
            a_2 = 1.
            xi_nu_2 = (1./2.) * (n[p]+1.)

            a_1 = 1. - xi_nu_2
            xi_nu_1 = (1./2.) * (a_1*n[q]+a_1)

            xi_nu_3 = 1. - xi_nu_2 - xi_nu_1

            x = xi_nu_1 * nu_1 + xi_nu_2 * nu_2 + xi_nu_3 * nu_3

            f = function(x)

            f_sub[0:3] += a_2*w[p] * a_1*w[q] * xi_nu_1 * f
            f_sub[3:6] += a_2*w[p] * a_1*w[q] * xi_nu_2 * f
            f_sub[6:9] += a_2*w[p] * a_1*w[q] * xi_nu_3 * f

    return f_sub * (1./2.) * A_sub
```